

PDF hosted at the Radboud Repository of the Radboud University Nijmegen

The following full text is a publisher's version.

For additional information about this publication click this link.

<http://hdl.handle.net/2066/30953>

Please be advised that this information was generated on 2022-08-23 and may be subject to change.

The Biological Role of the Brain Specific Creatine Kinase Energy System in Mice

A Behavioral Approach



The Biological Role of the Brain Specific Creatine Kinase Energy System in Mice

A Behavioral Approach

Een wetenschappelijke proeve op het gebied van
de Medische Wetenschappen

Proefschrift

ter verkrijging van de graad van doctor
aan de Radboud Universiteit Nijmegen,
op gezag van de rector magnificus prof. mr. S.C.J.J. Kortmann,
volgens besluit van het College van Decanen
in het openbaar te verdedigen op
maandag 17 december 2007
om 10:30 uur precies

door

Femke Streijger
geboren op 30 november 1976
te Nijmegen

Promotor:

Prof. dr. Bé Wieringa

Copromotor:

Dr. Catharina E.E.M. van der Zee

Manuscriptcommissie:

Prof. dr. Arend Heerschap

Prof. dr. Melly S. Oitzl

Dr. Gajja S. Salomons

Leids Universitair Medisch Centrum

VU Medisch Centrum Amsterdam

Printed by:

Drukkerij Print Partners Ipskamp te Enschede

ISBN nummer: 978-90-9022481-7

Table of Contents

| | | |
|-----------|---|-----|
| | Abbreviations | 9 |
| Chapter 1 | General introduction | 13 |
| Chapter 2 | Mice lacking the UbCKmit isoform of creatine kinase reveal slower spatial learning acquisition, diminished exploration and habituation, and reduced acoustic startle reflex responses | 39 |
| Chapter 3 | Structural and behavioral consequences of double deficiency for creatine kinases BCK and UbCKmit | 71 |
| Chapter 4 | Hair bundles are specialized for ATP delivery via creatine kinase | 109 |
| Chapter 5 | Deficiency for brain-type creatine kinases in mice causes defective thermoregulation | 169 |
| Chapter 6 | Complete brain-type creatine kinase deficiencies in mice affects seizure activity and removal of intracellular calcium | 207 |
| Chapter 7 | Summarizing discussion | 235 |
| | Nederlandse samenvatting | 253 |
| | Dankwoord | 259 |
| | Curriculum Vitae | 265 |
| | Publications | 267 |

Abbreviations

| | |
|------------------|---|
| ABRs | auditory brainstem evoked responses |
| ADP | adenosine diphosphate |
| AK1 | adenylate kinase 1 |
| Ap5A | adenosine 5',5"-P1,P5-pentaphosphate |
| Arc | hypothalamic arcuate nucleus |
| ATP | adenosine triphosphate |
| ATPases | adenosine triphosphatase |
| BAT | brown adipose tissue |
| BCK | cytosolic brain creatine kinase isoform |
| BCK-/- | mice lacking cytosolic brain creatine kinase isoform |
| BSA | bovine serum albumin |
| BW | bodyweight |
| Ca ²⁺ | calcium |
| cDNA | circular deoxyribonucleic acid |
| c-FOS | cellular FBR murine osteosarcoma |
| CK | creatine kinase |
| CK-/- | mice lacking both cytosolic brain creatine kinase and mitochondrial ubiquitous creatine kinase isoforms |
| CLIC5 | chloride intracellular channel-5 |
| CNS | central nervous system |
| Cr | creatine |
| DAB | diaminobenzidine tetrachloride |
| DAPI | 4',6-diamidino-2-phenylindole |
| DC | Deiters' cell |
| DNFB | dinitrofluorobenzene |
| 2DOG | 2-deoxyglucose |
| EDTA | ethylenediamine tetraacetic acid |
| EEG | electroencephalographic |
| EPLIN | epithelial lost in neoplasm |
| ES cells | embryonic stem cells |
| EST | expressed sequence tag |
| FFA | free fatty acids |
| GABA | aminobutyric acid |
| GAPDH | glyceraldehyde-3-phosphate dehydrogenase |
| H ⁺ | hydrogen |

Abbreviations

| | |
|----------------------------------|---|
| HEPES | 4-(2-hydroxyethyl)-1-piperazineethanesulfonic acid |
| H ₂ O ₂ | hydrogen peroxide |
| Hsc70 | heat shock cognate 70 |
| IHC | inner hair cell |
| IIP-MF | intra- infra-pyramidal mossy fibers |
| IF | intensity factor |
| K ⁺ | potassium |
| LC | liquid chromatography |
| Mg ⁺ | magnesium |
| mRNA | messenger ribonucleic acid |
| MR-spectroscopy | magnetic resonance spectroscopy |
| MS/MS | tandem mass spectrometry |
| MuDPIT | multidimensional protein identification technology |
| NA | noradrenaline |
| Na ⁺ | sodium |
| NaCl | sodium chloride |
| Na ₂ HPO ₄ | sodium hydrogen phosphate |
| NHERF1 | Na ⁺ -H ⁺ exchanger regulatory factor-1 |
| OHC | outer hair cell |
| ~P | phosphorus flux |
| PBS | phosphate buffered saline |
| PBS-T | PBS with Tween |
| PCr | phosphocreatine |
| PF | paraformaldehyde |
| pH | potential of hydrogen |
| Pi | inorganic phosphate |
| PMCA2 | plasma membrane Ca ²⁺ -ATPase-2 |
| PnC | nucleus reticularis pontis caudalis |
| POA | hypothalamic medial preoptic area |
| PTPRQ | protein tyrosine phosphatase, receptor type, Q |
| PTZ | pentylenetetrazole |
| PVN | hypothalamic paraventricular nucleus |
| RNA | ribonucleic acid |
| SCF | spectral count factor |
| SD | standard deviation |
| SDS | sodium dodecyl sulfate |
| SDS-PAGE | SDS-polyacrylamide gel electrophoresis |

| | |
|------------|---|
| SEM | standard error of the mean |
| SP-MF | supra-pyramidal mossy fibers |
| TG | triglyceride |
| TOF-MS | time-of-flight mass spectrometry |
| TIM | triosephosphate isomerase |
| UbCK | mitochondrial ubiquitous creatine kinase isoform |
| UbCKmit-/- | mice lacking mitochondrial ubiquitous creatine kinase isoform |
| UCP1 | uncoupling protein 1 |
| VLGR1 | very large G protein-coupled receptor-1 |
| WAT | white adipose tissue |
| wt | wildtype |

Chapter 1

General Introduction



1. General introduction

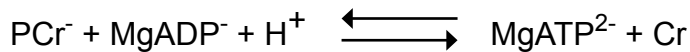
Cells in tissues such as skeletal and cardiac muscle, brain or sensory organs of vertebrates, sperm or the electric organs of rays, eels and fish, all depend on the immediate availability of vast amounts of energy. ATP is the universal currency for energy requiring processes in biological systems (Lehninger, 1982). Under normal conditions, oxidative phosphorylation and glycolysis are the major ATP synthetic pathways, but depending on cell type, also lipidolysis, serinolysis, and glutaminolysis may contribute (Erecinska and Silver, 1989; Clark and Sokoloff, 1999). Tight control of these pathways for energy homeostasis is thereby critical for normal physiology and survival. In a living cell, the energy flux is regulated to ensure that the rate of energy production and expenditure remain within acceptable limits. If the capacity of cells to generate or store energy is reduced, cell function(s) could be impaired depending on the margins of safety that exists between the amount of energy the cells can normally generate and their requirement. Cell suicide is initiated if the cell fails to maintain [ATP] above a certain critical level during some period of time (Izyumov et al, 2004). The concept, once held, of a single large intracellular reservoir of ATP, supplied by glycolytic and oxidative reactions, is nowadays recognized as no longer tenable. The level of immediate available ATP (i.e. the ATP “reserve”) that any given cell has available is rather limited, and can provide energy for only brief periods of activation (Ames, 2000). In tissues with high and fluctuating energy demands, additional energy reservoirs therefore seem necessary to buffer against excessive ATP depletion. One such a crucial intracellular energy reservoir is formed by the phosphagen phosphocreatine (PCr), which can provide high-energy phosphate to yield ATP via a reaction catalyzed by creatine kinase (CK).

1.2 Creatine kinase, more than just an energy buffer of the cell

1.2.1 The CK-PCr system

The creatine kinase-phosphocreatine (CK-PCr) energy system has undergone intensive investigation for over 150 years (Newsholme and Beis, 1996). Studies started in the mid 1830s with the discovery of creatine (from Greek *kreas*, flesh) isolated from meat extract (Chevreul, 1835). It took almost one hundred years before the finding

of a labile phosphate compound in muscle, characterized as phosphocreatine was reported (Eggleton and Eggleton, 1927; Fiske and Subbarow; 1927; Fiske and Subbarow, 1929). Meyerhof and Lohmann (1928) measured the heat of hydrolysis of this compound and placed it in the category of what are today called phosphagens or high-energy phosphate compounds. Not long after, Lohmann (1934) discovered creatine kinase and proposed that phosphate molecules from creatine phosphate combined with adenosine monophosphate to form ATP. After the discovery of ADP, Lehmann (1936) established the reversibility of the phosphate transfer between PCr and ADP, and described the now accepted CK reaction:



The creatine kinase enzyme (CK) catalyzes the reversible transfer of a phosphoryl group from phosphocreatine (PCr) to ADP, producing ATP and creatine (Cr). The equilibrium of the reaction is well to the right, so that only very low concentrations of ADP are required to stimulate production of ATP from PCr. This reaction together with the enzyme creatine kinase is often called the CK-PCr system. Cells and tissues like muscle and brain use the CK-PCr energy system to cope efficiently with high or alternating ATP requirements.

1.2.2 Creatine kinase isoenzymes

Nowadays there are four major CK isoenzymes known, which have been named after the tissues from which they were isolated. The isoenzymes have been characterized based on differences in gene and amino acid sequence, tissue localization and immunogenicity (for review see Wallimann, 1992). There are two cytosolic isoforms, the muscle (MCK) and brain (BCK) forms, which exist as dimers under physiological conditions. In cells where these enzymes are co-expressed, like in heart cells, cytosolic CK can exist as the MB heterodimer. MCK is predominantly found in differentiated striated muscle, while BCK is expressed in a number of tissues but is most abundant throughout the brain, approximately 5 fold lower in the stomach, 10-fold lower in the heart and barely detectable in liver.

There are also two mitochondrial isoforms of the enzyme, the ubiquitous (UbCKmit) and the sarcomeric (ScCK) forms, which generally exist as octamers but can be readily dissociated into dimers.

Based on their isoelectric point, they are sometimes referred to as acidic and basic mitochondrial CK, respectively (for review see Wyss et al., 1992). Both mitochondrial CK forms are located in the intermembrane space, along the entire inner membrane and also at peripheral contact sites where inner and outer membranes are in close proximity (Kottke et al., 1988; Biermans et al., 1990; Kottke et al., 1991; Brdiczka, 1994; Kottke et al., 1994). There, CK can directly transphosphorylate intramitochondrially produced ATP into PCr, which is then exported into the cytosol (Jacobus, 1985). Interestingly, the mitochondrial ScCK is usually co-expressed with the cytosolic MCK, whereas the mitochondrial UbCKmit appears to be mainly active where BCK is expressed (Wallimann et al., 1992).

1.2.3 Physiological function

For many years only the soluble form of creatine kinase was known, and the main physiological role ascribed to CK was that of a temporal energy buffer (for review see Wallimann et al. 1992). Even though the cellular pools of ATP are rather small (Ames, 2000), no significant change in overall ATP levels can be detected during activation of excitable tissues (Mommaerts & Wallner, 1967; Mommaerts et al., 1977; Seraydarian, 1980). This is because large intracellular PCr stores and a high CK activity phosphorylates ATP at a rate fast enough to cope with the transient high-energy demand crucial for proper cell functioning. As a direct consequence of the CK reaction also Cr is produced. This provides an additional feedback indicator of energy consumption, as Cr can act as a promoter of energy generation. Thus, PCr and Cr provide a buffer for keeping cellular ATP/ADP ratios balanced and the ATP pool highly charged. Providing ATP at appropriate rates to energy-consuming enzymes throughout the cell requires not only organized systems for generating ATP but also organized means of delivery. ATP and ADP diffusion through the cytoplasm is rather slow over distances measured in mm, and may represent a rate limiting factor in energy demanding systems operating at high rates in large cell like muscle cells or neurons. With the discovery of the mitochondrial isoenzymes, it now appears that CK-catalyzed phosphotransfer also acts a spatial energy buffer in concert to reduce the potential limitation cited above (Fig. 1).

In cells where both creatine kinases co-exist, the interplay between cytosolic and mitochondrial CK isoenzymes provides an efficient

energy shuttle system that plays a pivotal role in cellular energy both energy supply and distribution. According to a hypothetical concept, high-energy phosphate groups from glycolytic or OXPHOS-derived ATP may be passed directly from one enzyme molecule to the next in a series of linked reactions (Bessman and Geiger, 1981; Bessman and Carpenter, 1985; Walliman et al., 1992). This proposal is based on the observation that high energy phosphoryls undergo ten or more exchanges between ATP and PCr en route to ATPases, and on the finding that the rate of \sim P transfer is greater than expected from free diffusion of the substrates through the cytoplasm.

Besides the temporal and spatial energy buffer concepts, the CK-PCr system also works as a regulator of cellular energetics (Wallimann et al., 1992). It prevents a rise in intracellular free ADP and thus preserves the thermodynamic efficiency of ATPases even at high cellular ATP turnover. By this mechanism, an inactivation of cellular ATPases by rising ADP levels is avoided and a net loss of adenine nucleotides is prevented (Iyengar et al. 1982; Iyengar 1984). Another potential useful element of the system is its proton buffering capacity. Hydrolysis of ATP leads to proton production, but these protons are used when ATP levels are replenished in the CK reaction. In addition, the net production of inorganic \sim P stimulates glycolysis and glycogenolysis (Davuluri et al. 1981). In the absence of dephosphorylation of PCr, the inorganic phosphate levels could be rate limiting for these processes as suggested by Meyer et al. (1986).

1.3 The significance of creatine kinase in brain

The major ideas about the physiological of the CK-PCr system are based on studies of the skeletal muscle, involving the enzymes MCK and ScCK. The high activity of these CK's in muscle, as well as the phenotype of muscle-type deficient mice (Van Deursen et al., 1993; Steeghs et al., 1998; De Groof et al., 2001a; De Groof et al., 2001b) and the effects of Cr analogue on muscle function (Shoubridge and Radda 1984; Van Deursen et al. 1994; Wyss and Wallimann 1994), strongly indicates that CK is a key enzyme in muscle energy metabolism. Over the past years, a concept for creatine kinase function, the 'PCr-circuit' model, has evolved. Based on this concept, multiple functions for the CK/PCr-system have been proposed, such as an energy buffering function, regulatory functions, as well as an energy transport function, mostly based on studies with muscle.

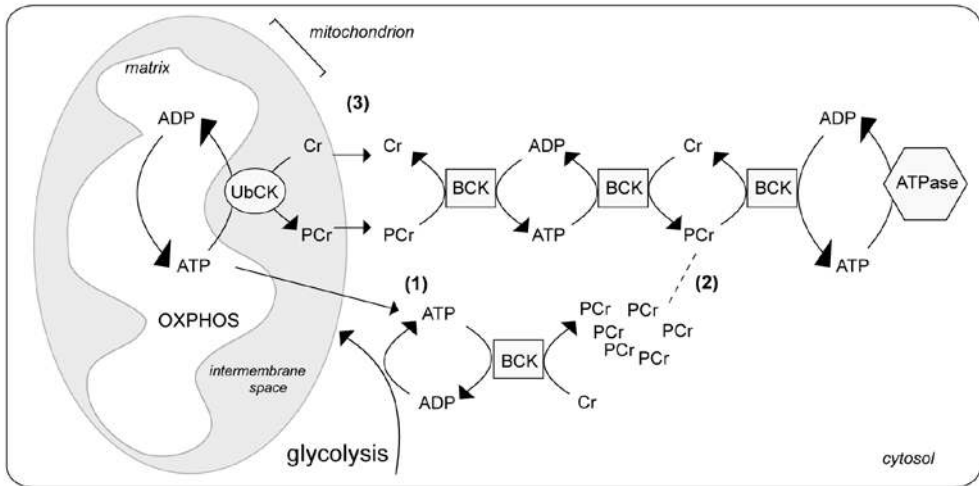


Figure 1: The CK-PCr energy system in brain cells. Under normal physiological conditions, the majority of ATP is produced by oxidative phosphorylation (OXPHOS) and glycolysis. During periods of low energy expenditure, the cytosolic BCK isoform can convert ATP and creatine (Cr) into ADP and phosphocreatine (PCr) (1). The produced PCr acts as a temporal energy buffer that can be used during periods of high and fluctuating energy demands (2). The CK-PCr system can also act as a spatial energy buffer, connecting sites of energy production to sites where energy consumption is high (3). UbCKmit (UbCK) can directly transphosphorylate intramitochondrially produced ATP into PCr. When exported into the cytosol, this PCr can be shuttled through the cytosol using BCK towards the site of energy consumption (ATPase).

Although activity of the CK system has been shown to correlate with brain activity (Sauter and Rudin, 1993; Chen et al, 1997; Holtzman et al., 1997; Kekelidze et al., 2001), it remains to be determined how essential the CK-PCr system is for cells in the central nervous system (CNS), and at what sites it is most critical. At just 2% of body mass, the human brain consumes nearly 20% of metabolic energy required for the whole body (Clarke and Sokoloff, 1999; Torrealdea et al., 2006). Energy requirement in brain is special because both neurons and glial cells (astrocytes and microglia) are highly dynamic, with elaborate peripheral processes that form distinct locales in the cell. During development and adulthood, brain cells have to invest a high percentage of their ATP, not only for “normal” maintenance of housekeeping functions but also for fuelling of molecular transport, intracellular communication, actomyosin-based dynamics during synaptogenesis, and for continuous dendritic spine or glial endfeet remodelling. In addition,

neurons and glial cells have to invest high and sudden amounts of ATP for fuelling of Ca^{2+} - and Na^+/K^+ -ATPases involved in electrogenic or ion-homeostasis activity, and for neurotransmitter cycling or neuroendocrine signalling (Barinaga, 1997; Bernstein and Bamburg, 2003; Streijger et al., 2007; Hertz 2007).

Existence of a CK-shuttle, with CK isoforms located at both the mitochondrial and cytosolic end-points of a cellular energy relay pathway, is now a commonly accepted concept (Wyss and Kaddurah-Daouk, 2000; Dzeja and Terzic, 2003; Streijger et al., 2007). Unfortunately, this model is rather uncritically presented as one metabolic entity in many reviews on cell energy metabolism and the question whether both end-points indeed co-exist in CK-expressing cells is hardly ever asked. It could thus very well be that capacities of the CK reactions in the mitochondrial inner-membrane space and at locations in the cytosol are in severe unbalance in various cell types (Streijger et al., 2007). In brain, both mitochondrial UbCKmit and cytosolic BCK are highly expressed. Recent findings have shown that UbCKmit was expressed selectively in neurons and localized in their mitochondria in dendrites, cell bodies, axons and terminals. By contrast, BCK was selective to astrocytes among glial populations, and was exclusive to inhibitory neurons among neuronal populations (Sisterman et al., 1995; Jost et al., 2002; Streijger et al. 2004; Tachikawa et al., 2004). These data strongly suggests that BCK and UbCKmit are certainly not always expressed at constant ratios in different brain areas, or are even not coupled at all in certain cell types. New available ISH data confirms this picture and demonstrate that BCK and UbCKmit mRNA levels vary profoundly across cell types (Tachikawa et al., 2004; Lein et al., 2007; also see <http://www.brain-map.org>, GENSAT at <http://www.ncbi.nlm.nih.gov/projects/gensat/>, and at <http://expression.gnf.org/cgi-bin/index.cgi#Q>). For a better understanding of the validity of the CK-shuttle concept or the existence of any form of intercellular cooperation of Cr-PCr metabolism we need to study regional and cell-type dependent variation in BCK vs. UbCKmit expression levels in more detail. Therefore, we will first need better classification of neuronal and glial cell-types of which several hundreds of sub-types may exist in various brain structures (Streijger et al., 2007).

1.3.1 Disturbed energy metabolism in neurodegenerative diseases

Substantial evidence indicates that bioenergetic dysfunction plays a role in the pathophysiology of cell death or dysfunction in a variety of neurodegenerative diseases such as Huntington's disease, Amyotrophic lateral sclerosis, Parkinson's disease, and Alzheimer disease (Palop et al., 2006; Rubinsztein, 2006). A common hallmark of these diseases is oxidative stress accompanied by a severely disturbed energy metabolism as well as a disturbed energetic status of the brain (Beal, 2000; Lin and Beal, 2006). For many of these disorders, impairments of the CK-PCr system in the regulation of brain ATP were described as well (Hemmer and Walliman, 1993). Dramatically decreased content of immunoreactive BCK and a reduction by up to 86% of total CK activity have been observed in the brain in Alzheimer's disease (Smith et al., 1991; Burbaeva et al., 1992; David et al., 1998; Aksenova et al., 1999; Bürklen et al., 2006). A comparable increase in protein oxidation and decrease in brain CK activity was observed in Pick's disease and diffuse Lewy body disease (Aksenova et al., 1999). To a lesser degree decreased activity of CK was observed in brains of patients with epilepsy, schizophrenia, and manic-depressive psychosis. Thus, proper functioning of the brain seems to be linked with the CK system and with Cr metabolism, although the causal relationships in many cases are not yet known.

If impairment of high-energy phosphate metabolism plays a critical role in the progression of neurodegenerative disease, then compounds that increase the cerebral energy reserve may be neuroprotective. The potential of creatine to be protective has been illustrated in several models of neurodegeneration (Carter et al., 1995; Brewer and Walliman, 2000; Sullivan et al., 2000; Wilken et al., 2000). In addition, creatine protects against neuronal loss in mice with chemically induced Parkinsonism (Matthews et al., 1998; Matthews et al., 1999) and appeared effective in transgenic mouse models of Amyotrophic lateral sclerosis and Huntington's disease (Klivenyi et al., 1999; Ferrante et al., 2000; Andreassen et al., 2001). Several factors have been postulated to contribute to the neuroprotective effects of oral Cr supplementation: improvement of energy and calcium homeostasis enhanced presynaptic glutamate uptake or protection of mitochondria from mitochondrial permeability transition (Brewer and Wallimann, 2000; Wyss and Kaddurah-Daouk, 2000; Kaemmerer et al., 2001). The relevance of these factors and the detailed mechanisms of action

in vivo are not yet clear. The only consistent conclusion that can be drawn so far is that neuroprotection depends on increases in Cr and PCr concentrations in the brain.

1.3.2 Creatine deficiency syndromes

In vertebrates, Cr is synthesized mostly in the liver and kidney and is then transported through the blood and taken up by the main target organs like muscle and brain via creatine transporters (Walker, 1979; Wyss and Kaddurah-Daouk, 2000). Biosynthesis of creatine involves two sequential steps. First, L-arginine: glycine amidinotransferase (AGAT) catalyzes the formation of guanidinoacetate (GAA), the immediate precursor of creatine. Subsequently, creatine is formed by S-adenosyl-L-methionine:N-guanidinoacetate methyltransferase (GAMT) by methyl group transfer from S-adenosyl-L-methionine to GAA (Walker, 1979, Schmidt et al., 2004). The importance of intact Cr metabolism in humans is highlighted by the identification of Cr deficiency syndromes characterized by a complete lack of Cr/PCr in the brain (Schultze 2003). Disorders of creatine metabolism arise from genetic alterations of AGAT, GAMT, and the creatine transporters (Stöcker et al., 1996; Salomons et al., 2000; Item et al., 2001). GAMT deficiency is the first identified inborn error of creatine metabolism in man. The clinical manifestation is heterogeneous, generally characterized by epilepsy, slow background activity in EEG, global developmental delay, failure of active speech, altered signal intensities in the basal ganglia, and extrapyramidal movement disorders (Stöckler et al., 1994; Stöckler et al. 1996; Ganesan et al., 1997, Schultze et al., 1997; Van der Knaap et al., 2000; Von Figura et al., 2001; Schutze 2003). GAMT knockout mice exhibit biochemical changes and the typical associated behavioral effects that are also observed in human GAMT deficiency (Schmidt et al., 2004). AGAT deficiency was recently identified in two sisters, 4 and 6 years of age (Bianchi et al., 2000; Item et al., 2001). The girls suffered from mild mental retardation and severe language delay. Finally, six patients with creatine transporter deficiency have been identified (Cecil et al., 2001; Salomons et al., 2001). Patients with this problem initially presented with mild mental retardation, and severe delay in speech and expressive language function. These cases emphasize the importance of creatine and the creatine kinase reaction for normal brain function such as psychomotor development and cognitive function.

1.3.3 Transgenic mice with ablated brain-CK gene function

Various data suggest that the BCK and UbCKmit isoforms are coupled into a fully functional PCr-ATP circuit but it is currently unclear to what extent brain energy metabolism relies on their presence (Wallimann et al., 1992; Kaldis et al., 1996). During the past 2-3 decades, the use of genetically altered mice has opened up a broad range of entirely new possibilities to study the physiological and structural role of proteins in cell growth, signaling, and metabolism. Although different approaches for reverse genetics are possible (with design of transgenic models that over-express either protein, express mutant protein, or no protein at all), our group has mainly focused on the generation of models with complete or partial enzyme deficiency. Using gene-knockout in embryonic stem cells we have generated transgenic mice deficient for either BCK (BCK^{-/-} mice), UbCKmit (UbCKmit^{-/-} mice), or both enzymes (CK^{--/--} mice) (Van Deursen and Wieringa, 1994; Steeghs et al., 1995; In 't Zandt et al., 2004). Immunohistochemical and zymogram analysis of whole brain-sections from wildtype and knockout mice revealed that single CK deficiency induced no compensation through changes in expression profile or activity of the remaining CK isoform (Jost et al., 2002; Streijger et al., 2007). Some studies have demonstrated MCK isotype expression in brain (Hemmer et al., 1994; Sistermans et al., 1995). However, with an antibody raised against an MCK specific peptide (Friedman and Perryman, 1991) we only found occasional α -specific labeling along the plasma membrane of a very limited number of neurons in the cortex (data not shown). Furthermore, MCK activity is absent in the brain extracts on zymograms.

Subsequent studies of aspects of brain physiology, and brain function, including behavior and learning did reveal, however, that CK ablation is not entirely neutral (Jost et al., 2002; In 't Zandt et al., 2004; Streijger et al., 2004; streijger et al., 2005; Shin et al., 2007; Streijger et al., 2007; Chapters 2-6). For phenotyping of brain functions in these mice, histo-anatomical analyses and biophysical approaches with MR-spectroscopy or MR-imaging were used. In addition, neurobehavioral approaches for monitoring of brain functions were employed. Hereto, a battery of different behavioral and learning paradigms was developed and used to study the relationship between phosphocreatine-creatine energetics and task performance. Tests used included habituation behavior and spatial learning tests, which specifically address hippocampal based brain functions as well as the acoustic startle reflex chal-

lence which probes the auditory-brainstem circuit. Also the response to seizure induction and other integral physiological features, including body temperature control, were monitored.

Both BCK^{-/-} and UbCKmit^{-/-} mice showed near normal levels of PCr. Furthermore, BCK or UbCKmit deficiency had no effect on development and life expectancy of these animals (Steeghs et al., 1995; Jost et al., 2002; In 't Zandt et al., 2004). This observation was unanticipated, especially in view of the reports of the creatine kinase syndromes. When assessing behavioral characteristics of the single mutant animals (Jost et al., 2002; Streijger et al., 2004; chapter 2), the data showed diminished open-field habituation, and an impairment in learning and memory functioning. In addition, the time-profile of chemically induced seizures in BCK^{-/-} and control animals differed (Jost et al., 2002). The behavioral defect was more pronounced in mice missing the entire BCK/UbCKmit system. These animals completely lack PCr as high-energy metabolite, however show rather normal basal ATP, Pi and pH levels (Jost et al., 2002; In 't Zandt et al., 2004). CK^{-/-} mice appeared viable, however their growth/development was affected, resulting in an overall smaller body posture (Streijger et al., 2005; chapter 3; chapter 5). Furthermore, the complete lack of CK in brain in these animals severely impaired spatial learning and was coupled to abnormal startle responses, hearing problems, thermoregulatory problems, and, and their response to chemical seizure induction appeared suppressed (Streijger et al., 2005; Shin et al., 2007; chapter 3-6). In contrast, the visual and motor functions, exploration behavior, and anxiety-related responses were not changed in CK^{-/-} mice, suggesting no global deficit in sensorimotor function, or motivation. Various effects on behavior were consistent with underlying anatomical changes in the hippocampus (Jost et al., 2002; streijger et al., 2004; streijger et al., 2005; chapter 2-3). Others can best be explained by loss of functional integrity (Shin et al., 2007; chapter 4; chapter 6).

Combined these findings therefore strongly support the crucial importance of the CK-PCr system in the brain for behavioral task performance and physiological regulation.

1.4 Outline thesis

The aims of my PhD study described in this thesis were to identify behavioral processes in mice that depend on the CK energy system and to examine how an impaired CK energy system in brain can cause

behavioral and physiological abnormalities. In this thesis I have described the first steps on a long road towards the delineation of the biological role the creatine kinases in brain energetics (**chapter 1-6**).

In **chapter 2**, we have addressed the significance of the ubiquitous mitochondrial creatine kinase (UbCKmit), as a follow up of studies of Jost et al. (2002) regarding the role of the cytosolic brain-type creatine kinase (BCK) in brain energy homeostasis. In analogy to these BCK studies, we decided to portray UbCKmit mice in more detail upon behavioral challenge in comparison to wildtype animals. In this study, the UbCKmit^{-/-} mice were analyzed for open field exploration and habituation, dry and wet maze spatial learning, T-maze spontaneous alternation, light-dark box anxiety, rotarod and nestbuilding activity, tests that were used earlier to phenotype the BCK single knockout group. Furthermore, tests of motor coordination and sensory abilities addressed specific questions about the role of a creatine kinase in coordination, visual and auditory function.

Next, we assessed the behavioral consequences of complete depletion of the CK-PCr system in transgenic mice without BCK and UbCKmit. In the single knockout mice there is no appreciable loss in PCr content with respect to wildtype levels, however in CK^{-/-} brain PCr is undetectable (Jost et al., 2002; In 't Zandt et al., 2004). Furthermore, given the broad distribution of CK in brain, we hypothesized that CK^{-/-} mice would be more affected than the BCK and UbCKmit single knockouts. Comparative analysis of wildtype, single and double knockout mice will allow us to assess the relative importance of the brain specific CK isoforms. In **chapter 3**, we describe how CK^{-/-} mice were subjected to a similar comprehensive battery of tests as used for the initial screening of both single knockout mice, which included tests for exploratory and locomotor activity, and cognitive performance. In addition, the anatomical features of the hippocampus and mossy fiber fields were measured, and correlated to exploration and spatial learning performance (Schwegler and Crusio, 1995). Speculating that fast energy is needed, we used the acoustic startle paradigm to investigate the impact of brain CK deficiency on the immediate reaction to sudden stimuli (**chapter 3**).

As a follow up study, in **chapter 4** we conducted additional hearing studies to get more detail upon the role of brain-type creatine kinase in hearing. As a measure of the sensitivity of the auditory system, we analysed the brainstem response to broadband click stimuli, which largely contain low-frequency components, and 8 kHz and 16

kHz tone bursts of CK^{-/-} mice. Furthermore, in collaboration with the group of dr. P.Gillespie we investigated BCK immunoreactivity in inner ear and brain, localization of creatine kinase B in hair bundles, and function role of BCK in the vestibular hearing system (**chapter 4**).

Under normal laboratory housing conditions, CK^{-/-} mice showed a higher mortality rate. We did notice that death was occasionally preceded by onset of severe hypothermia, and body temperatures as low as 28°C were observed. Strikingly, these sudden temperature drops were never observed in wildtypes or any of the single knockout mice. Thus, it appears that the lack of both creatine kinase isoforms can seriously affect thermoregulation. To address the question how CK double deficiency could lead to deregulation of the body temperature, we examine broad series of physiological parameters involved in thermoregulation. The measured variables include food intake, general activity, changes in white and brown fat depots, functioning of the neuronal circuitry, and BAT thermogenesis (**chapter 5**).

In the final chapter (**chapter 6**), we examined whether CK deficiency changes brain function characteristics. Generation of ATP, hence CK activity, is critical for CNS function. Activity of the CK system protects against cellular toxicity by ATP depletion during hypoxia or chemically induced mitochondrial dysfunction (Holtzman et al., 1998a; Holtzman et al., 1998b; Matthews et al., 1999). However, little direct evidence had been obtained about the physiological importance of the CK-PCr system during strenuous conditions. Other studies have shown that increased local cerebral glucose utilization and high ATP turnover is required during neuronal activity associated with seizures (El Hamdi et al., 1992; Holtzman et al., 1997). For that reason, we used pentylenetetrazole (PTZ)-induced seizures as an interpretable method for metabolic challenging. Changes in brain function potential in CK^{-/-} mice was based on electroencephalogram study and behavioral observation. The results of this study are described in **chapter 6**.

In the general discussion (**chapter 7**) the possible metabolic and cell-network changes that could cause the (behavioral) phenotype in the CK^{-/-} mice are discussed. In addition, experiments are suggested for future studies that should contribute to better knowledge of creatine kinase function(s) in neural activities at many levels.

References

- Aksenova MV, Aksenov MY, Payne RM, Trojanowski JQ, Schmidt ML, Carney JM, Butterfield DA, Markesbery WR (1999) Oxidation of cytosolic proteins and expression of creatine kinase BB in frontal lobe in different neurodegenerative disorders. *Dement Geriatr Cogn Disord* 10:158-165.
- Ames AIII (2000) CNS energy metabolism as related to function. *Brain Res Rev* 34:42-68.
- Andreassen OA, Dedeoglu A, Ferrante RJ, Jenkins BG, Ferrante KL, Thomas M, Friedlich A, Browne SE, Schilling G, Borchelt DR, Hersch SM, Ross CA, Beal MF (2001) Creatine increase survival and delays motor symptoms in a transgenic animal model of Huntington's disease. *Neurobiol Dis* 8:479-491.
- Barinaga, M (1997) What makes brain neurons run? *Science* 276:196-198.
- Beal MF (2000) Energetics in the pathogenesis of neurodegenerative diseases. *Trends Neurosci* 23:298-304.
- Bessman SP, Carpenter CL (1985) The creatine-creatine phosphate energy shuttle. *Annu Rev Biochem* 54:831-862.
- Bernstein BW, Bamberg JR (2003) Actin-ATP hydrolysis is a major energy drain for neurons *J Neurosci* 23:1-6.
- Bessman SP, Geiger PJ (1981) Transport of energy in muscle: the phosphorylcreatine shuttle. *Science* 211:448-452.
- Bianchi MC, Tosetti M, Fornai F, Alessandri' MG, Cipriani P, De Vito G, Canapicchi R (2000) Reversible brain creatine deficiency in two sisters with normal blood creatine level.. *Ann Neurol* 47:511-513.
- Biermans W, Bakker A, Jacob W (1990) Contact site between inner and outer mitochondrial membrane: a dynamic microcompartment for creatine kinase activity. *Biochim Biophys Acta* 1018:225-228.

Brdiczka D (1994) Function of the outer mitochondrial compartment in regulation of energy metabolism. *Biochim Biophys Acta* 1187:264-269.

Brewer GJ, Wallimann TW (2000) Protective effect of the energy precursor creatine against toxicity of glutamate and beta-amyloid in rat hippocampal neurons. *J Neurochem* 74:1968-1978.

Burbaeva GS, Aksenova MV, Makarenko IG (1992) Decreased level of creatine kinase BB in the frontal cortex of Alzheimer patients. *Dementia* 3:91-94.

Bürklen TS, Schlattner U, Homayouni R, Gough K, Rak M, Szeghalmi A, Wallimann T (2006) The Creatine Kinase/Creatine Connection to Alzheimer's Disease: CK Inactivation, APP-CK Complexes, and Focal Creatine Deposits *J Biomed Biotechnol* 2006:1-11.

Carter AJ, Muller RE, Scorn U, Stansky W (1995) Preoccupation with creatine enhances levels of creatine phosphate and prevents anoxic damage in rat hippocampal slices. *J Neurosci* 15:2691-2699.

Chen W, Zhu XH, Adriany G, Ugurbil K (1997) Increase of creatine kinase activity in the visual cortex of human brain during visual stimulation: a ³¹P magnetization transfer study. *Magn Reson Med* 38:551-557.

Chervil X. (1835) sur la composition critique due bouillon de viands. *J Pharm Sci Accessoires* 21:231-242.

Clarke DD, Sokoloff L (1999) *Basic Neurochemistry: Molecular, Cellular, and Medical Aspects*. Editors: Siegel GJ, Agranoff BW, Albers RW, Fisher SK, and Uhler MD, Lippincott-Raven, Philadelphia, pp637-669.

David S, Shoemaker M, Haley BE (1998) Abnormal properties of creatine kinase in Alzheimer's disease brain: correlation of reduced enzyme activity and active site photolabeling with aberrant cytosol-membrane partitioning. *Mol Brain Res* 54: 276-287.

Davuluri SP, Hird FJR, McLean RM (1981) A re-appraisal of the function and synthesis of phosphoarginine and phosphocreatine in muscle. *Comp Biochem Physiol* 69:329-336.

De Groof AJ, Smeets B, Groot Koerkamp MJ, Mul AN, Janssen EE, Tabak HF, Wieringa B (2001a) Changes in mRNA expression profile underlie phenotypic adaptations in creatine kinase-deficient muscles. *FEBS Lett* 506:73-78.

De Groof AJ, Oerlemans FT, Jost CR, Wieringa B (2001b) Changes in glycolytic network and mitochondrial design in creatine kinase-deficient muscles. *Muscle Nerve* 24:1188-1196.

De Groof AJ, Fransen JA, Errington RJ, Willems PH, Wieringa B, Koopman WJ (2002) The creatine kinase system is essential for optimal refill of the sarcoplasmic reticulum Ca^{2+} store in skeletal muscle. *J Biol Chem* 277:5275-5284.

Dzeja PP, Terzic A (2003) Phosphotransfer networks and cellular energetics. *J Exp Biol* 206:2039-2047.

Eggleton P, Eggleton GP (1927) The Inorganic Phosphate and a Labile Form of Organic Phosphate in the Gastrocnemius of the Frog. *Biochem J* 21:190-195.

El Hamdi G, de Vasconcelos AP, Vert P, Nehlig A (1992) An experimental model of generalized seizures for the measurement of local glucose utilization in the immature rat. I. Behavioral characterization and determination of lumped constant. *Brain Res Dev Brain Res* 69:233-242.

Erecinska M, Silver IA (1989) ATP and brain function. *J Cereb Blood Flow Metab* 9:2-19.

Ferrante RJ, Andreassen OA, Jenkins BG, Dedeoglu A, Kuemmerle S, Kubilus JK, Kaddurah-Daouk R, Hersch SM, Beal MF (2000) Neuroprotective effects of creatine in a transgenic mouse model of Huntington's disease. *J Neurosci* 20:4389-4397.

Fiske CH, Subbarow Y (1927) The nature of the "inorganic phosphate" in voluntary muscle. *Science* 65:401-403.

Fiske CH, Subbarow Y (1929) Phosphocreatine. *J Biol Chem* 81:629-679.

Friedman DL, Perryman MB (1991) Compartmentation of multiple forms of creatine kinase in the distal nephron of the rat kidney. *J Biol Chem* 266:22404-22410.

Ganesan V, Johnson A, Connelly A, Eckhardt S, Surtees RA (1997) Guanidinoacetate methyltransferase deficiency: new clinical features. *Pediatr Neurol* 17:155-157.

Hemmer W, Walliman T (1993) Functional aspects of creatine kinase in brain. *Dev Neurosci* 15:249-260.

Hemmer W, Zanolla E, Furter-Graves EM, Eppenberger HM, Wallimann T (1994) Creatine kinase isoenzymes in chicken cerebellum: Specific localization of brain-type creatine kinase in Bergmann glial cells and muscle-type creatine kinase in Purkinje neurons. *Eur J Neurosci* 6:538-549.

Hertz L, Peng L, Dienel GA (2007) Energy metabolism in astrocytes: high rate of oxidative metabolism and spatiotemporal dependence on glycolysis/ glycogenolysis. *J Cereb Blood Flow Metab* 27:219-249.

Holtzman D, Meyers R, Khait I, Jensen F (1997) Brain creatine kinase reaction rates and reactant concentrations during seizures in developing rats. *Epilepsy Res* 27:7-11.

Holtzman D, Brown M, O'Gorman E, Allred E, Wallimann T (1998a) Brain ATP metabolism in hypoxia resistant mice fed guanidinopropionic acid. *Dev Neurosci* 20:469-477.

Holtzman D, Togliatti A, Khait I, Jensen F (1998b) Creatine increases survival and suppresses seizures in the hypoxic immature rat. *Pediatr Res* 44:410-414.

In 't Zandt HJ, Renema WK, Streijger F, Jost C, Klomp DW, Oerlemans F, Van der Zee CEEM, Wieringa B, Heerschap A (2004) Cerebral creatine kinase deficiency influences metabolite levels and morphology in the mouse brain: a quantitative in vivo ¹H and ³¹P magnetic reso-

nance study. *J Neurochem* 90:1321-1330.

Item CB, Stockler-Ipsiroglu S, Stromberger C, Muhl A, Alessandri MG, Bianchi MC, Tosetti M, Fornai F, Cioni G (2001) Arginine : glycine amidinotransferase deficiency: the third inborn error of creatine metabolism in humans. *Am J Hum Genet* 69:1127-1133.

Iyengar MR (1984) Creatine kinase as an intracellular regulator. *J Muscle Res Cell Motil* 5:527-534.

Iyengar MR, Fluellen CE, Iyengar C (1982) Creatine kinase from the bovine myometrium: purification and characterization. *J Muscle Res Cell Motil* 3:231-246.

Izyumov DS, Avetisyan AV, Pletjushkina OY, Sakharov DV, Wirtz KW, Chernyak BV, Skulachev VP (2004) "Wages of fear": transient three-fold decrease in intracellular ATP level imposes apoptosis. *Biochim Biophys Acta* 1658:141-147.

Jost CR, Van der Zee CEEM, In 't Zandt HJ, Oerlemans F, Verheij M, Streijger F, Fransen J, Heerschap A, Cools AR, Wieringa B (2002) Creatine kinase B-driven energy transfer in the brain is important for habituation and spatial learning behavior, mossy fiber field size and determination of seizure susceptibility. *Eur J Neurosci* 15:1692-1706.

Kaemmerer WF, Rodrigues CM, Steer CJ, Low WC (2001) Creatine-supplemented diet extends Purkinje cell survival in spinocerebellar ataxia type 1 transgenic mice but does not prevent the ataxic phenotype. *Neuroscience* 103:713-724.

Kaldis P, Stolz M, Wyss M, Zanolla E, Rothen-Rutishauser B, Vorherr T, Wallimann T (1996) Identification of two distinctly localized mitochondrial creatine kinase isoenzymes in spermatozoa. *J Cell Sci* 109:2079-2088.

Kekelidze T, Khait I, Togliatti A, Benzecry JM, Wieringa B, Holtzman D (2001) Altered brain phosphocreatine and ATP regulation when mitochondrial creatine kinase is absent. *J Neurosci Res* 66:866-872.

Klivenyi, P Ferrante RJ, Matthews RT, Bogdanov MB, Klein AM, Andreassen OA, Mueller G, Wermer M, Kaddurah-Daouk R, Beal MF (1999) Neuroprotective effects of creatine in a transgenic animal model of amyotrophic lateral sclerosis. *Nat Med* 5:347-350.

Kottke M, Adam V, Riesinger I, Riesinger I, Bremm G, Bosch W, Brdiczka D, Sandri G, Panfili E (1988) Mitochondrial boundary membrane contact sites in brain: points of hexokinase and creatine kinase location, and control of Ca²⁺ transport. *Biochim Biophys Acta* 935:87-102.

Kottke M, Adams V, Wallimann T, Nalam VK, Brdiczka D (1991) Location and regulation of octameric mitochondrial creatine kinase in the contact sites. *Biochim Biophys Acta* 1061:215-225.

Kottke M, Wallimann T, Brdiczka D (1994) Dual electron microscopic localization of mitochondrial creatine kinase in brain mitochondria. *Biochem Med Metab Biol* 51:105-117.

Lehmann H (1936) Über die umesterung des adenylsäuresystems mit phosphagenen. *Biochem Z* 286:336-343.

Lehninger AL (1982) *Principles of Biochemistry*. Worth Publishers Inc., New York

Lein ES et al. (2007) Genome-wide atlas of gene expression in the adult mouse brain. *Nature* 445:168-176.

Lin MT, Beal MF (2006) Mitochondrial dysfunction and oxidative stress in neurodegenerative diseases *Nature* 443:787-795.

Lohman K (1934) Über die enzymatische aufspaltung der kreatinphosphorsäure; zugleich ein beitrag zum chemismus der muskelkontraktion. *Biochem Z* 271:264-277.

Matthews RT, Yang L, Jenkins BG, Ferrante RJ, Rosen BR, Kaddurah-Daouk R, Beal MF (1998) Neuroprotective effects of creatine and cyclocreatine in animal models of Huntington's disease. *J Neurosci* 18:156-163.

Matthews RT, Ferrante RJ, Klivenyi P, Yang L, Klein AM, Mueller G, Kaddurah-Daouk R, Beal MF (1999) Creatine and cyclocreatine attenuate MPTP neurotoxicity. *Exp Neurol* 157:142-149.

Meyer RA, Brown TR, Krilowicz BL, Kushmerick MJ (1986) Phosphagen and intracellular pH changes during contraction of creatine-depleted rat muscle. *Am J Physiol* 250:C264-C267.

Meyerhof O, Lohmann K (1928) Über die natürlichen Guanidinophosphorsäuren (Phosphagene) in der quergestreiften Muskulature. *Biochem Z* 196:22-48.

Mommaerts WFHM, Wallner A (1967) The breakdown of adenosine triphosphate in the contraction cycle of the frog sartorius muscle. *J Physiol* 193:343-357.

Mommaerts WF, Seraydarian K, Suh M, Kean CJ, Buller AJ (1977) The conversion of some biochemical properties of mammalian skeletal muscles following cross-reinnervation. *Exp Neurol* 55:637-653.

Newsholme EA, Beis I (1996) *Creatine and Creatine Phosphate: Scientific and Clinical Perspectives*. Editors: Conway MA and Clark JF, Academic Press, London, England, pp3-16.

Palop JJ, Chin J, Mucke L (2006) A network dysfunction perspective on neurodegenerative diseases. *Nature* 443:768-773.

Rubinsztein DC (2006) The roles of intracellular protein-degradation pathways in neurodegeneration. *Nature* 443:780-786.

Salomons GS, van Dooren SJ, Verhoeven NM, Cecil, KM, Ball WS, Degrauw TJ, Jakobs C (2001) X-linked creatine-transporter gene (SLC6A8) defect: a new creatine-deficiency syndrome. *Am J Hum Genet* 68:1497-1500.

Sauter A, Rudin M (1993) Determination of creatine kinase kinetic parameters in rat brain by NMR magnetization transfer. *J BioZ Chem* 268:13166-13171.

Schmidt A, Marescau B, Boehm EA, Renema WK, Peco R, Das A, Steinfeld R, Chan S, Wallis J, Davidoff M, Ullrich K, Waldschütz R, Heerschap A, De Deyn PP, Neubauer S, Isbrandt D (2004) Severely altered guanidino compound levels, disturbed body weight homeostasis and impaired fertility in a mouse model of guanidinoacetate N-methyltransferase (GAMT) deficiency. *Hum Mol Genet* 13:905-921.

Schulze A, Hess T, Wevers R, Mayatepek E, Bachert P, Marescau B, Knopp MV, De Deyn PP, Bremer HJ, Rating D (1997) Creatine deficiency syndrome caused by guanidinoacetate methyltransferase deficiency: diagnostic tools for a new inborn error of metabolism. *J Pediatr* 131:626-631.

Schultze A (2003) Creatine deficiency syndromes *Molecular and Cellular Biochemistry* 244:143-150.

Schwegler H, Crusio WE (1995) Correlations between radial-maze learning and structural variations of septum and hippocampus in rodent. *Behav Brain Res* 67:29-41.

Seraydarian MW (1980) Heart Creatine Kinase. Editors: Jacobus WE, Ingwall JS, Williams & Wilkins, Baltimore, London, pp. 82-90

Shin JB, Streijger F, Beynon A, Peters T, Gadzala L, McMillen D, Bystrom C, van der Zee CEEM, Wallimann T, Gillespie PG (2007) Hair bundles are specialized for ATP delivery via creatine kinase. *Neuron* 53:371-386.

Shoubridge EA, Radda GK (1984) A ³¹P-nuclear magnetic resonance study of skeletal muscle metabolism in rats depleted of creatine with the analogue betaguanidinopropionic acid. *Biochim Biophys Acta* 805:79-88.

Sisternans EA, De Kok, YJM, Peters W, Ginsel LA, Jap PHK, Wieringa B (1995) Tissue- and cell-specific distribution of creatine kinase B: A new and highly specific monoclonal antibody for use in immunohistochemistry. *Cell Tissue Res* 280:435-446.

Smith CD, Carney JM, Starke-Reed PE, Oliver CN, Stadtman ER, Floyd RA, Markesbery WR (1991) Excess brain protein oxidation and enzyme dysfunction in normal aging and in Alzheimer disease. *Proc Natl Acad Sci USA* 88:10540-10543.

Steeghs K, Oerlemans F, De Haan A, Heerschap A, Verdoodt L, De Bie M, Ruitenbeek W, Benders A, Jost C, Van Deursen J, Tullson P, Terjung R, Jap P, Jacob W, Pette D, Wieringa B (1998) Cytoarchitectural and metabolic adaptations in muscles with mitochondrial and cytosolic creatine kinase deficiencies. *Mol Cell Biochem* 184:183-194.

Steeghs K, Oerlemans F, Wieringa B (1995) Mice deficient in ubiquitous mitochondrial creatine kinase are viable and fertile. *Biochim Biophys Acta* 1230:130-138.

Stöckler S, Holzbach U, Hanefeld F, Marquardt I, Helms G, Requart M, Hanicke W, Frahm J (1994) Creatine deficiency in the brain: a new, treatable inborn error of metabolism. *Pediatr Res* 36:409-413.

Stöckler S, Isbrandt D, Hanefeld F, Schmidt B, Von Figura K (1996) Guanidinoacetate methyltransferase deficiency: the first inborn error of creatine metabolism in man. *Am J Hum Genet* 58:914-922.

Streijger F, Jost CR, Oerlemans F, Ellenbroek BA, Cools AR, Wieringa B, Van der Zee CEEM (2004) Mice lacking the UbCKmit isoform of creatine kinase reveal slower spatial learning acquisition, diminished exploration and habituation, and reduced acoustic startle reflex responses. *Mol Cell Biochem* 256-257:305-318

Streijger F, Oerlemans F, Ellenbroek BA, Jost CR, Wieringa B, Van der Zee CEEM (2005) Structural and behavioral consequences of double deficiency for creatine kinases BCK and UbCKmit. *Behav Brain Res* 157:219-234.

Streijger F, In 't Zandt HJA, Renema WK, Oerlemans F, Heerschap A, Kuiper J, Pluk H, Jost C, Van der Zee CEEM, Wieringa B (2007) Developmental and Functional Consequences of Disturbed Energetic Communication in Brain of Creatine Kinase Deficient Mice: Understanding CK's role in fuelling of behavior and learning. Editor: Valdur Saks, Wiley Book Series, in press

Sullivan PG, Geiger JD, Mattson MP, Scheff SW (2000). Dietary supplement creatine protects against traumatic brain injury. *Ann Neurol* 48:723-729.

Tachikawa M, Fukaya M, Terasaki T, Ohtsuki S, Watanabe M (2004) Distinct cellular expressions of creatine synthetic enzyme GAMT and creatine kinases uCK-Mi and CK-B suggest a novel neuron-glia relationship for brain energy homeostasis. *Eur J Neurosci* 20:144-160.

Torrealea FJ, D'Anjou A, Graña M (2006) Energy aspects of the synchronization of model neurons. *Phys rev* 74:1-6.

Van der Knaap MS, Verhoeven NM, Maaswinkel-Mooij P, Pouwels PJ, Onkenhout W, Peeters EA, Stockler-Ipsiroglu S, Jakobs C (2000) Mental retardation and behavioral problems as presenting signs of a creatine synthesis defect. *Ann Neurol*, 47:540-543.

Van Deursen J, Heerschap A, Oerlemans F, Ruitenbeek W, Jap P, Ter Laak H, Wieringa B (1993) Skeletal muscles of mice deficient in muscle creatine kinase lack burst activity. *Cell* 74:621-631.

Van Deursen J, Jap P, Heerschap A, Ter Laak H, Ruitenbeek W, Wieringa B (1994) Effects of the creatine analogue beta-guanidinopropionic acid on skeletal muscles of mice deficient in muscle creatine kinase. *Biochim Biophys Acta* 1185:327-335.

Van Deursen J, Wieringa B (1994) Approaching the multifaceted nature of energy metabolism: inactivation of the cytosolic creatine kinases via homologous recombination in mouse embryonic stem cells. *Mol Cell Biochem* 133-134:263- 274.

Von Figura K, Hanefeld F, Isbrandt D, Stöckler-Ipsiroglu S (2001) The metabolic and molecular basis of inherited disease. Editors: Scriver CR, Beaudet AL, Sly WS, Valle D, McGraw Hill, New York, pp1897-1908.

Wallimann T, Wyss M, Brdiczka D, Nicolay K, Eppenberger HM (1992) Intracellular compartmentation, structure and function of creatine kinase isoenzymes in tissues with high and fluctuating energy demands: the phosphocreatine circuit for cellular energy homeostasis. *Biochem*

J 281:21-40.

Walker JB (1979) Creatine: biosynthesis, regulation, and function. *Adv Enzymol Relat Areas Mol Biol* 50:177-242.

Wilken B, Ramirez JM, Probst I, Richter DW, Hanefeld F (2000) Anoxic ATP depletion in neonatal mice brainstem is prevented by creatine supplementation. *Arch Dis Child Fetal Neonatal Ed* 82:F224–F227.

Wyss M, Wallimann (1994) Creatine metabolism and the consequences of creatine depletion in muscle. *Mol Cell Biochem* 133-134:51-66.

Wyss M, Kaddurah-Daouk R (2000) Creatine and creatinine metabolism. *Physiol Rev* 80:1107-1213.

Chapter 2

Mice lacking the UbCKmit isoform of creatine kinase reveal slower spatial learning acquisition, diminished exploration and habituation, and reduced acoustic startle reflex responses.

Femke Streijger¹, Carolina R. Jost¹, Frank Oerlemans¹, Bart A. Ellenbroek², Alexander R. Cools², Bé Wieringa¹ and Catharina E.E.M. Van der Zee¹.

¹ Department of Cell Biology, NCMLS, Radboud University Nijmegen Medical Centre, Nijmegen, The Netherlands.

² Department of Psychoneuro-pharmacology, Radboud University Nijmegen Medical Centre, Nijmegen, The Netherlands.



Abstract

Brain-type creatine kinases BCK (cytosolic) and UbCKmit (mitochondrial) are considered important for the maintenance and distribution of cellular energy in the central nervous system. Previously, we have demonstrated an abnormal behavioral phenotype in mice lacking the BCK creatine kinase isoform, regarding exploration, habituation, seizure susceptibility and spatial learning. The phenotype in these mice was associated with histological adaptations in the hippocampal mossy fiber field size.

Here, mice lacking the ubiquitous mitochondrial creatine kinase isoform (UbCKmit^{-/-} mice) showed, when subjected to a similar battery of behavioral tasks, diminished open field habituation and slower spatial learning acquisition in the Morris water maze task, but normal sensory or motor functions. Furthermore, a reduced acoustic startle response was observed in UbCKmit^{-/-} mice, suggesting that the unconditioned reflexive responsiveness is not optimal. Our findings suggest a role for mitochondrial CK-mediated high-energy phosphoryl transfer in synaptic signaling in the acoustic signal response network and hippocampal-dependent learning circuitry of brain. Finally, we demonstrate that UbCKmit has a widespread occurrence in the cell soma of neuronal nuclei along the rostro-caudal axis of the brain, i.e., cortex, midbrain, hindbrain, cerebellum and brainstem, similar to the occurrence of BCK. This may explain the similarity of phenotypes in mice lacking BCK or UbCKmit. We predict that the remaining functional intactness of the cytosolic BCK reaction and perhaps the compensatory role of other phosphoryl transfer systems are sufficient to sustain the energy requirements for basic sensory, motor and physiological activities in UbCKmit^{-/-} mice.

1. Introduction

Of the four genes for different creatine kinase (CK) subunits, two are mainly expressed in brain, i.e. the cytosolic brain-type creatine kinase (BCK) and the ubiquitous mitochondrial creatine kinase (UbCKmit) genes (Walliman et al., 1992; Jost et al., 2002). Here, these members of the family of creatine kinase genes specify the dimeric cytosolic BCK and the di- or octameric mitochondrial UbCKmit proteins, which are supposed to play an important role in the maintenance of energy

homeostasis and the distribution of high-energy phosphoryl groups between different subcellular locales in brain cells (Walliman et al., 1992; Wyss and Kaddurah-Daouk, 2000).

Functional energy maintenance of the brain, where ATP can be formed by mitochondrial oxidative phosphorylation and (an)aerobic glycolysis and is consumed in electrogenic activity of Ca^{2+} , Na^+/K^+ ATPases, glutamine-glutamate neurotransmitter cycling, and molecular synthesis and transport of cell constituents (Barinaga, 1997), is still an ill understood and much debated aspect of metabolism. Especially the role of astrocytes and neurons, the coupling of carbohydrate (mainly glucose) utilization to O_2 consumption, and the sharing of fuel for local energy production between these two cell types is a focus of intense research and discussion (Tsacopoulos and Magistretti, 1996; Deitmer, 2000; Chih et al., 2001; Dienel and Hertz, 2001). At the global level, it has been demonstrated by ^{31}P magnetic resonance spectroscopy that there is a strong correlation between physiological activity and CK-mediated exchange of high-energy phosphoryls between γ -ATP and phosphocreatine (PCr) in brain (Sauter and Rudin, 1993). This suggests that - as in many other tissues with high and fluctuating energy demand - the phosphorus flux ($\sim\text{P}$) through the CK reaction contributes to the maintenance of local ATP/ADP ratios (Walliman et al., 1992; Wyss and Kaddurah-Daouk, 2000; Bessman and Carpenter, 1985; O'Gorman et al., 1996; Schlattner, 1997).

Creatine kinases in brain might not only serve directly in energy homeostasis, however, they can also exert a broad protective role, as shown by creatine (or creatine analogue) feeding in animal models for seizures, hypoxia, or neurodegenerative disorders (Tsuji et al., 1995; Holtzman et al., 1998) like Huntington's disease, Parkinson's disease, and amyotrophic lateral sclerosis (Matthews et al., 1998; Matthews et al., 1999; Ferrante et al., 2000; Klivenyi et al., 2000). Also the beneficial effects of creatine feeding in children with inborn errors in creatine synthesis (Van Deursen et al., 1993) point into this direction.

Deficiency in the CK system of muscle tissue introduced by genetic ablation of MCK, or both MCK and ScCKmit leads to extensive metabolic remodeling, as has been reported previously (Van Deursen et al., 1993; Steeghs et al., 1997; In 't Zandt et al., 2000b; De Groof et al., 2001; De Groof et al., 2002). In addition, a recently published study from our group regarding cytosolic BCK gene ablation demonstrated that also brain can metabolically compensate loss of CK activity. Ini-

tially, no gross abnormalities in brain anatomy or home cage behavior were seen in BCK^{-/-} mutants. However, upon more detailed histological analysis and a battery of tests of behavioral challenges, mice deficient for BCK revealed diminished habituation and spatial learning acquisition (Jost et al., 2002). Since these animals also demonstrated a prolonged pre-seizure jerks period and a much later onset of the chemically-induced seizures, a slower rate or profile of synaptic transmission was suggested. BCK deficient mice also contained a larger intra-infra-pyramidal mossy fiber field size (Jost et al., 2002). These findings suggested that physiological and morphological adaptation occurred in the metabolic and structural network in the brain of these animals, presumably to provide improved physiological sustenance.

Mice deficient for the UbCKmit gene had been generated in our lab (Steeghs et al., 1995) and also appeared to be viable and fertile, again showing no obvious abnormalities in general (home cage) behavior (Steeghs et al., 1995). Here, in analogy to our BCK studies, we decided to portray them in more detail upon behavioral challenge and comparison to wildtype animals. We focused in this study on open field exploration and habituation, and water maze spatial learning acquisition, thereby controlling for motor and visual functions. Furthermore, the ability to quickly respond (assuming that fast energy is needed) in a sensory hearing and motor reflex was tested in the acoustic startle reflex test. We discuss our results in the context of new data on the cell-type distribution of UbCKmit and speculation about its putative metabolic role in the brain.

2. Material and methods

All procedures involving animals were approved by the Animal Care Committee of the University of Nijmegen and conformed to the Dutch Council for Animal Care and the NIH guidelines. All efforts were made to reduce the number of animals used.

2.1 Generation and genotyping of UbCKmit deficient (UbCKmit^{-/-}) mice

Procedures involved in the construction of the targeting vector, the generation of UbCKmit^{-/-} mice, and the genotype analysis by PCR, have been described in detail elsewhere (Steeghs et al., 1995; Jost et

al., 2002).

2.2 Creatine kinase isoenzyme activity assay

Extracts for analysis of creatine kinase isoenzyme activities were prepared by homogenizing freshly excised brain in a 1:5 dilution (w/v) of buffer containing 50 U/ml heparin, 250 mM sucrose, 2 mM EDTA, 10 mM Tris-HCl, and complete protease inhibitor complex (Boehringer Mannheim, Germany) at pH 7.4 and 4°C. Zymogram analysis was performed as described previously (Steeghs et al., 1997) and developed using the colorimetric detection kit from Sigma diagnostics (procedure number 715-EP).

2.3 Body weights

The body weights of male and female wildtype and UbCKmit^{-/-} mice were determined at 3 months of age.

2.4 Histochemistry and immunocytochemistry

Adult mice (3-5 months old, n=4 per genotype group) were anaesthetized and perfused transcardially with 15 ml of 0.1 M phosphate-buffered saline followed by 30 ml freshly prepared 4% paraformaldehyde in 0.1 M phosphate buffer (pH 7.4). Brains were removed, post-fixed overnight in the same fixative, prepared for paraffin-embedding, and subsequently cut on the cryostat and mounted on Superfrost Plus microscope slides (Menzel Gläser, Braunschweig, Germany). For histochemical analyses, haematoxylin and eosin staining was applied to determine the overall structure of the brain along its rostrocaudal axis in every 50th dewaxed-paraffin (5 µm) section. For immunocytochemical analyses, dewaxed-paraffin (5 µm) sections were taken to 70% ethanol. Endogenous peroxidase activity was quenched by 30-min incubation in 0.375% H₂O₂ in methanol, and nonspecific binding sites were blocked by incubation in 1% bovine serum albumin fraction V (Sigma, St Louis, MO, USA) and 2% normal donkey serum in phosphate-buffered saline. Sections were incubated overnight at 4°C with primary rabbit anti-UbCKmit antibody #253 (1:4000 to 1:10000; Friedman and Perryman, 1991), and the next day washed and incubated for 45 min at room temperature with the secondary antibody Biotin spp.-conju-

gated donkey antirabbit (Jackson-ImmunoResearch, Westgrove, PA, USA). Staining procedures were completed using the avidin-biotin-horseradish peroxidase system in the Vectastain ABC kit (Vector laboratories, Burlingame, CA, USA), and peroxidase activity was revealed by 0.03% H₂O₂ and 2.5 mM diaminobenzidine tetrachloride (DAB). Sections were counterstained in haematoxylin, dehydrated, cleared in xylene, and coverslipped with Eukitt (Kindler AG, Germany).

2.5 Behavioral analysis

2.5.1 Animals

Adult male wildtype and UbCKmit^{-/-} mice (3-5 months old, 25-33 g) were used for the behavioral phenotyping. The mice were housed in the central animal facility with the temperature controlled at 21°C, and an artificial 12:12 h light:dark cycle (lights on at 07.00 am). Fourteen days before starting the behavioral test battery, all mice were individually housed in Macrolon type II cages, with food and water available ad libitum. Two cohorts of mice performed the open field, the rotarod and the Morris water maze acquisition, probe and visible platform task, with 2 wk intervals between the different tests. To avoid interference with behavioral outcome due to training history (McIlwain et al., 2001) two additional groups of mice were used for the acoustic startle reflex paradigm.

2.5.2 Open field

To analyze explorative behavior mice were placed individually in a square open field (40x40x30 cm) with white plexiglass walls, and videotaped for 30 min. Behavioral records were analyzed later in three blocks of 10 min for the duration (in sec) of walking, wall leaning, rearing, sitting, rearing, and grooming. These open field parameters were defined as follows: walking, movement of its hind paws and forepaws with a minimal distance of 1 cm, wall leaning, standing on its hind legs, the mouse places one or two forepaws against the wall, rearing, the mouse stands upright on the hind legs, while the forepaws are not touching any surface, sitting, no movements of the hind paws and forepaws for a duration of 2 sec, and grooming, washing (parts of) its body. In addition, the total number of faeces droppings during the 30

min was recorded as well.

By applying a computer-assisted walking pattern analysis (provided by Ir. D. Heeren, University of Nijmegen, The Netherlands) the video-taped sessions were further used to calculate the total walking distance during the 30 min observation, to determine the walking pattern, and the potential formation of a “home-base”. A “home-base” is here defined as a 10x10 cm area (usually one of the corners of the field) where the mouse spends > 20% of its time. Formation of such a “home-base” is an indication of habituation (Sakic et al., 1994; Tchernichovski and Golani, 1995).

2.5.3 Rotarod

To control for motor functions such as balance and motor co-ordination, mice were individually placed on a rotarod. During a 400 sec time interval the acceleration of the rod resulted in a gradual increase from 0 to 38 rpm. The time (in sec) each mouse was able to stay, by keeping walking, on the rod was measured. Mice were subjected to one pre-trial (data not used), and three test trials with a maximum of 400 sec and a 30 min inter-trial rest interval.

2.5.4 Morris Water Maze

To investigate spatial learning abilities, mice were placed in a black pool (120 cm diameter) filled with water (21-22°C; made opaque by the addition of milk powder), at different starting positions and were supposed to find the submerged platform by using distant visual cues in the room. The spatial cues were present on the four walls in the test room at a distance of ~0.5 m. To facilitate videocamera tracing of the mouse, a strip of white tape (width 10 cm) was taped along the top/inside perimeter of the pool to prevent dark reflection. The 8 cm-diameter round platform was submerged 1 cm below the water surface and placed in the middle of the NW quadrant. During the acquisition, probe, and visual test, the latency (in sec) to find the platform was determined, as well as total distance (m), and average swim speed (cm/s).

Acquisition test. Adult male wildtype and UbCKmit^{-/-} mice performed six acquisition trials (maximal swimming time 120 sec; 30 sec on the platform; inter-trial interval 30 min) per day during three consecutive

days. Starting positions were: E, W, N, S, W, S.

Probe test. A single probe trial was performed, at 30 min following the last trial on day 3, in which the platform was removed from the swimming pool. Mice were allowed to swim for 120 sec and the time spent swimming and searching in the NW quadrant (where the platform had been located) was recorded.

Visible platform test. One week later, the visual test (4 trials) with the platform visibly located above the water level (and at a different location each trial), was performed to account for visual and/or motor impairments in the swimming pool.

2.5.5 Acoustic startle reflex

Startle reactivity was measured using a startle response system (SR-LAB, San Diego Instruments, San Diego, CA, USA). The startle chamber consisted of a non-restrictive Plexiglas cylinder (4 cm diameter), resting on a Plexiglas platform inside the ventilated and sound attenuated chamber. A high-frequency loudspeaker inside the chamber produced both a continuous background noise of 70 dB and the various acoustic stimuli. Vibrations of the platform, produced by the whole-body startle response of the mouse, were detected and transduced by a piezoelectric accelerometer mounted underneath the platform, connected to an automated system. Each mouse was placed inside the cylinder for 5 min. with a background noise of 70 dB to habituate before the first startle stimuli were given.

Prepulse inhibition and habituation. The first block (f) of the testing session consisted of 5 separate 120 dB startle pulse trials. The middle portion of the session (m) consisted of 4 blocks with each block containing: (1) two startle pulse alone trials (120 dB burst), (2) four prepulse trials, in which 72, 74, 78, or 86 dB stimuli preceded the 120 dB burst, and (3) a no stimulus trial (only the 70 dB background noise). These 7 trials were presented in a pseudo-random order. The last part of the testing session (l) consisted again of a block with 5 separate 120 dB startle pulse trials.

Threshold. The hearing threshold trial consisted of five blocks of 10 different sound levels -no stimulus (70 dB), 90, 95, 100, 105, 110, 120, 130, 140, or 150 dB- presented in a pseudo-random order.

The (pre)pulses consisted of a 20 ms sound burst. The interval between the onset of the prepulse and the onset of the startle pulse was

100 ms. The startle response was measured during a 50 ms period, commencing at the onset of the startle pulse, with an amplitude read-out expressed in arbitrary units.

2.6 Statistics

Animal weights and behavioral data are presented as means \pm SEM, and the statistical analysis involved one-way ANOVA, ANOVA with repeated measures, post hoc t-test, and paired t-test, using the SPSS 9.0 statistical software package. Statistical significance was set at $P < 0.05$.

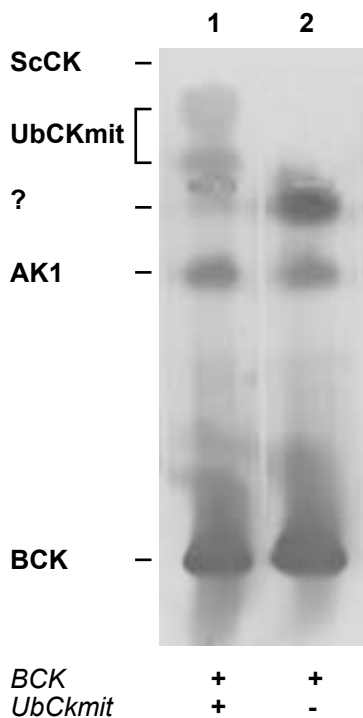


Figure 1: Zymogram activity assay of creatine kinase (CK) isoenzymes in brain homogenates. Lane 1, brain homogenate from a wildtype mouse shows the octameric (upper dash) and dimeric (lower dash) ubiquitous mitochondrial CK isoform (UbCKmit) and the dimeric cytosolic brain-type CK isoform (BCK). Both muscle-type CK isoforms, i.e., cytosolic MCK (not indicated) and mitochondrial sarcomeric ScCK, are absent. Lane 2, brain homogenate from a UbCKmit^{-/-} mouse shows the absence of both octameric and dimeric UbCKmit, but normal activity of dimeric BCK (see also Steeghs et al., 1995; Jost et al., 2002). An unidentified phosphorus transfer enzyme activity, presumably originating from contaminating blood cells, is indicated by a question mark. Both wildtype (lane 1) and UbCKmit^{-/-} (lane 2) mice exhibit also normal levels of adenylate kinase 1 (AK1).

3. Results

3.1 Phenotyping of UbCKmit^{-/-} mice

Homozygous UbCKmit^{-/-} mice with a NeoR cassette replacing the exon 7-8 area of both UbCKmit gene copies were generated by targeted mutagenesis in ES cells as reported (Steeghs et al., 1995). Breeding colonies of UbCKmit^{-/-} mice and wildtype controls with a mixed C57Bl/6 x 129/Sv inbred background were maintained as separate cohorts for over several years. Creatine kinase isoenzyme characterization using zymogram assays demonstrated presence of octameric and dimeric UbCKmit protein and dimeric cytosolic brain-type creatine kinase (BCK), but complete absence of sarcomeric muscle-type creatine kinase isoforms (ScCK) in the wildtype brain (Fig. 1, lane 1). Comparison of the enzyme profiles of UbCKmit^{-/-} mice (Fig. 1, lane 2) and wildtype animals (Fig. 1, lane 1) confirmed that UbCKmit^{-/-} mice completely lacked UbCKmit activity, but exhibited normal levels of BCK and also adenylate kinase 1 (AK1) (Fig. 1, lane 1, 2).

Using monitoring during a period of several years, newborn UbCKmit^{-/-} mice in our colony always showed a normal development compared with wildtype animals, when kept under standard housing conditions (see also Steeghs et al., 1995). They gained weight at the same rate as the wildtypes, were fertile and showed a normal life expectancy of about 2 years. Adult 3 months old female UbCKmit^{-/-} and wildtype mice demonstrated a similar average body weight (Fig. 2). Likewise, 3 months old male UbCKmit^{-/-} animals were not different from age-matched wildtype males either (Fig. 2).

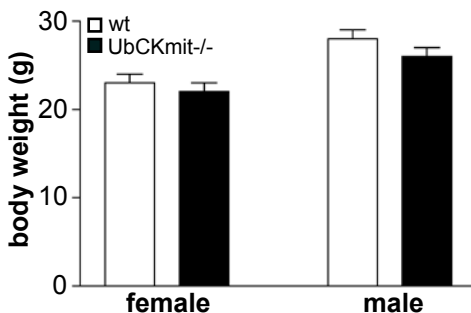


Figure 2: Body weights. Adult (3 months old) female wildtype (wt) and UbCKmit^{-/-} mice show a similar average body weight. Male UbCKmit^{-/-} mice of 3 months of age are not different from age-matched male wildtypes (wt) either.

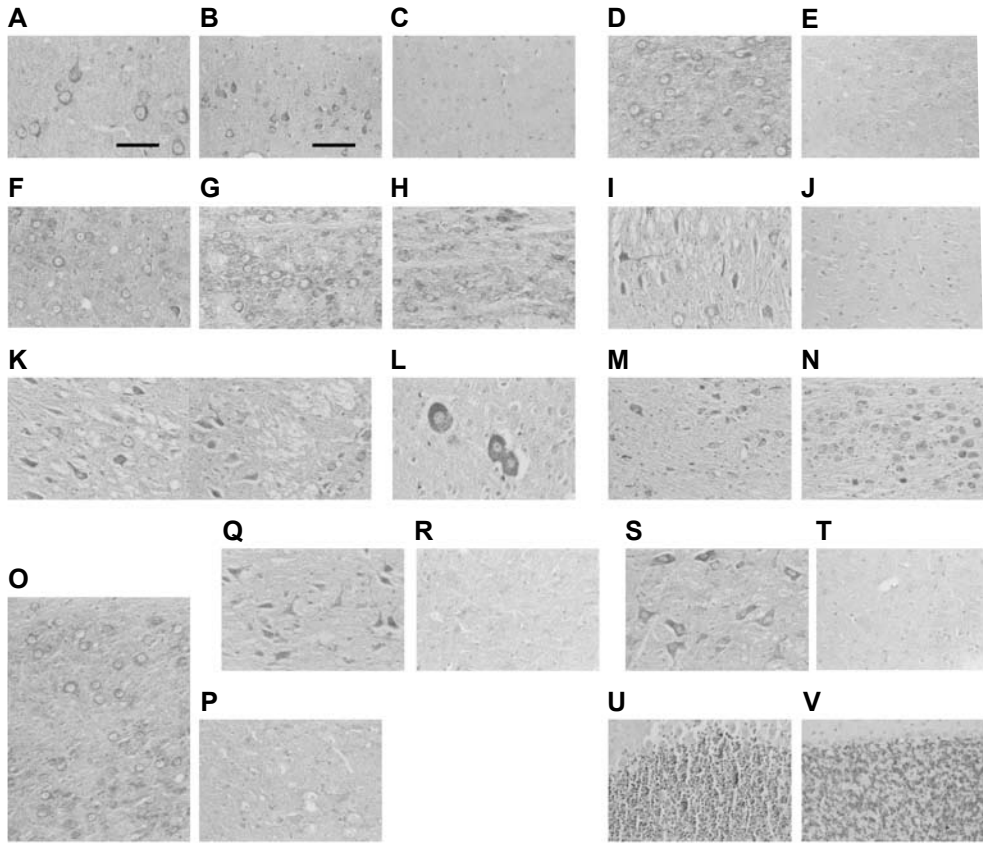


Figure 3: Immunolocalization of ubiquitous mitochondrial creatine kinase (*UbCKmit*) in the brain. Immunolabelled coronal paraffin sections (5 mm) of wildtype brain (counterstained with haematoxylin and eosin) show localization of *UbCKmit* in various regions and neuronal nuclei along the rostrocaudal axis of the brain. (A, B) Cerebral cortex layer V pyramidal neurons, (C) corresponding section from *UbCKmit*^{-/-} mouse served as control and lacked *UbCKmit* expression, as expected. (D) Red nucleus magnocellular and (E) corresponding *UbCKmit*^{-/-} control section. (F) Thalamic ventral posteromedial nucleus, (G) reticulo tegmental nucleus pons, and (H) the pontine nuclei. (I, K) Mesencephalic trigeminal nucleus, with (J) corresponding *UbCKmit*^{-/-} section. (L) Large trigeminal nucleus cells located adjacent to the aquaduct. (M) Lateral superior olive and paraolivary nucleus, and (N) the trapezoid body. (O) Lateral cerebellar nucleus, with (P) corresponding *UbCKmit*^{-/-} control section. (Q) Facial nucleus, (S) prepositus hypoglossal nucleus, and (R, T) the respective *UbCKmit*^{-/-} control sections. (U) Glomeruli of the cerebellar granular cell layer, with (V) the corresponding *UbCKmit*^{-/-} control section. Bar in A (for A, L), 50 μ m. Bar in B (for B-K and M-V), 80 μ m.

3.2 Cellular distribution of UbCKmit in brain

The spatial distribution of the UbCKmit isoform in brain tissue of wildtype mice was immunohistochemically assessed using an antiserum raised against a UbCKmit-specific peptide (AASERRRLYPPSA, residues 1-13). Positive staining for UbCKmit antiserum was observed in the soma and neurites of neurons in several regions and nuclei along the rostral-caudal axis of the brain. In the forebrain area of wildtype mice the cortex layer V pyramidal neurons were clearly stained (Fig. 3A (larger magnification) and B), whereas in UbCKmit^{-/-} control sections no immunoreactivity was seen (Fig. 3C). In the midbrain clear immunoreactivity was observed in cells from the red nucleus magnocellular (Fig. 3D, with corresponding UbCKmit^{-/-} control section in E), the thalamic ventral posteromedial nucleus (Fig. 3F), the reticulo tegmental nucleus pons (Fig. 3G), and the pontine nuclei (Fig. 3H). Furthermore, the mesencephalic trigeminal nucleus (containing cell bodies from the 5th cranial nerve) located more laterally (Fig. 3I, K, with corresponding negative control in J), or located adjacent to the aqueduct as quite large cells (Fig. 3L, larger magnification) were clearly positive for UbCKmit antiserum. Immunoreactive cells were also seen in the ventral part of the midbrain in the lateral superior olive/paraolivary nucleus (Fig. 3M) and the trapezoid body (Fig. 3N). The deep cerebellar nuclei were obviously UbCKmit-positive, with the lateral cerebellar nucleus shown in Fig. 3O and the corresponding UbCKmit^{-/-} section in Fig. 3P. Brainstem nuclei that appeared positive for UbCKmit comprised the facial nucleus (containing cell bodies of the 7th cranial nerve; Fig. 3Q and negative control in R), and the prepositus hypoglossal nucleus (with cell bodies of the 12th cranial nerve, Fig. 3S and UbCKmit^{-/-} control section in T). Finally, the glomeruli within the granular cell layer of the cerebellum of wildtype mice were positively immunostained for UbCKmit antiserum (Fig. 3U), whereas in corresponding control sections of the UbCKmit^{-/-} animals immunostaining was absent (Fig. 3V). These observations indicate that UbCKmit is ubiquitously present in the cell soma of various specific neuronal nuclei in different brain regions.

3.3 Behavioral testing

Based on the previously reported behavioral phenotype of mice lacking the cytosolic brain creatine kinase isoform (BCK^{-/-} mice) regard-

ing exploration, habituation, seizure susceptibility and spatial learning (Jost et al., 2002), we investigated the impact of UbCKmit deficiency on behavioral performances. Before starting the different tests, mice were observed in their cage for homecage locomotion, fur appearance, breeding, development and individual body temperature. These general observations did not reveal obvious abnormalities, confirming initial findings (Steeghs et al., 1995). Subsequently, a battery of behavioral tests was used to evaluate explorative behavior, motor and balance performances, spatial learning, and startle response behavior. Specifically, these tests included the open field, rotarod task, Morris water maze spatial learning acquisition test and probe test, the visible platform test, and the acoustic startle reflex, and were applied to adult male wildtype and UbCKmit^{-/-} mice.

3.3.1 UbCKmit^{-/-} mice show less active explorative behavior

Wildtype mice (n=8) were observed for 30 min in the open field, and demonstrated active exploration and locomotion activity, i.e., mainly walking (450 out of 600 sec) and wall leaning and rearing (98/600 sec) with less time sitting and grooming (52/600 sec) in the first 10-min period (Fig. 4). In the second and third 10-min periods wildtype mice revealed significantly less walking ($F(1,7) = 7.66, P < 0.028$) and more grooming ($F(1,7) = 16.05, P < 0.005$) compared to the first period (Fig. 4A; Fig. 4E), indicating habituation to the new environment. UbCKmit^{-/-} mice (n=8) performed during the entire 30 min period a less active explorative behavior, as assessed by less rearing ($F(1, 14) = 5.29, P < 0.037$) and more sitting ($F(1,14) = 4.66, P < 0.049$), compared to the wildtype group (Fig. 4C-D). In contrast, the explorative behavioral parameters walking and wall leaning were not significantly different between both genotype groups (Fig. 4A-B). The total walking distance during the 30 min period was not different either between the wildtype animals (42 ± 4 m) and the UbCKmit^{-/-} mice (35 ± 3 m). The number of faeces droppings per 30 min period was higher in the UbCKmit^{-/-} group (Fig. 4F).

3.3.2 UbCKmit^{-/-} mice show reduced habituation

Habituation is defined by changes in the explorative pattern instigated by information assessed over time by the animals, regarding

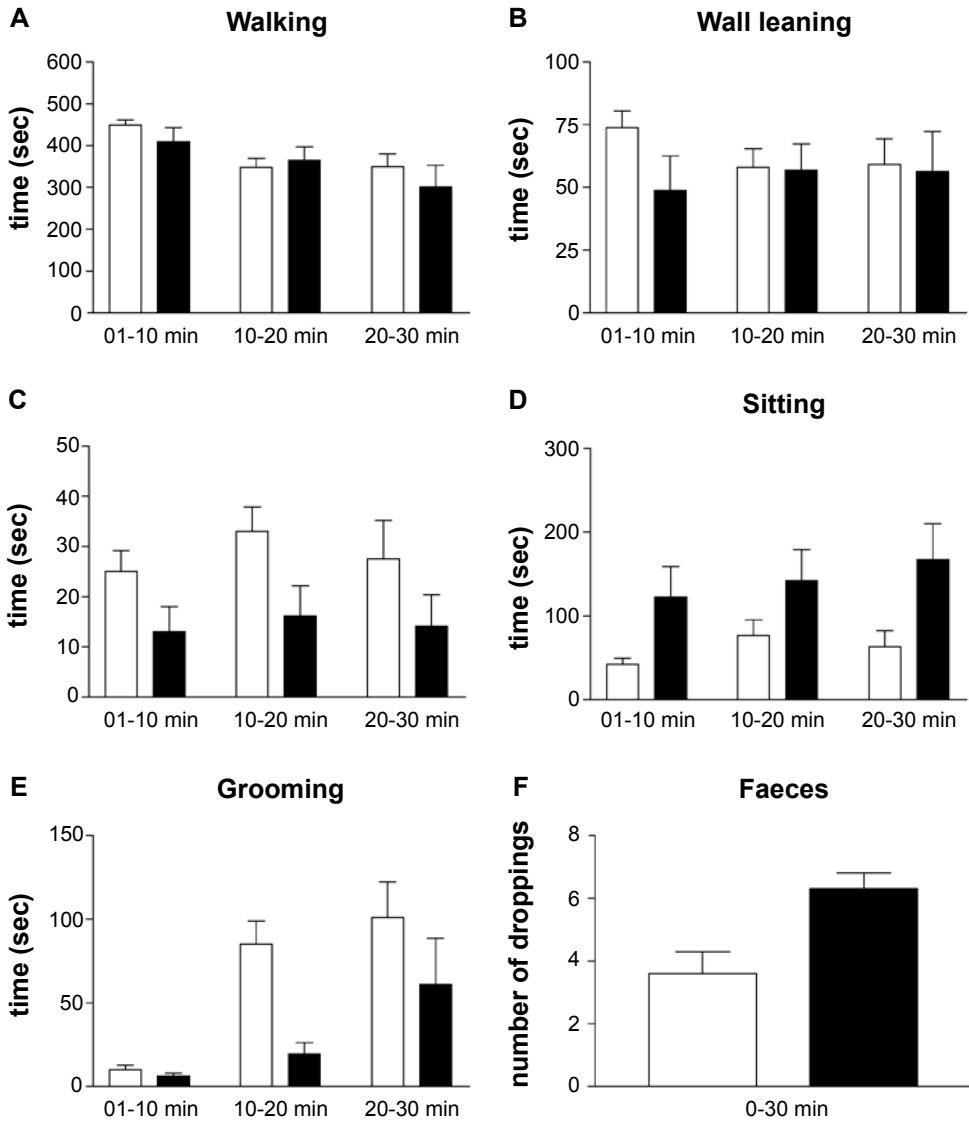


Figure 4: Open field behavior. (A-F) Open field activity parameters, like (A) walking, (B) wall leaning, (C) rearing, (D) sitting, (E) grooming, and (F) faeces droppings, were observed during a 30-min period and scored in three 10 min periods for adult male wildtype (wt, white bars) and UbCKmit^{-/-} mice (grey bars). Wildtype animals display active exploration of the open field environment during the first 10 min, but reduced walking, and more sitting and grooming in the second (10-20 min) and third (20-30 min) periods. This decrease in active exploration behavior over time is referred to as “habituation”. UbCKmit^{-/-} mice, in contrary, show less active explorative behavior demonstrated by less rearing and more sitting, compared to wildtype mice, throughout the 30 min period. In addition, the reduced level of grooming in UbCKmit^{-/-} mice, scored in all three 10 min periods, is indicative for a less distinct habituation. Note the difference in time-scales for five of the six different parameters.

their novel environment. These behavioral changes are reflected by reduced exploration behavior (less walking, wall leaning, and rearing) and increased non-explorative behavior, like grooming. Habituation is clearly seen for the wildtype animals as revealed by less walking over time and more grooming, as mentioned above (Fig. 4A; Fig. 4E). Although UbCKmit^{-/-} mice showed a similar reduction in walking, the total amount of time spent grooming during the 30 min period was significantly lower in UbCKmit^{-/-} mice when compared to that in wildtype mice ($F(1,14) = 7.10$, $p < 0.018$; Fig. 4E). In addition, the walking pattern analysis (not shown) revealed that seven out of eight wildtype mice created a homebase, usually a corner area where the mouse spends $> 20\%$ of its time, and another indication for habituation (Sakic et al., 1994; Tchernichovski and Golani, 1995; Jost et al., 2002). Four out of eight UbCKmit^{-/-} mice did not create a homebase during the 30 min open field task, showing a tendency for less habituation than the wildtypes, although this difference did not reach significance.

3.3.3 UbCKmit^{-/-} mice demonstrate slower spatial learning acquisition

The Morris water maze is used to examine spatial learning, i.e. the ability of the individual mice to orientate in the pool using surrounding distal cues. This type of learning is dependent on the integrity of the hippocampal structure. The spatial learning performance was assessed in the previously mentioned two groups of wildtype ($n=8$) and UbCKmit^{-/-} ($n=8$) mice. First in an acquisition test consisting of 6 trials per day during three days, and secondly in one single probe trial of 2 min duration. Wildtype mice showed a clear learning curve (significant effect of trials, $F(1,7) = 60.02$, $P < 0.0001$; Fig. 5A). They showed an initial high latency for trial block 1 (~90 sec) followed by fast decreasing latencies to find the hidden platform in subsequent trial blocks 2 and 3 of the first day (~55 sec). Latencies in wildtype mice were reduced further during day 2 and 3 to ~15 sec. The UbCKmit^{-/-} mice also learned over time (significant effect of trials, $F(1,7) = 7.13$, $P < 0.032$), but they demonstrated significantly increased latencies to find the platform in the water maze acquisition test, when compared to the wildtype animals ($F(1,14) = 7.36$, $P < 0.017$; Fig. 5A). This difference was still apparent at day 3, when UbCKmit^{-/-} mice needed an average of ~50 sec to reach the platform, compared to only ~15 sec for

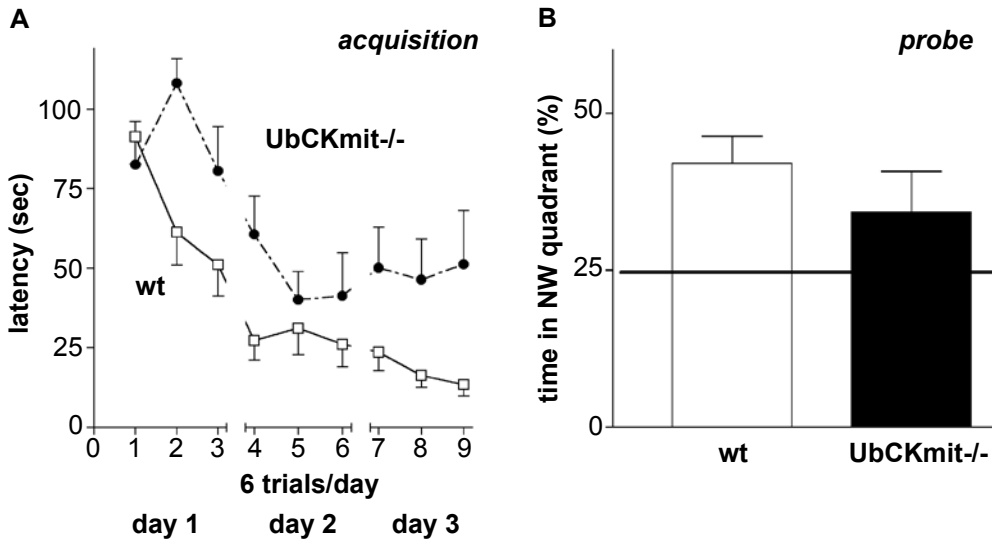


Figure 5: Spatial learning in the Morris water maze. (A) Adult male UbCKmit^{-/-} mice (black circles) show a significantly higher latency to find the submerged platform in the water maze, compared with adult male wildtype mice (wt, white squares), suggesting a slower spatial learning acquisition. Each symbol depicted is the average of two trials; the acquisition test consisted of six trials per day, during three consecutive days. (B) At the end of day 3 the probe test (with the platform now removed from the pool) demonstrated that the wildtype (wt, white bar) and the UbCKmit^{-/-} (black bar) mice all spent significantly more time (i.e., more than the chance level of 25% of the total time) swimming and searching in the northwest (NW, learning) quadrant than in the other pool quadrants, indicating that not only the wildtype animals but -in the end- also the UbCKmit^{-/-} mice had acquired the task.

the wildtype mice. The probe test, with the platform removed from the pool, is a second approach to confirm the spatial learning ability of the animals, and is performed at the end of acquisition test day 3. Compared to the $25 \pm 2\%$ chance to be in the NW quadrant as determined in a group of 8 naive animals (see 25% line in Fig. 5B), wildtype and UbCKmit^{-/-} mice spent significantly more time swimming and searching in this area than in the other pool areas during the probe test (Fig. 5B; one-way ANOVA, $F(2,23) = 3.58$, $P < 0.046$, followed by post hoc t-tests, $P < 0.01$). Analysis of the swimming pattern (not shown) revealed differences in searching strategy, which in turn affected the latency. Within the UbCKmit^{-/-} group several mice showed some floating behavior, especially during the initial trials; one animal of this group

showed severe floating in the probe trial as well, resulting in a lower group average of % time spent in the NW quadrant. Wildtype animals were swimming more directly towards the platform, demonstrating a more effective strategy to find the platform.

Taken together, we conclude that the UbCKmit^{-/-} mice as a group were initially slower in the spatial learning acquisition test, caused by a different searching strategy. However, they did learn over time, and the probe test confirmed that these UbCKmit^{-/-} mice had mastered the task to locate the platform in the pool.

3.3.4 UbCKmit^{-/-} mice have no visual or motor impairments

In order to exclude any possible visual or motoric impairments that might cause the observed differences in spatial learning performance, both mouse groups were tested in a visible platform swimming task and in the rotarod motor coordination and balance test. The average latency (\pm SEM) to swim in the pool to the “visible” platform, now raised 1 cm above water level, was similar for wildtype (12 ± 2 sec) and UbCKmit^{-/-} (14 ± 3 sec) mice. Interestingly, there was no floating occurring in the last 3 (out of 4) trials of the visual test in the latter group. In addition, UbCKmit^{-/-} mice did not differ from wildtype animals in their motor coordination and balance on the rotarod. The average time that they were able to stay on the rotarod was 326 ± 21 versus 338 ± 20 sec, respectively. Taken together, the observed increased latencies in the water maze acquisition test are not likely the outcome of a visual or motor function deficit.

3.3.5 Acoustic startle reflex response is reduced in UbCKmit^{-/-} mice

In order to investigate whether animals with a deficit in their brain energy-metabolism show an impairment in their immediate reaction to sudden stimuli, two additional groups of wildtype and UbCKmit^{-/-} mice were tested in the acoustic startle reflex set-up. Both wildtype and UbCKmit^{-/-} mice demonstrated a background response amplitude of around ~40 arbitrary units during the no stimulus (70 dB) trials (Fig. 6A). This response was defined as the basal activity of individual mice. The wildtype mice (n=9) showed maximal startle amplitudes of around ~400 arbitrary units as response to the 120 dB startle pulses (Fig. 6A). The maximal startle amplitude values in the three consecutive trial

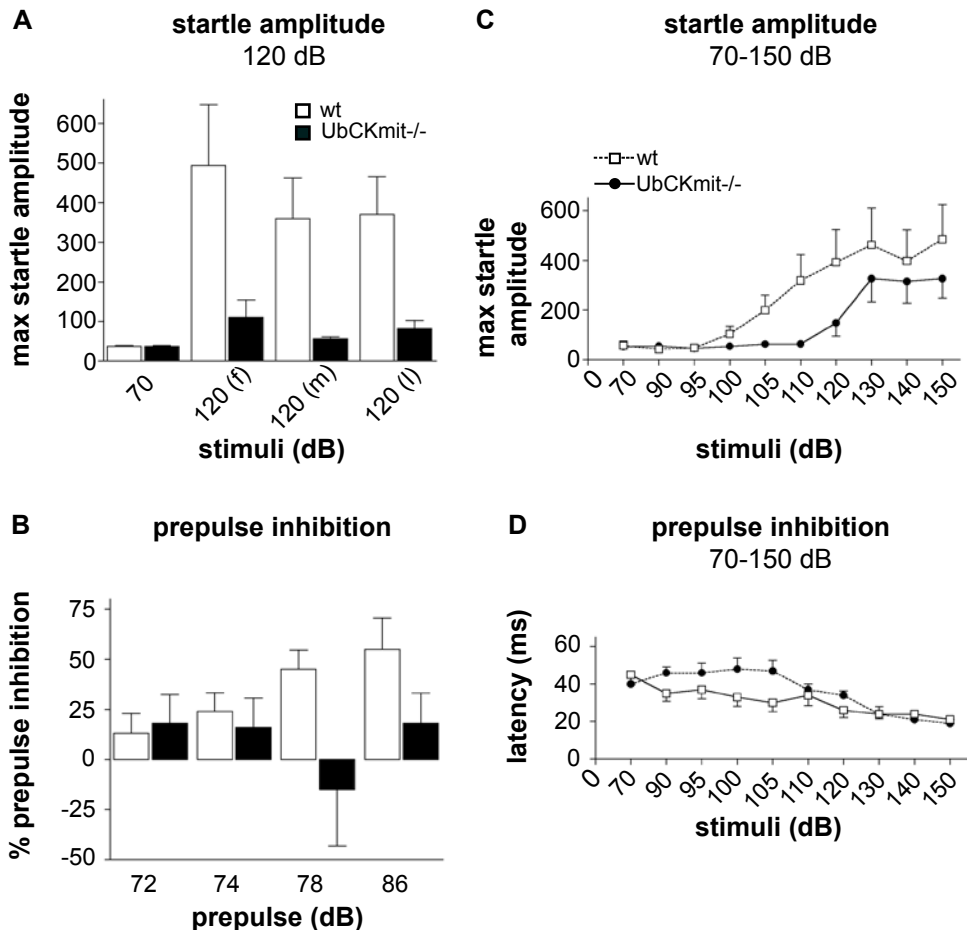
blocks (f, m, l) did not show a significant decrease over time (ANOVA repeated measures, within trial effect; $F(1,8) = 1.77$, $P > 0.2$; Fig. 6A), indicating that no habituation occurred in the wildtype animals. The UbCKmit^{-/-} mice (n=8) also showed no habituation to the 120 dB startle pulses (within trial effect; $F(1,7) = 0.61$, $P > 0.4$; Fig. 6A). However, the UbCKmit^{-/-} mice demonstrated a significantly reduced startle response (around ~80-100 arbitrary units), compared to the wildtype animals (group by trial interaction; $F(1,15) = 7.1$, $P < 0.02$; Fig. 6A).

3.3.6 UbCKmit^{-/-} mice show no prepulse inhibition

Prepulse inhibition is defined as the suppression of the 120 dB pulse-induced startle response when this stimulus pulse is preceded by a weak prepulse (+2, +4, +8, or +16 dB above background). This prepulse inhibition of the startle response was calculated by applying the following formula: $100 - [100 * (\text{the startle amplitude following a 120 dB pulse preceded by a prepulse} / \text{the startle amplitude following a 120 dB pulse alone})]$, and was expressed as “percentage prepulse inhibi-

Figure 6: *Acoustic startle reflex response.* (A) For both wildtype (wt, white bars) and UbCKmit^{-/-} (grey bars) mice the response amplitude following background noise (70 dB) was around 40 arbitrary units, indicating that their basal activity was similar. A possible habituation of the response to the acoustic startle stimulus of 120 dB was measured by comparing the average maximal startle amplitude following 5-8 separate 120 dB startle pulses in the first (f), middle (m), and last (l) trial blocks. No habituation to the startle pulse is observed in wildtype or UbCKmit^{-/-} mice. Notably, UbCKmit^{-/-} mice show a much lower startle response amplitude than the wildtype animals. (B) Prepulse inhibition of the startle response was recorded by offering 4 blocks of trials with each block containing four prepulse trials, in which a 72, 74, 78, or 86 dB stimulus preceded the 120 dB startle pulse, and is expressed as percentage inhibition of the pulse response. Wildtype (white bars) mice show a clearcut prepulse inhibition of the startle response (up to 55%) following a prepulse of +16 dB above background. In contrast, UbCKmit^{-/-} (grey bars) mice did not demonstrate prepulse inhibition of their (lower) startle response. (C) Startle response threshold. The startle response to acoustic stimuli of increasing intensity (ranging from 70 - 150 dB) resulted in increasingly higher response amplitudes up to 100-130 dB, after which it was leveling off, in wildtype mice (wt, white squares). UbCKmit^{-/-} mice (black circles) demonstrated an increasing amplitude response upon increasing sound levels as well, but the rise became only apparent after receiving higher stimuli levels (120-130 dB). This indicated a higher threshold for UbCKmit^{-/-} mice, compared to wildtypes. (D) The startle latency, the time (in ms) after which the maximal startle amplitude is recorded, is measured for a range of stimuli (70 - 150 dB) in wildtype (white squares) and UbCKmit^{-/-} (black circles) mice.

tion". The wildtype mice revealed a clearcut prepulse inhibition, which increased with increasing prepulse intensities (within trial effect; $F(1,8) = 9.1$, $P < 0.02$; Fig. 6B). The strongest prepulse inhibition ($55 \pm 16\%$) was shown following the +16 dB above background prepulse (Fig. 6B). UbCKmit^{-/-} mice, on the other hand, did not show a significant prepulse inhibition (within trial effect; $F(1,7) = 0.89$, $P > 0.4$; Fig. 6B). In addition, when both genotype groups were compared, and taking all prepulse trials into account, the prepulse inhibition in the wildtype animals was significantly higher than in the UbCKmit^{-/-} mice (group by trial; $F(1,15) = 6.43$, $P < 0.023$; Fig. 6B).



3.3.7 UbCkmit^{-/-} mice show higher threshold of startle response

In order to investigate whether the differences in startle response between wildtype and UbCKmit^{-/-} mice may be due to a hearing deficit, we evaluated the startle responses to startle stimuli of increasing intensity (within the range of 70-150 dB). The wildtype mice showed increasing startle amplitudes following increasing sound levels (within trial effect; $F(1,8) = 8.50$, $P < 0.02$; Fig. 6C). Relatively low amplitudes were observed with 70, 90, and 95 dB stimulus levels. This was followed by a rapid 4.5-fold increase in the startle response amplitude following pulse levels ranging from 100-130 dB (Fig. 6C). Higher pulse levels (i.e., 140 or 150 dB) did not further augment the maximal startle amplitude (Fig. 6C). In addition, the startle amplitude threshold curve shown for our wildtype animals (Fig. 6C) is very similar to the startle response threshold values observed in a group of C57Bl/6 mice ($n=10$, not shown). Like for our wildtype group, the UbCKmit^{-/-} mice also demonstrated an increasing amplitude response upon increasing sound levels (within subjects-contrasts; $F(1,15) = 0.83$, $P > 0.4$; Fig. 6C). Their response amplitudes only started to rise after receiving 120-130 dB stimuli levels, indicating a higher threshold in UbCKmit^{-/-} mice (130 dB and higher, ~300 arbitrary units), compared to wildtype animals (110 dB, ~300 arbitrary units, 120 dB, ~400 arbitrary units; Fig. 6C).

The startle latency, the time (in ms) after which the maximal startle amplitude is recorded, was determined for both genotype groups (Fig. 6D). Wildtype, as well as UbCKmit^{-/-}, animals demonstrated a decrease in startle latency upon increasing stimuli ranging from 70-150 dB (Fig. 6D). Although in UbCKmit^{-/-} mice significantly higher latencies were seen following stimuli in the range of 90-105 dB ($F(1,15) = 11.31$, $P < 0.004$), the latency following the 120 dB startle pulse was not different from that in wildtypes (Fig. 6D).

4. Discussion

We have now addressed the significance of the ubiquitous mitochondrial creatine kinase (UbCKmit), in addition to the previously published findings by Jost and colleagues (Jost et al., 2002) regarding the role of the cytosolic brain-type creatine kinase (BCK) in brain energy homeostasis. We present here evidence that (i) UbCKmit is present in the

cell soma of specific nuclei in many different brain regions, and that UbCKmit deficiency results in (ii) reduced open-field exploration and habituation, (iii) slower spatial learning acquisition, and (iv) diminished acoustic startle response and lack of prepulse inhibition.

It is of note that specific immunostaining for UbCKmit has not only been shown in brain, but also occurs in kidney, heart, smooth muscle containing organs like uterus, placenta and vessel walls, as well as in photoreceptor cells of the retina and in spermatozoa (Walliman et al., 1992; Steeghs et al., 1995). Here we only concentrated on its distribution in brain, showing that the expression pattern of UbCKmit appeared fairly similar to that for BCK. Clear positive cytosolic BCK staining was present in the soma of neurons throughout the brain, in the neurons of the deeper cortical layers, and in the hippocampus, mid-brain nuclei, and deep cerebellar nuclei, Purkinje cells, and glomeruli of the cerebellar granular layer (Jost et al., 2002). Mitochondrial immunostaining for UbCKmit reported here was in the soma of cortical (layer V pyramidal) neurons, in midbrain red nucleus, thalamic nuclei, and olivary nucleus and trapezoid body cells. Furthermore, pontine nuclei, tegmental cells and cell bodies of the trigeminal, facial, hypoglossal cranial nerves, as well as the glomeruli of the cerebellar granular layer and the deep cerebellar nuclei were found to be UbCKmit positive.

Although we still lack semiquantative data on the cell-type and subcellular distribution of both isoenzymes, our data support a picture in which BCK and UbCKmit are co-expressed in the same neuronal nuclei, in various regions of the brain (see also Jost et al., 2002). Preliminary findings from quantitative ^1H and ^{31}P MR-spectroscopy of BCK and UbCKmit deficient brains corroborate this interpretation (In 't Zandt, 2000a). In this latter study it was demonstrated that PCr, ATP, Pi and Cr levels as well as pH were still absolutely normal in single mutants, suggesting that the remaining cytosolic BCK reaction could compensate for loss of UbCKmit activity, and vice versa. Double knockout mice lacking both BCK and UbCKmit differed in that they lacked all PCr and had significant lower total creatine levels, but the ATP concentration was still intact (unpublished findings, In 't Zandt HJA, Wieringa B, Heerschap A). These results are somewhat reminiscent to findings in muscle (Van Deursen et al., 1993; Steeghs et al., 1997) and demonstrate that it is important to have at least one end of the cytosolic-mitochondrial Cr-PCr shuttle intact. It now becomes urgent to measure high-energy phosphorus fluxes through the remain-

ing BCK end point in brains of our UbCKmit deficient mice. In our ^{31}P magnetic resonance spectroscopy study of BCK deficient animals we noticed a strongly reduced metabolic phosphorus flux rate (Jost et al., 2002), indicating that channeling of the CK reaction through mitochondria is a compartmentalized process, with restricted access. Loss of UbCKmit activity, representing approximately 25-30% of total CK activity in brain, may have similar effects, but it is also conceivable that the BCK reaction can more easily compensate for loss of UbCKmit, due to its more widespread distribution through the cytosolic compartment, and simply because it represents a larger fraction of total CK activity in brain (70-75%). Experimental approaches that could distinguish between these possibilities require acquisition of magnetic resonance spectra with high time resolution and have not been conducted until now.

Whatever the situation, our zymogram results of brain homogenates of wildtype and UbCKmit $^{-/-}$ mice showed that the absence of UbCKmit did not induce any increase in the level of dimeric BCK activity, neither did it affect the level of another phosphotransfer enzyme, adenylate kinase 1 (AK1). Currently, we are performing mRNA profiling studies on cDNA arrays and semi-quantitative proteomics studies (like those performed for muscle CK deficient mice; De Groof et al., 2001; De Groof, 2002a), to see whether any adaptational response may compensate for the loss of UbCKmit.

4.1 Diminished open field habituation and spatial learning acquisition

As behavioral phenotyping provides one of the most sensitive tests for brain-metabolic and structural alterations (or adaptations, if any) we subjected our animals to a series of behavioral challenges. When observed in the open field test, UbCKmit $^{-/-}$ mice revealed diminished rearing and increased sitting, indicating less explorative behavior. However, the reduction in total time spent grooming, and the fact that only half of the UbCKmit $^{-/-}$ animals showed the formation of a home base, suggested diminished open field habituation as another explanation. Information assessed in time by a mouse about its novel environment can lead to changes in its explorative pattern, which is called habituation. For instance, behavioral parameters like reduced walking and increased sitting, combined with more grooming often indicate habituation. However, sitting can also be a form of (anxiety-related)

freezing. As we could not distinguish between habituation-related sitting and anxiety-induced sitting it is possible that the sitting behavior in the first 10 min consisted of more freezing behavior, whereas in the third block sitting was more a result of habituation. Also, reduced rearing and increased faeces production in the open field are used as anxiety-related indicators. When an animal displays rearing behavior in a novel environment, the animal is more vulnerable to predation (Crusio and Abeelen, 1987). Furthermore, the reduced amount of grooming and the higher number of boluses observed in UbCKmit^{-/-} mice might also be explained as a form of anxiety, indicating that the UbCKmit^{-/-} mice are less adaptive to a novel environment. This does not mean that the UbCKmit^{-/-} mice will never adapt to the open field situation, but they may simply need more time (we only observed for 30 min). Notably, habituation to a novel environment is considered one of the most elementary forms of learning (Sakic et al., 1994; Gerlai, 2000).

The UbCKmit^{-/-} mice also demonstrated a slower hippocampal-dependent spatial learning acquisition, but did develop spatial memory over time. This was not only evident after comparing latencies in the first trials with those in the last few trials, but also confirmed in the probe trial. Although floating (by some of the UbCKmit^{-/-} mice) did contribute to a certain extent to the increased latency to find the platform, the fact that the visible platform test of four trials was performed with no floating at all, demonstrates also a difference in search-strategy among the two genotype groups. Since no differences were found between wildtype and UbCKmit^{-/-} animals regarding their rotarod performance or during the visible platform trials, we conclude that the observed slower spatial learning acquisition was not due to any form of visual or motor function deficit.

4.2 Acoustic startle reflex and creatine kinase action

One other approach to evaluate the animals' response to situations of fast energy demand in brain is the acoustic startle reflex test, where mice have to react fast and immediately to sudden acoustic stimuli (resulting in a measurable startle response). Wildtype animals showed a clear startle response, which was 10-fold the basal activity amplitude. In contrast, a much reduced startle response of only 2-fold the basal activity was observed in UbCKmit^{-/-} mice. In addition, wildtype mice demonstrated a clearcut prepulse inhibition (up to 55%) of the startle

response, whereas UbCKmit^{-/-} mice did not show prepulse inhibition at all. Coupling between startle responses and prepulse inhibition responses has been reported in numerous studies with humans (Swerdlow et al., 2001), rats (Ellenbroek et al., 1996; Swerdlow et al., 2001) and different inbred strains of mice (Paylor and Crawley, 1997). Since habituation to the 120 dB startle stimulus was not observed in our animals (even not after 18 trials), it is not likely that the lower startle response amplitude measured in UbCKmit^{-/-} mice is due to habituation. The height of the startle response amplitude and the extent of prepulse inhibition can vary among the different mouse strains (Paylor and Crawley, 1997). Therefore, an extra group of C57Bl/6 mice (representing one of the two background strains) was tested, but the startle response was indeed similar to that of the wildtype group. To explain our findings, one might suggest that the absence of prepulse inhibition of the startle response observed in UbCKmit^{-/-} animals is due to the fact that a reduction in response cannot be measured because of the already quite low startle response amplitude. Although we cannot completely exclude this possibility, two other cohorts of genetically-modified mice (lacking BCK or both BCK/UbCKmit) demonstrated similarly low levels of startle response amplitude (~100 arbitrary units), but did show clear prepulse inhibition of their startle response (unpublished observations, Streijger F, Ellenbroek BA, Van der Zee CEEM). Another explanation for the lower startle response observed in UbCKmit^{-/-} mice could be a hearing deficit. To investigate this possibility, mice have been exposed to increasing pulse sound levels and their startle response amplitude levels were measured. A curve of increasing amplitudes following increasing dB stimuli was shown for the wildtypes, and was similar to the curve from C57Bl/6 mice (own observations, Streijger F). UbCKmit^{-/-} mice showed a shift in the startle response curve (amplitude goes up later / at higher dB), which is interpreted as a higher hearing threshold. The possibility is therefore still open that we have to explain the lower startle response and lack of prepulse inhibition by a diminished hearing function. The circuitry mediating the acoustic startle response includes the auditory nerve, the cochlear root neurons, the nucleus reticularis pontis caudalis (PnC), and the spinal motor neuron (Swerdlow et al., 2001). However, many additional brain structures are involved in the regulation of prepulse inhibition (Swerdlow et al., 2001). The “feed-forward” inhibition model is often used to explain the prepulse inhibition (Koch et al., 1993; Swerdlow et al., 2001). After the prepulse

activates the cochlear root and PnC, one of these regions then directly or indirectly activates cells in the pontine tegmentum, in the area of the pedunculo-pontine nucleus. These pedunculo-pontine nucleus cells directly innervate, and apparently inhibit, the PnC such that its response to the startling stimulus is reduced (Koch et al., 1993; Swerdlow et al., 2001). Since the UbCKmit protein is present in the pontine nuclei and tegmental area, it is feasible that the lack of this enzyme in mitochondria affects efficient neurotransmission (as mentioned by Jost and colleagues (2002) in this brain circuit.

It is assumed that brain activity, including action potentials, Na^+ / K^+ ATPase activity and neurotransmission, requires fast and fluctuating energy (i.e. ATP; Barinaga, 1997) largely fed through the Cr/PCr-CK circuitry. Neurons are inextricably bound up with glial cells morphologically, but also functionally. Neuron-glia interactions involve synaptic transmission and strengthening, neurotransmitter cycling, as well as glucose and lactate exchange, although a shared role by neurons and astrocytes in the provision of fuel for energy production is still debated [Tsacopoulos and Magistretti, 1996; Deitmer, 2000; Chic et al., 2001; Dienel and Hertz, 2001; Shulman et al., 2001; Field and Stevens-Graham, 2002). The expression of UbCKmit in the cell soma of neurons (but so far not shown in glia) and BCK in both neuronal and glial cells (Jost et al., 2002) would support a shared exchange of energy.

The reduced habituation and slower spatial learning acquisition now observed in UbCKmit^{-/-} mice have also been reported in our study of BCK^{-/-} mice (Jost et al., 2002). In that study findings were compatible with impairment in synaptic signaling as the most likely explanation. Altered synaptic signaling was also proposed to underlie changes in global chemically-evoked seizure induction in BCK^{-/-} mice (Jost et al., 2002). Now again, our results with the startle response and prepulse inhibition tests suggested that lack of UbCKmit (directly or indirectly) renders the synaptic circuitry in brain less efficient in coping with sensory-induced, activity-related, energy challenges. For our UbCKmit^{-/-} animals, we still have to study whether an altered rate or profile of neurotransmission, and associated morphological changes, as seen for the hippocampal mossy fiber area in BCK^{-/-} brains, may be involved. If so, additional issues have to be explained for both types of brain CK mutants, namely (i) how behavioral tasks require extra activity in terms of increased energetic-demand, (ii) how CK-mediat-

ed mitochondrial and cytosolic energy relay systems are coupled to stimulated synaptic activity and (iii) which are the remaining molecular networks involved in CK mutant brain.

Acknowledgements

This work was supported by NWO Program grants #901-01095 and #901-01191 (to B.W.). We thank dr. K. Steeghs for her contribution to the initial phase of this study, H. Croes for help in paraffin histological analysis and our colleagues in the Central Animal Facility for help and advice with the animal care.

References

Barinaga M (1997) What makes brain neurons run? *Science* 276:196-198.

Bessman SP, Carpenter CL (1985) The creatine-creatine phosphate energy shuttle. *Annu Rev Biochem* 54:831-862.

Chih C-P, Lipton P, Roberts EL Jr (2001) Do active cerebral neurons really use lactate rather than glucose? *Trends Neurosci* 24:573-578.

Crusio WE, van Abeelen JH (1987) Zinc-induced peripheral anosmia and behavioral responses to novelty in mice: a quantitative-genetic analysis. *Behav Neural Biol* 48:63-82.

Gerlai RT (2000) Genotype x environment interaction: an old problem in a new field. *Trends Neurosci* 23:450.

De Groof AJC, Oerlemans F, Jost CR, Wieringa, B (2001) Changes in glycolytic network and mitochondrial design in creatine kinase deficient muscle. *Muscle Nerve* 24:1188-1196.

De Groof AJC (2002) Cellular remodeling in creatine kinase-deficient muscles: adaptive changes and regulatory mechanisms. ISBN 90-9015729-8 Thesis book, University of Nijmegen, The Netherlands: 2002

Deitmer JW (2000) Glial strategy for metabolic shuttling and neuronal function. *BioEssays* 22:747-752

Dienel DA, Hertz L (2001) Glucose and lactate metabolism during brain activation. *J Neurosci Res* 66:824-838.

Ellenbroek BA, Budde S, Cools AR (1996) Prepulse inhibition and latent inhibition: the role of dopamine in the medial prefrontal cortex. *Neuroscience* 75:535-542.

Ferrante RJ, Andreassen OA, Jenkins BG, Dedeoglu A, Kuemmerle S, Kubilus JK, Kaddurah-Daouk R, Hersch SM, Beal MF (2000) Neuro-

protective effects of creatine in a transgenic mouse model of Huntington's disease. *J Neurosci* 20:4389-4397.

Fields RD, Stevens-Graham B (2002) New insights into neuron-glia communication. *Science* 298:556-562.

Friedman DL, Perryman MB (1991) Compartmentation of multiple forms of creatine kinase in the distal nephron of the rat kidney. *J Biol Chem* 266:22404-22410.

Holtzman D, Togliatti A, Khait I, Jensen F (1998) Creatine increases survival and suppresses seizures in the hypoxic immature rat. *Pediatr Res* 44:410-414.

In 't Zandt HJA (2000a) Quantitative ^1H and ^{31}P MR-spectroscopy and -imaging reveal changes in metabolite levels and morphology of creatine kinase (CK) -deficient mouse brain. ISBN 90-64642054: Thesis book Chpt 7, University of Nijmegen, The Netherlands.

In 't Zandt HJA, Klomp DWJ, Oerlemans F, Wieringa B, Hilbers CW, Heerschap A (2000b) Proton MR spectroscopy of wildtype and creatine deficient mouse skeletal muscle: dipole-dipole coupling effects and postmortem changes. *Magn Res Med* 43: 517-524.

Jost CR, Van der Zee CEEM, in 't Zandt HJA, Oerlemans F, Verheij M, Streijger F, Fransen J, Heerschap A, Cools AR, Wieringa B (2002) Creatine kinase B-driven energy transfer in the brain is important for habituation and spatial learning behavior, mossy fiber field size and determination of seizure susceptibility. *Eur J Neurosci* 15:1692-1706.

Klivenyi P, Ferrante RJ, Matthews RT, Bogdanov MB, Klein AM, Andreassen OA, Mueller G, Wermer M, Kaddurah-Daouk R, Beal MF (1999) Neuroprotective effects of creatine in a transgenic animal model of amyotrophic lateral sclerosis. *Nat Med* 5:347-350.

Koch M, Kungel M, Herbert H (1993) Cholinergic neurons in the pedunculopontine tegmental nucleus are involved in the mediation of prepulse inhibition of the acoustic startle response in the rat. *Exp Brain Res* 97:71-82.

Matthews RT, Yang L, Jenkins BG, Ferrante RJ, Rosen BR, Kaddurah-Daouk R, Beal MF (1998) Neuroprotective effects of creatine and cyclocreatine in animal models of Huntington's disease. *J Neurosci* 18:156-163.

Matthews RT, Ferrante RJ, Klivenyi P, Yang L, Klein AM, Mueller G, Kaddurah-Daouk R, Beal MF (1999) Creatine and cyclocreatine attenuate MPTP neurotoxicity. *Exp Neurol* 157:142-149.

McIlwain KL, Merriweather MY, Yuva-Paylor LA, Paylor R (2001) The use of behavioral test batteries: Effects of training history. *Physiol Behav* 73:705-717.

O'Gorman E, Beutner G, Wallimann T, Brdiczka D (1996) Differential effects of creatine depletion on the regulation of enzyme activities and on creatine-stimulated mitochondrial respiration in skeletal muscle, heart, and brain. *Biochim Biophys Acta* 1276:161-170.

Paylor R, Crawley JN (1997) Inbred strain differences in prepulse inhibition of the mouse startle response. *Psychopharmacol* 132:169-180.

Sakic B, Szechtman H, Talangbayan H, Denburg SD, Carbotte RM, Denburg JA (1994) Disturbed emotionality in autoimmune MRL-lpr mice. *Physiol Behav* 56:609-617.

Sauter A, Rudin M (1993) Determination of creatine kinase kinetic parameters in rat brain by NMR magnetization transfer. Correlation with brain function. *J Biol Chem* 268:13166-13171.

Schlattner U (1997) Adenylate kinase isoforms in higher plants. *Recent Res Devel in Phytochem* 1:439-465.

Shulman RG, Hyder F, Rothman DL (2001) Cerebral energetics and the glycogen shunt: neurochemical basis of functional imaging. *Proc Natl Acad Sci USA* 98:6417-6422.

Steeghs K, Oerlemans F, Wieringa B (1995) Mice deficient in ubiquitous mitochondrial creatine kinase are viable and fertile. *Biochim Biophys Acta* 1230:130-138.

Steeghs K, Benders A, Oerlemans F, De Haan A, Heerschap A, Ruitenbeek W, Jost C, Van Deursen J, Perryman B, Pette D, Bruckwilder M, Koudijs J, Jap PH, Veerkamp J, Wieringa B (1997) Altered Ca^{2+} responses in muscles with combined mitochondrial and cytosolic creatine kinase deficiencies. *Cell* 89:93-103.

Stockler S, Isbrandt D, Hanefeld F, Schmidt B, Von Figura K (1996) Guanidinoacetate methyltransferase deficiency: the first inborn error of creatine metabolism in man. *Am J Hum Genet* 58:914-922.

Swerdlow NR, Geyer MA, Braff DL (2001) Neural circuit regulation of prepulse inhibition of startle in the rat: current knowledge and future challenges. *Psychopharmacol* 156:194-215.

Tchernichovski O, Golani I (1995) A phase plane representation of rat exploratory behavior. *J Neurosci Methods* 62:21-27.

Tsacopoulos M, Magistretti PJ (1996) Metabolic coupling between glia and neurons. *J Neurosci* 16:877-885.

Tsuji M, Allred E, Jensen F, Holtzman D (1995) Phosphocreatine and ATP regulation in the hypoxic developing rat brain. *Brain Res Dev Brain Res* 85:192-200.

Van Deursen J, Heerschap A, Oerlemans F, Ruitenbeek W, Jap PH, ter Laak H, Wieringa B (1993) Skeletal muscle of mice deficient in muscle creatine kinase lack burst activity. *Cell* 74:621-631.

Wallimann T, Wyss M, Brdiczka D, Nicolay K, Eppenberger HM (1992) Intracellular compartmentation, structure and function of creatine kinase isoenzymes in tissues with high and fluctuating energy demands: the "phosphocreatine circuit" for cellular energy homeostasis. *Biochem J* 281:21-40.

Wyss M, Kaddurah-Daouk R (2000) Creatine and creatine metabolism. *Physiol Rev* 80:1107-1213.

Chapter 3

Creatine kinase double deficiency in brain results in reduced hippocampus and total brain size with impaired dry and wet maze spatial learning, lower nestbuilding activity, and diminished acoustic startle reflex responses.

Femke Streijger¹, Frank Oerlemans¹, Bart A. Ellenbroek², Carolina R. Jost³, Bé Wieringa¹ and Catharina E.E.M. Van der Zee¹

¹ Department of Cell Biology, NCMLS, Radboud University Nijmegen Medical Centre, Nijmegen, The Netherlands.

² Department of Psychoneuro-pharmacology, Radboud University Nijmegen Medical Centre, Nijmegen, The Netherlands.

³ LUMC, University of Leiden, The Netherlands.

In Behavioral Brain Research 2005
Volume 157:219-234



Abstract

The cytosolic brain-type creatine kinase (BCK) isoform and the mitochondrial ubiquitous creatine kinase (UbCKmit) isoform are both important for the maintenance and distribution of cellular energy in neurons and astrocytes. Previously, we reported that mice deficient for BCK or UbCKmit each showed a surprisingly mild phenotype, probably due to reciprocal functional compensation by the remaining creatine kinase. Mice lacking both creatine kinase isoforms (referred to as CK^{-/-} mice) showed, besides a lower body weight, a more severe behavioral phenotype including impaired spatial learning in both a dry and a wet maze, reduced nestbuilding activity and diminished acoustic startle reflex responses. In contrast, their visual and motor functions, exploration behavior, prepulse inhibition and anxiety-related responses were not changed, suggesting no global deficit in sensorimotor function, hearing or motivation. Morphological analysis of CK^{-/-} brains revealed a reduction of ~7% in wet brain weight and hippocampal size, a ~15% smaller regio inferior and relatively larger suprapyramidal, and intra-infra-pyramidal mossy fiber areas.

These results suggest that lack of both creatine kinase isoforms that are predominantly expressed in brain, possibly affect brain connectivity during postnatal development and renders the synaptic circuitry in adult brain less efficient in coping with sensory or cognitive activity related challenges.

1. Introduction

Due to high and fluctuating energy demands, the maintenance of energy homeostasis in the brain requires tight coupling between energy production and consumption, like during the performance of sensory, motor, emotional and cognitive tasks (Fox et al., 1988; Belliveau et al., 1991; Beal, 1992; Erecinska and Silver, 1994; Ikonomidou and Turski, 1996; Barinaga, 1997; Khakh, 2001). Electrogenic activity of Ca²⁺, Na⁺/K⁺ ATPases, neurotransmitter cycling, molecular synthesis and transport of motility of cell constituents, especially in actin-based processes, all require ATP (Barinaga, 1997; Bernstein and Bamberg, 2003). The creatine kinase (CK) reaction ($\text{MgATP}^{2-} + \text{Cr} \leftrightarrow \text{MgADP}^- + \text{PCr}^{2-} + \text{H}^+$) is important for the maintenance of energy homeostasis, storage, and (fast) distribution of high-energy phosphoryl groups

(Bessman and Carpenter, 1985; O’Gorman et al., 1996; Walliman et al., 1992; Wyss and Kaddurah-Daouk, 2000; In ‘t Zandt et al., 2000; In ‘t Zandt et al., 2004). The cytosolic brain-type creatine kinase (BCK) is present in neurons and glia throughout the brain (Jost et al., 2002). It has been proposed that BCK levels are more predominant in astrocytes and oligodendrocytes than in neurons (Molloy et al., 1992; Shen et al., 2002), but this may differ between glial and neuronal subtypes. The ubiquitous mitochondrial creatine kinase (UbCKmit) is localized in various specific neuronal nuclei along the rostro-caudal axis of the brain (Walliman et al., 1992; Wyss and Kaddurah-Daouk, 2000; Jost et al., 2002; Shen et al., 2002; Boero et al., 2003; Streijger et al., 2004). The cytosolic and mitochondrial end points of the CK circuit may therefore not co-exist in all cell types throughout the brain.

Mice lacking the BCK (BCK^{-/-}; Jost et al., 2002) or the UbCKmit (UbCKmit^{-/-}; Steeghs et al., 1995; Streijger et al., 2004) isoforms were viable and fertile, and showed no gross abnormalities in brain anatomy or home cage behavior. However, a battery of behavioral tests demonstrated for both genotype groups diminished habituation behavior, slower spatial learning and reduced acoustic startle response (Jost et al., 2002; Streijger et al., 2004). Furthermore, BCK^{-/-} mice demonstrated reduced explorative behavior, a prolonged pre-seizure period and a much later onset of the chemically induced full-seizures. Histological analyses revealed that BCK^{-/-} brains contained a larger intra-infra-pyramidal mossy fiber field size (Jost et al., 2002), however no obvious change was observed (F. Streijger, unpublished observations) in UbCKmit^{-/-} brains.

The behavioral changes in both single knockout groups motivated us to evaluate the impact of creatine kinase double deficiency in brain on behavioral performance. In this study several cohorts of CK^{-/-} mice are compared to wildtype cohorts in a behavioral test battery including a wet and dry spatial learning task, the open field and the acoustic startle reflex test. Additionally, histological brain analyses are performed. We present evidence that total CK deficiency in brain severely impairs spatial learning, nestbuilding activity and startle reflex responses. Our brain morphology findings raise the possibility that the behavioral effects do not only have a purely metabolic/physiological basis, but are also due to effects on the development of the cellular-synaptic circuitry involved in sensory-induced activity regulation.

2. Materials and methods

2.1. Generation of the CK^{-/-} mice and genotype analysis

All procedures involving animals were approved by the Animal Care Committee of the University of Nijmegen, the Netherlands and conformed to the Dutch Council for Animal Care and the NIH guidelines.

BCK^{-/-} single knockout mice (Jost et al., 2002) and UbCKmit^{-/-} single knockout mice (Steeghs et al., 1995; Streijger et al., 2004)(both 25% 129/Ola - 75% C57BL/6) were interbred to obtain heterozygous BCK/UbCKmit^{+/-} offspring. Siblings with only one wildtype CK allele (either BCK^{+/-}UbCKmit^{-/-} or BCK^{-/-}UbCKmit^{+/-}) were mated with double knockout (BCK^{-/-}UbCKmit^{-/-}) partners resulting in the generation of mice lacking both CK isoforms (further referred to as CK^{-/-} mice) in sufficiently high numbers. Polymerase Chain Reaction (PCR) analysis was employed to distinguish mutated and wildtype alleles and follow their segregation behavior. The following BCK specific primers were used: BCKfor2, 5'-GAT GCA GAC CTC GCT GAC CTT G-3', a forward primer located in intron 1; B-CKKrev2, 5'-GAA TAC AAG GTG GTG GCC AGA GTG AG-3' a reverse primer located in intron3, and NeoHyg-back, 5'-GGC CTG GGT GGA GAG GCT TTT T-3', a reverse primer located in the promotor region of the neomycin resistance gene. Amplified PCR products were analyzed on agar gels to separate wildtype (720 bp) and mutant (400 bp) derived fragments. UbCKmit specific primers were: Ubex8, 5'-GCA GCG TCT TTG ACA TCT CTA-3', a forward primer located in exon8; Ubex9, 5'-GAC GCC GTT CAG AGT CAA TCA-3', a reverse primer located in exon9 and a neomycin resistance gene primer. Agarose gel analysis shows a 600 bp wildtype and a 480 bp mutant PCR product.

2.2. Zymogram analysis and enzyme activity

Extracts for zymogram analysis and total creatine kinase activities were prepared by homogenizing freshly excised brain in a 1:5 dilution (w/v) of buffer containing 50 U/ml heparin, 250 mM sucrose, 2 mM EDTA, 10 mM Tris-HCl (pH: 7.4) and complete protease inhibitor complex (Boehringer Mannheim, Germany) at 4°C. Zymogram analysis was performed as described (Steeghs et al., 1997) and developed using the colorimetric detection kit (Sigma diagnostics; procedure number

715-EP). Total creatine kinase activity (units/mg) was measured using a creatine kinase N-acetyl activated kit (Boehringer Mannheim).

2.3. Body weight

The body weights of wildtype and CK^{-/-} male and female mice were determined in the first 3-4 months of life.

2.4. Timm's staining and quantification of mossy fiber fields

The Timm sulphide silver staining procedure (Danscher, 1981; Van der Zee et al., 1995) was used to stain the Zn²⁺-containing mossy fibers in the hippocampus. In short, adult mice (7-10 months of age) were anaesthetized and transcardially perfused with 15 ml 0.9% NaCl (saline) followed by 30 ml sodium sulphide perfusion medium (0.37 M Na₂S.9H₂O, 0.3 M sucrose, 0.1 M NaH₂PO₄.H₂O). The brains were removed and immediately frozen in dry ice and stored at -70°C. Horizontal, 30-µm sections of the hippocampal area at the mid-septo-temporal level were cut on a cryostat and mounted on chromium potassium sulphate (chrom alum)-coated glass slides. The sections were developed in the dark for 60 min in a 60:30:10 ml mixture of gum arabic (50 g/100 ml developing mixture), 0.5 M hydroquinone and citrate buffer (1.2 M citric acid, 0.8 M sodium citrate); 0.5 ml of a 1-M silver nitrate solution was added per 100 ml developing mixture.

From each brain four hippocampal sections covering the mid-septo-temporal range (between 2.7 and 3.3 mm ventral to bregma, 150 µm apart) were selected and analyzed. For both the left and right sides of the hippocampus, the area size of the hilus, the intra- infra-pyramidal mossy fibers (IIP-MF) terminal fields, the supra-pyramidal mossy fibers (SP-MF) projection fields, the regio inferior (consisting of the hippocampal CA3 fields plus the hilus) and the hippocampus (comprising the dentate gyrus and the regio inferior) were determined using a computer-assisted image analysis system. The mean size value per area was calculated for each mouse and then averaged per genotype group. In addition, the relative sizes of the IIP-MF, SP-MF and hilus were expressed as a percentage of the regio inferior (Jost et al., 2002). In addition, as a measure for total brain size the total wet brain weight was analyzed for both groups.

2.5. Behavioral analysis

2.5.1. Animals

Adult male wildtype and CK^{-/-} mice (lacking both BCK and UbCK-mit isoforms) were used for behavioral phenotyping at the age of 3-6 months. All mice were housed in the central animal facility with temperature controlled at 21°C, and an artificial 12:12 h light:dark cycle (lights on at 07.00 am). Fourteen days before starting the behavioral test battery, the mice were individually housed in Macrolon type II cages, with food and water available ad libitum. All testing was performed between 8:00 am - 17:00 pm.

The first cohort of mice performed the cotton test and the light-dark box. The second group of animals conducted the open field, the Morris water maze, the rotarod, the circular hole board and the T-maze continuous alternation task, with 1-wk to 1-month intervals between tests. A third cohort of 6-10 month old male mice was used for the acoustic startle paradigm.

2.5.2. Nestbuilding

Nestbuilding activity as assessed with the cotton collection test (Lynch, 1980; Sluyter et al., 1999) was performed in the room the mice normally resided. Adult male mice were housed individually, and provided with water ad libitum. During the 4-day experiment food pellets were placed on the bottom of the cage, which was covered with only a thin layer of sawdust. A pre-weighed amount of cotton (~10 g, 100% hydrophilic cotton) was provided in the food hopper of each cage lid, and the cotton remaining in the hopper was weighed on each of the four consecutive days. Nests were removed daily, and additional pre-weighed cotton was added to the food hopper if necessary. Nestbuilding activity was expressed as the amount of cotton collected per day.

2.5.3. Light-dark box

According to a previously described light-dark box paradigm (Crawley and Goodwin, 1980) anxiety was tested in a light-dark box (also known as black and white test or two compartment activity box). The test chamber consists of a closed, dark compartment (L: 16 cm, W: 16

cm, H: 16 cm) and an open, lit compartment (L: 24 cm, W: 16 cm, H: 16 cm). A lamp (2 x 8 Watt type TL 218N 220V-50Hz 0.165 (0.27)A) at 16 cm above the floor delivered 230 lux illumination in the light compartment. The mouse was initially placed in the light compartment and subsequently observed for 10 min (starting after the first crossing from light to dark). The parameters measured were latency (sec) before entering the dark compartment (latency L-D), latency of the second crossing from dark to light (latency D-L), the total time spent in the light compartment (%), total time spent in the dark compartment (%), total number of crossings, rearing frequency in the light compartment, and the number of defecation.

2.5.4. Circular hole board

Spatial learning ability of the mice was tested in the circular hole board (dry maze) similar to a previously described method (Grootendorst et al., 2001), with some minor changes. In short, mice were placed in the middle of the 12-circular hole board and were supposed to find the escape tunnel, which is at a fixed location, by using distant visual cues in the room. The spatial cues were present on the four walls in the test room at a distance of ~0.5 m. The circular hole board consists of a large, white circular board (110 cm diameter) containing 12 concentric holes (4 cm diameter) at a distance of 9 cm from the rim. The maze was affixed at 90 cm above the floor by a tripod. The holes can be open or closed when connected with an open escape tunnel (s-shaped), or a closed tube (5 cm depth), respectively. Only in close proximity to the hole, the mouse could recognize whether the hole is open or closed. The open escape tunnel ended in the homecage of the animal, which was placed underneath the circular hole board. To correct for possible odor cues, two additional cages with used sawdust were placed underneath the board.

Habituation and handling. During the pre-training, an s-shaped tube is placed inside the homecage for the mice to explore (similar tubes are used during the acquisition). The mice were handled and habituated to the testing procedure by placing them individually inside an open cylinder positioned around a hole with an escape tunnel, allowing the mice to enter the escape tunnel freely (within 120 sec) during 2 handling sessions per day for 3 days. When animals did not enter freely, they were gently guided into the tunnel. Also, before starting the acquisition

trials all mice were individually placed once on the board for 5 min with all holes closed.

Acquisition. The mouse was placed in an open cylinder in the center of the board with eleven holes closed and one hole connected to an escape tunnel, at a fixed position in respect to the spatial cues, leading to the homecage. After 30 sec the cylinder was lifted and the mouse could start to explore the board for maximally 2 min and exit via the escape tunnel. During the acquisition trials (2 trials per day for 9 days) a hole visit was scored when the animal was in contact with the hole (closed or open). Two successive visits to the same hole were counted separately if the animal visited another hole in between, or moved away over a distance of at least his own body length. The time to find the escape tunnel was registered as the escape latency (sec), a visit to a closed hole was registered as an error. The return to the homecage via the escape tunnel is the reward, which serves as a positive motivation to learn about the location of the open escape hole. After each trial the board and escape tunnel were cleaned and the board turned so another hole would be at the fixed position.

Probe. Each mouse was allowed to explore the holeboard, now with all holes closed. During the 2 min probe trial the number of holes visited in the NE quadrant (where the escape tunnel was located previously) or NW, SE, SW quadrants (each containing three holes) was scored using a video-tracking computer analysis program made by D. Heeren (University of Nijmegen). The percentage of hole visits was calculated for each quadrant and compared to (25%) chance level. After 2 min, a randomly determined hole was connected to the escape tunnel and positioned above the homecage, so the mouse would leave the board through the escape tunnel.

2.5.5. T-maze

Spontaneous alternation behavior was tested in a T-maze apparatus like described before (Crusio et al., 1990; Gerlai, 1998)(L: 75 cm, W: 12 cm, H: 20 cm). The walls of the maze were made of transparent Plexiglas and were glued to a dark gray Plexiglas square bottom. Three removable doors were used to block off the two goal stems and a 24-cm compartment at the beginning of the start arm. Visual cues were present on the four walls of the testing room, about 0.5-1.0 m away from the maze. After each individual mouse, but not in between

trials of one test session, the T-maze was thoroughly cleaned.

The procedure consisted of one forced trial and 14 choice trials and involved location specific blockade of entries to certain arms of the maze by removable doors. Mice were individually placed in the 24-cm start compartment of the T-maze. After 5 sec, the start arm door was removed and the mice were allowed to explore the start arm and one of the goal arms of the maze. Entry to the other arm was blocked, creating a forced trial. The mice explored the areas available to them and eventually re-entered the start arm and moved down to the start compartment, after which that door was closed for 5 sec. Meanwhile, the door blocking one of the goal arms was opened, and the second trial began. Now the mice could choose between the two goal arms. After the mouse had chosen and entered one goal arm half way down, the other arm was closed. The mice left the explored goal arm and moved down to the start compartment again, closing the start-door for 5 sec. Then, the testing cycle continued with another free choice trial, up to a total of 14 free choice trials, without picking up the animals. The time to complete the 15 trials was measured, the consecutive choices made by the mice were recorded, and the overall alternation rate during the 14 free choice trials was calculated (0% = no alternation, 100% = alternation at each trial, 50% = random choice).

2.5.6. Open field

To analyze explorative behavior mice were placed individually in a square open field (L: 40, W: 40, H: 30 cm) with white Plexiglas walls, and videotaped for 30 min. Behavioral records were analyzed later in three blocks of 10 min for the duration (sec) of walking, wall leaning, rearing, sitting and grooming. These open field parameters were defined as follow: walking, movement of its hind paws and forepaws with a minimal distance of 1 cm, wall leaning, standing on its hind legs, the mouse places one or two forepaws against the wall, rearing, the mouse stands upright on the hind legs, while the forepaws are not touching any surface, sitting, no movements of the hind paws and forepaws for a duration of 2 sec, and grooming, washing (parts of) its body. In addition, the total number of faces during the 30 min was recorded as well.

By applying a computer-assisted walking pattern analysis (Heeren and Cools, 2000) the videotaped sessions were further used

to calculate the total walking distance during the 30 min observation, to determine the walking pattern, and the potential formation of a homebase. A homebase is here defined as a 10x10 cm area (usually one of the corners of the field) where the mouse spends more than 20% of its time. Formation of such a homebase is an indication of habituation (Sakic et al., 1994; Tchernichovski and Golani, 1995).

2.5.7. Morris water maze

To investigate spatial learning abilities, mice were placed in a black pool (120 cm diameter) filled with water (21-22°C; made opaque by the addition of milk powder) at different starting positions and were supposed to find the submerged platform by using distant visual cues in the room. Spatial cues were present on the four walls in the test room at a distance of ~0.5 m. To facilitate video camera tracing of the mouse, a strip of white tape (width 10 cm) was taped along the top/inside perimeter of the pool to prevent dark reflection. The 8 cm diameter round platform was submerged 1 cm below the water surface and placed in the middle of the NW quadrant. Parameters measured were the latency (sec) to find the platform and the time spent (sec) in the training quadrant. During all trials the experimenter was present, and always located in the same position in the room.

Acquisition. Adult male wildtype and CK-*−/−* mice performed six acquisition trials (maximal swimming time 120 sec; 30 sec on the platform; inter-trial interval 60 min) per day during three consecutive days. Starting positions were: E, W, N, S, W, E. After the 2-min swim the mice were placed back in their homecage. Underneath the cage a heating pad is placed and also a paper towel is available inside the cage for additional drying and heat.

Probe. All mice performed a single probe trial, at 30 min following the last trial on day 3, in which the platform was removed from the swimming pool. Mice were allowed to swim for 120 sec and the time spent swimming and searching in the NW quadrant (where the platform had been located) was recorded using a video-tracking computer analysis program made by D. Heeren (University of Nijmegen).

Visible platform. 5 days later, the visual test (4 trials) with the platform visibly located above the water level (and at a different location each trial), was performed to account for visual and/or motor impairments in the swimming pool.

2.5.8. Rotarod

To control for motor functions such as balance and motor co-ordination, mice were individually placed on a rotarod. During a 400 sec time interval the acceleration of the rod resulted in a gradual increase from 0 to 38 r.p.m. The time (sec) each mouse was able to stay on the rod, by keeping walking and balancing, was measured. Mice were subjected to one pre-trial (data not used), and three test trials with a maximum of 400 sec and a 30 min inter-trial rest interval.

2.5.9. Acoustic startle reflex

Startle reactivity was measured using a startle response system (SR-LAB, San Diego Instruments, San Diego, CA, USA). The startle chamber consisted of a non-restrictive Plexiglas cylinder (4 cm diameter), resting on a Plexiglas platform inside a ventilated and sound attenuated chamber. A high-frequency loudspeaker inside the chamber produced both a continuous background noise of 70 dB and the various acoustic stimuli. Vibrations of the platform, produced by the whole-body startle response of the mouse, were detected and transduced by a piezoelectric accelerometer mounted underneath the platform, connected to an automated system. Each mouse was placed inside the cylinder for 5 min with a background noise of 70 dB to habituate before the first startle stimuli were given.

Prepulse inhibition and habituation. The first part (f) of the testing session consisted of 5 separate 120 dB startle pulse trials. The middle portion of the session (m) consisted of 4 blocks with each block containing: (1) two startle pulse alone trials (120 dB burst), (2) four prepulse trials, in which 72, 74, 78, or 86 dB stimuli preceded the 120 dB burst, and (3) a no stimulus trial (only the 70 dB background noise). These 7 trials were presented in a pseudo-random order. The last part of the testing session (l) consisted again of a block with 5 separate 120 dB startle pulse trials.

Threshold. The hearing threshold trial consisted of five blocks of 10 different sound levels -no stimulus (70 dB), 90, 95, 100, 105, 110, 120, 130, 140, or 150 dB- presented in a pseudo-random order.

The (pre)pulses consisted of a 20 ms sound burst. The interval between the onset of the prepulse and the onset of the startle pulse was 100 ms. The startle response was measured during a 50 ms pe-

riod, commencing at the onset of the startle pulse, with an amplitude read-out expressed in arbitrary units.

2.6. Statistics

Animal body weights, brain area sizes and behavioral test data are presented as means \pm SEM. The statistical analysis involved a Boltzmann sigmoidal curve-fitting, paired t-test, student's t-test, one-way ANOVA and ANOVA repeated measures, using the SPSS 9.0 statistical software package. For any statistical comparison within or between groups the F-value or t-value is given with the corresponding P value. Statistical significance was set at $P < 0.05$.

3. Results

3.1. Confirmation of enzymatic consequences for CK^{-/-} mice

Creatine kinase isoenzyme characterization using zymogram assays demonstrated the presence of dimeric cytosolic brain-type creatine kinase (BCK) and octameric and dimeric mitochondrial UbCKmit protein, but complete absence of muscle-type creatine kinase isoforms (MCK or ScCK) in the wildtype brain (Fig. 1A, lane 1). The enzyme profiles confirmed that UbCKmit^{-/-} (Fig. 1A, lane 2) and BCK^{-/-} (Fig. 1A, lane 3) single knockout brains lack only UbCKmit or BCK, respectively, whereas the CK^{-/-} (Fig. 1A, lane 4) mouse brain homogenates completely lack both the isoenzymes BCK and UbCKmit. Wildtype, both single knockout and double knockout brains exhibited normal levels of adenylate kinase 1 (Fig. 1A, lane 1-4). The total creatine kinase (CK) enzyme activity was measured in the first weeks after birth for C57BL/6 (one of the two background strains) and BCK^{-/-} brains (Fig. 1B; one animal per time point). The data for the C57BL/6 demonstrated a postnatal increase of the total CK enzyme activity, with a peak between 3-6 weeks of age (Fig. 1B). A similar CK enzyme activity pattern was observed for the 129-substrain (the other background strain; data not shown). Mice lacking brain-type creatine kinase also showed a postnatal increase, but the total CK enzyme activity was ~67% lower. The remaining ~33% of the CK enzyme activity represents the mitochondrial UbCKmit still present in BCK^{-/-} brains (Fig. 1B).

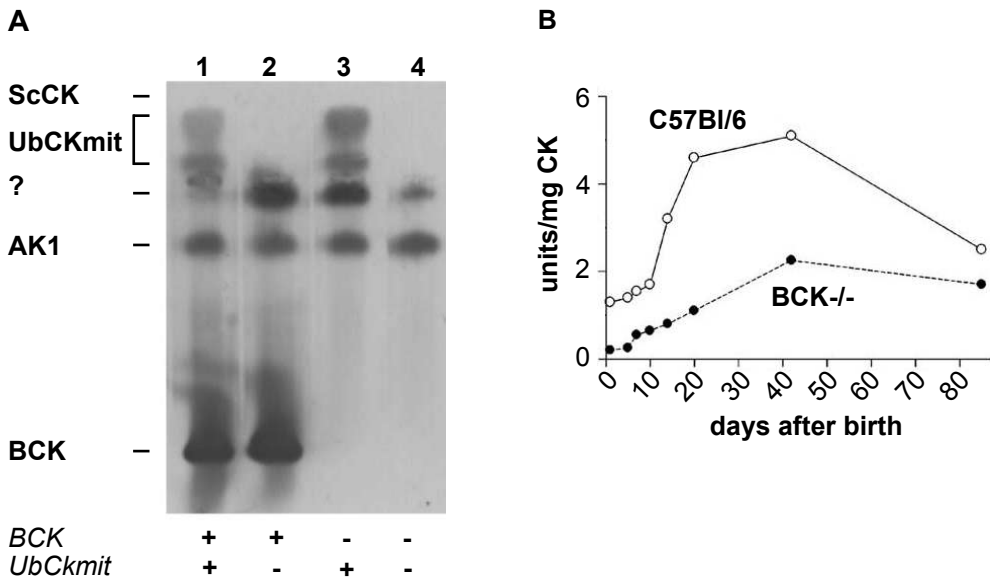


Figure 1: Zymogram analysis and enzyme activity of creatine kinase isoenzymes in brain homogenates. (A) Lane 1, brain homogenate from a wildtype mouse shows the presence of the dimeric cytosolic brain-type CK isoform (BCK) and the octameric (upper dash) and dimeric (lower dash) ubiquitous mitochondrial CK isoform (UbCKmit). Both muscle-type isoforms, i.e., cytosolic MCK (not indicated) and mitochondrial sarcomeric Sc-CK, are absent. Lane 2, brain homogenate from a UbCKmit^{-/-} single knockout mouse shows the absence of both octameric and dimeric UbCKmit, but normal activity of dimeric BCK. Lane 3, a BCK^{-/-} single knockout mouse demonstrates the absence of BCK. Lane 4, the CK^{-/-} mouse shows the complete absence of both BCK and UbCKmit isoforms. An unidentified phosphorus transfer enzyme activity, presumably originating from contaminating blood cells, is indicated by a question mark. Adenylate kinase-1 (AK1) is present in equal amounts in all four lanes. (B) The total creatine kinase enzyme activity in C57BL/6 mouse brains (open circles) demonstrates a postnatal increase. BCK^{-/-} mouse brains (closed circles) show a ~67% decrease in total CK activity, indicating that the remaining ~33% is attributable to UbCKmit.

3.2. CK^{-/-} mice have lower body weights

Longitudinal weight measurements indicated that both male (Fig. 2A) and female (Fig. 2B) CK^{-/-} mice gained weight more slowly than their male and female wildtype littermates, as shown by Boltzman sigmoidal curve fitting. At 3 months of age, the average body weight is still reduced in CK^{-/-} male mice (22 ± 1 g, $n=19$; $P < 0.001$) compared to that of wildtype mice (28 ± 1 g, $n=19$). Also, 3 months old female

CK^{-/-} mice showed a significant and persistent lower body weight (19 ± 0.5 g, $n=20$; $P < 0.001$) in comparison with aged-matched female wildtypes (22 ± 0.5 g, $n=6$).

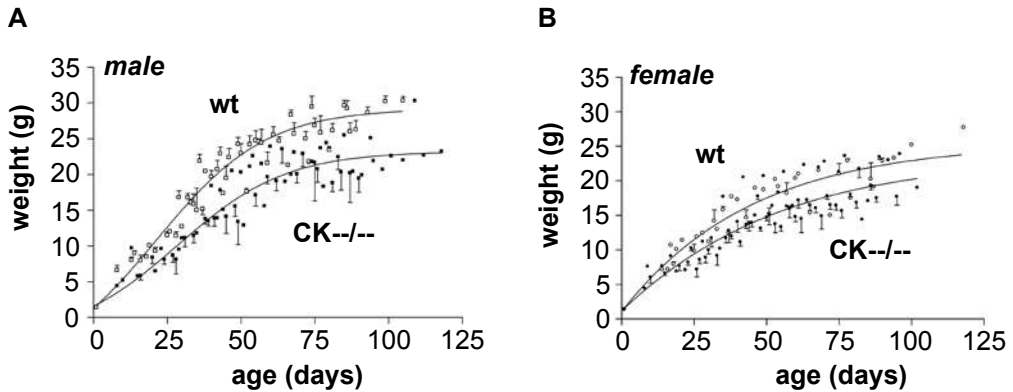


Figure 2: *Body weights.* The body weights of wildtype (wt; open symbols) and CK^{-/-} mice (closed symbols) male and female mice as determined every two weeks in the first 3-4 months of life. CK^{-/-} mice gained weight more slowly than their male (A) and female (B) wildtype littermates.

3.3. CK^{-/-} mice show impaired spatial learning in a wet and dry maze

3.3.1 Morris water maze

The Morris water maze is used to examine spatial learning, i.e. the ability of individual mice to orientate in a novel environment using surrounding distal cues (spatial map). Spatial learning in the water-maze was analyzed during acquisition sessions in which the animals have to locate a submerged hidden platform. Performance of mutant and wildtype animals was compared in groups, from which one wt and one mutant had to be removed because of excessive floating and an obvious lack of swimming ability, respectively. For the wildtype group ($n=9$) the escape latencies decreased across training (main effect of trial; $F(1,8) = 122.8$, $P < 0.0001$) with an average escape latency of 100 ± 6 sec in the first two trials and 14 ± 3 sec during the last two trials, indicating spatial learning (Fig. 3A). The CK^{-/-} mice ($n=9$) also demon-

strated a decrease in average latency over time, however the escape latencies remained significantly higher compared with the wildtype group ($F(1,16) = 11.4, P < 0.004$). The average escape latencies in the last trials for the CK^{-/-} mice (53 ± 8 sec) were almost 4 times higher than in those observed in wildtype mice (14 ± 3 sec), indicating impaired spatial learning (Fig. 3A).

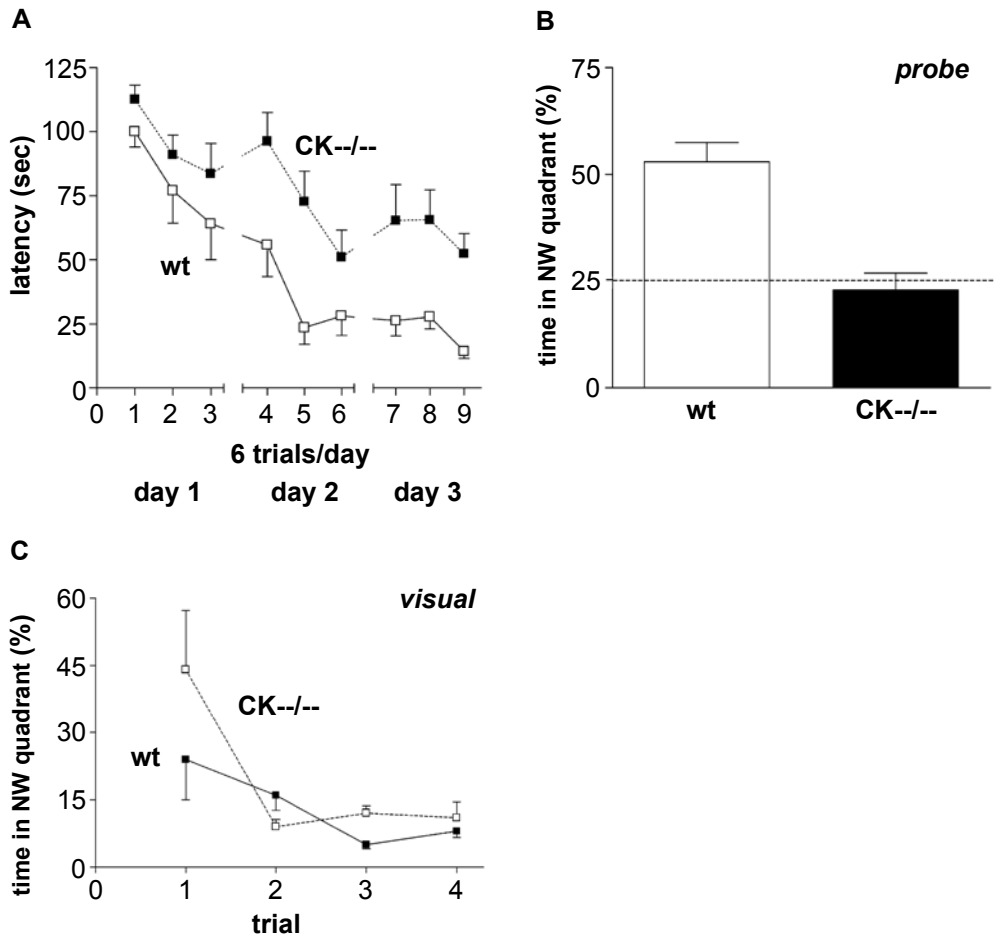


Figure 3: Spatial learning in the Morris water maze. Compared to wildtype (wt; open squares) animals, CK^{-/-} mice (closed squares) displayed a significantly higher latency to find the submerged platform (A), demonstrated no specific searching in the trainings quadrant during the probe test (B), and do not differ from the wildtypes in the visual platform task (C), indicating severely impaired spatial learning.

The probe test, with the platform now removed from the pool, serves to confirm the presence or absence of spatial learning ability of the animals (Fig. 3B). The wildtype animals spent $53.0 \pm 4.5\%$ of their time searching in the NW quadrant, where the platform was initially situated, indicating a preferable search in the training quadrant. The CK^{-/-} mice spent only $22.9 \pm 3.9\%$ of the 2 min probe trial time in the NW quadrant, which was significantly lower compared to the wildtype group ($F(1,16) = 25.9$, $P < 0.0001$; Fig. 3B), and equal to the 25% chance level. Taking together, the higher escape latencies in the acquisition phase and the non-specific searching performance in the probe trial demonstrated impaired spatial learning in the wet maze for CK^{-/-} mice.

3.3.2 12-Circular hole board

In order to confirm the impaired spatial learning ability of the CK^{-/-} mice and to account for several swimming related (stress) factors; (Hölscher, 1990; Wishaw and Tomie, 1990; Gerlai, 2001; Iivonen et al., 2003), a dry-version of analysis of spatial orientation learning was performed on the circular hole board (dry maze). When latencies to find the escape hole and the numbers of errors made before finding the correct hole were measured, wildtype mice ($n=8$) showed a learning curve (main effect of trial; $F(1,7) = 5.8$, $P < 0.047$) with an initial latency of 19 ± 5 sec for trial day 1 and an average latency of 9 ± 2 sec on trial day 9 (Fig. 4A). Also, wildtype mice became more accurate over time in the localization of the exit hole, which is expressed by the decreasing number of visits to closed holes, registered as errors (Fig. 4B). The CK^{-/-} mice ($n=10$) revealed no clear decline in latency. Moreover, they demonstrated significantly increased escape latencies during the 9 session days, when compared with the wildtype animals ($F(1,16) = 9.196$, $P < 0.008$; Fig. 4A). The CK^{-/-} mice were less accurate over time in finding the escape hole, i.e., they made significantly more errors than the wildtype mice ($F(1,16) = 8.566$, $P < 0.01$; Fig. 4B). During the last session, CK^{-/-} mice still visited about 7 other holes before they reached the escape hole, which is two times more errors than the wildtype mice (3 ± 1 errors; Fig. 4B).

To confirm that the mice showed spatial learning in locating the escape hole, a probe trial was conducted with all holes closed. The number of holes visited in the NE quadrant (where the escape hole

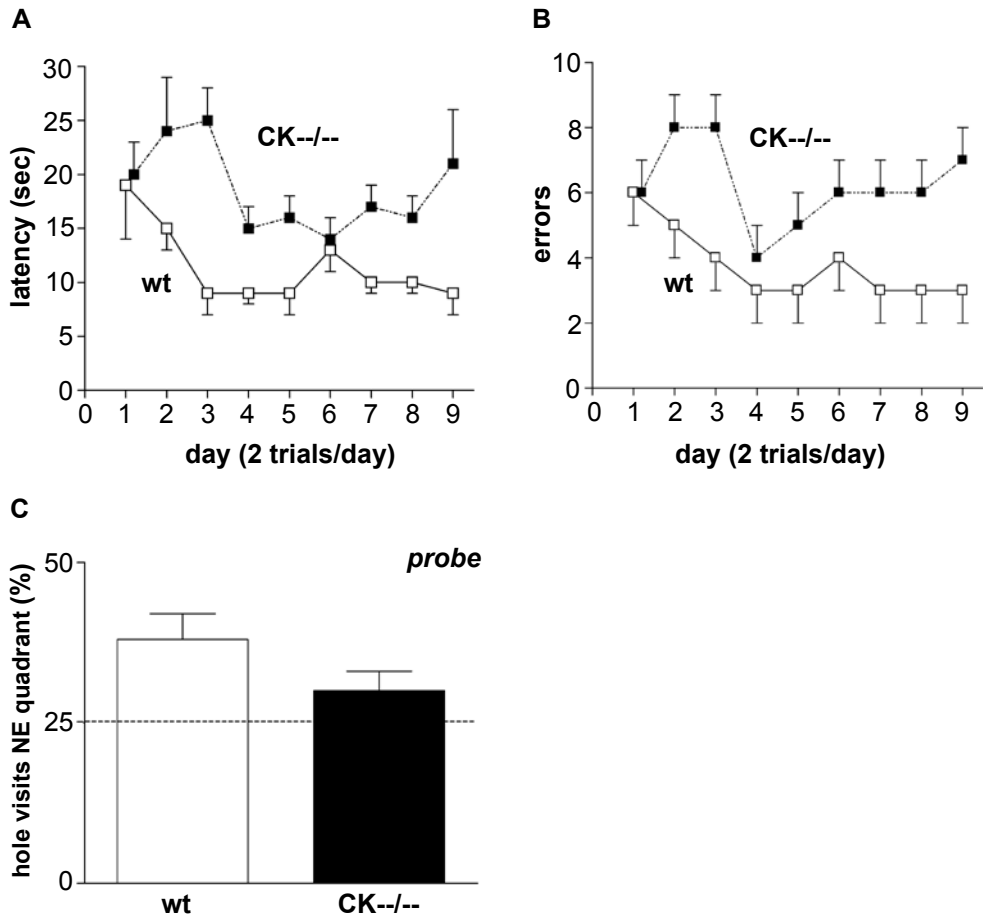


Figure 4: *Spatial learning in the circular hole board.* Compared to wildtype (wt; open squares) animals, CK-/- mice (closed squares) showed a significantly higher latency (A), and made more errors (B) during the effort to find the escape hole. The probe test (C) showed that the percentage of hole visits in the previously correct quadrant was not different from chance level, indicating a severe spatial learning deficit for the CK-/- mice.

had been located; Fig. 4C) and the other quadrants was recorded. The wildtype animals visited significantly more holes in the NE quadrant ($38.4 \pm 4\%$) than in the other areas of the board (NE vs. SE quadrant: $P < 0.009$; NE vs. NW quadrant: $P < 0.047$; NE vs. SW quadrant: $P < 0.017$; Fig. 4C). However, the CK-/- mice appeared not to search specifically, and were visiting only $29.4 \pm 3\%$ of the total number of hole visits in the NE quadrant which was not significantly different from

25% chance level (Fig. 4C). These results revealed that the CK^{-/-} mice did not learn the position of the escape hole, indicating impaired spatial learning which corroborates the findings from the water maze test.

3.4. Cued performance and motor coordination is normal in CK^{-/-} mice

To analyze whether the observed learning impairment could be due to a performance defect involving visual or motor dysfunction, the wildtype and CK^{-/-} mice conducted a water maze visual platform swimming task and the so-called rotarod task. During the visual task, the platform in the water maze was raised above the surface of the water. The average latency for the wildtype mice (n=9) to reach the platform is 13 ± 3 sec (Fig. 3C). The CK^{-/-} mice (n=9) were not different from the wildtype group regarding their average latency (19 ± 3 sec; Fig. 3C). The rotarod test is routinely used to study motor coordination and balance. The total time the animals could keep their balance and stay walking on top of the rotating rod was for CK^{-/-} animals 333 ± 22 sec (n=9), which was not different from the wildtype group (331 ± 24 sec, n=9). These findings from the visual task and the rotarod indicated that the reduced spatial learning ability of the CK^{-/-} mice is not caused by visual or motor deficiencies.

3.5. CK^{-/-} mice show similar open field exploration and habituation

Wildtype mice (n=10) were observed in the open field and demonstrated active exploration and locomotion activity (Fig. 5). During 30 min (divided in 3 blocks of 10 min) the time spent sitting decreased, whereas rearing and grooming increased (Fig. 5C-E). The CK^{-/-} mice (n=10) demonstrated similar open field locomotion behavior as wildtype mice. The time spent walking, wall leaning, rearing and sitting during the different time periods was similar for both groups (Fig. 5A-D). While grooming was decreased for CK^{-/-} mice compared to wildtype mice (77.7 ± 24.5 sec and 176.4 ± 42 sec, respectively; total grooming time during the entire 30 min period; Fig. 5E), this was however not statistically significant ($F(1,18) = 4.115$, $P < 0.058$). During the 30 min period, both groups displayed similar walking patterns and homebase formation (data not shown). In addition, the total walking distance was

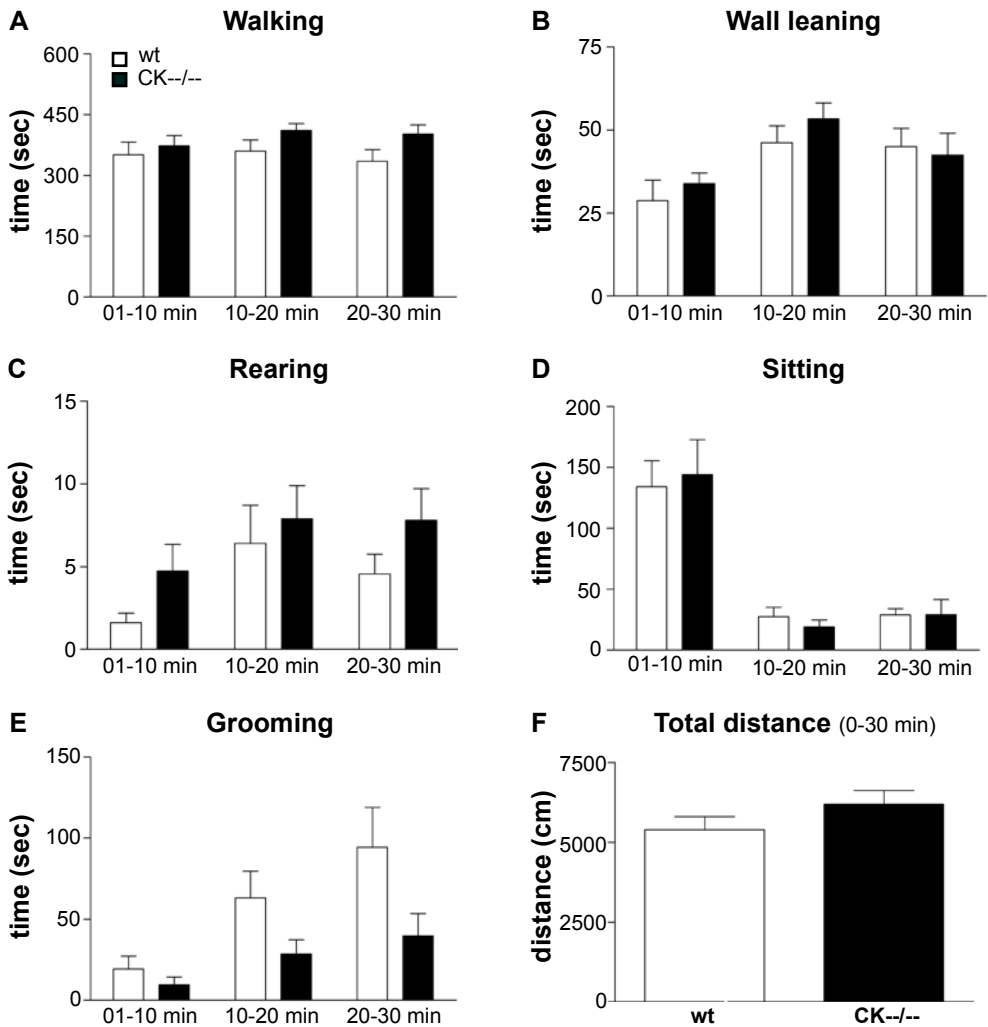


Figure 5: Open field behavior. Open field activity parameters such as walking (A), wall leaning (B), rearing (C), sitting (D), and grooming (E) were observed during a 30 min period and scored in three 10 min blocks. The total distance traveled is shown in (F). Although grooming seemed decreased in CK^{-/-} mice (black bars), no significant differences were found for either of the open field parameters, when compared to wildtype (wt; white bars) mice.

not different either between the wildtype animals (54 ± 4 m) and the CK^{-/-} mice (62 ± 4 m; Fig. 5F). The overall results demonstrate that CK double deficiency does not influence explorative behavior during the open field test. Using the formation of a homebase as indication for habituation, the CK^{-/-} mice demonstrated a similar habituation like

the wildtype animals.

3.6. CK^{-/-} mice show no differences in anxiety response

The parameters analyzed in the light-dark box are indicators of anxiety-related responses. This test is based on the tendency of mice to prefer and explore a dimly lit, concealed area and avoid a brightly lit, open area. The wildtype mice (n=8) preferred the dark compartment above the light compartment. Of the total time of 10 min the animals spent 78% in the dark compartment, while only 22% in the light compartment. After the first transition between the two chambers (latency L-D), the wildtype mice repeatedly entered the light and dark chambers. During their time in the light chamber the wildtype mice showed rearing behavior. The CK^{-/-} mice (n=7) demonstrated a similar preference for the dark chamber (75% of the total time). The first transition from light to dark and from dark to light observed in CK^{-/-} mice was not different from wildtype animals. Also, no differences were found for the rearing frequency in the light chamber, the total number of crossings and the number of defecation between the genotype groups. The results for the light-dark box suggested that there was no difference between wildtype and CK^{-/-} mice in their anxiety-related response.

3.7. CK^{-/-} mice show reduced nestbuilding activity

Nestbuilding behavior is expressed as the amount of cotton collected per day, used to build a nest. The wildtype mice (n=9) showed an average cotton collection of about 4-5 gram cotton per day, with increasing amounts over time (Fig. 6). The CK^{-/-} mice (n=7), however, collected significantly less cotton (0.5-1.5 gram per day; Fig. 6) over the 4-day period when compared to the wildtype group ($F(1,14) = 61.162$, $P < 0.0001$). These results suggest a 4-fold decrease in nestbuilding activity for the CK^{-/-} mice (Fig. 6). This might indicate reduced habituation to, or increased fear for, new elements in the otherwise familiar environment.

3.8. CK^{-/-} mice show normal spontaneous alternation behavior

Both genotype groups were tested in the T-maze continuous alternation task (Gerlai, 1998), which is based on the phenomenon of spon-

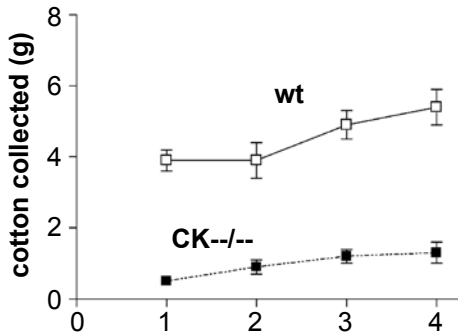


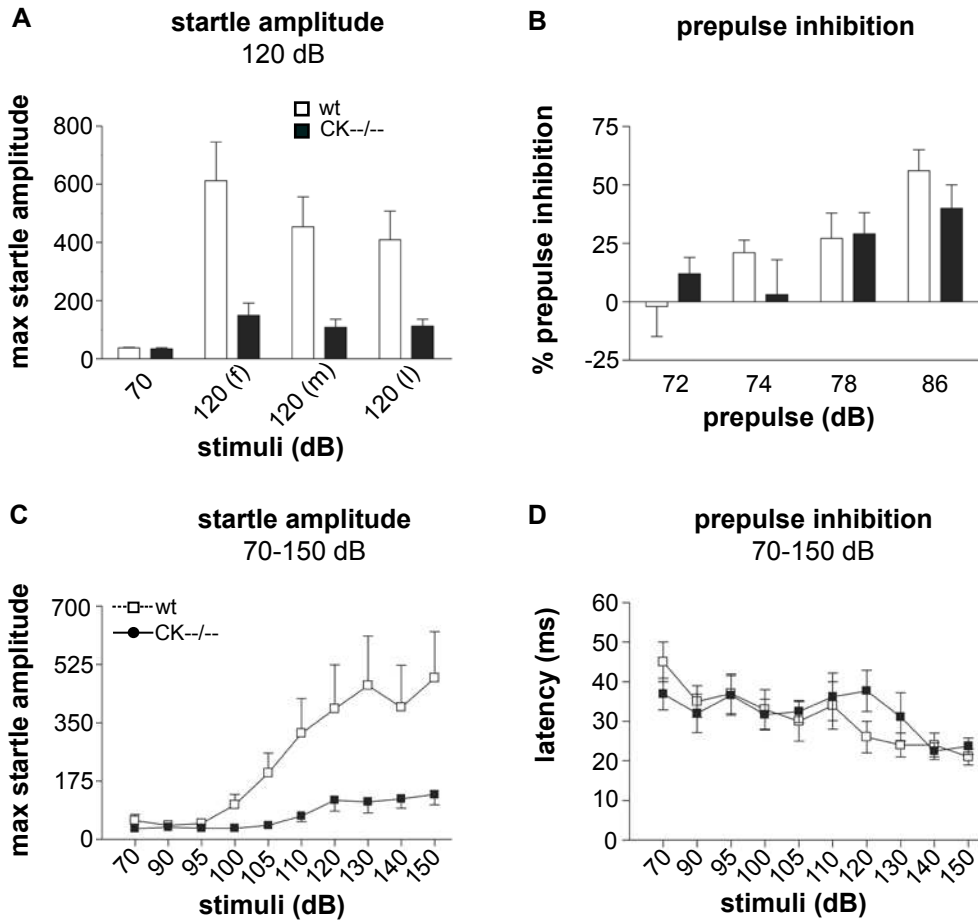
Figure 6: *Nestbuilding activity.* The amount of cotton gathered during four consecutive days for nestbuilding by CK^{-/-} mice (closed squares) was significantly lower than that collected by wildtype (wt; open squares) mice.

taneous alternation by mice. Wildtype animals (n=8) and CK^{-/-} mice (n=6) performed well in the T-maze continuous alternation task. Both groups demonstrated an alternation rate of ~60%. The average time to complete the 15 trials was 19 ± 3 min for the wildtype animals and 17 ± 3 min (data not shown) for the CK^{-/-} mice, which was not significantly different either. The results of the T-maze continuous alternation task indicate that CK^{-/-} mice display similar exploratory behavior when compared to wildtype mice.

3.9. Acoustic startle reflex

3.9.1. Acoustic startle reflex response is reduced in CK^{-/-} mice

To investigate whether animals with a deficit in their brain energy-metabolism show an impairment in their immediate reaction to sudden stimuli, separate cohorts of wildtype (n=17) and CK^{-/-} mice (n=13) were tested in the acoustic startle reflex set-up (Fig. 7). Both groups were characterized in a baseline startle session (a background noise of 70 dB). Data from the no stimulus trials indicated that the wildtype and CK^{-/-} mice both have similar levels of basal activity of around ~40 arbitrary units in the restraining tube (Fig. 7A). The wildtype mice showed an average maximal startle amplitude of ~500 arbitrary units as response to the 120 dB startle pulses (Fig. 7A). However, the acoustic startle response to the 120 dB startle pulse was strongly reduced in the CK^{-/-} mice (Fig. 7A). Their startle response amplitude of ~130 arbitrary units was significantly lower compared to that of wildtype animals ($F(1,28) = 9.274$, $P < 0.005$; Fig. 7A).



3.9.2. Prepulse inhibition is not altered in CK^{-/-} mice

Prepulse inhibition is defined as the reduction in 120-dB startle stimulus response when a weak prepulse (+2, +4, +8, or +16 dB above background, i.e., stimuli of 72, 74, 78 and 86 dB) precedes the 120 dB stimulus pulses. The prepulse itself is too low to elicit a startle response. The prepulse inhibition of the startle response is expressed as a percentage (Fig. 7B). The wildtype mice revealed a clearcut prepulse inhibition, which increased with increasing prepulse intensities (within trial effect; $F(1,16) = 31.7$, $P < 0.0001$; Fig. 7B). The strongest prepulse inhibition ($56 \pm 9\%$) was shown following the +16 dB above background. CK^{-/-} mice also showed an increasing prepulse inhibition of the startle response (within trial effect, $F(1,12) = 7.7$, $P < 0.017$;

Figure 7: Acoustic startle reflex response. (A) For both wildtype (wt, white bars) and CK^{-/-} (black bars) mice the response amplitude following background noise (70 dB) was around 40 arbitrary units, indicating that their basal activity was similar. A possible habituation of the response to the acoustic startle stimulus of 120 dB was measured by comparing the average maximal startle amplitude following 5-8 separate 120 dB startle pulses in the first (f), middle (m), and last (l) trial blocks. No habituation to the startle pulse was observed in wildtype or CK^{-/-} mice. Notably, CK^{-/-} mice showed a significantly lower startle response amplitude than the wildtype animals. (B) Prepulse inhibition of the startle response was recorded by offering 4 blocks of trials with each block containing four prepulse trials, in which a 72, 74, 78, or 86 dB stimulus preceded the 120 dB startle pulse, and was expressed as percentage inhibition of the pulse response. Both wildtype (wt, white bars) and CK^{-/-} (black bars) mice showed prepulse inhibition of the startle response following prepulses of +8 dB and +16 dB above background. (C) Startle response threshold. Acoustic stimuli of increasing intensity (ranging from 70-150 dB) resulted in increasingly higher response amplitudes in wildtype mice (wt, open squares). CK^{-/-} mice (black squares) demonstrated significantly lower response amplitudes, even upon acoustic stimuli in the highest range. (D) The startle latency, the time (msec) after which the maximal startle amplitude was recorded, was measured following stimuli in the range from 70-150 dB in wildtype (wt, open squares) and CK^{-/-} (closed squares) mice.



Fig. 7B), with a prepulse inhibition of $40 \pm 10\%$ for the strongest prepulse of +16 dB. Thus, these data revealed that both genotype groups demonstrated prepulse inhibition.

3.9.3. CK^{-/-} mice show a decreased startle response profile

To investigate whether the differences in startle reflex response (Fig. 7A) between wildtype (n=9) and CK^{-/-} mice (n=7) may be due to a hearing deficit, we evaluated the startle reflex responses to startle stimuli of increasing intensity (within the range of 70 - 150 dB; Fig. 7C). The wildtype mice showed increasing startle amplitudes following increasing sound levels (within trial effect; $F(1,8) = 8.50$, $P < 0.02$; Fig. 7C). Relatively low amplitudes were observed with 70-105 dB stimulus levels. This was followed by a rapid increase in the startle response amplitude following stimuli ranging from 110-150 dB (Fig. 7C). Data revealed that the CK^{-/-} mice had significantly reduced startle amplitudes in the range of 70-150 dB compared to the wildtype group ($F(1,14) = 4.878$, $P < 0.044$; Fig. 7C). The CK^{-/-} mice showed a startle response amplitude profile of almost 3.5 times lower than the wildtype mice upon increasing sound levels.

The startle latency, the time (ms) after which the maximal startle amplitude is recorded, was determined for both genotype groups (Fig. 7D). Wildtype, as well as the CK-/-, animals demonstrated a similar decrease in startle latency upon increasing stimuli ranging from 70-150 dB.

3.10. Smaller hippocampus, regio inferior area and brain weight in CK-/- mice

The mossy fibers located inside hippocampus are axons and axon collaterals of the dentate granule cells projecting to the hilus and the CA3 pyramidal cell layer. The terminal field of the hippocampal mossy fibers located superficial to the pyramidal cell layer is called the supra-pyramidal mossy fiber area (SP-MF). Also a small extent terminates within or below the pyramidal cell layer named the intra- infra-pyramidal mossy fiber (IIP-MF) area (Fig. 8A, courtesy H.P. Lipp) Subtle anatomical variations in the hippocampus mossy fiber fields have been shown to co-vary with behavioral variations in a number of tasks (Schwegler and Crusio, 1995; Laghmouch et al., 1997), therefore the hippocampus and mossy fiber field areas of wildtype and CK-/- brains have been analyzed histologically (Table 1 and Fig. 8).

The Timm's staining, used to visualize the Zinc-containing mossy fibers, showed no difference in the absolute values of the hilus, SP-MF and IIP-MF area between both genotype groups. However, the

Table 1. Hippocampal mossy fibre fields in wildtype and CK-/- knockout mice

| area ($\times 10^3 \mu\text{m}^2$) | wildtype (n=6) | CK-/- (n=6) |
|--------------------------------------|--|---|
| hippocampus | 2346 \pm 36 | 2180 \pm 56* |
| regio inferior | 705 \pm 12 | 601 \pm 24** |
| IIP-MF | 17 \pm 0.8 (2.5 \pm 0.1) ^a | 17 \pm 1.3 (3.0 \pm 0.2) ^a |
| SP-MF | 73 \pm 2.2 (10.4 \pm 0.3) ^a | 73 \pm 2.3 (12.1 \pm 0.2) ^{a***} |
| hilus | 87 \pm 3.2 (12.5 \pm 0.4) ^a | 79 \pm 5.3 (13.2 \pm 0.8) ^a |

Values presented as mean \pm SEM.

IIP-MF, intra-infra-pyramidal mossy fibres; SP-MF, supra-pyramidal mossy fibres; ^a Percentage of regio-inferior (CA3 + hilus)

Statistical difference (one-way ANOVA) between groups of animals, * P < 0.03; ** P < 0.003; *** P 0.001.

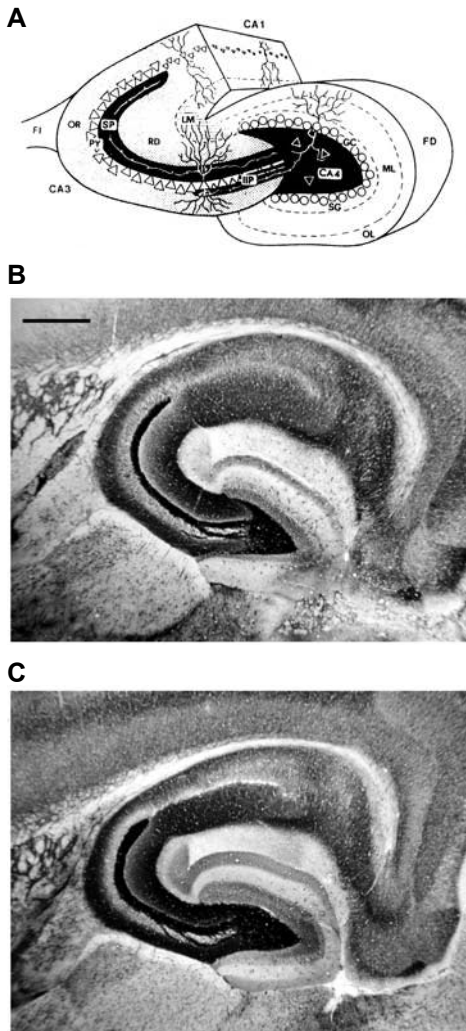


Figure 9: Mossy fiber projection fields. (A) Schematic drawing of the hippocampus with the CA3 pyramidal (PY) cell layer and the mossy fiber (dentate gyrus granule cell (GC) axon) projection fields (in black): the intra-infrapyramidal (IIP) mossy fiber area, the suprapyramidal (SP) mossy fiber field and the hilus (CA4). Other hippocampal areas indicated are FD, fascia dentata, FI, fimbria, LM, stratum lacunosum-moleculare, ML and OL, dentate gyrus middle and outer molecular layer, OR, stratum oriens, RD, stratum radiatum, SG, supragranular layer. Courtesy of W.E. Crusio & H.P. Lipp. (B, C) Representative examples of Timm-stained horizontal hippocampal sections, at the midseptotemporal level, showed for CK^{-/-} mice (C) a smaller regio inferior (CA3 area plus the hilus) but a relatively larger IIP-MF and SP-MF area, compared to wildtype animals (B). Bar in B (for B, C), 440 μm .

size of the regio inferior (CA3 area plus the hilus) was significantly reduced ($F(1,11) = 15.6$, $P < 0.003$; Table 1) in the CK^{-/-} brains ($n=6$) compared to wildtype brains ($n=6$), i.e. an estimated reduction in the range of $\sim 15.0\%$. As a result the relative size of the SP-MF area of the CK^{-/-} brains ($12.1 \pm 0.2\%$) was significantly larger than that of wildtype brains ($10.4 \pm 0.3\%$; $F(1,11) = 23.4$, $P < 0.001$; Table 1). The relative size of the IIP-MF area also seemed larger in CK^{-/-} ($3.0 \pm 0.2\%$) than in wildtype ($2.5 \pm 0.1\%$) brains, however this did not reach significance (Table 1). In addition, besides a reduced regio inferior size, a significantly decreased total hippocampal area within the same

brain sections was measured, revealing a 7.0% reduction in the absolute size value for the CK^{-/-} hippocampus when compared to the wildtype hippocampus ($F(1,11) = 6.2$, $P < 0.032$; Table 1).

Two additional genotype cohorts (wt: $n=6$, bodyweight: 27.3 ± 1.2 g; CK^{-/-}: $n=6$, bodyweight: 18.0 ± 0.2 g) were used to determine wet brain weights. In comparison with wildtypes, the data revealed a ~6.3% reduction for CK^{-/-} mice, indicating an overall smaller brain (CK^{-/-}: 0.43 ± 0.001 g vs. wildtype: 0.46 ± 0.01 g; $F(1,11) = 15.99$, $P < 0.003$), besides their reduced regio inferior and hippocampal areas.

4. Discussion

In addition to previously published findings regarding deficiency for BCK (Jost et al., 2002) or UbCKmit (Streijger et al., 2004) alone, we now have addressed the significance of double deficiency for both brain-type creatine kinases (see also Table 2 for comparisons). Based on their distribution and the assumption that CK activity would be essential for normal brain function (Ross and Bluml, 1996; Wys and Kaddurah-Daouk, 2000), a prominent phenotype in double knockout animals was expected.

We now provide evidence that CK^{-/-} mice have (i) diminished body and brain weights, (ii) smaller hippocampus/regio inferior areas with relatively larger suprapyramidal and intra-infra-pyramidal mossy fiber fields, and demonstrate (iii) severely impaired spatial learning in the circular hole board dry maze and the Morris water maze, (iv) strongly reduced nestbuilding activity, and (v) significantly decreased startle reflex responses and profile.

4.1. Creatine kinase deficiency affects behavior

Since the BCK and UbCKmit kinases are expressed throughout the brain including the hippocampus, deficiency of both enzymes was expected to have a severe impact on hippocampus mediated spatial learning processes. Previous studies revealed for both BCK^{-/-} (Jost et al., 2002) and UbCKmit^{-/-} mice (Streijger et al., 2004) a slower spatial learning but eventually they acquired the task, as shown in a probe test. Here, we report that the CK^{-/-} mice are more severely impaired in spatial learning ability observed in both the Morris water maze and the circular hole board. This was evidenced by longer escape latencies

and a failure to exhibit correct searching in the target quadrant during the probe trial (Gerlai, 2001). This impairment cannot be attributed to gross sensorimotor impairments or to deficits in escape motivation or simple associative learning processes because the CK^{-/-} mice performed normally in the visible platform task, the light-dark box and

Table 2. Comparative (behavioral) analysis of single and double CK knockout mice.

| | UbCKmit^{-/-} (Streijger et al., 2004) | BCK^{-/-} (Jost et al., 2002) | CK^{-/-} |
|--------------------------|--|---|-------------------------|
| rotarod | - | - | - |
| light-dark box | n.d. | - | - |
| T-maze | n.d. | - a | - |
| open field | +/- | + | - |
| Morris water maze | | | |
| acquisition | - a | + a | + |
| probe test | - a | - a | + |
| visual test | - | - | - |
| hole board test | | | |
| acquisition | - a | + a | + |
| probe test | - a | - a | + |
| cotton collection | + | + a | ++ |
| acoustic startle | | | |
| startle response | + | + a | + |
| prepulse inhibition | - b | - a | - |
| startle profile | +/- | + a | ++ |
| mossy fibre area | | | |
| IIP-MF | - a | + | +/- |
| SP-MF | - a | - | +/- |
| hippocampus | - a | - | + |
| brain weight | - a | - a | + |
| body weight | - | - | + |

n.d.: not done; (-) not affected (not different from wildtype; +/-) slightly affected; (+) affected; (++) largely affected; IIP-MF: intra-infra-pyramidal mossy fibres; SP-MF: supra-pyramidal mossy fibres.

^a Unpublished observations

^b Not different from wildtypes at 130 dB; Streijger et al. (2004) reported the absence of prepulse inhibition at 120 dB.

the rotarod. Interestingly, the severity and characteristics of the spatial learning impairment observed in our CK^{-/-} mice is highly reminiscent of that previously reported for aged 24 months old BCK^{-/-} mice (Jost et al., 2002). Apparently, an age-related decline in mitochondrial (in this case UbCKmit) function in aged BCK^{-/-} single knockout mice culminates in a situation that mimics the complete knockout of the creatine kinase system. Indeed, mitochondrial decay has been associated with memory loss and particularly with age-dependent cognitive impairment (Wallace, 1999; Liu et al., 2002) and CK enzymes are particularly vulnerable to ageing and stress related (oxidative) damage (Wendt et al., 2003).

Previously, the open field test revealed increased exploration behavior for BCK^{-/-} mice (Jost et al., 2002) and a diminished habituation in both BCK^{-/-} and UbCKmit^{-/-} groups (Streijger et al., 2004). Surprisingly, CK^{-/-} mice demonstrated overtly similar open field exploration as the wildtype animals, with only a tendency for reduced grooming. In addition, the relative good performance of the CK^{-/-} mice in the spontaneous alternation task is supportive evidence for unaltered exploration motivation and locomotion, corroborating the findings from the open field.

When providing cotton in the foodhopper, the wildtype animals collected increasing amounts of cotton over time, which has been related to habituation and experience (Sluyter et al., 1999). Since the CK^{-/-}s collected hardly any cotton, it could be assumed that these mice have reduced habituation to, or increased fear for, new elements in an otherwise familiar environment. Notably, separate BCK^{-/-} and UbCKmit^{-/-} groups both showed a reduction in nestbuilding activity, but less severe than CK^{-/-} mice (F. Streijger and C.E.E.M. Van der Zee, unpublished observation).

Recently, we found that BCK^{-/-} and UbCKmit^{-/-} mice demonstrated a four-fold lower startle response, and that both genotype groups showed prepulse inhibition (Streijger et al., 2004; F. Streijger and C.E.E.M. Van der Zee, unpublished observation). In this study, the CK^{-/-} mice revealed a similar 4-fold startle response decrease, which was confirmed by the acoustic startle profile (stimuli in the range of 70-150 dB). The acoustic startle profile, however, did not exclude the possibility of a (partial) hearing deficit. Based on the observation that CK^{-/-} mice displayed a prepulse inhibition response to the 86 dB prepulse, which is only 14 dB above the threshold prepulse of 72

dB, we concluded that their hearing is normal. Although the lower startle amplitude may also be explained by a general later onset of the response reaction, this is not very likely because the startle latency of CK^{-/-} mice was not altered. In addition, the lower average body weight of CK^{-/-} animals does not seem to contribute to the lower startle response, since the UbCKmit^{-/-} and BCK^{-/-} single knockout mice displayed similarly low startle amplitudes upon the 120 dB stimulus, while having normal body weights (Jost et al., 2002; Streijger et al., 2004).

Taken together our findings strongly suggest that, in the startle reflex brain circuitry, which includes the auditory nerve, the cochlear root neurons, the nucleus reticularis pontis caudalis, and the spinal motor neuron (Swerdlow et al., 2001), the full absence of the brain-type creatine kinases energy shuttle has created a new situation with impaired or rewired neurotransmission.

4.2. The role of creatine kinase in brain

Our earlier studies revealed that mice with either cytosolic BCK or mitochondrial UbCKmit deficiency revealed only a mild phenotype upon behavioral testing (Table 2). A ³¹P magnetic resonance spectroscopy of whole brain showed a reduced, but not entirely blocked, phosphorus exchange capacity (i.e., ~P flux) for BCK^{-/-} animals, and both single knockouts displayed unchanged PCr peaks (Jost et al., 2002; In 't Zandt et al., 2000; In 't Zandt et al., 2004). These results support a model in which enzymes still present at the cytosolic BCK or mitochondrial UbCKmit endpoint can reciprocally compensate for the loss of enzymes at the other endpoint of the CK shunt. However, it is still unclear whether the contributions of the cytosolic and mitochondrial enzymes are coupled in a cell autonomous fashion, as if every single cell is a metabolic isolate, or whether PCr (and Cr and ATP) can also be shunted and shared between adjacent neural and glial cells, across gap-junctional connections or other pathways for metabolic cooperation. We do know, however, that complete absence of both brain-type creatine kinases results in complete disappearance of the PCr peak in CK^{-/-} brain. Unexpectedly, levels of free Cr are slightly higher but ATP and pH levels are surprisingly normal (In 't Zandt et al., 2000; In 't Zandt et al., 2004).

To explain all our findings at the mechanistic level we must distinguish between two extremes, namely that global CK absence affects either (i) the global cellular distribution and/or connectivity in the CNS, or (ii) only the metabolic status (and thus the cellular performance under challenge) in cells in essential brain regions coupled to behavior and cognition. Based on the following pieces of evidence we favor the first model, but cannot exclude a combination of effects. We noticed that CK^{-/-} mice display, besides a lower body weight, also a significantly reduced overall brain size. In addition, a smaller hippocampus and regio inferior area was observed. However, the relative sizes for the supra-pyramidal and intra- infra-pyramidal mossy fiber projection fields did not remain in proportion, but were increased. Since BCK^{-/-} brains contained only larger intra- infra-pyramidal field sizes (Jost et al., 2002), CK^{-/-} brains appear to be more affected.

It is interesting to note that the BCK and UbCKmit proteins are increasingly expressed after the first postnatal week and reach a maximum in expression level around the time of most intense neuritogenesis and neurogenesis. Assuming that phosphotransfer through the CK system has not only a role in neuronal physiology, but also may be involved in cell differentiation or actin-based cell motility (a major ATP consuming process in brain; Bernstein and Bamburg, 2003), like axon outgrowth and growth cone motility (Gungabissoon and Bamburg, 2003), it is conceivable that CK absence affects postnatal development. Further study is necessary to examine if development of neuronal connections, including the process of postnatal pruning (Bagri et al., 2003) in the mossy fiber projection fields, is particularly sensitive or just one feature of a more general effect on neuron-glia cell distribution throughout the brain.

In conclusion, we here provided evidence that the complete lack of CK in brain alters behavior and severely impairs spatial learning, nestbuilding activity, and startle responses. Our present findings raise the possibility that these effects do not only have a purely metabolic/physiological basis, but are also due to effects on the development of the cellular-synaptic circuitry involved in sensory-induced activity regulation. Of importance will be the determination of the molecular processes that sense the impairment in the high-phosphoryl energy transfer system and translate this in altered axonal outgrowth or synapse formation.

Acknowledgement

This work was supported by NWO Program grants 901-01095 and 901-01191 (to B. Wieringa) and a NMR facility grant (to A. Heerschap) from the Dutch Organization for Scientific Research (NWO, Medical Sciences). We thank Dr. M. Oitzl for her assistance with the set-up of the circular hole board test, and our colleagues in the Central Animal Facility for help and advice with the animal care.

References

Bagri A, Cheng HJ, Yaron A, Pleasure SJ, Tessier-Lavigne M (2003) Stereotyped pruning of long hippocampal axon branches triggered by retraction inducers of the semaphorin family. *Cell* 113:285-299.

Barinaga M (1997) What makes brain neurons run? *Science* 276:196-198.

Beal MF (1992) Does impairment of energy metabolism result in excitotoxic neuronal death in neurodegenerative illnesses? *Ann Neurol* 31:119-130.

Belliveau JW, Kennedy DN Jr, McKinstry RC, Buchbinder BR, Weisskoff RM, Cohen MS, Vevea JM, Brady TJ, Rosen BR (1991) Functional mapping of the human cortex by magnetic resonance imaging. *Science* 254:716-719.

Bernstein BW, Bamburg JR (2003) Actin-ATP hydrolysis is a major energy drain for neurons. *J Neurosci* 23:1-6.

Bessman SP, Carpenter CL (1985) The creatine-creatine phosphate energy shuttle. *Annu Rev Biochem* 54:831-862.

Boero J, Qin W, Cheng J, Woolsey TA, Strauss AW, Khuchua Z (2003) Restricted neuronal expression of ubiquitous mitochondrial creatine kinase: changing patterns in development and with increased activity. *Mol Cell Biochem* 244:69-76.

Crawley J, Goodwin FK (1980) Preliminary report of a simple animal behavior model for the anxiolytic effects of benzodiazepines. *Pharmacol Biochem Behav* 13:167-170.

Crusio WE, Bertholet JY, Schwegler H (1990) No correlations between spatial and non-spatial reference memory in a T-maze task and hippocampal mossy fiber distribution in the mouse. *Behav Brain Res* 41:251-259.

Danscher G (1981) Histochemical demonstration of heavy metals. A revised version of the sulphide silver method suitable for both light and electron microscopy. *Histochemistry* 71:1-16.

Erecinska M, Silver IA (1994) Ions and energy in mammalian brain. *Prog Neurobiol* 43:37-71.

Fox PT, Raichle ME, Mintun MA, Dence C (1988) Nonoxidative glucose consumption during focal physiologic neural activity. *Science* 241:462-464.

Gerlai R (1998) A new continuous alternation task in T-maze detects hippocampal dysfunction in mice. A strain comparison and lesion study. *Behav Brain Res* 95:91-101.

Gerlai R (2001) Behavioral tests of hippocampal function: simple paradigms complex problems (Review). *Behav Brain Res* 25:269-277.

Grootendorst J, de Kloet ER, Vossen C, Dalm S, Oitzl MS (2001) Repeated exposure to rats has persistent genotype-dependent effects on learning and locomotor activity of apolipoprotein E knockout and C57Bl/6 mice. *Behav Brain Res* 125:249-259.

Gungabissoon RA, Bamberg JR (2003) Regulation of growth cone actin dynamics by ADF/cofilin. *J Histochem Cytochem* 51:411-420.

Heeren DJ, Cools AR (2002) Classifying postures of freely moving rodents with the help of Fourier descriptors and a neural network. *Behav Res Methods Instrum Comput* 32:56-62.

Hölscher C (1999) Stress impairs performance in spatial water maze learning tasks. *Behav Brain Res* 100:225-235.

Iivonen H, Nurminen L, Harri M, Tanila H, Puolivali J (2003) Hypothermia in mice tested in Morris water maze. *Behav Brain Res* 141:207-213.

Ikonomidou C, Turski L (1996) Neurodegenerative disorders: Clues from glutamate and energy metabolism. *Crit Rev Neurobiol* 10:239-

263.

In 't Zandt, HJA. Quantitative ^1H and ^{31}P MR-spectroscopy and -imaging reveal changes in metabolite levels and morphology of creatine kinase (CK) -deficient mouse brain. Thesis book: University of Nijmegen, The Netherlands. ISBN # 9064642054; 2000. p.141-163.

In 't Zandt, HJA, Renema WKJ, Streijger F, Jost C, Klomp DWJ, Oerlemans F, Van der Zee CEEM, Wieringa B, Heerschap, A (2004) Cerebral creatine kinase deficiency influences metabolite levels and morphology in the mouse brain: a quantitative in vivo ^1H and ^{31}P Magnetic resonance study. *J Neurochem* 90:1321-1330.

Jost RJ, Van der Zee CEEM, in 't Zandt HJA, Oerlemans F, Verheij M, Streijger F, Franssen J, Heerschap A, Cools AR and Wieringa B (2002) Creatine kinase B-driven energy transfer in the brain is important for habituation and spatial learning behavior, mossy fiber field size and determination of seizure susceptibility. *Eur J Neurosci* 15:1692-1702.

Khakh BS (2001) Molecular physiology of P2X receptors and ATP signaling at synapses. *Nature reviews* 2:165-174.

Laghmouch A, Bertholet JY, Crusio WE (1997) Hippocampal morphology and open-field behavior in *Mus musculus domesticus* and *Mus spretus* inbred mice. *Behav Genet* 27:67-73.

Liu J, Head E, Gharib AM, Yuan W, Ingersoll RT, Hagen TM, Cotman CW, Ames BN (2002) Memory loss in old rats is associated with brain mitochondrial decay and RNA/DNA oxidation: partial reversal by feeding acetyl-L-carnitine and/or R- α -lipoic acid. *Proc Natl Acad Sci USA* 99:2356-2361.

Lynch CB (1980) Response to divergent selection for nesting behavior in *Mus musculus*. *Genetics* 96:757-765.

Molloy GR, Wilson CD, Benfield P, de Vellis J, Kumar S (1992) Rat brain creatine kinase messenger RNA levels are high in primary cultures of brain astrocytes and oligodendrocytes and low in neurons. *J Neurochem* 59:1925-1932.

O'Gorman E, Beutner G, Wallimann T, Brdiczka D (1996) Differential effects of creatine depletion on the regulation of enzyme activities and on creatine-stimulated mitochondrial respiration in skeletal muscle, heart, and brain. *Biochim Biophys Acta* 1276:161-170.

Ross BD, Bluml S (1996) New aspects of brain physiology. *NMR Biomed* 9:279-296.

Sakic B, Szechtman H, Talangbayan H, Denburg SD, Carbotte RM, Denburg JA (1994) Disturbed emotionality in autoimmune MRL-lpr mice. *Physiol Behav* 56:609-617.

Schwegler H, Crusio WE (1995) Correlations between radial-maze learning and structural variations of septum and hippocampus in rodent. *Behav Brain Res* 67:29-41.

Shen W, Willis D, Zhang Y, Schlattner U, Wallimann T, Molloy GR (2002) Expression of creatine kinase isoenzyme genes during post-natal development of rat brain cerebellum: evidence for transcriptional regulation. *J Biochem* 367:369-380.

Sluyter F, Marican CC, Crusio WE (1999) Further phenotypical characterisation of two substrains of C57BL/6J inbred mice differing by a spontaneous single-gene mutation. *Behav Brain Res* 98:39-43.

Steeghs K, Benders A, Oerlemans F, De Haan A, Heerschap A, Ruitenbeek W, Jost C, Van Deursen J, Perryman B, Pette D, Bruckwilder M, Koudijs J, Jap PH, Veerkamp J, Wieringa B (1997) Altered Ca²⁺ responses in muscles with combined mitochondrial and cytosolic creatine kinase deficiencies. *Cell* 89:93-103.

Steeghs K, Oerlemans F, Wieringa B (1995) Mice deficient in ubiquitous mitochondrial creatine kinase are viable and fertile. *Biochim Biophys Acta* 1230:130-138.

Streijger F, Jost RJ, Oerlemans F, Ellenbroek BA, Cools AR, Wieringa B, van der Zee CEEM (2004) Mice lacking the UbCKmit isoform of creatine kinase reveal slower spatial learning acquisition, diminished exploration and habituation, and reduced acoustic startle reflex re-

sponses. *Mol Cell Biochem* 256-257:305-318.

Swerdlow NR, Geyer MA, Braff DL (2001) Neural circuit regulation of prepulse inhibition of startle in the rat: current knowledge and future challenges. *Psychopharmacology* 156:194-215.

Tchernichovski O, Golani I (1995) A phase plane representation of rat exploratory behavior. *J Neurosci Methods* 62:21-27.

Van der Zee CEEM, Rashid K, Le K, Moore K-A, Stanisiz J, Diamond J, Racine RJ, Fahnestock M (1995) Intraventricular administration of antibodies to nerve growth factor retards kindling and blocks mossy fiber sprouting in adult rats. *J Neurosci* 15:5316-5323.

Wallace DC (1999) Mitochondrial diseases in man and mouse. *Science* 283:1482-1488.

Wallimann T, Wyss M, Brdiczka D, Nicolay K, Eppenberger HM (1992) Intracellular compartmentation, structure and function of creatine kinase isoenzymes in tissues with high and fluctuating energy demands: the 'phospho-creatine circuit' for cellular energy homeostasis. *Biochem J* 281:21-40.

Wendt S, Schlatter U, Walliman T (2003) Differential effects of peroxynitrite on human mitochondrial creatine kinase isoenzymes - Inactivation, octamer destabilization, and identification of involved residues. *J Biol Chem* 278:1125-1130.

Whishaw IQ, Tomie JA (1996) Of mice and mazes: similarities between mice and rats on dry land but not water mazes. *Physiol Behav* 60:1191-1197.

Wyss M, Kaddurah-Daouk R (2000) Creatine and creatine metabolism. *Physiol Rev* 80:1107-1213.

Chapter 4

Hair Bundles Are Specialized for ATP Delivery via Creatine Kinase

Jung-Bum Shin¹, Femke Streijger², Andy Beynon³, Theo Peters³,
Laura Gadzala¹, Debra McMillen⁴, Cory Bystrom⁴, Catharina E.E.M.
Van der Zee², Theo Wallimann⁵, and Peter G. Gillespie¹

¹ Oregon Hearing Research Center and Vollum Institute, Oregon Health and Science University, Portland, OR 97239, USA.

² Department of Cell Biology, NCMLS, Radboud University Nijmegen Medical Centre, 6500 HB Nijmegen, The Netherlands.

³ Department of Otorhinolaryngology, Radboud University Nijmegen Medical Centre, 6500 HB Nijmegen, The Netherlands.

⁴ Proteomics Shared Resource, Oregon Health & Science University, Portland, OR 97239, USA

⁵ Institute of Cell Biology, ETH-Zurich, Hoenggerberg, CH-8093 Zurich, Switzerland.

In Neuron 2007

Volume 53:371-386.

Abstract

When stimulated strongly, a hair cell's mechanically sensitive hair bundle may consume ATP too rapidly for replenishment by diffusion. To provide a broad view of the bundle's protein complement, including those proteins participating in energy metabolism, we used shotgun mass spectrometry methods to identify proteins of purified chicken vestibular bundles. In addition to cytoskeletal proteins, proteins involved in Ca^{2+} regulation, and stress-response proteins, many of the most abundant bundle proteins that were identified by mass spectrometry were involved in ATP synthesis. After β -actin, the cytosolic brain isoform of creatine kinase was the next most abundant bundle protein; at 0.5 mM, creatine kinase is capable of maintaining high ATP levels despite 1 mM/s ATP consumption by the plasma-membrane Ca^{2+} -ATPase. Consistent with this critical role in hair bundle function, the creatine kinase circuit is essential for high-sensitivity hearing as demonstrated by hearing loss in creatine kinase knockout mice.

1. Introduction

Hair cell mechanotransduction is direct; displacement of the mechanically sensitive hair bundle leads to immediate gating of cation-selective transduction channels. Although metabolic energy apparently is not required for mechanotransduction itself, ATP is essential for myosins that carry out adaptation of the transduction current (Gillespie and Cyr, 2004) and bundle assembly (Lin et al., 2005). Moreover, treadmilling actin (Schneider et al., 2002), and phosphoinositide turnover (Hirono et al., 2004) also require ATP consumption. Quantitatively, the most significant drain on ATP levels in the hair bundle is probably Ca^{2+} pumping by the plasma-membrane Ca^{2+} -ATPase isoform 2 (PMCA2). Even with the low concentrations of Ca^{2+} that bathe the hair bundle, Ca^{2+} carries a substantial fraction of the transduction current (Lumpkin et al., 1997; Ricci and Fettiplace, 1998); moreover, bundle PMCA2 removes the majority of the entering Ca^{2+} (Lumpkin and Hudspeth, 1998), which can occur at a rate of >1 mM/s (Ricci and Fettiplace, 1998; Yamoah et al., 1998; see supplemental data).

Hair bundles consist of dozens of stereocilia, typically 2-15 μm in length, each of which is packed with actin filaments. Stereocilia have no mitochondria and thus might rely on diffusion of ATP from mitochon-

dria located at their bases. However, diffusion cannot deliver sufficient ATP to stereocilia tips to maintain Ca^{2+} pumping (see Discussion), suggesting that stereocilia use alternative methods for delivering ATP to PMCA2 and other ATPases.

Understanding how hair bundles maintain energy homeostasis has been hampered by our limited knowledge of proteins present in the bundle. Although several methods for bundle isolation have been developed (Neugebauer and Thurm, 1984; Tilney et al., 1989; Shepherd et al., 1989; Gillespie and Hudspeth, 1991), the scarcity of hair cells has prevented thorough cataloging of bundle proteins. Another approach, identification of “deafness genes,” has successfully discovered proteins which are essential for and specific to the inner ear (Petit, 2006), but this approach fails to identify proteins important for bundle function that play indispensable roles elsewhere.

Recent technical advances have made mass spectrometry into a practical tool for identification and quantification of hair bundle proteins. Here we report the characterization of the proteins from hair bundles of the chicken utricle, a vestibular organ; we note that a large number of proteins consistently detected in the preparation are involved in energy metabolism. Not only are glycolytic enzymes abundant, but the cytosolic brain isoform of creatine kinase is present at high enough levels to be primarily responsible for ATP delivery to PMCA2 and other bundle ATPases. Consistent with that conclusion, mice lacking brain creatine kinase have vestibular dysfunction and reduced hearing sensitivity.

2. Materials and Methods

2.1 Hair bundle isolation

Bundle isolation from E20 utricles of White Leghorn chicken (*Gallus domesticus*) embryos was carried out as described previously (Gillespie and Hudspeth, 1991) with modifications for chicken (supplemental data). While the White Leghorn strain is different from the Red Jungle Fowl strain (*Gallus gallus*) used for genome sequencing, DNA from the two strains differs in sequence by only ~1% (http://www.ensembl.org/Gallus_gallus/index.html). Because mass spectrometry peptide identification tolerates small numbers of amino acid differences (specified when setting the search parameters), this level of se-

quence difference should have had little effect on protein identification. Moreover, amino acid sequence differences between proteins of the two strains will likely be much less than the 1% difference seen at the DNA level. Measurement of total protein and quantitative immunoblotting was performed as described in the supplemental data.

2.2 Mass spectrometry via LC-MS/MS and MuDPIT

Agarose plugs containing hair bundles were dried in a vacuum centrifuge. The agarose was rehydrated with 10 mM DTT, minced, and incubated at 35°C for 30 min. Iodoacetamide was added to 15 mM and the samples were incubated in the dark for 30 min. The samples were dried, then trypsin (20 ng/ml; Sequencing Grade Modified Trypsin, Promega) was added to reswell the agarose; the sample was sonicated during rehydration. The sample was then adjusted to 10% acetonitrile and digested overnight at 37°C. Peptides were extracted via two additions of 80 μ l of 1% formic acid, each followed by sonication. Acidified peptides were desalted on a StageTip (Proxeon), dried, and resuspended in 1% formic acid containing 2.5 mM ammonium acetate.

Tryptic peptides from digests were analyzed by nano-LC-MS/MS. Chromatography was achieved using an Eksigent nanoLC to generate a gradient using the following chromatographic conditions: mobile phase A: water, acetonitrile, formic acid, trifluoroacetic acid (95, 4.89, 0.1, 0.01, v/v/v/v); mobile phase B: acetonitrile, isopropanol, water, formic acid, trifluoroacetic acid (80, 10, 9.89, 0.1, 0.01, v/v/v/v/v). Mobile phase B was ramped from 2% to 45% over 40 min, increased to 80% in 5 min, and held for 5 min before being returned to starting conditions. Flow was regulated at 200 nl/min and directed through a 75 μ m \times 15 cm column packed in-house with Astrosil (5 μ m particle size, 100 Å pore size, C18 reverse phase chemistry; Stellar Phases) coupled to a 5 μ m tapered emitter (New Objectives). Prior to analytical chromatography, 5 μ l of tryptic digest was injected onto a 150 μ m \times 2 cm sample trap packed with Poros R10; the trap was washed with mobile phase A to remove salts and contaminants, then was switched in-line with the analytical column. Tandem mass spectrometry data was collected using a QSTAR XL hybrid time-of-flight mass spectrometer (Applied Biosystems) under the following conditions: spray voltage 1800V-1900V; TOF-MS scan mass-to-charge value (m/z) 400-1600,

0.5 s; TOF-MS/MS scan m/z 50-2000, 2.0 s, 90 s exclusion; data dependent product ion acquisition of the three most abundant +2 and +3 ions from the TOF-MS scan.

For MuDPIT, the instrumentation described above was used with the following changes. A 5 cm, lab-packed SCX column was prepared for ion-exchange chromatography (Polysulfoethyl A, 5 μm particle size, 300 \AA) as instructed by the manufacturer. Analytical columns of 75 and 50 μm diameter were used at flow rates of 200 or 100 nl/min , respectively. Tryptic peptides from a hair bundle digest were injected onto the SCX column and the breakthrough was analyzed as the first fraction. Additional pools of peptides were displaced from the ion exchange column via ammonium acetate injections (5, 10, 15, 20, 25, 30, 35, 40, 45, 50, 75, 100, 150, and 300 mM); each eluate was separately run on nano-LC-MS/MS as described above.

2.3 Mass spectrometry via GeLC-MS/MS

Hair bundle proteins were resolved by 1D SDS-PAGE; individual lanes of Sypro Orange-stained gels were cut into ~45 individual slices using a 2DiDx sample preparation robot (Leap Technologies). Individual gel slices were placed in a ZipPlate (Millipore), which was used as a filter to facilitate tryptic digestion. Gel slices were destained in two changes of 100 mM ammonium bicarbonate in 30% methanol, dried with neat acetonitrile, reduced with 10 mM DTT, and alkylated with 50 mM iodoacetamide. After washing and drying, approximately 100 ng of sequencing grade trypsin in 20 mM ammonium bicarbonate was added to each sample along with sufficient buffer to completely immerse the gel slices in buffer. Digestion proceeded overnight at 37°C. After acidifying samples with 10 μl of 1% formic acid, the peptide extract was collected by centrifugation; the gel slices were further extracted with two additions each of 50% and 70% acetonitrile. Peptide extracts were brought to near dryness before being resuspended in 10 μl of 0.1% formic acid in preparation for nano-LC-MS/MS.

2.4 Protein identification

Monoisotopic masses for database searching were generated using Distiller (Matrix Science) and submitted to X! Tandem for protein identification. Masses were searched against the Ensembl database

(Ensembl Gallus gallus WASHUC 1, v 37.1) with the following parameters: fixed modification, cysteine carbamidomethylation; variable modification, methionine oxidation; one missed cleavage allowed; digest agent, trypsin; refinement modifications, methionine oxidation and N/Q deamidation, as well as one point mutation allowed; no removal of redundant spectra; precursor and fragment ion mass tolerances of 100 ppm and 0.2 Da, respectively.

We generated Table 1 as follows. Protein isoforms identified with the same set of peptides were inspected manually to determine the most abundant isoform; this step applied to actin, creatine kinase, tubulin, and enolase. Because of contamination by human skin keratin, we manually deleted all intermediate filament identifications. Likewise, hemoglobin identifications were removed, as they resulted from red blood cell contamination (data not shown). We wrote a Mathematica 5.0 program to automatically select proteins that fit the criteria we used for Table 1.

2.5 Immunocytochemistry

Auditory and vestibular organs from chicken embryos (E20) were dissected in chicken saline and processed for immunocytochemistry (supplemental data). The antibodies for GAPDH, CLIC5, NHERF, and BCK required an unmasking procedure to expose the antigenic sites. Organs were fixed as usual in formaldehyde, then boiled in a citrate-based antigen unmasking solution (Vector Laboratories, Burlingame CA) for 5-10 min in a microwave. Organs were then washed in PBS and blocked in blocking solution as usual. The unmasking procedure inhibits phalloidin binding, presumably by disrupting F-actin structure; in experiments requiring antigen unmasking, actin counterstaining was achieved using a monoclonal anti- β -actin antibody (AC-15, Sigma; 1:400). AC-15 only detected stereocilia actin after unmasking.

2.6 ATP determination

Bullfrog hair cells were isolated in low-calcium saline (110 mM NaCl, 2 mM KCl, 2 mM MgCl₂, 0.1 mM CaCl₂, 3 mM D-glucose, and 10 mM HEPES [pH 7.25]) as described previously (Hirono et al., 2004). Total ATP was quantified using the Enliten luciferin/luciferase kit (Promega) using methods described in the supplemental data.

2.7 Magnesium green fluorescence

Bullfrog hair cells were isolated as described above; 3 mM Magnesium Green AM dye (Invitrogen Molecular Probes) was included in the dissociation solution. After hair cells had settled, the solution was replaced by standard saline (low-calcium saline with 4 mM CaCl₂) containing 6.66 mM Mg Green AM. After 20 min of dye loading time, cells were washed with standard saline and allowed to de-esterify for an additional 20 min. Cells were viewed with a Plan Apochromat 603 (1.40 NA) oil lens on a Nikon TE 300 inverted microscope with a Bio-Rad MRC 1024 confocal imaging system. For inhibition of creatine kinase, a 10 mM stock solution of DNFB was diluted to a final concentration of 10 mM in the experimental chamber. Before adding DNFB, the basal Mg Green fluorescence was monitored for at least 6 min in order to ensure a relatively stable baseline. Image analysis was performed using ImageJ software; data were fitted to single-exponential functions.

2.8 Analysis of creatine kinase knockout mice

To obtain heterozygous BCK/UbCKmit^{+/-} mice, BCK^{-/-} single-knockout mice (Jost et al., 2002) and UbCKmit^{-/-} single-knockout mice (both 25% 129/Ola and 75% C57BL/6) were interbred. Breeding between heterozygous pairs generated heterozygous siblings, homozygous siblings with wildtype CK alleles (BCK/UbCKmit^{+/+}), and homozygous double-knockout siblings (BCK^{-/-}UbCKmit^{-/-}). Homozygous siblings were interbred to generate two separate lines with the same genetic background: (1) wildtype mice, and (2) mice lacking both CK isoforms (CK^{-/-} mice; Streijger et al., 2005). Histological analysis, ABR measurements, and vestibular tests were carried out as described in the supplemental data.

2.9 Mechanotransduction and adaptation

Mechanotransduction currents were measured from bullfrog sacculi with a two-compartment transepithelial voltage-clamp apparatus (Corey and Hudspeth, 1983), as described in the supplemental data.

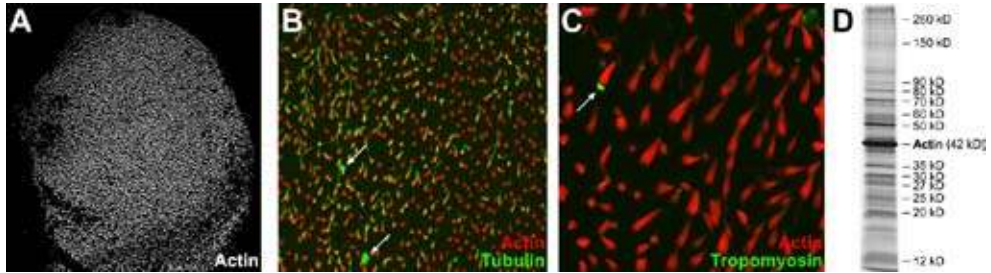


Figure 1: Chicken Utricle Hair Bundle Isolation. (A) Purified hair bundles, embedded in agarose, stained with phalloidin to highlight actin. Panel is $1121 \times 1121 \mu\text{m}$. (B) Purified hair bundles stained with phalloidin (red) and anti-tubulin (green). Note presence of kinocilia in most bundles but only minimal soma tubulin contamination (arrow, example of soma tubulin). Panel is $192 \times 192 \mu\text{m}$. (C) Purified hair bundles stained with phalloidin (red) and anti-tropomyosin (green). Note the scarcity of cuticular plates (arrow, example of cuticular plate). Panel is $96 \times 96 \mu\text{m}$. (D) One-dimensional SDS-PAGE separation of purified hair bundle proteins; gel was silver-stained. Migration positions corresponding to actin and major bundle bands are indicated.

3. Results

3.1 Chicken hair bundle purification

We used a modification of the twist-off method (Gillespie and Hudspeth, 1991) to purify hair bundles from embryonic day 20 (E20) chicken utricles (Fig. 1A); at this age, utricles have $>20,000$ hair cells (Goodyear et al., 1999) and the vestibular system is functional (Jones and Jones, 1996). Purity of the bundle preparation was assessed by immunolabeling isolated bundles with tubulin antibodies (to detect cell bodies), tropomyosin antibodies (to detect cuticular plates), MitoTracker (to detect mitochondria), and DAPI (to detect nuclei). Kinocilia were isolated along with most hair bundles and were well stained with anti-tubulin; by contrast, little additional tubulin staining was seen (Fig. 1B; see also Fig. 3A). Cuticular plates were rare; tropomyosin labeling was associated with about 1 in every 50 bundles (Fig. 1C). No Mito-Tracker or DAPI staining was detected, suggesting the absence of mitochondrial or nuclear contamination (data not shown). Although these experiments indicated that there was minimal contamination of the bundle preparation, we cannot exclude that some individual preparations may have had contaminating cell bodies, and hence a few nuclei or mitochondria. Because the somatic volume exceeds the bundle volume

by more than 20-fold, a small number of copurified cell bodies might skew the set of bundle proteins. Nevertheless, we are confident that our bundle isolations are sufficiently clean enough to achieve a high enrichment of bundle proteins. Indeed, the amount of PMCA2 immunoblot signal normalized to total protein increased 80-fold in bundles compared with whole utricles (data not shown), suggesting that substantial enrichment was achieved with the bundle isolation.

As in frog hair bundles (Gillespie and Hudspeth, 1991), a protein that comigrated with actin (42 kDa) was the predominant protein in purified bundles (Fig. 1D), accounting for 25%-50% of the protein in the bundles. Another 15 or so proteins appeared reproducibly as major bands in the preparation (Fig. 1D).

3.2 Mass spectrometry identifies abundant hair bundle proteins

Although hair bundle proteins are scarce, mass spectrometry has sufficient sensitivity to detect many proteins of the bundle preparation. We used bundles from ~100 chicken utricles (1-2 μ g of total bundle protein) for each of five complementary shotgun mass spectrometry experiments (see Table S1 in the supplemental data). In one approach, 1D PAGE protein separation-nanocapillary LC-MS/MS analysis (GeLC-MS/MS; Rezaul et al., 2005), we separated purified bundle proteins using one-dimensional SDS-PAGE, cut gel slices with a robot, and separately digested the 35-45 slices with trypsin. Each sample was subsequently analyzed with reverse-phase liquid chromatography-tandem mass spectrometry (LC-MS/MS). In other experiments, we directly digested agarose-embedded hair bundles with trypsin, then analyzed bundle peptides either directly with LC-MS/MS or the MuDPIT method (Washburn et al., 2001), which introduces a cation-exchange step prior to LC-MS/MS.

Using the X! Tandem search algorithm accessed via the Global Protein Machine interface (Craig et al., 2004), we searched mass spectrometry data against the Ensembl database of predicted chicken proteins derived from the chicken genome sequencing project (International Chicken Genome Sequencing Consortium, 2004). Because assignment algorithms do not absolutely identify proteins, confidence in protein identification depends on the search stringency. We used two measures that indicate the confidence of each identification. The log of the expectation value, $\log(e)$, indicates the probability that the

Table 1. Chicken utricle hair bundle proteins.

| Rank, IF | Rank, SCF | Identifier | Best # | Best log(e) | Best count | MW (kDa) | IF | SCF | Name |
|----------|-----------|---------------------|--------|-------------|------------|----------|--------|--------|--|
| 1 | 1 | ENSGALP00000002101 | 5 | -573.9 | 259 | 41.8 | 0.3373 | 0.2789 | Beta-actin (ACT5_CHICK) |
| 2 | 2 | ENSGALP00000018742 | 5 | -296.2 | 107 | 42.9 | 0.0651 | 0.0543 | Creatine kinase B (KCRB_CHICK) |
| 3 | 3 | ENSGALP00000023278 | 5 | -291.7 | 44 | 35.7 | 0.0406 | 0.0345 | Glyceraldehyde-3-phosphate dehydrogenase (G3P_CHICK) |
| 4 | 4 | ENSGALP00000005475 | 4 | -101.3 | 29 | 12.1 | 0.0297 | 0.0324 | Parvalbumin 3 (PRVU_CHICK) |
| 5 | 10 | ENSGALP00000016260 | 3 | -37.5 | 7 | 16.8 | 0.0152 | 0.0142 | Calmodulin (CaM) |
| 6 | 7 | ENSGALP00000010510 | 5 | -239.6 | 45 | 70.8 | 0.0145 | 0.0157 | Heat shock cognate 70 |
| 7 | 5 | ENSGALP00000013964 | 5 | -190.0 | 38 | 43.5 | 0.0139 | 0.0166 | Tubulin beta-2C (TUBB2C) |
| 8 | 8 | ENSGALP00000021618 | 5 | -66.1 | 25 | 36.3 | 0.0132 | 0.0157 | L-lactate dehydrogenase B (LDHB_CHICK) |
| 9 | 18 | ENSGALP00000017577 | 4 | -30.1 | 11 | 19.1 | 0.0129 | 0.0098 | Anterior gradient homolog (AG-3 protein) |
| 10 | 9 | ENSGALP00000026911 | 5 | -140.4 | 19 | 28.2 | 0.0125 | 0.0142 | Chloride intracellular channel protein 5 (CLIC5) |
| 11 | 14 | ENSGALP00000019165 | 4 | -37.6 | 6 | 12.2 | 0.0118 | 0.0118 | Histone H4 |
| 12 | 6 | ENSGALP00000023396 | 4 | -77.7 | 15 | 22.7 | 0.0114 | 0.0166 | Triosephosphate isomerase (TPIS_CHICK) |
| 13 | 11 | ENSGALP00000027650 | 5 | -162.5 | 36 | 68.4 | 0.0113 | 0.0133 | Radixin (RADI_CHICK) |
| 14 | 20 | ENSGALP00000019162 | 3 | -33.2 | 6 | 15.6 | 0.0102 | 0.0095 | Histone H2A |
| 15 | 13 | ENSGALP00000019365 | 5 | -111.0 | 15 | 37.5 | 0.0094 | 0.0120 | Annexin A5 |
| 16 | 15 | ENSGALP00000016978 | 4 | -202.6 | 31 | 50.8 | 0.0090 | 0.0109 | Tubulin alpha-1 (TBA1_CHICK) |
| 17 | 22 | ENSGALP00000011961 | 3 | -49.9 | 14 | 20.9 | 0.0090 | 0.0090 | Phosphatidylethanolamine-binding protein (PEBP) |
| 18 | 17 | ENSGALP00000003737 | 5 | -197.7 | 30 | 50.2 | 0.0086 | 0.0101 | Alpha-enolase (ENO1) |
| 19 | 19 | ENSGALP00000004164 | 5 | -166.4 | 27 | 70.9 | 0.0085 | 0.0097 | Fimbrin (FIMB_CHICK) |
| 20 | 16 | ENSGALP00000003012 | 4 | -101.5 | 18 | 35.6 | 0.0079 | 0.0102 | Malate dehydrogenase mitochondrial (MDH) |
| 21 | 21 | ENSGALP00000008988 | 5 | -121.2 | 19 | 39.0 | 0.0075 | 0.0093 | NHERF1 |
| 22 | 12 | ENSGALP00000012878 | 4 | -149.7 | 22 | 44.6 | 0.0072 | 0.0127 | Phosphoglycerate kinase (PGK_CHICK) |
| 23 | 24 | ENSGALP00000004703 | 4 | -20.3 | 7 | 19.3 | 0.0063 | 0.0068 | Ubiquitin (UBIQ_CHICK) |
| 24 | 26 | ENSGALP00000003665 | 3 | -20.4 | 4 | 12.7 | 0.0059 | 0.0059 | Calretinin (CALB2) |
| 25 | 25 | ENSGALP00000014374 | 5 | -62.6 | 10 | 36.5 | 0.0056 | 0.0064 | Malate dehydrogenase cytoplasmic |
| 26 | 29 | ENSGALP00000008647 | 3 | -21.5 | 10 | 20.7 | 0.0056 | 0.0056 | ADP-ribosylation factor 1 (ARF1) |
| 27 | 23 | ENSGALP00000004182 | 4 | -35.9 | 10 | 29.2 | 0.0054 | 0.0086 | 14-3-3 protein epsilon (14-3-3E) |
| 28 | 31 | ENSGALP00000001474 | 4 | -106.4 | 22 | 72.0 | 0.0054 | 0.0054 | GRP 78/BIP (GRP78_CHICK) |
| 29 | 28 | ENSGALP00000016523 | 4 | -83.4 | 33 | 83.4 | 0.0049 | 0.0057 | Heat shock protein HSP 90-beta (HS90B_CHICK) |
| 30 | 35 | ENSGALP00000016629 | 3 | -40.5 | 8 | 22.3 | 0.0047 | 0.0047 | Peroxiredoxin 1 |
| 31 | 27 | ENSGALP000000034108 | 4 | -117.7 | 18 | 58.0 | 0.0045 | 0.0058 | Pyruvate kinase muscle isozyme (KPYK_CHICK) |
| 32 | 30 | ENSGALP00000002695 | 5 | -111.9 | 13 | 60.6 | 0.0042 | 0.0054 | ATP synthase H+ transporting mitochondrial F1 alpha |

Table 1. Continued

| Rank, IF | Rank, SCF | Identifier | # | Best log(e) | Best count | MW (kDa) | IF | SCF | Name |
|----------|-----------|--------------------|---|-------------|------------|----------|--------|--------|--|
| 33 | 40 | ENSGALP00000018498 | 3 | -65.8 | 25 | 64.6 | 0.0039 | 0.0039 | Heat shock protein HSP 90-alpha (Q5ZIC0_CHICK) |
| 34 | 37 | ENSGALP00000017765 | 5 | -141.8 | 22 | 86.4 | 0.0038 | 0.0043 | EPLIN (epithelial protein lost in neoplasm) |
| 35 | 34 | ENSGALP00000017773 | 5 | -309.2 | 51 | 257.2 | 0.0036 | 0.0049 | Protein tyrosine phosphatase RQ (PTPRQ) |
| 36 | 42 | ENSGALP00000032508 | 3 | -33.4 | 7 | 27.7 | 0.0035 | 0.0035 | Glutathione transferase omega |
| 37 | 32 | ENSGALP00000025499 | 4 | -28.1 | 3 | 15.7 | 0.0034 | 0.0050 | Superoxide dismutase |
| 38 | 36 | ENSGALP00000018265 | 4 | -64.2 | 7 | 24.4 | 0.0034 | 0.0045 | 47 kDa heat shock protein (HSP47_CHICK) |
| 39 | 33 | ENSGALP00000010167 | 4 | -53.0 | 9 | 42.1 | 0.0033 | 0.0050 | L-lactate dehydrogenase A (LDHA_CHIC) |
| 40 | 39 | ENSGALP00000025573 | 4 | -258.7 | 34 | 147.5 | 0.0032 | 0.0042 | Myosin-VI |
| 41 | 38 | ENSGALP00000013574 | 4 | -93.3 | 13 | 50.4 | 0.0032 | 0.0043 | Protein disulfide-isomerase A3 |
| 42 | 44 | ENSGALP00000020744 | 4 | -113.5 | 15 | 92.3 | 0.0024 | 0.0029 | GRP94 (endoplasmic) (ENPL_CHICK) |
| 43 | 43 | ENSGALP00000020268 | 5 | -61.3 | 13 | 73.3 | 0.0024 | 0.0031 | Protein disulfide isomerase family A member 4 |
| 44 | 45 | ENSGALP00000007934 | 3 | -98.5 | 12 | 62.1 | 0.0022 | 0.0022 | Glucose phosphate isomerase |
| 45 | 48 | ENSGALP00000007997 | 3 | -26.2 | 5 | 31.2 | 0.0020 | 0.0020 | Voltage-dependent anion-selective channel protein 2 (VDAC-2) |
| 46 | 41 | ENSGALP00000026461 | 3 | -22.0 | 4 | 28.7 | 0.0020 | 0.0037 | 14-3-3 protein theta (14-3-3T) |
| 47 | 47 | ENSGALP00000000304 | 4 | -95.3 | 13 | 73.4 | 0.0018 | 0.0022 | Dihydropyrimidinase-related protein 2 (DRP-2) |
| 48 | 46 | ENSGALP00000013267 | 4 | -63.1 | 9 | 49.5 | 0.0016 | 0.0022 | GDP dissociation inhibitor 2 |
| 49 | 51 | ENSGALP00000014371 | 3 | -44.6 | 8 | 95.1 | 0.0015 | 0.0015 | Novel Ensembl prediction |
| 50 | 52 | ENSGALP00000007703 | 3 | -145.0 | 16 | 137.1 | 0.0012 | 0.0014 | Plasma membrane Ca ²⁺ ATPase 2 (ATP2B2) |
| 51 | 49 | ENSGALP00000011689 | 3 | -36.0 | 5 | 44.1 | 0.0012 | 0.0019 | Protein disulfide isomerase |
| 52 | 50 | ENSGALP00000009371 | 3 | -41.6 | 5 | 50.5 | 0.0011 | 0.0016 | Elongation factor 1-alpha 2 (EF-1-alpha-2) |
| 53 | 53 | ENSGALP00000003850 | 3 | -23.1 | 3 | 57.8 | 0.0010 | 0.0010 | T-complex protein 1 zeta-2 subunit |
| 54 | 54 | ENSGALP00000025506 | 3 | -21.6 | 3 | 64.5 | 0.0009 | 0.0009 | Malic enzyme 1 NADP(+)-dependent cytosolic |
| 55 | 55 | ENSGALP00000017926 | 3 | -26.7 | 6 | 62.4 | 0.0009 | 0.0009 | Phosphoglucomutase 1 |
| 56 | 56 | ENSGALP00000018987 | 3 | -25.4 | 4 | 61.0 | 0.0009 | 0.0009 | T-complex protein 1 alpha subunit (TCP-1-alpha) |
| 57 | 57 | ENSGALP00000011233 | 3 | -36.7 | 5 | 86.8 | 0.0008 | 0.0008 | 6-phosphofructokinase type C |
| 58 | 58 | ENSGALP00000002625 | 3 | -37.5 | 3 | 56.8 | 0.0006 | 0.0006 | Vacuolar H-ATPase B subunit osteoclast isozyme |
| 59 | 59 | ENSGALP00000008236 | 3 | -102.2 | 13 | 192.2 | 0.0004 | 0.0006 | Clathrin heavy chain |

Proteins were listed if they were (1) identified in at least three of five experiments (see Table S1), (2) had a log(e) of -20 or better in at least one experiment, and (3) had a total spectral count of three or more in at least one experiment. Key: Rank IF, rank order based on intensity factor (IF); Rank SCF, rank order based on spectral counting (spectral count factor; SCF); Identifier, Chicken Ensembl database reference identifiers; #, number of mass spectrometry experiments protein was identified in; Best log(e), lowest log(e) score for protein; Best count, largest spectral count for protein; MW (kDa), molecular mass in kDa; IF, intensity factor score; SCF, spectral count factor score; Name, descriptive name, with chicken gene name indicated in some cases.

identification occurred by chance (Fenyo and Beavis, 2003); the spectral count is the number of MS/MS spectra that were matched to the protein, and is approximately proportional to the abundance of the protein in the sample (Liu et al., 2004; Old et al., 2005). A total of 59 proteins were identified from the chicken hair bundle preparation using the following stringent selection criteria: $\log(e)$ score of < -20.0 in at least one experiment, spectral count of three or more in at least one experiment, and identification in a minimum of three of five mass spectrometry runs (Table 1). Although many other proteins were provisionally identified in our experiments (Table S1; supplemental data), the stringency of our selection conditions gives us confidence that the proteins in Table 1 were correctly identified.

We used two methods for obtaining an estimate of the amount of each protein in the preparation. In the first, we summed the raw ion-current intensities of all matched peaks in MS/MS spectra for a given protein, summed the intensities for each data set, then determined the relative intensity contribution of each protein, which we assumed to be proportional to protein mass (Powell et al., 2004; Prochasson et al., 2005). To compare approximate molar abundance, we normalized the data by dividing by molecular masses; we termed the resulting index an intensity factor (IF; Table 1). Because ion-current intensities vary depending both on mass spectrometer settings and on properties of each peptide, including recovery, capacity for ionization, and fragmentation properties (Ong and Mann, 2005), this quantitation method will be more accurate for proteins identified with large numbers of independent peptides, which is the case for the majority of the proteins in Table 1.

The ion-current intensity quantitation values were corroborated by quantitation using spectral counting, where the abundance of a protein in the original sample is considered to be proportional to the number of MS/MS spectra collected. Again, the ratio of spectral counts for a given protein relative to total spectral counts was adjusted for each protein molecular mass, yielding a spectral count factor (SCF; Table 1). Although quantitation with the two methods agreed well (Table 1; rank order correlation coefficient of 0.98), both measures should be considered to be only approximations of protein abundance.

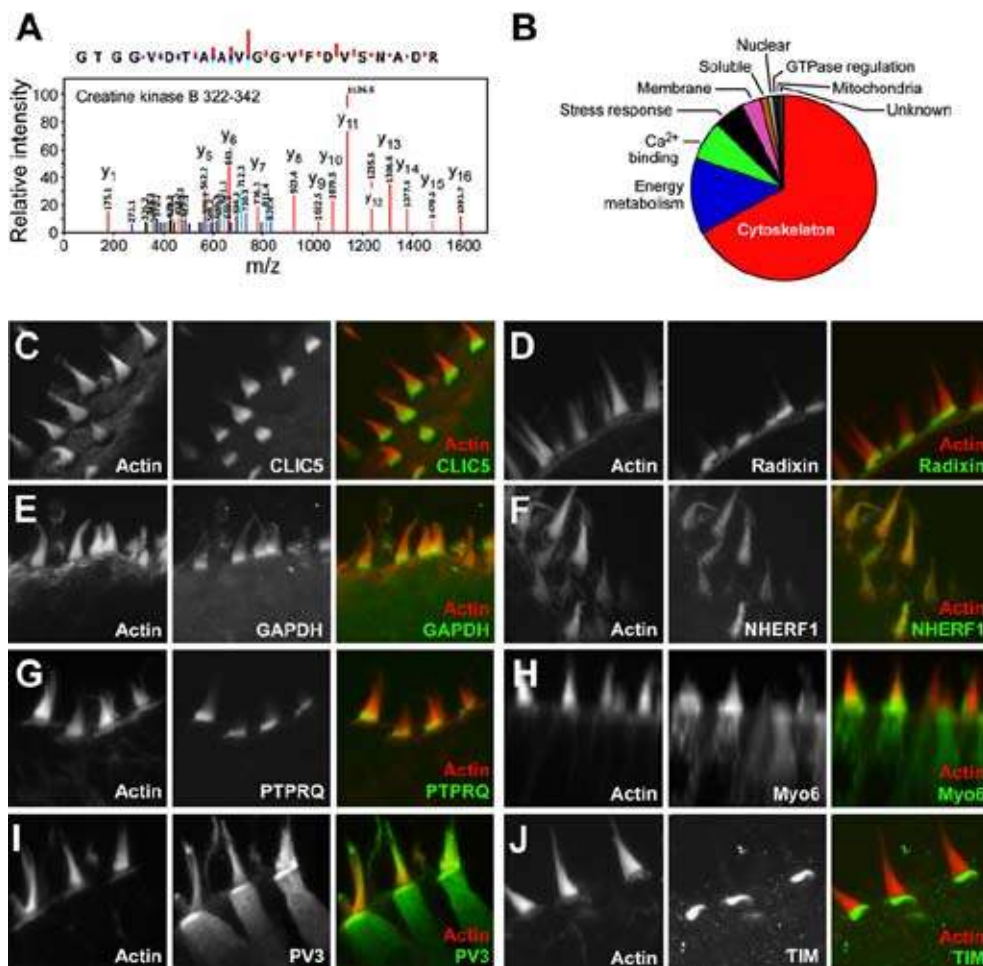
3.3 Classification of abundant hair bundle proteins

Our mass spectrometry results allowed us to identify what are likely the most abundant hair bundle proteins. As expected, cytoskeletal proteins dominated; the protein with the largest intensity and spectral-count factors was β -actin (Table 1). In addition, other cytoskeletal proteins known to be present in bundles (fimbrin, radixin, tubulin) were also prominent. On the basis of its apparent abundance and colocalization with radixin, we have argued that chloride intracellular “channel” 5 (CLIC5) is also a cytoskeletal protein (Gagnon et al., 2006). Na^+ - H^+ exchanger regulatory factor 1 (NHERF1), a widely expressed scaffolding protein that also interacts with radixin (Shenolikar et al., 2004), was also present. Another cytoskeletal protein consistently detected was epithelial lost in neoplasm (EPLIN), which has been shown to crosslink actin filaments and prevent filament branching (Maul et al., 2003). Finally, we detected two T-complex polypeptides, which are specialized chaperones for tubulin (Lopez-Fanarraga et al., 2001) and actin (Liang and MacRae, 1997).

Proteins involved in sequestration and removal of Ca^{2+} were also readily identified, including the mobile Ca^{2+} buffers parvalbumin 3 (Heller et al., 2002), calmodulin (Walker et al., 1993), and calretinin (Edmonds et al., 2000), as well as PMCA2 (Dumont et al., 2001). At least one other transmembrane protein, PTPRQ (Goodyear et al., 2003), was detected, as were two peripheral membrane proteins, annexin A5 and phosphatidylethanolamine binding protein. Two mitochondrial membrane proteins, ATP synthase a subunit and voltage-dependent anion-selective channel protein 2, were detected, suggesting a small amount of mitochondrial contamination of the bundle preparation. Several proteins involved in stress responses were noted, including heat shock cognate 70 (Hsc70), which has been detected in hair cells previously (Neely et al., 1991).

Several less-abundant proteins expressed from deafness genes (e.g., myosin-VIIIa, cadherin 23, espin, harmonin, and very large G protein-coupled receptor 1 (VLGR1) were detected in one or more mass spectrometry runs, but did not meet the stringent criteria used for Table 1 (data not shown). More sensitive or exhaustive mass spectrometry experiments should permit more consistent detection of these scarce proteins.

Finally, a striking result was the abundance of proteins involved



in energy metabolism, including the cytosolic brain isoform of creatine kinase (creatine kinase B or BCK; Fig. 2A); the glycolytic enzymes glyceraldehyde-3-phosphate dehydrogenase (GAPDH), triosephosphate isomerase (TIM), enolase, and pyruvate kinase; and lactate dehydrogenase. By molar abundance, energy metabolism proteins account for 14% of the bundle, second only to cytoskeletal proteins (Fig. 2B). Most proteins involved in glycolysis, particularly those necessary for ATP production, were reproducibly detected (supplemental data).

3.4 Validation of mass spectrometry identification

Because some proteins identified in the hair bundle preparation might be from contaminating fractions, we used immunocytochemistry to validate many of the more significant identifications. Several proteins were clearly enriched in hair bundles, including CLIC5, radixin, GAPDH, NHERF, and PTPRQ (Fig. 2C-G). CLIC5, radixin, GAPDH, and PTPRQ each localized to the base of the hair bundle, although it is not clear that their patterns overlap precisely. By contrast, NHERF1 was distributed throughout the stereocilia. Others, like myosin-VI and parvalbumin 3 (Fig. 2H-I), were present both in bundles and somas; both were distributed in bundles relatively uniformly, although parvalbumin 3 apparently also concentrated in cuticular plates. Localization of these antigens in P4-P8 rat utricles was similar to that in chicken (data not shown). In a few cases, we identified proteins present in the bundle preparation that were clearly concentrated in other cellular locations, including TIM, which was located in the cuticular plate (Fig. 2J), and ATP synthase, which was concentrated in the apical end of the hair cell soma (data not shown).

3.5 Protein quantitation in hair bundles

Because both ion-current intensity and spectral counting quantitation methods indicated that BCK was the next most abundant hair bundle protein after actin, we corroborated this result using quantitative immunoblotting. BCK was readily detected in immunoblots of chicken utricle (Fig. 3A) and bullfrog sacculus (data not shown) hair bundle proteins. Using purified chicken brain BCK (Hornemann et al., 2000) as a standard, we found that bundles of one E20 chicken utricle contained 2.0 ± 0.4 ng of BCK ($n=4$; Fig. 3B). Separate quantitation of actin indicated

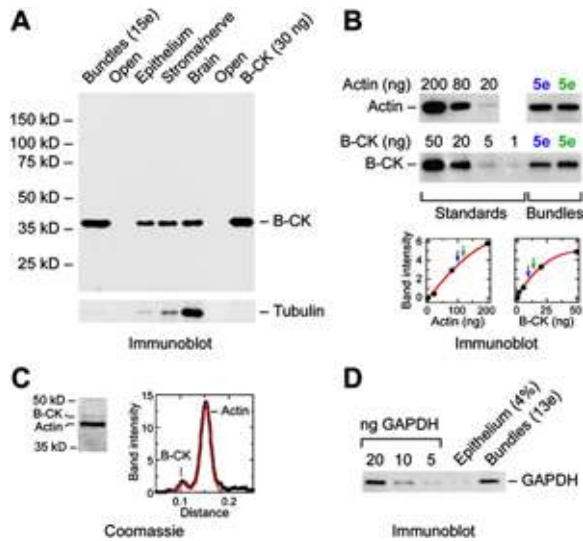


Figure 3: Detection and Quantitation of Hair Bundle Creatine Kinase B and GAPDH. (A) BCK immunoreactivity in inner ear and brain. Loading: hair bundles from 15 chicken utricles; 0.1 utricular equivalent of sensory epithelium (Epithelium); 0.1 utricular equivalent of utricular residue after scraping off sensory epithelium, containing stroma and nerve (Residual); $\sim 3 \mu\text{g}$ brain protein (Brain); and 30 ng purified BCK. Probed with anti-BCK (top); stripped and reprobed with anti-tubulin (bottom). (B) BCK quantitation by immunoblotting. Two samples of bundles from five chicken utricles each (5e) and various amounts of purified actin or BCK were detected with actin and BCK antibodies. Blots were scanned and analyzed to calculate BCK and actin in the bundles from a chicken utricule. Standard curves (below) were fit with second-order (actin) or third-order (BCK) polynomials; signals corresponding to actin and BCK bundle samples, coded in blue or green, are indicated with arrows. (C) BCK:actin ratio in hair bundles from gel scanning. Hair bundles were separated by SDS-PAGE; gel was stained with Coomassie blue. (Left) Region corresponding to BCK and actin is shown; the band labeled as BCK comigrates with authentic chicken BCK. (Right) Plot of Coomassie signal with distance along molecular mass axis of gel (black). Data were fit with a sum of two Gaussian curves (red); the area corresponding to BCK was 12% of that corresponding to actin. (D) GAPDH quantitation by immunoblotting. Purified chicken GAPDH, 4% of a whole chicken utricule, or bundles from 13 chicken utricles each were detected with anti-GAPDH. The utricule and bundle lanes have approximately the same amount of total protein loaded (210 ng); the stronger intensity of the bundle band indicated that GAPDH is substantially enriched in bundles over whole epithelium.

it was present at 16 ± 3 ng per utricule ($n=4$). Because we did not adjust these values for recovery of bundles with the twist-off method (20%-50%), the actual amounts of actin and BCK per ear equivalent are approximately 2-fold greater. Using a fluorescence assay for total protein,

we found that bundles of one chicken utricle, not adjusted for recovery, contained 16 ± 4 ng total protein; a whole utricle contained 5.3 ± 0.4 μ g. Although these results suggested that actin made up 100% of the bundle protein, inefficiencies in protein extraction for the total-protein assay probably led to the apparent discrepancy.

These quantitative immunoblotting results indicated that actin is about 8-fold more abundant in hair bundles than BCK. In an alternative method of determining this ratio, we scanned a Coomassie-stained gel of hair bundle proteins in the region corresponding to BCK and actin (Fig. 3C). Assuming that both proteins bind similar amounts of dye, integration indicated that the peak corresponding to actin was 8.2-fold more intense than that corresponding to BCK. These values are close to the 5-fold difference determined by mass spectrometry, suggesting that ion-current intensity and spectral counting measures are reasonably accurate for abundant bundle proteins. To estimate the concentration of BCK in bundles, we considered that actin's concentration is approximately 4 mM in frog saccule bundles (Jacobs and Hudspeth, 1990; Gillespie and Hudspeth, 1991); if actin is at a similar concentration in chicken bundles, then the BCK concentration is ~ 0.5 mM.

Quantitative immunoblotting indicated that the bundles of each ear (not adjusted for recovery) contained 1.6 ± 0.4 ng GAPDH ($n=3$; Fig. 3D). This value indicates that GAPDH is present at one-eighth of the molar concentration of actin, which is almost identical to the estimate from mass spectrometry; this ratio corresponds to a GAPDH concentration of 0.5 mM in bundles. At 102 ± 22 ng per μ g of total protein, GAPDH is 5-fold more abundant in bundles than in whole utricle (18 ± 2 ng GAPDH/ μ g).

3.6 Localization of creatine kinase B in the inner ear

In the chicken utricle, BCK immunolabeling was concentrated in hair cells, in both stereocilia and kinocilia (Fig. 4A-C). Immunolabeling of stereocilia and hair cell somas, but not kinocilia, was blocked by coincubation of the primary antibody with purified BCK, demonstrating that stereocilia labeling is specific, but also that at least some of the kinocilium labeling is nonspecific (Fig. 4D-E). Unexpectedly, BCK was present at much lower levels in chicken basilar papilla (data not shown). BCK was also expressed at high levels in bullfrog saccular hair cells, although levels varied from cell to cell (Fig. 4F-I). Robust de-

tection in vestibular organs required an antigen unmasking step (Shi et al., 2001); we suspect that the need for unmasking could arise from localization of BCK in the actin-filament cores of stereocilia.

BCK was also present in hair bundles of mouse inner and outer hair cells (Fig. 4J-L; supplemental data). In addition, as previously reported (Spicer and Schulte, 1992), we detected strong BCK immunoreactivity in Deiters' cells, particularly in their phalanges and apical surfaces (Fig. 4M-R; supplemental data).

3.7 Functional role of creatine kinase B in hair bundles

If creatine kinase maintains ATP levels in hair bundles, inhibition of the enzyme should permit bundle ATPases to reduce the concentration of ATP. We measured ATP levels in isolated bullfrog saccular hair cells incubated in saline containing 100 mM CaCl_2 . Under control conditions, we detected ~ 1 fmol ATP per cell. Inhibition of creatine kinase with 10 mM dinitrofluorobenzene (DNFB; Infante and Davies, 1965) decreased ATP levels by about 30% (Fig. 5B). Inhibition of hair cell PMCA with 20 mM carboxyeosin (Gatto and Milanick, 1993) increased ATP levels several-fold, suggesting that Ca^{2+} pumping was a major energy load on isolated hair cells (Fig. 5B). To determine whether the effect of DNFB was specific to hair bundle creatine kinase, we used the dye Magnesium Green (Mg Green) to indirectly measure ATP levels (Leysens et al., 1996). Because Mg^{2+} binds ~ 10 -fold more tightly to ATP than to ADP, hydrolysis of ATP releases Mg^{2+} , which can be detected as increased dye fluorescence (Fig. 5A). In isolated bullfrog hair cells loaded with the acetoxymethylester form of Mg Green, inhibition of creatine kinase by DNFB caused a significant rise in fluorescence in hair bundles, with an initial rate of fluorescence increase ($1.3\% \text{ min}^{-1}$) that was more than 6-fold greater than the increase in somas (Fig. 5C; supplemental data).

We used the bullfrog sacculus transepithelial microphonic preparation (Corey and Hudspeth, 1983) to measure the rate of adaptation of the mechanotransduction current, which should indirectly report ATP levels. As adaptation depends on myosins (Stauffer et al., 2005), depletion of ATP should slow adaptation once ATP levels fall in the range of myosin's Michaelis-Menten constant (K_m) for ATP, ~ 0.2 mM (Gillespie and Cyr, 2004; supplemental data). Although Ca^{2+} pumping also depends on the concentration of ATP, with a K_m of < 1 μM (Cara-

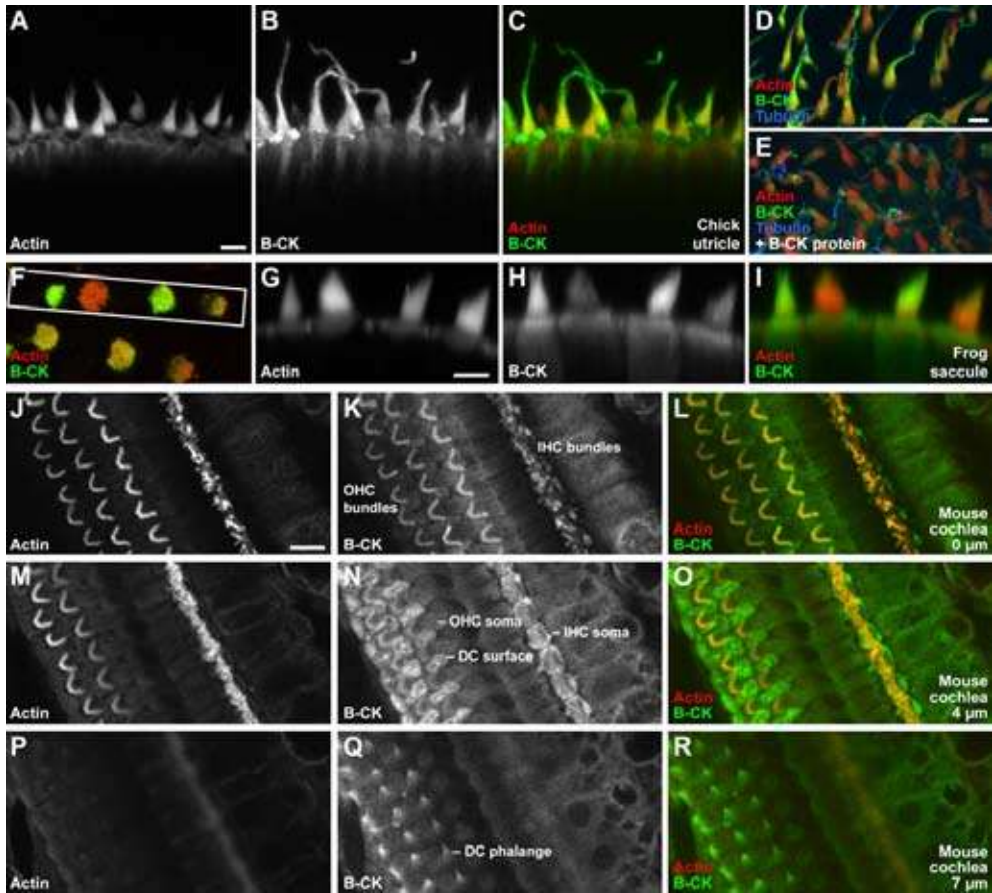
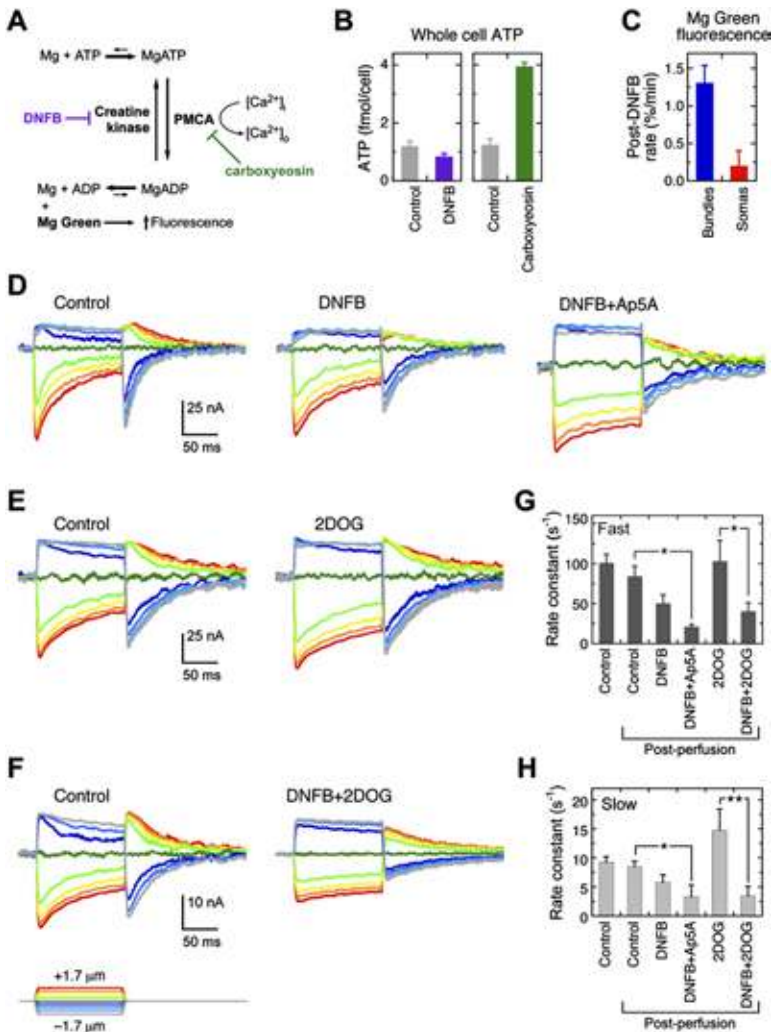


Figure 4: Localization of Creatine Kinase B in Hair Bundles. (A-R) Immunolabeling with rabbit anti-chicken BCK antibody (Kaldis et al., 1996). (A-C) BCK localization in chicken utricle hair bundles. Antigen unmasking used. Projection of seven confocal sections, each 1 μm apart. (D-E) Antibody specificity control with chick utricle. Antigen unmasking used. Excess purified BCK protein blocks anti-BCK labeling in stereocilia; block in kinocilium is incomplete, however. (F-I) BCK localization in frog saccule hair cells. (F) single x-y plane from a z-stack of saccular epithelium. Region used for x-z reslice is indicated by white box. (G-I) Reslice from z-series of (F), showing cross-sections through hair cells. (J-R) BCK localization in mouse cochlea. Antigen unmasking used. IHC, inner hair cell; OHC, outer hair cell; DC, Deiters' cell. Optical sections at three indicated depths reveal labeling in hair bundles, somas of inner hair cells, and Deiters' cells. Scale bars: bar in (A) (5 μm) also applies to (B-C); bar in (D) (5 μm) also applies to (E); bar in (G) (5 μm) also applies to (H-I); bar in (J) (10 μm) also applies to (K-R).



foli, 1992), PMCA2 will be more resistant to ATP depletion. Our stimuli were relatively large (0.4-1.7 mm) and slow (10%-90% rise time of 4 ms); although we detected fast and slow components of adaptation (8 ± 1 ms and 49 ± 3 ms, respectively), both probably arose from myosin slipping down actin filaments under tension (supplemental data).

After a 30 min DNFB perfusion, rate constants for fast and slow components of adaptation were reduced by $\sim 40\%$ compared with a control perfusion (Fig. 5D, 5G, and 5H), although the effects were not statistically significant ($P = 0.054$ and $P = 0.091$, respectively). Additional application of the adenylate kinase inhibitor Ap5A decreased

Figure 5: *Creatine kinase inhibition increases ATP hydrolysis and slows adaptation in hair bundles.* (A) Creatine kinase and PMCA are major sources of ATP synthesis and hydrolysis, respectively, in hair bundles. ATP consumption can be monitored indirectly with Mg Green; because the affinity of Mg^{2+} for ADP is much less than for ATP, hydrolysis of ATP will increase free Mg^{2+} levels. Rephosphorylation of ADP by creatine kinase will keep free Mg^{2+} levels low; inhibition of creatine kinase (by DNFB) should elevate Mg^{2+} , increasing Mg Green fluorescence. (B) ATP levels in isolated bullfrog hair cells after treatment with DNFB or carboxyeosin. ATP in approximately seven cells was measured with luciferin/luciferase assay. These experiments are representative of three independent experiments. Error bars = SEM. (C) Average rate of increase (initial slope) of Mg Green fluorescence from first six points (12 min) of each cell, individually fit with single-exponential functions ($n=19$). The difference between bundles and somas is significant (** $P < 0.02$). Error bars = SEM. (D) Transduction currents before (left) and after (middle) 30 min treatment with 100 μ M DNFB; right traces show transduction currents after 500 μ M Ap5A was added to the apical solution as well. (E) Transduction currents before (left) and after (right) 30 min treatment with 5 mM 2DOG; 5 mM pyruvate was included in apical and basal solutions. (F) Transduction currents before (left) and after (right) 30 min treatment with 100 μ M DNFB and 5 mM 2DOG; 5 mM pyruvate was included in apical and basal solutions. (G) Fast adaptation rate constants before (control; $n=32$) and 30 min post-perfusion with control salines ($n=10$); 100 μ M apical and basal DNFB ($n=10$); 100 μ M DNFB apical and basal followed by 500 μ M apical Ap5A ($n=3$); 5 mM 2-deoxyglucose and 5 mM pyruvate in glucose-free salines ($n=5$); 100 μ M DNFB, 5 mM 2-deoxyglucose, and 5 mM pyruvate in glucose-free salines ($n=7$). Significance (two-tailed Student's t test) indicated by * $P < 0.05$; ** $P < 0.02$. Significance for the Control-DNFB comparison was $p = 0.056$. Error bars = SEM. (H) Slow adaptation rate constants; same epithelia as (G). Significance for the Control-DNFB comparison was $P = 0.091$. Error bars = SEM.

fast and slow components even further (Fig. 5D, 5G, and 5H), however, suggesting that this enzyme helps to maintain ATP levels by scavenging ADP (Gillespie and Hudspeth, 1993). The glycolysis inhibitor 2-deoxyglucose (2DOG), when applied along with pyruvate (to supply energy for oxidative phosphorylation), did not slow adaptation; however, the combination of DNFB and 2DOG reduced adaptation rates substantially and significantly (Fig. 5E-H). The open probability (P_o) at rest rose substantially when DNFB was paired with either Ap5A or 2DOG, consistent with elevated ADP levels (Gillespie and Hudspeth, 1993).

3.8 The creatine kinase circuit is required for normal hearing and balance

PMCA2 is essential for hearing (Kozel et al., 1998; Street et al., 1998), and efficient PMCA2 activity may be necessary for cochlear amplification (LeMasurier and Gillespie, 2005). If outer hair cell BCK is needed to supply PMCA2 with sufficient ATP, then BCK's absence should adversely affect the ability of the cochlea to detect faint sounds. We measured the auditory brainstem response (ABR), a measure of the sensitivity of the auditory system, in mice deficient in BCK (BCK^{-/-}) (Jost et al., 2002). In addition, because overexpression from the ubiquitous mitochondrial creatine kinase isoform (UbCKmit) apparently can compensate for BCK in knockout mice, we used double-knockout mice lacking BCK and UbCKmit (further referred to as CK^{-/-}) (Streijger et al., 2005). At the light microscopic level, no differences in cochlear morphology were noticed between wildtype mice and CK^{-/-} mice at ages of 6, 15, and 30 days (data not shown). Demonstrating the specificity of the mouse cochlea immunolocalization (Fig. 4J-R), labeling by the BCK antibody was essentially eliminated in BCK^{-/-} and CK^{-/-} mice (Fig. S1; supplemental data).

Although ABRs to broad band click stimuli, which largely contain low-frequency components, were not significantly different between the three groups, the sensitivity of the auditory system to the 8 kHz and 16 kHz tone bursts was reduced substantially in CK^{-/-} mice compared with wildtype mice and BCK^{-/-} mice (Fig. 6A-B). Thresholds were elevated by 20-30 dB, which indicates that the sound pressure required to reach a detectable signal in the brainstem was 10-to 30-fold greater. BCK^{-/-} mice showed thresholds elevated similarly to those CK^{-/-} mice for the 32 kHz tone burst stimulus; both were significantly different from wild-type mice ($P < 0.01$). Although neither BCK^{-/-} nor CK^{-/-} mice showed overt circling behavior (Jost et al., 2002; Streijger et al., 2005), an indication of severe vestibular dysfunction, we observed more subtle signs of a malfunctioning vestibular system in both groups by using tail-suspension and swim tests. When compared to WT animals, which were all characterized by normal vestibular function, BCK^{-/-} mice showed a mild defect, whereas CK^{-/-} double knockout mice had a more substantial vestibular dysfunction (Fig. 6C).

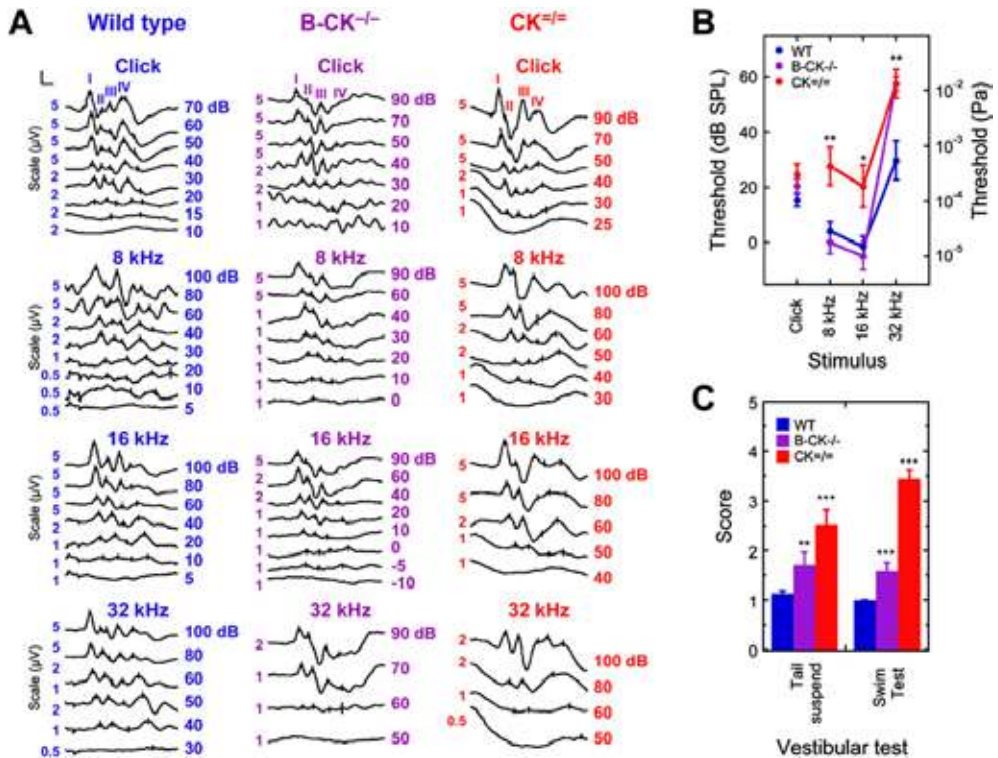


Figure 6: Auditory Brainstem Responses and Vestibular Behavior in Creatine Kinase Knockout Mice. (A) Typical ABRs evoked with a click stimulus (top) and with tone bursts of 8, 16, and 32 kHz (bottom) for WT, BCK^{-/-}, and CK^{-/-} mice. ABRs are shown at different descending stimulus intensity levels in dB re 20 μ Pa (dB SPL). Reproducible ABRs at lower stimulation intensities in response to 32 kHz tone burst stimuli were not elicited from BCK^{-/-} and CK^{-/-} mice; CK^{-/-} mice also showed higher thresholds in response to 8 kHz and 16 kHz tone burst stimuli. The vertical axis scale was adjusted for readability at higher stimulation levels; scale bar in upper left signifies 1.5 ms and the appropriate vertical scale (indicated to the left of each trace). (B) Mean auditory brainstem thresholds. CK^{-/-} mice showed significantly elevated hearing thresholds compared with BCK^{-/-} and WT mice for 8 and 16 kHz (ANOVA, ** $P < 0.01$ and * $P < 0.05$, respectively). For the 32 kHz tone burst, both BCK^{-/-} and CK^{-/-} mice showed significantly elevated auditory thresholds compared with WT (ANOVA, ** $P < 0.01$). Significance in (B) and (C) is indicated by * $P < 0.05$; ** $P < 0.01$; and *** $P < 0.001$. Error bars = SE. (C) Vestibular dysfunction in creatine kinase-deficient mice. Applying the tail-suspension and swim tests, each with scores ranging from 1 (normal vestibular function) to 5 (severe vestibular dysfunction), indicated normal vestibular function for WT mice ($n=30$). BCK^{-/-} single-knockout mice ($n=17$) showed a mild vestibular dysfunction; dysfunction in CK^{-/-} double-knockout mice ($n=17$) was more severe. Error bars = SE.

4. Discussion

Hair bundles are optimized for maintenance of ATP levels via phosphocreatine buffering. The high concentration of BCK in bundles suggests that if phosphocreatine levels are sufficiently high, bundles can maintain millimolar ATP levels even as PMCA2 or other ATPases consume prodigious amounts of ATP. Thus, processes that rely on ATP, such as fast and slow adaptation (Stauffer et al., 2005), can continue to operate efficiently; although mechanotransduction does not rely directly on ATP levels, optimal sensitivity does.

4.1 Hair bundle proteins

We identified 59 proteins that, by stringent criteria, are present in our hair bundle preparation. Many of these proteins are not specifically concentrated in bundles; hair bundles are not closed compartments, so they will contain proteins that can diffuse from the soma. Proteins that are not exclusively located in bundles can nevertheless be essential for bundle function; for example, BCK is also located in cell bodies (Fig. 4). Other proteins are enriched in bundles; for example, we did not detect fimbrin, radixin, CLIC5, or annexin A5 in mass spectrometry experiments using whole chicken epithelium, despite their abundance in mass spectrometry experiments using isolated bundles (data not shown).

The list of proteins identified in the hair bundle preparation includes a few that are present at high levels in fractions that contaminate the purified bundles, such as the mitochondrial ATP synthase and histones H2a and H4, which are present in nuclei. Other proteins, such as the heat shock proteins Hsc70 and GRP78, are at high concentrations in cell somas, although a modest amount of each may be soluble in bundles. Nevertheless, our ongoing validation experiments indicate that most proteins in Table 1 are authentic bundle proteins.

Have we missed any abundant hair bundle proteins because of an incomplete database? The majority of the genes in the chicken Ensembl database are predicted by automated gene-build analysis (Curwen et al., 2004), which relies on cross-referencing with the deeply annotated human and mouse databases. When we searched our ion-peak lists against human and mouse databases, very few additional proteins were identified, none of which meet the criteria used for Table

1 (data not shown). We thus believe that we have identified the majority of the abundant hair bundle proteins, although we do not suggest that our list is complete; membrane proteins in particular are likely to be underrepresented.

4.2 Glycolysis in hair bundles

Components of the glycolytic pathway from GAPDH onward were all present in hair bundles. (The one exception, phosphoglycerate mutase, was present in two out of five mass spectrometry experiments and thus did not qualify for inclusion in Table 1.) TIM was also present in the bundle preparation but probably derived from contaminating cuticular plates; its localization there would ensure that any diffusing dihydroxyacetone phosphate would be converted to glyceraldehyde-3-phosphate prior to entering stereocilia. Moreover, lactate dehydrogenase was present at high levels; because this enzyme converts NADH to NAD⁺, it would regenerate NAD⁺ consumed by GAPDH. Lactate presumably then diffuses to hair cell (or supporting cell) mitochondria for use in oxidative phosphorylation.

That glycolytic enzymes are present in stereocilia is not surprising; many of these enzymes bind specifically to actin (Arnold et al., 1971; Bronstein and Knull, 1981; Mejean et al., 1989). Because the concentration of stereocilia actin is so high compared with the cell soma, these glycolytic enzymes should be concentrated in bundles. Interestingly, GAPDH can associate with membranes (Hsu and Molday, 1990) as well as with actin (Bronstein and Knull, 1981), suggesting that GAPDH might be a membrane-to-cytoskeleton crosslinker in stereocilia.

If the relevant mass spectrometry identifications are valid, our results suggest that hair bundle glycolysis proceeds via glyceraldehyde-3-phosphate reduction and subsequent steps, rather than relying on glucose transport from the endolymph into bundles. This arrangement allows the bundle to generate a net of four ATP molecules per glucose, rather than only two if hexokinase and phosphofructokinase steps are required. Those two ATPs are still consumed by the cell, but distantly from the bundle. In rod outer segments and red blood cells, glycolysis can generate ATP at 0.1 mM/s (Hsu and Molday, 1994). The stereocilia Ca²⁺ entry rate, and hence ATP consumption rate, can be estimated from the transduction channel P_o, single channel conduct-

ance, membrane potential, and fraction of the current carried by Ca^{2+} (Figure 7 legend). If P_o is 0.1 and 100% of entering Ca^{2+} is extruded by PMCA2, stereocilia will consume ATP at 0.12 mM/s ATP. Because GAPDH, rate limiting for the second half of glycolysis, has a bundle concentration similar to that in rod outer segments (Hsu and Molday, 1990), glycolysis could be sufficient for ATP generation by quiescent bundles. Also indicating the significance of glycolysis for bundles, adaptation is slowed much more substantially when creatine kinase inhibition is coupled with inhibition of glycolysis.

4.3 Hair bundles cannot rely on ATP diffusion

Although glycolysis might provide sufficient ATP for stereocilia with channels at their rest P_o , stereocilia with transduction channels at an increased P_o may need >1 mM/s ATP. Can diffusion supply enough ATP to make up the difference? Modeling the stereocilium as a one-dimensional diffusion space, the concentration of ATP should fall linearly between its source and its sink, the site of consumption. To simplify the calculations, we assume that $[\text{ATP}]$ at the base of a stereocilium is fixed at 2 mM by the mitochondria clustered nearby, and that all ATP is consumed by PMCA2 at stereocilia tips, near the site of Ca^{2+} entry. Fick's first law gives:

$$Q = D \cdot a \cdot \frac{d[\text{ATP}]}{dx} \quad (1)$$

where Q is the ATP diffusion rate, D is the diffusion coefficient of ATP in cytoplasm, and a is the cross-sectional area of the stereocilium. Because the central assumption in this model is that ATP diffusion is sufficient for extrusion, $Q = R$, where R is the ATP consumption rate. We approximate the effect of glycolysis by subtracting the estimated glycolysis rate (g) from R . The concentration at distance x from the source is thus:

$$[\text{ATP}]_x = [\text{ATP}]_o - x \cdot \frac{R - g}{D \cdot a} \quad (2)$$

Although this equation suggests that glycolysis could provide enough ATP at a resting P_o of 0.1, elevating P_o to 0.25 causes the ATP con-

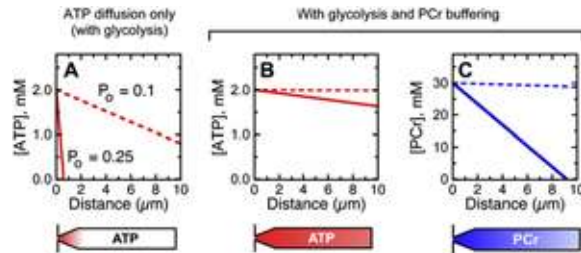


Figure 7: Modeling Spatial Buffering of ATP by Creatine Kinase and Phosphocreatine. (A) [ATP] spatial profile in absence of PCr buffering. One-dimensional source-sink model used as described in text. Parameters used: [ATP] at base fixed at 2 mM, 60 mV membrane potential, single channel conductance of 100 pS; 3% of current carried by Ca^{2+} , channel P_o of 0.1 (dashed lines) or 0.25 (solid lines), 100% of Ca^{2+} pumped out by bundle PMCA (117 $\mu\text{M/s}$), glycolysis rate of 110 $\mu\text{M/s}$, diffusion coefficient for ATP in cytoplasm of $3.5 \times 10^{-10} \text{ m}^2 \text{ s}^{-1}$ (Bowen and Martin, 1964; Yoshizaki et al., 1987), and stereocilia radius of 200 nm. Diagram of stereocilium below indicates depletion of ATP (red); narrowing of stereocilium at base was not considered in modeling. (B) Effect on [ATP] of adding PCr buffering. Parameters: same as (A) with [PCr] at base fixed at 30 mM, ATP/ADP ratio of 25, K' (equilibrium constant for creatine kinase reaction) of 100, and diffusion constant for PCr of $4.9 \times 10^{-10} \text{ m}^2 \text{ s}^{-1}$. ATP levels remain nearly constant, even with elevated P_o . (C) [PCr] gradient. $J_{\text{PCr}}/J_{\text{ATP}}$ ratio was 91. When P_o is elevated, PCr levels fall toward stereocilium tip but remain in the millimolar range.

centration to drop below zero in less than 1 μm (Figure 7A). This unreasonable result shows that the central assumption of the model cannot be correct.

4.4 Creatine kinase controls ATP levels in hair bundles

Because isolated frog hair cells are 1-2 pl in volume (Edmonds et al., 2000) and contain 1-2 fmol of ATP, their resting ATP concentration was $\sim 1 \text{ mM}$. This concentration may have been artificially low as these cells may be loaded with Na^+ (Shi et al., 2005), increasing ATP consumption by the Na^+/K^+ -ATPase. Inhibition of creatine kinase by DNFB decreased ATP levels, which suggests that substantial amounts of ATP must be delivered in hair cells by phosphocreatine and creatine kinase. Because inhibition of PMCA increased ATP levels, a calcium pump must continuously consume large amounts of ATP. We therefore conclude that the creatine kinase is essential for maintaining ATP lev-

els in hair cells, and that PMCA is a major drain on ATP. Moreover, the spatially restricted Mg Green fluorescence increase seen in hair bundles in response to DNFB suggests that ATP consumption by bundle PMCA2 drives bundle creatine kinase activity.

Slowing of adaptation by DNFB, particularly when coupled with adenylate kinase or glycolysis inhibition, supports a critical role for creatine kinase in hair bundles. Although the effect of DNFB alone on adaptation was not profound, the concentration of ATP might have been reduced by ten-fold or more without dramatically slowing myosins, depending on myosin's K_m for ATP and the resting ATP level (supplemental data). Moreover, the degree to which DNFB reduces ATP will depend on the amount of creatine kinase present in bundles. For example, 100 mM DNFB reduces creatine kinase activity in muscle by 75% without reducing the ATP consumption rate substantially (Dzeja et al., 1996); likewise, an excess of creatine kinase in hair bundles would blunt the effects of DNFB. The effects of DNFB were enhanced by adenylate kinase inhibition, suggesting that this enzyme normally removes ADP that otherwise inhibits adaptation (Gillespie and Hudspeth, 1993); likewise, glycolysis inhibition synergizes with DNFB, consistent with a role for glycolysis in basal ATP maintenance.

As it ranked second in the hair bundle preparation by spectral counting and ion-current intensities, we confirmed with quantitative immunoblotting that BCK was highly abundant in chicken utricle hair bundles. At 0.5 mM and with a maximal activity of 250 s^{-1} (Hornemann et al., 2000), BCK could regenerate ATP at $>200 \text{ mM s}^{-1}$ if ADP and phosphocreatine levels were well above their K_m values (0.2 and 2 mM, respectively; Hornemann et al., 2000). Although the actual rate will be lower, as ADP levels should be maintained well below 0.2 mM, hair bundles have a sufficiently high concentration of BCK to allow the reaction to be near equilibrium, even during high ATP consumption or DNFB inhibition.

The high concentration of BCK allows for spatial buffering of ATP by facilitated diffusion. As ATP is consumed in stereocilia, creatine kinase uses phosphocreatine to immediately restore ATP levels; the required flux of ATP into stereocilia thus can be replaced nearly entirely by phosphocreatine flux. Assuming that the creatine kinase reaction is at equilibrium, Meyer et al. (1984) showed that the ratio of phosphocreatine flux (J_{PCr}) to ATP flux (J_{ATP}) into a compartment is:

$$\left(\frac{J_{\text{PCR}}}{J_{\text{ATP}}}\right) = \left(\frac{D_{\text{Cr}(t)}}{D_{\text{Ad}(t)}}\right) \cdot \left(\frac{C_{\text{Cr}(t)}}{C_{\text{Ad}(t)}}\right) \cdot K' \cdot \left(\frac{R + 1}{R + K'}\right)^2 \quad (3)$$

where $D_{\text{Cr}(t)}$ is the diffusion coefficient for creatine and phosphocreatine (assumed to be identical), $D_{\text{Ad}(t)}$ is the diffusion coefficient for ADP and ATP, $C_{\text{Cr}(t)}$ is total creatine+phosphocreatine concentration, $C_{\text{Ad}(t)}$ is the ADP+ATP concentration, R is the ATP-to-ADP concentration ratio, and K' is the apparent equilibrium constant. If the concentration of ATP in the cell body is 2 mM, phosphocreatine is 30mM, $R = 25$, and $K' = 100$ (Meyer et al., 1984), the flux ratio would be ~ 90 ; over 98% of the high-energy phosphate bonds would thus enter stereocilia as phosphocreatine, not ATP. Although phosphocreatine will also be depleted from stereocilia, if the concentration in the soma is sufficiently high, phosphocreatine will remain high enough to maintain fast creatine kinase activity.

Phosphocreatine will be regenerated either by creatine kinase associated with glycolytic enzymes (Kraft et al., 2000) or through mitochondrial creatine kinase utilization of ATP formed by oxidative phosphorylation (Kay et al., 2000). Phosphocreatine would be synthesized in the apical region of the hair cell, rich in mitochondria, and diffuse to stereocilia; creatine would diffuse back. Strong evidence for similar compartmentalized phosphocreatine-creatine circuits comes from sperm cells (Tombes and Shapiro, 1985) and retinal photoreceptors (Hemmer et al., 1993), although the rate of ATP consumption in stereocilia appears to be substantially larger.

Although our modeling is simplistic, we believe that it captures the essential role for creatine kinase in hair bundles, i.e., to temporally and spatially buffer ATP. Although a more realistic reaction-diffusion model, including Ca^{2+} buffering, Ca^{2+} extrusion along the stereocilia, kinetic constants for the Ca^{2+} pump and creatine kinase, and the effects of the stereocilia taper, would improve quantitative predictions, it would be very unlikely to substantially alter our principal qualitative conclusions.

4.5 Creatine kinase B in hearing and balance

Creatine kinase is necessary for normal hearing and balance. CK^{-/-} mice have vestibular dysfunction and significantly elevated ABR

thresholds in the middle and upper regions of the auditory range of mice (8-32 kHz). Mice lacking only BCK show a deterioration of the auditory threshold only at 32 kHz, suggesting that compensation by UbCKmit can protect hearing throughout most of the auditory range. Consistent with creatine kinase's importance in the cochlea, phosphocreatine concentrations rise 4-fold from apex to base in the guinea pig organ of Corti (Krzanowski and Matschinsky, 1971). The elevation of ABR threshold at high frequencies is similar to results seen with mice with only one functional copy of PMCA2 (McCullough and Tempel, 2004). Several cell types in the ear besides hair cells might rely on creatine kinase; in particular, BCK levels are high in phalanges of Deiters' cells. Because these mitochondria-free phalanges are tens of micrometers in length, even a small amount of ATP must be generated locally (supplemental data); the concentration of BCK may not be proportional to its importance for cochlear function. The ABR results are thus consistent with an essential role for BCK in hair cells and, in particular, hair bundles.

In conjunction with the results for CK^{-/-} mice, the high concentration of PMCA2 in hair bundles (Dumont et al., 2001), the necessity of PMCA2 for hearing (Kozel et al., 1998; Street et al., 1998), and the calculated need for facilitated diffusion of ATP, we propose that hair bundle BCK is responsible for maintaining bundle ATP levels despite high PMCA2 activity (Figure 7). In muscle, the efficiency of the sarcoplasmic reticulum Ca²⁺ pump depends critically on the local ATP/ADP ratio, which is maintained at a high level by pump-coupled creatine kinase (Rossi et al., 1990); accordingly, mice with a double knockout of muscle-type and sarcomeric mitochondrial creatine kinase genes show substantially altered calcium homeostasis and compromised muscle relaxation (Steeghs et al., 1997). We thus propose that hair cells elevate BCK to manage the energetically demanding task of Ca²⁺ homeostasis.

Acknowledgments

All genotype-specific mice mentioned were generated by the laboratory of Bé Wieringa (NCMLS, Radboud University Nijmegen Medical Centre, The Netherlands). We thank Bill Roberts (University of Oregon) for help with the diffusion calculations. Bé Wieringa and members of the Gillespie laboratory provided valuable comments on the

manuscript. This work was supported by a Postdoctoral Research Fellowship from the German Research Foundation (to J.B.S), NIH grants R21 DC006097, R01 DC002368, and P30 DC005983 (to P.G.G.), and Swiss National Science Foundation grant 3100AO-102075 (to T.W.).

References

Arnold H, Henning R, Pette D (1971) Quantitative comparison of the binding of various glycolytic enzymes to F-actin and the interaction of aldolase with G-actin. *Eur J Biochem* 22:121-126.

Bowen WJ, Martin HL (1964) The diffusion of adenosine triphosphate through aqueous solutions. *Arch. Biochem Biophys* 107:30-36.

Bronstein WW, Knull HR (1981) Interaction of muscle glycolytic enzymes with thin filament proteins. *Can J Biochem* 59:494-499.

Carafoli E (1992) The Ca^{2+} pump of the plasma membrane. *J Biol Chem* 267:2115-2118.

Corey DP, Hudspeth AJ (1983) Analysis of the microphonic potential of the bullfrog's sacculus. *J Neurosci* 3:942-961.

Craig R, Cortens JP, Beavis RC (2004) Open source system for analyzing, validating, and storing protein identification data. *J Proteome Res* 3:1234-1242.

Curwen V, Eyraas E, Andrews TD, Clarke L, Mongin E, Searle SM, Clamp M (2004) The Ensemble automatic gene annotation system. *Genome Res* 14:942-950.

Dumont RA, Lins U, Filoteo AG, Penniston JT, Kachar B, Gillespie PG (2001) Plasma membrane Ca^{2+} -ATPase isoform 2a is the PMCA of hair bundles. *J Neurosci* 21:5066-5078.

Dzeja PP, Zeleznikar RJ, Goldberg ND (1996) Suppression of creatine kinase-catalyzed phosphotransfer results in increased phosphoryl transfer by adenylate kinase in intact skeletal muscle. *J Biol Chem* 271:12847-12851.

Edmonds B, Reyes R, Schwaller B, Roberts WM (2000) Calretinin modifies presynaptic calcium signaling in frog saccular hair cells. *Nat Neurosci* 3:786-790.

Fenyo D, Beavis RC (2003) A method for assessing the statistical significance of mass spectrometry-based protein identifications using general scoring schemes. *Anal Chem* 75:768-774.

Gagnon LH, Longo-Guess CM, Berryman M, Shin JB, Saylor KW, Yu H, Gillespie PG, Johnson KR (2006) The chloride intracellular channel protein CLIC5 is expressed at high levels in hair cell stereocilia and is essential for normal inner ear function. *J Neurosci* 26, 10188-10198.

Gatto C, Milanick MA (1993) Inhibition of the red blood cell calcium pump by eosin and other fluorescein analogues. *Am J Physiol* 264:C1577-C1586.

Gillespie PG, Cyr JL (2004) Myosin-1c, the hair cell's adaptation motor. *Annu Rev Physiol* 66:521-545.

Gillespie PG, Hudspeth AJ (1991) High-purity isolation of bullfrog hair bundles and subcellular and topological localization of constituent proteins. *J Cell Biol* 112:625-640.

Gillespie PG, Hudspeth AJ (1993) Adenine nucleoside diphosphates block adaptation of mechano-electrical transduction in hair cells. *Proc Natl Acad Sci USA* 90:2710-2714.

Goodyear RJ, Gates R, Lukashkin AN, Richardson GP (1999) Hair-cell numbers continue to increase in the utricular macula of the early posthatch chick. *J Neurocytol* 28:851-861.

Goodyear, R.J., Legan, P.K., Wright, M.B., Marcotti, W., Oganessian, A., Coats, S.A., Booth, C.J., Kros, C.J., Seifert, R.A., Bowen-Pope, D.F., and Richardson, G.P. (2003). A receptor-like inositol lipid phosphatase is required for the maturation of developing cochlear hair bundles. *J. Neurosci.* 23, 9208-9219.

Heller S, Bell AM, Denis CS, Choe Y, Hudspeth AJ (2002) Parvalbumin 3 is an abundant Ca^{2+} buffer in hair cells. *J Assoc Res Otolaryngol* 3:488-498.

Hemmer W, Riesinger I, Wallimann T, Eppenberger HM, Quest AF (1993) Brain-type creatine kinase in photoreceptor cell outer segments: role of a phosphocreatine circuit in outer segment energy metabolism and phototransduction. *J Cell Sci* 106:671-683.

Hirono M, Denis CS, Richardson GP, Gillespie PG (2004) Hair cells require phosphatidylinositol 4,5-bisphosphate for mechanical transduction and adaptation. *Neuron* 44:309-320.

Hornemann T, Rutishauser D, Wallimann T (2000) Why is creatine kinase a dimer? Evidence for cooperativity between the two subunits. *Biochim Biophys Acta* 1480:365-373.

Hsu SC, Molday RS (1990) Glyceraldehyde-3-phosphate dehydrogenase is a major protein associated with the plasma membrane of retinal photoreceptor outer segments. *J Biol Chem* 265:13308-13313.

Hsu SC, Molday RS (1994) Glucose metabolism in photoreceptor outer segments. Its role in phototransduction and in NADPH-requiring reactions. *J Biol. Chem* 269:17954-17959.

Infante AA, Davies RE (1965) The effect of 2,4-dinitrofluorobenzene on the activity of striated muscle. *J Biol Chem* 240:3996-4001.

International Chicken Genome Sequencing Consortium (2004) Sequence and comparative analysis of the chicken genome provide unique perspectives on vertebrate evolution. *Nature* 432, 695-716.

Jacobs RA, Hudspeth AJ (1990) Ultrastructural correlates of mechano-electrical transduction in hair cells of the bullfrog's internal ear. *Cold Spring Harb Symp Quant Biol* 55:547-561.

Jones SM, Jones TA (1996) Short latency vestibular evoked potentials in the chicken embryo. *J Vestib Res* 6:71-83.

Jost CR, Van der Zee CEEM, In 't Zandt HJ, Oerlemans F, Verheij M, Streijger F, Fransen J, Heerschap A, Cools AR, Wieringa B (2002) Creatine kinase B-driven energy transfer in the brain is important for habituation and spatial learning behavior, mossy fiber field size and de-

- termination of seizure susceptibility. *Eur. J Neurosci* 15:1692-1706.
- Kaldis P, Stolz M, Wyss M, Zanolla E, Rothen-Rutishauser B, Vorherr T, Wallimann T (1996) Identification of two distinctly localized mitochondrial creatine kinase isoenzymes in spermatozoa. *J Cell Sci* 109:2079-2088.
- Kay L, Nicolay K, Wieringa B, Saks V, Wallimann T (2000) Direct evidence for the control of mitochondrial respiration by mitochondrial creatine kinase in oxidative muscle cells in situ. *J Biol Chem* 275:6937-6944.
- Kozel PJ, Friedman RA, Erway LC, Yamoah EN, Liu LH, Riddle T, Duffy JJ, Doetschman T, Miller ML, Cardell EL, Shull GE (1998) Balance and hearing deficits in mice with a null mutation in the gene encoding plasma membrane Ca^{2+} -ATPase isoform2. *J Biol Chem* 273:18693-18696.
- Kraft T, Hornemann T, Stolz M, Nier V, Wallimann T (2000) Coupling of creatine kinase to glycolytic enzymes at the sarcomeric I-band of skeletal muscle: a biochemical study in situ. *J Muscle Res Cell Motil* 21:691-703.
- Krzanowski JJJ, Matschinsky FM (1971) A phosphocreatine gradient opposite to that of glycogen in the organ of Corti and the effect of salicylate on adenosine triphosphate and P-creatine in cochlear structures. *J Histochem Cytochem* 19:321-323.
- LeMasurier M, Gillespie PG (2005) Hair-cell mechanotransduction and cochlear amplification. *Neuron* 48:403-415.
- Leysens A, Nowicky AV, Patterson L, Crompton M, Duchen MR (1996) The relationship between mitochondrial state, ATP hydrolysis, $[\text{Mg}^{2+}]_i$ and $[\text{Ca}^{2+}]_i$ studied in isolated rat cardiomyocytes. *J Physiol* 496:111-128.
- Liang P, MacRae TH (1997) Molecular chaperones and the cytoskeleton. *J Cell Sci* 110:1431-1440.

Liu H, Sadygov RG, Yates JR, III (2004) A model for random sampling and estimation of relative protein abundance in shotgun proteomics. *Anal Chem* 76:4193-4201.

Lin HW, Schneider ME, Kachar B (2005) When size matters: the dynamic regulation of stereocilia lengths. *Curr Opin Cell Biol* 17:55-61.

Lopez-Fanarraga M, Avila J, Guasch A, Coll M, Zabala JC (2001) Review: postchaperonin tubulin folding cofactors and their role in microtubule dynamics. *J Struct Biol* 135:219-229.

Lumpkin EA, Hudspeth AJ (1998) Regulation of free Ca^{2+} concentration in hair-cell stereocilia. *J Neurosci* 18:6300-6318.

Lumpkin EA, Marquis RE, Hudspeth AJ (1997) The selectivity of the hair cell's mechano-electrical-transduction channel promotes Ca^{2+} -flux at low Ca^{2+} -concentrations. *Proc Natl Acad Sci USA* 94:10997-11002.

Maul RS, Song Y, Amann KJ, Gerbin SC, Pollard TD, Chang DD (2003) EPLIN regulates actin dynamics by cross-linking and stabilizing filaments. *J Cell Biol* 160:399-407.

McCullough BJ, Tempel BL (2004) Haplo-insufficiency revealed in deafwaddler mice when tested for hearing loss and ataxia. *Hear Res* 195:90-102.

Mejean C, Pons F, Benyamin Y, Roustan C. (1989) Antigenic probes locate binding sites for the glycolytic enzymes glyceraldehyde3-phosphate dehydrogenase, aldolase and phosphofructokinase on the actin monomer in microfilaments. *Biochem J* 264:671-677.

Meyer RA, Sweeney HL, Kushmerick MJ (1984) A simple analysis of the "phosphocreatine shuttle". *Am J Physiol* 246:C365-C377.

Neely JG, Thompson AM, Gower DJ (1991) Detection and localization of heat shock protein 70 in the normal guinea pig cochlea. *Hear Res* 52:403-406.

Neugebauer DC, Thurm U (1984) Chemical dissection of stereovilli from fish inner ear reveals differences from intestinal microvilli. *J Neurocytol* 13:797-808.

Old WM, Meyer-Arendt K, Aveline-Wolf L, Pierce KG, Mendoza A, Sevinsky JR, Resing KA, Ahn NG (2005) Comparison of label-free methods for quantifying human proteins by shotgun proteomics. *Mol Cell Proteomics* 4:487-1502.

Ong SE., Mann M (2005) Mass spectrometry-based proteomics turns quantitative. *Nat Chem Biol* 1:252-262.

Petit C (2006) From deafness genes to hearing mechanisms: harmony and counterpoint. *Trends Mol Med* 12:57-64.

Powell DW, Weaver CM, Jennings JL, McAfee KJ, He Y, Weil PA, Link AJ (2004) Cluster analysis of mass spectrometry data reveals a novel component of SAGA. *Mol Cell Biol* 24:7249-7259.

Prochasson P, Florens L, Swanson SK, Washburn MP, Workman JL (2005) The HIR corepressor complex binds to nucleosomes generating a distinct protein/DNA complex resistant to remodeling by SWI/SNF. *Genes Dev* 19:2534-2539.

Rezaul K, Wu L., Mayya V, Hwang SI, Han D (2005) A systematic characterization of mitochondrial proteome from human T leukemia cells. *Mol Cell Proteomics* 4:169-181.

Ricci AJ, Fettiplace R (1998). Calcium permeation of the turtle hair cell mechanotransducer channel and its relation to the composition of endolymph. *J Physiol* 506:159-173.

Rossi AM, Eppenberger HM, Volpe P, Cotrufo R, Wallimann T (1990) Muscle-type MM creatine kinase is specifically bound to sarcoplasmic reticulum and can support Ca^{2+} uptake and regulate local ATP/ADP ratios. *J Biol Chem* 265:5258-5266.

Schneider ME, Belyantseva IA, Azevedo RB, Kachar B (2002) Rapid renewal of auditory hair bundles. *Nature* 418:837-838.

Shenolikar S, Voltz JW, Cunningham R, Weinman EJ (2004) Regulation of ion transport by the NHERF family of PDZ proteins. *Physiology (Bethesda)* 19:362-369.

Shepherd GMG, Barres BA, Corey DP (1989) "Bundle-blot" purification and initial protein characterization of hair cell stereocilia. *Proc Natl Acad Sci USA* 86:4973-4977.

Shi SR, Cote RJ, Taylor CR (2001) Antigen retrieval techniques: current perspectives. *J Histochem Cytochem* 49:931-937.

Shi X, Gillespie PG, Nuttall AL (2005) Na⁺ influx triggers bleb formation on inner hair cells. *Am J Physiol Cell Physiol* 288:C1332-C1341.

Spicer SS, Schulte BA (1992) Creatine kinase in epithelium of the inner ear. *J Histochem Cytochem* 40:185-192.

Stauffer EA, Scarborough JD, Hirono M, Miller ED, Shah K, Mercer JA, Holt JR, Gillespie PG. (2005) Fast adaptation in vestibular hair cells requires myosin-1c activity. *Neuron* 47:541-553.

Steeghs K, Benders A, Oerlemans F, De Haan A, Heerschap A, Ruitenbeek W, Jost C, Van Deursen J, Perryman B, Pette D, Bruckwilder M, Koudijs J, Jap P, Veerkamp J, Wieringa B (1997) Altered Ca²⁺ responses in muscles with combined mitochondrial and cytosolic creatine kinase deficiencies. *Cell* 89:93-103.

Street VA, McKee-Johnson JW, Fonseca RC, Tempel BL, Noben-Trauth K (1998) Mutations in a plasma membrane Ca²⁺-ATPase gene cause deafness in deafwaddler mice. *Nat Genet* 19:390-394.

Streijger F, Oerlemans F, Ellenbroek BA, Jost CR, Wieringa B, Van der Zee CEEM (2005) Structural and behavioral consequences of double deficiency for creatine kinases BCK and UbCKmit. *Behav Brain Res* 157:219-234.

Tilney MS, Tilney LG, Stephens RE, Merte C, Drenckhahn D, Cotanche DA, Bretscher A (1989) Preliminary biochemical characterization of the stereocilia and cuticular plate of hair cells of the chick cochlea. *J Cell*

Biol 109:1711-1723.

Tombes RM, Shapiro BM (1985). Metabolite channeling: a phosphoryl-creatine shuttle to mediate high energy phosphate transport between sperm mitochondrion and tail. *Cell* 41:325-334.

Walker RG, Hudspeth AJ, Gillespie PG (1993) Calmodulin and calmodulin-binding proteins in hair bundles. *Proc Natl Acad Sci USA* 90:2807-2811.

Washburn M.P, Wolters D, Yates J.R. III. (2001) Large-scale analysis of the yeast proteome by multidimensional protein identification technology. *Nat Biotechnol* 19:242-247.

Yamoah EN, Lumpkin EA, Dumont RA, Smith PJ, Hudspeth AJ, Gillespie PG (1998) Plasma membrane Ca^{2+} -ATPase extrudes Ca^{2+} from hair cell stereocilia. *J Neurosci* 18:610-624.

Yoshizaki K, Nishikawa H, Watari H (1987) Diffusivities of creatine phosphate and ATP in an aqueous solution studied by pulsed field gradient ^{31}P NMR. *Jpn J Physiol* 37:923-928.

S1. Supplemental background

S1.1 ATP consumption and demands in hair bundles

Although other hair-bundle processes may require ATP, myosin activity, treadmilling actin, phosphoinositide turnover, and Ca^{2+} pumping are amenable to quantitative estimation of ATP consumption. We calculate ATP consumption in frog stereocilia, for which substantial quantitative data are available; these calculations show that the hair-bundle Ca^{2+} pump is likely to account for the lion's share of ATP consumption in an average frog stereocilium of 0.8 fl (Gillespie and Hudspeth, 1991).

Myosins. Frog stereocilia probably each have fewer than 5000 myosin molecules (Hasson et al., 1997); at a realistic actin-activated hydrolysis rate of 1 s^{-1} , myosin ATP hydrolysis would be $\sim 10 \mu\text{M s}^{-1}$.

PIP2 turnover. Given the area of a typical lipid ($0.7 \times 0.7 \text{ nm}$) and the surface area of an average frog stereocilium ($8 \times 10^{-12} \text{ m}^2$), each stereocilium contains ~ 107 phospholipids; PIP2 is likely to account for $\ll 5\%$ of this total. Given that the entire stereocilia PIP2 pool apparently turns over in less than 5 min (Hirono et al., 2004), PIP2 resynthesis requires $< 3 \mu\text{M s}^{-1}$ ATP.

Actin treadmilling. Stereocilia actin filaments treadmill as rapidly as $0.04 \text{ subunit s}^{-1}$ (Rzadzinska et al., 2004), which requires 1 ATP per subunit. Given that a frog stereocilium might contain as many as 1000 parallel filaments, ATP would be consumed at $\sim 1 \mu\text{M s}^{-1}$.

Ca^{2+} pumping. For a 100 pS transduction channel (Denk et al., 1995) and a -60 mV membrane potential, with a P_o of 0.1, ATPase-dependent removal of an ion of +2 charge accounting for 3% of the total transduction current (Lumpkin et al., 1997) will require consumption of $> 100 \mu\text{M s}^{-1}$ of ATP. When channel $P_{\text{open}} = 1$, the consumption rate is $> 1000 \mu\text{M s}^{-1}$.

Although myosins do not consume prodigious amounts of ATP, they require ATP levels to be maintained for efficient activity. The K_m for ATP for myosin-1c motility is $\sim 200 \mu\text{M}$ (Gillespie et al., 1999), indicating that ATP levels need to be maintained at millimolar levels to prevent

concentration-dependent fluctuations in enzyme activity. In addition, as ATP hydrolysis produces ADP, which inhibits myosin-1c with a K_i of $\sim 20 \mu\text{M}$ (Gillespie et al., 1999), maintenance of high a high ATP:ADP ratio is essential for sustained, efficient myosin activity.

S2. Supplemental results

S2.1 Identification of proteins by mass spectrometry

The five mass spectrometry runs used to generate Table 1 are summarized in Supplemental Table 1. Hair bundles from 105-125 chicken utricles were used in each experiment.

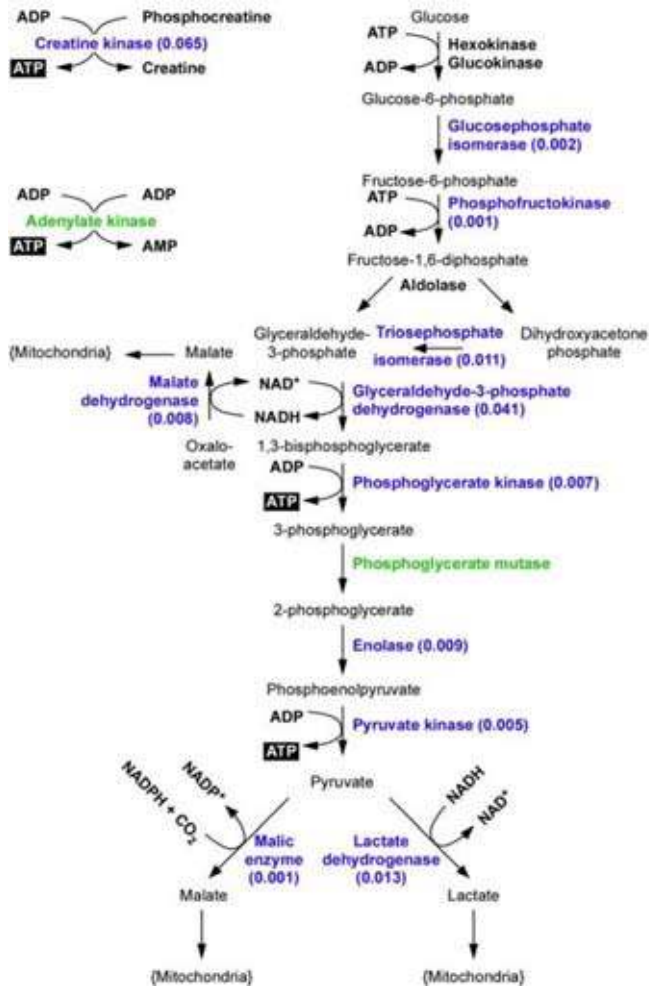
Supplemental Table 1. Chicken utricle mass spectrometry experiments.

| experimental name | experimental type | Mass spectrometer | # protein identification ($\log(e) < -1.0$) |
|--------------------------|--------------------------|--------------------------|---|
| CH1_A123 | LC-MS/MS | Q TRAP4000 | 77 |
| CHI182 | LC-MS/MS | QSTAR XL | 48 |
| CHI191 | GeLC-MS/MS | QSTAR XL | 168 |
| CHI223 | MuDPIIT | QSTAR XL | 305 |
| CHI239 | MuDPIIT | QSTAR XL | 134 |

Chicken utricle mass spectrometry experiments. Five mass spectrometry experiments were performed. Indicated are type of experiment, mass spectrometer used for analysis, and the number of protein identifications reported by Global Protein Machine, using X! Tandem searches, with a $\log(e)$ of -1.0 or better.

S2.2 Bundle proteins involved in ATP metabolism

Proteins involved in energy metabolism and identified in the hair-bundle preparation by mass spectrometry are displayed in Supplemental Fig. 1. Several proteins that did not meet the stringent criteria used for Table 1 are also indicated here. For example, adenylate kinase 1 (AK1) was identified in only two mass spectrometry runs and hence was not included in Table 1; nevertheless, we infer from the transduction experiments that it too plays an important role in bundle nucleotide metabolism.



Supplemental Figure 1 (left): Hair-bundle abundances of proteins involved in energy metabolism. Energy metabolism pathways, focusing on glycolysis. Enzymes labeled in blue were identified reproducibly by mass spectrometry (Table 1); intensity factors for each enzyme are indicated. Phosphoglycerate mutase and adenylate kinase were identified in 2/5 experiments (indicated by green labeling).

Curiously, two enzymes of malate metabolism, malic enzyme and malate dehydrogenase, were reproducibly present in the hair-bundle preparation. Malic enzyme can catalyze the production of malate from pyruvate (Hassel, 2001), while malate dehydrogenase interconverts malate and oxaloacetate (Goward and Nicholls, 1994). Like lactate dehydrogenase, malate dehydrogenase would recycle bundle NAD^+ dur-

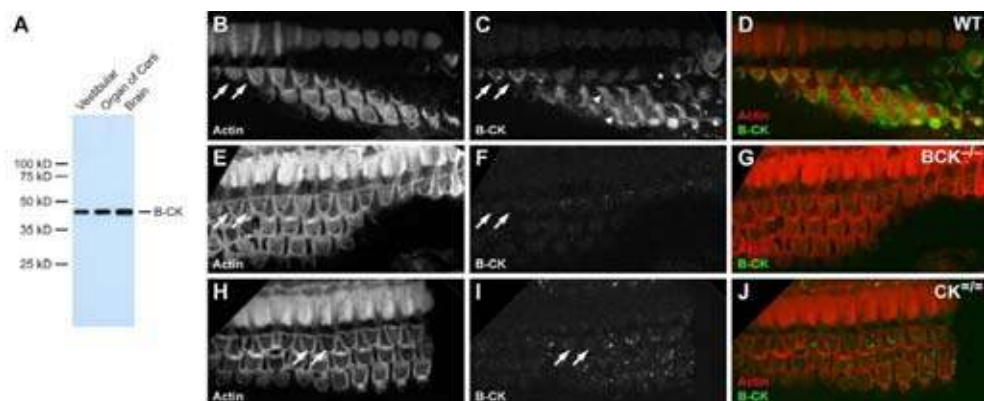
ing malate synthesis, transferring reducing equivalents to mitochondria via the malate-aspartate shuttle (McKenna et al., 2006). Although pathways involving malate may provide a second route for pyruvate metabolism, the significance of malic enzyme and malate dehydrogenase in hair bundles remains to be determined.

S2.3 Controls for cochlea BCK immunolocalization

In order to validate the BCK immunocytochemistry results, we carried out immunocytochemistry on mouse cochlea tissue using a polyclonal rabbit antibody against mouse BCK (gift of Dr. B. Wieringa). This antibody recognizes a single band of the appropriate molecular mass in mouse brain, cochlea, and vestibular organs (Supplemental Fig. 2A). Mice (10 months of age) were sacrificed and pericardially perfusion-fixed with 3% formaldehyde/PBS; temporal bones were removed, further fixed in 3% formaldehyde/PBS for 1 hour, and stored in PBS. Immunocytochemistry was carried out as described below. The resulting staining in mouse cochleas (Supplemental Fig. 2) was comparable to the staining in rat cochleas obtained with the rabbit anti-chicken BCK antibody (Fig. 4). Supplemental Fig. 2B-D shows tilted optical sections through the organ of Corti; arrows indicate hair bundles of outer hair cells, arrowheads point to the apical surfaces of Deiters' cells, and asterisks to Deiters' cell phalanges. Hair bundles were consistently labeled, although Deiters' cell labeling was usually stronger.

We further confirmed the specificity of the rabbit anti-mouse BCK antibody by staining cochleas from BCK^{-/-} knockout and CK^{-/-} double-knockout mice. No staining besides modest background staining was found in organ of Corti from BCK^{-/-} or CK^{-/-} mice (Supplemental Fig. 2E-J).

Consistent BCK labeling in cochlea with both antibodies required an antigen unmasking step, i.e., incubation of fixed organs in citrate/EDTA buffer at 60°C for 10 min. At higher temperatures (100°C), we observed speckled labeling in hair bundles with both antibodies in WT, BCK^{-/-}, and CK^{-/-} mice, suggesting that this labeling is an artifact of the unmasking procedure. As is well known anecdotally, some antibodies show artifactual labeling of stereocilia, which can be particularly problematic in the cochlea. Knockout mice offer the opportunity to unequivocally separate specific from nonspecific labeling of antibodies; the results shown here allow us to confirm the localization



Supplemental Figure 2: Controls for cochlea immunolabeling. A: Immunoblot with mouse tissues using rabbit polyclonal anti-mouse BCK antibody. B-J: Immunocytochemistry with the rabbit polyclonal anti-mouse BCK antibody. For each cochlea, five confocal sections, taken 1 μm apart, were subject to z-projection (maximum intensity), giving a single flattened image (shown). Arrows, bundles of outer hair cells; BCK labeling is seen in WT but not knockout organ of Corti. The apical surfaces (arrowheads) and phalanges (asterisks) of Deiters' cells are labeled. Dimensions of each panel are 47 x 94 μm .

of BCK to hair cells of the mouse.

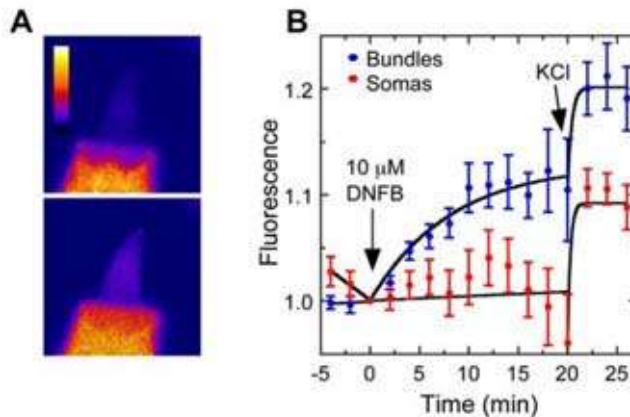
The abundance of BCK in Deiters' cells (Spicer and Schulte, 1992) could reflect a need for energy at the apical surface of these cells. Mitochondria are sparse at best at the ends of the long phalangeal processes of Deiters' cells (Engstrom, 1967); consistent with that observation, the mitochondrial potential dye tetramethyl rhodamine methyl ester (TMRM+) shows little or no labeling of Deiters' cell phalange apical terminals, despite strongly labeling hair cells (X. Shi and A.F. Nuttall, personal communication). Even if the requirements for ATP at Deiters' cell apical surfaces are modest, delivery of high-energy phosphates by facilitated diffusion would be required because of the length (tens of micrometers) of the phalanges.

S2.4 DNFB effects on Mg Green fluorescence

Mg Green fluorescence increased substantially in hair bundles, but not hair-cell somas, after treatment with 10 μM DNFB (Supplemental Fig. 3). Higher concentrations of DNFB led to swelling of isolated hair cells, which interfered with accurate measurements with this nonratiometric

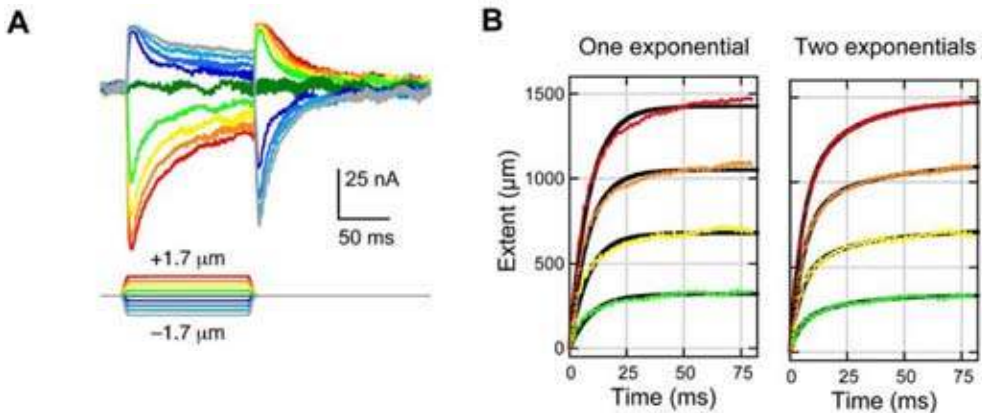
dye. Consequences of higher (100 μM) DNFB concentrations were not seen in the intact epithelium transduction assay, perhaps because the low Na^+ -, low Ca^{2+} -endolymph bathing apical surfaces prevented cation loading of hair cells via transduction channels. As a control, KCl depolarization induced a substantial rise of Mg Green signal in both compartments (Supplemental Fig. 3B, arrow), consistent with accelerated ATP turnover in response to depolarization-mediated Ca^{2+} entry and subsequent Ca^{2+} pumping.

While some hair bundles had large (>30%) increases in hair-bundle Mg Green fluorescence upon DNFB treatment, others had much lower fluorescence increases. The fluorescence signal depends on dye loading, resting intracellular Mg^{2+} levels, and ATP hydrolysis. Variability in DNFB-stimulated fluorescence may arise because some isolated hair cells were already Ca^{2+} loaded, so that their bundles were already depleted of ATP and hence resistant to creatine kinase inhibition. Indeed, imaging with the Ca^{2+} indicator fluo-3 suggested that the isolated hair cells were relatively Ca^{2+} loaded; consistent with that interpretation, we saw no significant change in fluo-3 signal upon DNFB treatment (data not shown).



Supplemental Figure 3: *DNFB inhibition causes rise in Mg Green fluorescence in hair bundles.* A: Confocal images of hair cells loaded with Mg Green. Top, control (0 min); bottom, 11 min after addition of DNFB. Images pseudocolored as indicated in linear scale. B: Averaged Mg Green fluorescence data from bundles ($n=19$) and somas ($n=18$). Data were normalized to fluorescence values at 0 min. Means \pm SEM are indicated; data were fit with single-exponential functions.

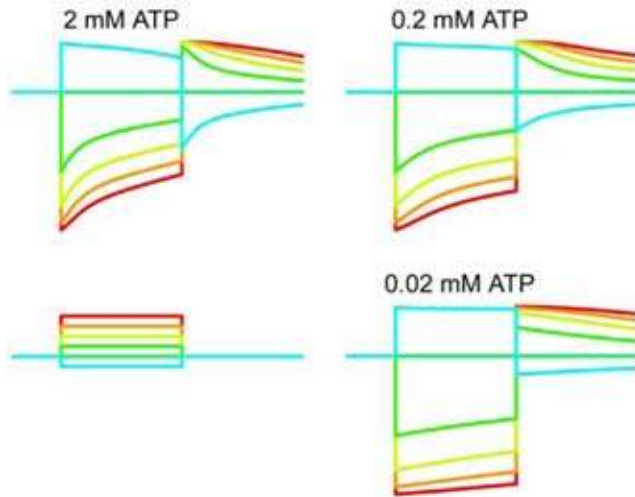
The absolute change in the concentration of ADP associated with the increased Mg Green signal is difficult to determine. The signal will be influenced by the concentrations of Mg^{2+} , Ca^{2+} , and adenine nucleotides; moreover, calibration of the response to give an absolute value for Mg^{2+} is difficult if not impossible (Leysens et al., 1996). For this reason we suggest that the Mg Green response be seen a strictly qualitative indication that ATP hydrolysis is increased in bundles, rather than somas, with DNFB application.



Supplemental Figure 4: *Two components of adaptation.* A: Transduction currents from a control sacculus. Note rapid adaptation to positive and negative displacements, and overshoots after the stimuli end with amplitudes that indicate the amount of adaptation during the stimulus. B: Extent of adaptive shift from inferred-shift analysis (data points), fit with single (left) or double (right) exponential functions. Double-exponential fit is much better than single-exponential fit.

S2.5 Two components of adaptation

Adaptation data, obtained by inferred-shift analysis, were fit best with double exponential functions (Supplemental Fig. 4). The inferred-shift method relies on one principal assumption, that adaptation is described by a pure shift of the displacement-response curve, without a change in its shape. This assumption is valid for bullfrog sacculus hair cells (Stauffer et al., 2005; Cheung and Corey, 2006). Similar to results from single bullfrog hair cells (Shepherd and Corey, 1994; Stauffer et al., 2005), the total extent of adaptation was a linear function of displacement, with a slope of 0.89.



Supplemental Figure 5: *Modeling slowing of adaptation during loss of [ATP].* Fast and slow adaptation rates (Fig. 5) were weighted by myosin velocity, assuming K_m for ATP of 0.2 mM. Stimuli were -0.4 to $1.6 \mu\text{m}$, in steps of $0.4 \mu\text{m}$, and 100 ms in duration.

However, we do not interpret the fast component of adaptation here to be the same as “fast adaptation” (Stauffer et al., 2005; Cheung and Corey, 2006), which requires much faster displacement stimuli. Indeed, the amplitude of our fast component ($\sim 50\%$ of the displacement) is much too large and its time constant much too slow (Stauffer et al., 2005). Instead, we suggest that our fast component is a combination of “fast adaptation,” unresolved in our experiments, and myosin movement.

S2.5 Modeling consequences of [ATP] decline for adaptation

To simulate the effects of ATP depletion on transduction currents, we modified our model for bullfrog saccular hair cells (Hirono et al., 2004) to include the concentration of ATP in estimates of adaptation rates. We used the simple hypothesis that adaptation rate constants would be weighted by the fractional myosin ATPase rate:

$$\text{fractional rate} = \frac{[\text{ATP}]}{[\text{ATP}] + K_m} \quad (\text{S1})$$

using a K_m of 0.2 mM. Not unexpectedly, a ten-fold reduction of [ATP], from 2 mM to 0.2 mM, only slowed adaptation rates by a factor of two, producing simulated currents very similar to those with higher [ATP]. Only with a further ten-fold reduction was adaptation slowed prominently (Supplemental Fig. 5).

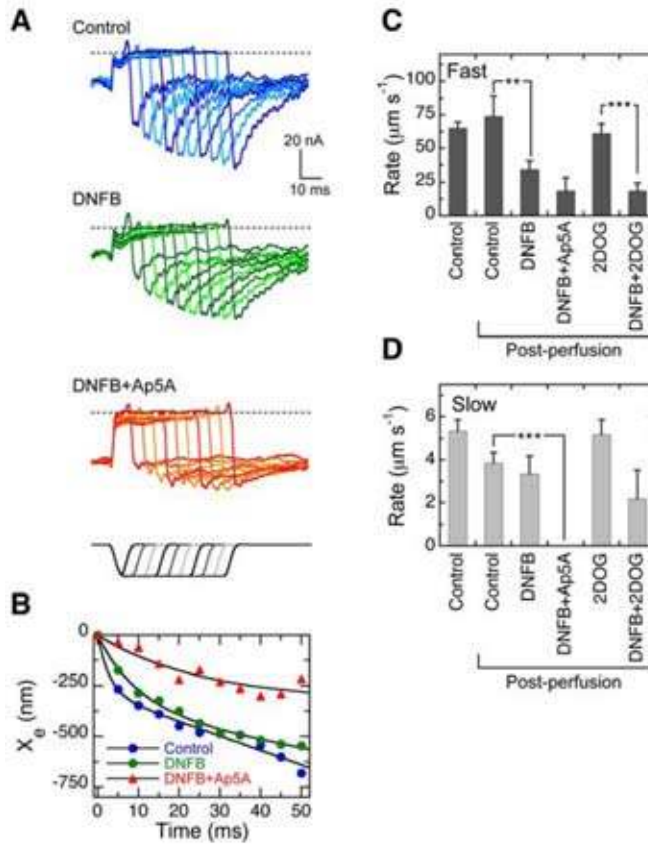
These simulations show that the modest effects of DNFB on adaptation rates (Fig. 5; Supplemental Fig. 6) could reflect a substantial decrease in hair bundle

S2.6 DNFB effects on negative adaptation

To measure the rate of negative adaptation, where gating-spring tension is reduced and motors can move unimpeded by opposing forces, we gave large inhibitory displacements for varying lengths of time. Upon return of the bundle to the resting position, an overshoot current appeared that reflected the amount of negative adaptation during the stimulus. By determining the inferred shift of the displacement-current curve corresponding to the amplitude of the overshoot current, we could estimate the adaptive shift during the stimulus (Stauffer et al., 2005). Negative adaptation was robust in the transepithelial microphonic preparation and, like in single frog and mouse hair cells, the resulting shift data were fit well with a model assuming a sum of fast exponential and slow linear components (Supplemental Fig. 6). Adaptive shifts were ~5-fold faster than that seen in isolated hair cells (Stauffer et al., 2005), perhaps because of reduced Ca^{2+} loading occurring with low- Ca^{2+} endolymph bathing the hair bundles.

The combination of DNFB and Ap5A significantly slowed fast and slow components of negative adaptation (Supplemental Fig. 6), consistent with previous evidence (Gillespie and Hudspeth, 1993) that adenylate kinase prevented slowing of adaptation by ADP, a potent Myo1c inhibitor (Gillespie et al., 1999). In addition, fast and slow components of negative adaptation were slowed by the combination of DNFB and 2DOG (Supplemental Fig. 6), consistent with a contribution of stereocilia glycolysis to maintenance of ATP levels there.

Somewhat surprisingly, DNFB had a stronger effect on fast negative adaptation than on slow (Supplemental Fig. 6C-D). A possible interpretation is that the resting point of the transduction apparatus, which controls the degree of fast adaptation, is sensitive to the concentration of ATP. As discussed for positive adaptation, an excess



Supplemental Figure 6: Inhibition of adaptation to negative displacements by DNFB.

A: Transduction currents from a single epithelium in response to $-1.7 \mu\text{m}$ negative displacements of varying durations. Top, control; middle, 30 min after perfusion with $100 \mu\text{M}$ DNFB in the apical and basal solutions; and bottom, 10 min after further addition of $500 \mu\text{M}$ Ap5A to the top compartment. Dashed line approximately indicates trans-epithelial current with channels closed. B: Inferred shift analysis showing adaptive shift during stimulus presentations of (A). Data were fit with a sum of exponential and linear components (control, DNFB) or a single exponential (DNFB+Ap5A). C: Fast adaptation rates before (control; $n=32$) and 30 min post-perfusion with control salines ($n=10$); $100 \mu\text{M}$ apical and basal DNFB ($n=10$); $100 \mu\text{M}$ DNFB apical and basal followed by $500 \mu\text{M}$ apical Ap5A ($n=3$); 5 mM 2-deoxyglucose and 5 mM pyruvate in glucose-free salines ($n=5$); $100 \mu\text{M}$ DNFB, 5 mM 2-deoxyglucose, and 5 mM pyruvate in glucose-free salines ($n=7$). Significance (two-tailed Student's t-test) indicated by: **, $P < 0.02$; ***, $P < 0.01$. Significance for the Control-DNFB/Ap5A comparison was $P = 0.083$. D: Slow adaptation rates; same epithelia as (C). Significance for the DNFB-DNFB/2DOG comparison was $P = 0.087$.

of creatine kinase could prevent DNFB from dramatically reducing the concentration of ATP, and as long as adenylate kinase can scavenge ADP, slow adaptation may be relatively unaffected. Inhibition of adenylate kinase with Ap5A would then slow adaptation from the combination of reduced ATP and increased ADP.

S2.7 Auditory brainstem response latencies

Because ABR latencies appeared prolonged (Fig. 6), we measured peak I latencies (Supplemental Table 2). Analyses of variance and post hoc tests, with factor group and ABR peak I latency as the dependent variable, were performed to analyze between-group differences (SPSS, one-way ANOVA with Bonferroni, SPSS 12.0.1). For 8-32 kHz pure-tone stimuli, peak I latencies were significantly prolonged in CK^{-/-} mice, compared to WT controls ($P < 0.02$).

In a given mouse strain, latencies shorten as stimulus intensity is increased (Mitchell et al., 1996); the increase in latency seen with the CK^{-/-} mice may simply reflect decreased sensitivity of the auditory periphery.

Supplemental Table 2. ABR peak I latencies.

| | n | click JI latency (ms) | SD | n | 8 kHz JI latency (ms) | SD | n | 16 kHz JI latency (ms) | SD | n | 32 kHz JI latency (ms) | SD |
|--------------------|---|-----------------------------|------|---|-----------------------------|------|---|------------------------------|------|---|------------------------------|------|
| wt | 8 | 1.47 | 0.08 | 8 | 1.66 | 0.18 | 8 | 1.75 | 0.14 | 8 | 1.79 | 0.18 |
| BCK ^{-/-} | 4 | 1.45 | 0.04 | 4 | 1.80 | 0.23 | 4 | 1.81 | 0.14 | 4 | 1.86 | 0.07 |
| CK ^{-/-} | 8 | 1.54 | 0.17 | 8 | 2.01 ^{***} | 0.22 | 8 | 1.98 ^{**} | 0.14 | 7 | 2.06 ^{***} | 0.09 |

Mean latencies and standard deviations of peak I of ABR in mice in response to a click and high-frequency tone burst stimuli for wild type (WT), BCK^{-/-} and CK^{-/-}. Statistically significant differences in comparison with wild type is indicated with asterisk (** $P < 0.02$; *** $P < 0.01$).

S3. Supplemental experimental procedures

S3.1 Hair-bundle isolation

Chicken embryos (E18-E20) were sacrificed by decapitation; utricles were dissected out in chicken saline (155 mM NaCl, 6 mM KCl, 2 mM MgCl₂, 4 mM CaCl₂, 3 mM D-glucose, 10 mM HEPES, pH 7.25) and the otolithic membranes were removed without protease treatment. After adhering utricles to a glass coverslip coated with Cell-Tak (BD Biosciences), a solution of chicken saline containing 4% low-melting-point agarose (Gibco-BRL), maintained at 40°C, was flowed into the chamber; the agarose was then allowed to solidify at 4°C. The solid agarose plug then was trimmed and introduced on to a stage, utricles facing up. Using a dissection microscope, utricles were pulled away from the gel surface, perpendicular to the bundles. Bundles then were removed by cutting a block of agarose containing the bundles, spearing the block with the tungsten needle, and transferring it to a microfuge tube. All steps after the initial dissection were performed under a laminar-flow hood in order to reduce keratin contamination.

S3.2 Total protein measurement

Total protein was measured in a fluorescence plate reader using with a CBQCA protein quantitation kit (Molecular Probes/Invitrogen). Isolated hair bundles from 10-15 chicken utricles (agarose gel volume ~5 µl) or one whole utricle were mixed with 140 µl (or 1 ml for whole utricle) 0.1 M borate buffer (pH 9.3) containing 0.1 % SDS, sonicated for 2 min, and incubated for 30 min at 4°C to allow protein extraction. After a short microfuge centrifugation at 12.000 rpm, 135 µl of the bundle extract (or appropriate volume of whole utricle extract) was sampled for protein quantitation using the CBQCA protein quantitation kit (Molecular Probes, Invitrogen). BSA was used as the quantitation standard. Control experiments were carried out to ensure that the agarose embedding the bundles did not interfere with protein quantitation.

S3.3 Quantitative immunoblotting

Agarose plugs containing bundles from chicken utricles each were diluted with sample buffer and heated for 5 min; proteins were separated

by SDS-PAGE and transferred to blotting membranes essentially as described previously (Dumont et al., 2001). Known amounts of purified actin (Cytoskeleton, Inc.), recombinant BCK (Hornemann et al., 2000), and GAPDH (Sigma) were used as standards. BCK concentration was determined using ultraviolet absorbance (a 1 mg/ml solution has an OD₂₈₀ of 0.87). Rabbit poly-clonal antibodies against chicken BCK have been described (Kaldis et al., 1996); immunoblots were probed anti-BCK antibody diluted 1:200. Rabbit polyclonal antibodies against mouse BCK were generated in the laboratory of Dr. B. Wieringa; although not previously published, they have been shown to be highly specific for BCK. This anti-mouse BCK antibody was used at 1:2000. Detection used a horseradish-peroxidasebased chemiluminescence detection system (Super Signal West Pico; Pierce); exposed X-ray films were digitized with a flat-bed scanner. Quantitation of standards and unknowns was carried out with ImageJ.

S3.4 Immunocytochemistry

Tissues were fixed for 25 min in 3% formaldehyde. After blocking for 1 hr with 1% bovine serum albumin, 3% normal donkey serum, and 0.2% saponin in PBS, organs were incubated with primary antibodies overnight at room temperature in blocking buffer. After incubation in primary antibody, organs were washed 3 x 5 min with PBS and incubated with secondary antibodies (7.5 µg/ml Cy5-conjugated donkey anti-rabbit IgG, donkey anti-mouse IgG, donkey anti-goat IgG, Jackson ImmunoResearch Laboratories, West Grove, PA) and 0.25 µM FITC-phalloidin (Sigma) in the blocking solution for 1-3 hr. Finally, organs were washed 5 times in PBS and mounted in Vectashield (Vector, Burlingame, CA). Samples were viewed with a Plan Aporchromat 60x (1.40 NA) oil lens on a Nikon TE 300 inverted microscope with a Bio-Rad MRC 1024 confocal imaging system. In order to obtain profile views from hair bundles, fixed and stained sacculi were mechanically disrupted using fine forceps while tissues were in Vectashield. In other cases, profile views were reconstructed from confocal Z-stacks using the "Reslice" function in ImageJ software. Antibodies against BCK were described in the previous section. Other primary antibodies, used in a 1:100 dilution unless otherwise noted, were obtained from: goat anti-GAPDH antibody (V-18), goat anti-TIM antibody (N-21), and rabbit anti-enolase antibody (H-300), all from Santa Cruz

Biotechnology; rabbit anti-GRP78 antibody, rabbit anti-Histone H2 antibody, and mouse monoclonal anti-tropomyosin antibody (TM311), all from AbCam; mouse monoclonal anti-HSP70 antibody, from Stressgen Bioreagents; rabbit anti-CLIC5a antibody (Berryman et al., 2004), from Mark Berryman; rabbit anti-radixin antibody (Pataky et al., 2004) (1:400), from Jim Hudspeth; rabbit anti-PTPRQ (1:400), from Guy Richardson; rabbit anti-NHERF antibody (N7286) and mouse monoclonal anti- α -tubulin antibody (1:400), from Sigma. Specificity of the goat anti-GAPDH antibody, goat anti-TIM antibody, and the rabbit anti-BCK antibody was demonstrated by antibody blocking control experiments using antigenic GAPDH and TIM peptides (Abcam; 1:100) or purified recombinant BCK (5 μ g/ml final concentration) respectively. In each case, the peptide or protein was preincubated with the antibody for 15 min.

S3.5 ATP determination

Isolated hair cells were evenly dispersed in saline solution, and 100 μ l aliquots were taken for each experiment. DNFB (Sigma) was added to a final concentration of 10 μ M (diluted from a 10 mM stock solution in chloroform). 5-(6-) carboxyeosin (Invitrogen Molecular Probes) was added to final concentration of 20 μ M (diluted from a 20 mM stock solution in DMSO). Control hair cells were incubated with equivalent volumes of chloroform or DMSO respectively. To account for background ATP in the dissociation solution, we allowed hair cells to settle and sampled 100 μ l of the cell-free saline for ATP measurement. ATP was extracted from cells by mixing the cell suspension with 3 volumes of 0.5% TCA, and the solution was neutralized by adding equal volumes of Trisacetate buffer pH 7.8. Neutralized extract (10 μ l) was pipetted into 96-well microplates and luminescence was measured in a Veritas Microplate Luminometer (Turner BioSystems). Luminometer settings were: 100 μ l injection volume of luciferin/luciferase assay reagent, 2 sec delay time after reagent injection, and 10 sec signal integration time. For each set of experiments, the average number of hair cells per aliquot was determined. Aliquots of hair cell suspension were pipetted onto a culture dish and allowed to settle and hair cells were counted. All experiments were carried out in triplicate; error bars represent standard deviation.

S3.6 Transepithelial microphonic preparation

We used a transepithelial voltage clamp preparation (Corey and Hudspeth, 1983; Kroese et al., 1989) to measure mechanotransduction. Frog sacculi were dissected in standard saline, then mounted across a plastic disk using Vetbond butylcyanoacrylate adhesive (WPI). The disk was placed in a two-compartment apparatus, which allowed separate solutions on the sacculus' apical and basolateral sides. Unless otherwise indicated, the basal surface of the preparation was perfused with oxygenated depolarizing saline (95 mM NaCl, 17 mM KCl, 2 mM MgCl₂, 4 mM CaCl₂, 3 mM D-glucose, 10 mM HEPES, pH 7.25), which decreases hair-cell input resistance and decreases depolarization induced by mechanotransduction (Corey and Hudspeth, 1983). By preventing depolarization, a rapid decrease in transduction current due to reduced driving force is eliminated. The apical surface was perfused with oxygenated frog endolymph (123.5 mM KCl, 0.25 mM CaCl₂, 3 mM D-glucose, 10 mM HEPES, pH 7.25).

To restrict measurement to hair cells with similar directional sensitivity, the otolithic membrane was peeled away from most of the sensory epithelium, leaving the membrane attached to only a few hundred hair cells at the abneural edge (Corey and Hudspeth, 1983). Maximum transduction currents varied from preparation to preparation because of nonidentical peeling. Stimuli were delivered with a one-dimensional piezoelectric bimorph, filtered at 100 Hz, and were coupled to the otolithic membrane with a solid glass rod, pulled to ~0.2 mm diameter and flattened on its bottom surface.

The transepithelial potential was clamped at 0 mV with a voltage-clamp circuit. The signal was amplified (~107 V/A), filtered at 1 kHz, and digitized at 5 kHz. Fast and slow positive adaptation rates were extracted from the data using inferred-shift analysis (Shepherd and Corey, 1994), as described previously (Hirono et al., 2004; Stauffer et al., 2005). Negative adaptation rates were determined as described previously (Hirono et al., 2004; Stauffer et al., 2005).

Because inhibition by DNFB develops slowly (Infante and Davies, 1965), we perfused the apical and basal chambers with 100 μM DNFB for 30 min. Control sacculi were perfused with endolymph and depolarizing saline for 30 min; there was a modest decrease in rates of fast and slow adaptation over that time period.

In experiments with 2DOG, we eliminated D-glucose from the

medium and substituted 5 mM 2DOG. We also included 5 mM pyruvate, which should supply energy through oxidative phosphorylation, bypassing glycolysis. We reasoned that this would prevent ATP depletion in the cell soma, which might otherwise prevent maintenance of the ion gradients that allow transduction currents to flow.

S3.7 Histological analysis

Inner ears of 6, 15 and 30 day old wild type and CK^{-/-} mice were isolated and immersion-fixed for 1 day in 4% formaldehyde, decalcified in 10% ethylenediaminetetraacetic acid (EDTA) for 3, 5 and 7 days, respectively, and embedded in glycol methacrylate (JB4). Cochlear sections (2 μ m) were stained with toluidine blue.

S3.8 Auditory brainstem response measurements

Auditory brainstem responses (ABR) were recorded differentially by using needle electrodes (vertex for positive, bilateral mastoids for negative, and halfway tail for ground). Clicks (100 μ s) and high frequency (8 kHz, 16 kHz and 32 kHz) tone burst stimuli (1 ms rise/fall, 3 ms plateau time) were presented with a stimulus rate of 30 pulses per s in a soundfield presented by a high-frequency tweeter (Elac Jet III) placed 6 cm in front of each ear. A standard clinical recording EEG-system (5-channel Synergy, Oxford Instruments) with an internal stimulator was used to obtain the click-evoked ABR; for the higher tone burst frequencies, the same EEG-system was modified to obtain external trigger pulses from an external computer/stimulator that was developed to generate high-frequency stimuli using a digital-to-analog converter (6062E; National Instruments). Loudness levels were calibrated according to IEC 61672-2 standards (2004) using a Bruel & Kjaer Analyzer type 2260 and corrected for the soundfield. Mice were i.p. anesthetized with ketamine (200 mg/kg) and xylazine (14 mg/kg). The analysis time window was set at 15 ms, including a pre-stimulus time of 1.5 ms to assess the baseline, followed by a time window of 13.5 ms from onset of stimulus. EEG-signals were recorded using 100-3000 Hz band pass filter settings, auto-reject mode set at 100 μ V and 60 Hz notch-filter on. All averaged signals were obtained at different stimulus levels according to standard audiometric top-down procedures; ABR-peaks were identified according to the Jewett & Williston nomencla-

ture (Jewett and Williston, 1971). The auditory hearing threshold was defined as the level in decibels at which no reproducible ABR peak morphology was recognized in the ipsilateral measured ear.

S3.9 Vestibular tests

Vestibular function was evaluated using two previously described methods (Kiernan et al., 1999), albeit slightly modified for this study.

S3.9.1 Tail suspension-reaching response.

The mouse was held in the air by the tail at 1 m above, and slowly lowered into a cage; behavior was scored on a 1-5 scale. Scoring: 1, hanging straight down and stretched out with its forelimbs towards the sawdust (normal vestibular function); 2, curling slightly with its body but mostly hanging straight down; 3, curling towards its belly and now and then moving its head upwards; 4, head tilting (to one side) and curling towards its belly; 5, severe head bobbing and curling strongly towards its belly (severe vestibular dysfunction).

S3.9.2. Swim test

The mouse was placed in a cage half-filled with lukewarm (24°C) water and swimming ability including balance in the water was scored on a 1-5 scale. Scoring: 1, normal swimming behavior: after being placed in water, the mouse quickly resurfaced with a “whipping” motion of its tail, managed to keep its back, head, nose and tail above the surface of water, and showed good swimming with all 4 limbs (normal vestibular function); 2, head only above water, showed swimming but with head tilted slightly to one side; 3, eyes at water level, spine slightly distorted, head tilted and swimming with difficulty; 4, strongly distorted spine, head or body tilted to one side, more floating than swimming; 5, whole body submerged, distorted body and head position, not able to swim (severe vestibular dysfunction).

References

Cheung EL, Corey DP (2006) Ca^{2+} changes the force sensitivity of the hair-cell transduction channel. *Biophys J* 90:124-139.

Corey DP, Hudspeth AJ (1983) Analysis of the microphonic potential of the bullfrog's sacculus. *J Neurosci* 3:942-961.

Denk W, Holt JR, Shepherd GM, Corey DP (1995) Calcium imaging of single stereocilia in hair cells: localization of transduction channels at both ends of tip links. *Neuron* 15:1311-1321.

Dumont RA, Lins U, Filoteo AG, Penniston JT, Kachar B, Gillespie PG (2001) Plasma membrane Ca^{2+} -ATPase isoform 2a is the PMCA of hair bundles. *J Neurosci* 21:5066-5078.

Engstrom H (1967) The ultrastructure of the sensory cells of the cochlea. *J Laryngol Otol* 81:687-715.

Gillespie PG, Gillespie SK, Mercer JA, Shah K, Shokat KM (1999) Engineering of the myosin-I β nucleotide-binding pocket to create selective sensitivity to N6-modified ADP analogs. *J Biol Chem* 274:31373-31381.

Gillespie PG, Hudspeth AJ (1991) High-purity isolation of bullfrog hair bundles and subcellular and topological localization of constituent proteins. *J Cell Biol* 112:625-640.

Gillespie PG, Hudspeth AJ (1993) Adenine nucleoside diphosphates block adaptation of mechano-electrical transduction in hair cells. *Proc Natl Acad Sci USA* 90:2710-2714.

Goward CR, Nicholls DJ (1994) Malate dehydrogenase: a model for structure, evolution, and catalysis. *Protein Sci* 3:1883-1888.

Hassel B (2001) Pyruvate carboxylation in neurons. *J Neurosci Res* 66:755-762.

Hasson T, Gillespie PG, Garcia JA, MacDonald RB, Zhao Y, Yee AG, Corey DP (1997) Unconventional myosins in inner-ear sensory epithelia. *J Cell Biol* 137:1287-1307.

Hirono M, Denis CS, Richardson GP, Gillespie PG (2004) Hair cells require phosphatidylinositol 4,5-bisphosphate for mechanical transduction and adaptation. *Neuron* 44:309-320.

Hornemann T, Rutishauser D, Wallimann T (2000) Why is creatine kinase a dimer? Evidence for cooperativity between the two subunits. *Biochim Biophys Acta* 1480:365-373.

Infante AA, Davies RE (1965) The effect of 2,4-dinitrofluorobenzene on the activity of striated muscle. *J Biol Chem* 240:3996-4001.

Jewett DL, Williston JS (1971) Auditory-evoked far field averaged potentials from the scalp of humans. *Brain Pathol* 94:681-696.

Kaldis P, Stolz M, Wyss M, Zanolla E, Rothen-Rutishauser B, Vorherr T, Wallimann T (1996) Identification of two distinctly localized mitochondrial creatine kinase isoenzymes in spermatozoa. *J Cell Sci* 109:2079-2088.

Kiernan AE, Zalzman M, Fuchs H, Hrabe de Angelis M, Balling R, Steel K P, Avraham KB (1999) Tailchaser (Tlc): a new mouse mutation affecting hair bundle differentiation and hair cell survival. *J Neurocytol* 28:969-985.

Kroese AB, Das A, Hudspeth AJ (1989) Blockage of the transduction channels of hair cells in the bullfrog's sacculus by aminoglycoside antibiotics. *Hear Res* 37:203-217.

Leyssens A, Nowicky AV, Patterson L, Crompton M, Duchen MR (1996) The relationship between mitochondrial state, ATP hydrolysis, $[Mg^{2+}]_i$ and $[Ca^{2+}]_i$ studied in isolated rat cardiomyocytes. *J Physiol* 496:111-128.

Lumpkin EA, Marquis RE, Hudspeth AJ (1997) The selectivity of the hair cell's mechano-electrical-transduction channel promotes Ca^{2+} flux

at low Ca^{2+} concentrations. *Proc Natl Acad Sci USA* 94:10997-11002.
McKenna MC, Waagepetersen HS, Schousboe A, Sonnewald U (2006) Neuronal and astrocytic shuttle mechanisms for cytosolic-mitochondrial transfer of reducing equivalents: current evidence and pharmacological tools. *Biochem Pharmacol* 71:399-407.

Mitchell C, Kempton JB, Creedon T, Trune D (1996) Rapid acquisition of auditory brainstem responses with multiple frequency and intensity tone-bursts. *Hear Res* 99:38-46.

Pataky F, Pironkova R, Hudspeth AJ (2004) Radixin is a constituent of stereocilia in hair cells. *Proc Natl Acad Sci USA* 101:2601-2606.

Rzadzinska AK, Schneider ME, Davies C, Riordan GP, Kachar B (2004) An actin molecular treadmill and myosins maintain stereocilia functional architecture and self-renewal. *J Cell Biol* 164:887-897.

Shepherd GMG, Corey DP (1994) The extent of adaptation in bullfrog saccular hair cells. *J Neurosci* 14:6217-6229.

Spicer SS, Schulte BA (1992) Creatine kinase in epithelium of the inner ear. *J Histochem Cytochem* 40:185-192.

Stauffer EA, Scarborough JD, Hirono M, Miller ED, Shah K, Mercer JA, Holt JR, Gillespie PG (2005) Fast adaptation in vestibular hair cells requires myosin-1c activity. *Neuron* 47:541-553.

Chapter 5

Deficiency for brain-type creatine kinases in mice causes defective thermoregulation

Femke Streijger¹, Frank Oerlemans¹, Antonio C. Bianco², Miriam O. Ribeiro³, Helma Pluk¹, Bé Wieringa¹, Catharina E.E.M. Van der Zee¹.

¹ Department of Cell Biology, NCMLS, Radboud University Nijmegen Medical Centre, Nijmegen, The Netherlands

² Department of Medicine, Thyroid Section, Division of Endocrinology, Diabetes and Hypertension, Brigham and Women's Hospital and Harvard Medical School, Boston, Massachusetts

³ Department of Biosciences, School of Biological, Exact and Experimental Sciences, Mackenzie University, São Paulo, Brazil

in preparation



Abstract

The cytosolic brain-type creatine kinase (BCK) and mitochondrial ubiquitous creatine kinase (UbCKmit) have an important role in cellular energy homeostasis in astrocytes and neurons. Both creatine kinase (CK) isoforms are expressed throughout the prepubescent and adult period in many different brain areas, including the hypothalamus.

In this study, we suggest the involvement of CK in both body temperature homeostasis and cold induced thermo-alterations in mice. With both brain-type CK isoforms being absent, the basal body temperature reproducibly dropped $\sim 1.0^{\circ}\text{C}$ below normal each day during the early morning period. The CK $^{-/-}$ mice exhibited decreased weight gain associated with less white and brown fat accumulation and smaller brown adipocytes. Also, circulating levels of glucose, triglycerides and leptin were reduced relative to wildtypes. CK $^{-/-}$ mice developed severe hypothermia during a 24-hour cold challenge, but exogenously administered noradrenaline was able to increase brown adipose tissue thermogenesis. Cold induction of UCP1 mRNA was also normal, indicating that brown adipose tissue responsiveness is not impaired in absence of CK. Surprisingly, the number of c-Fos immunoreactive neurons in specific hypothalamic nuclei after a cold challenge was higher in CK $^{-/-}$ mice than in wildtypes.

Combined, these findings indicate that the defective thermoregulation is not due to reduced locomotion, food intake, or gross deficits in brown adipose tissue physiology. Rather, our findings point to perturbed metabolic sensing and signaling processes for activation of cold-responses in the hypothalamus, possibly in combination with altered neuronal transmission in other areas of the CK $^{-/-}$ mouse brain.

1. Introduction

In tissues like muscle and brain, the often high and fluctuating ATP demands require strict maintenance of energy homeostasis with tight coupling between energy production and consumption. One of the enzymes that play a key role in the buffering and fast transfer of cellular fuel in a wide variety of tissues is creatine kinase (Bessman and Carpenter, 1985; Walliman et al., 1992; O’Gorman et al., 1996; Wyss and Kaddurah-Daouk, 2000; In ‘t Zandt et al., 2004). Creatine kinase (CK)

isoenzymes catalyse the synthesis of phosphocreatine (PCr) and its subsequent use in the regeneration of ATP by the reaction $\text{MgATP}^{2-} + \text{Cr} \leftrightarrow \text{MgADP}^- + \text{PCr}^{2-} + \text{H}^+$. In brain, two isoforms of creatine kinase are present, each encoded by separate genes, i.e. the cytosolic brain creatine kinase (BCK) and the mitochondrial ubiquitous creatine kinase (UbCKmit). We have shown that mice deficient for both BCK and UbCKmit (CK^{-/-} mice) have a severely abnormal phenotype (Shin et al., 2007; Streijger et al., 2005) characterized by a permanently reduced body weight, impaired spatial learning, low nestbuilding activity, impaired hearing, and abnormal morphology of the hippocampus in the brain.

In this study, we examined the possible role of CK in thermoregulation. We noticed that some CK^{-/-} mice incidentally succumbed due to a sudden and severe drop in body temperature, which occasionally could decrease to 28°C (unpublished observation). Strikingly, these sudden temperature drops were never observed in wildtypes or any of the single knockout mice (BCK^{-/-} or UbCKmit^{-/-}). Responses to maintain normal body temperature are coordinated by neuroendocrine interactions and the autonomic nervous system. The control of body temperature takes place in the central nervous system at different locations and levels in the spinal cord, the lower brainstem, and hypothalamus (Bahshad et al., 1999; Nagashima et al., 2000; Oldfield et al., 2002; Romanovsky et al., 2007). Of the sites in the hypothalamus the preoptic area, the paraventricular, dorsomedial, and ventromedial nuclei, and the posterior and lateral hypothalamic areas are the critical areas mediating temperature homeostasis in mammals. Brown adipose tissue (BAT), muscle, or the tail veins (Romanovsky et al., 2007) are the most important effector systems for heat loss compensation.

In order to advance our understanding of how body temperature is regulated in CK^{-/-} mice, we monitored their baseline temperature profile and investigated the capacity to maintain thermal homeostasis by exposing the animals to a 24-hour cold challenge. Through a series of experiments, we evaluated the key elements of thermal physiology in our mutant mice including thermogenic functioning of BAT. Furthermore, c-Fos immunostaining within specific hypothalamic neuronal nuclei and UCP1 mRNA response in BAT were used as indicators of neuronal signaling activity following cold exposure. As creatine kinases are generally important for energy metabolism and homeostasis, we also studied if the thermoregulatory defects in CK^{-/-} mice

are associated with abnormalities in food intake, body composition, or energy expenditure. Although several aspects of integral physiology appeared altered when CK is absent, our combined findings suggest that inefficient neuronal transmission may be a dominant factor in the thermoregulatory defect.

2. Materials and methods

All procedures involving animals were approved by the Animal Care Committee of the Radboud University Nijmegen Medical Centre conform the guidelines of the Dutch Council for Animal Care and the NIH. All efforts were made to reduce the number of animals used.

2.1 Animals

The generation of brain-type creatine kinase double knockout mice (further referred to as CK^{-/-} mice) and genotype analysis was described in detail elsewhere (Streijger et al. 2005). Adult (3-8 months) male CK^{-/-} mice and age-matched wildtype mice with the same genetic background (25% 129/Ola and 75% C57BL/6) were used for phenotyping. As reported earlier, body weight of adult CK^{-/-} mice (~23 g) is significantly less than that of wildtype mice (~31 g; Streijger et al., 2005). To adjust for the lower bodyweight of the CK^{-/-} mice, for some experimental set-ups we also tested wildtype animals with equally low bodyweight and tissue weight distribution (6 weeks old; ~22 g).

2.2 General housing conditions

All mice were housed in the central animal facility with room temperature controlled at 21°C, and an artificial 12h:12 h light:dark cycle (lights on at 07:00). The mice were housed in Macrolon type II cages with food and water available ad libitum. The animals were group housed, unless mentioned differently. Each cage was supplied with a mouse igloo, which serves as environmental enrichment and provides security and nesting area for mice (PLEXX, Elst, The Netherlands).

2.3 Body temperature measurements at room temperature

To minimize handling induced stress on measuring body temperature, the ELAMS animal identification and body temperature monitoring systems was used (PLEXX, Elst, The Netherlands). Temperature-sensitive transponders (model IPTT-300) were subcutaneously implanted into the thorax region of adult male mice from each genotype. The body temperatures of mice during the course of experiment were recorded using the wireless scanner (model DAS-5004, PLEXX, Elst, The Netherlands). To obtain a 30-hour profile, body temperature was recorded for 3x30 hours with a 3-hour interval. For each time point the average body temperature (°C) was calculated.

2.4 Body temperature response upon cold exposure

Body temperatures were first measured at room temperature (~21°C; 21:00) and then with 6h intervals during subsequent 24-hour cold exposure (4°C) using temperature-sensitive transponders (as described in section 2.3). If the body temperature of any mouse dropped below 28°C, the animal was removed from the cold and placed back at room temperature for recovery. Animals were housed together (3 or 4 animals per cage) in standard housing conditions.

2.5 Body temperature response upon fasting

Adult wildtype and CK^{-/-} mice were fasted for 12 hours. Body temperatures were first measured at room temperature (~21°C; 17:00) and then after 5, 8, 12 hours during subsequent fasting using temperature-sensitive transponders (as described in section 2.3). Body temperatures during arousal were recorded 30 min after the animals were given free access to food.

2.6 Daily food intake

Mice were individually housed and had unrestricted access to a pre-weighted (~200 g) amount of pellets in the foodhopper. For three days, food intake was measured every 24 hours (09:00) and calculated as the average amount of pellets eaten/per day (g).

2.7 Motor activity profile

To assess basal activity, mice were tested in an activity cage (Cools et al., 1986). With seven test set-ups the locomotor activity of seven mice at a time could be measured simultaneously. The activity cages (36 cm×24 cm×25 cm) were equipped with three photoelectric cells 2 mm above the floor. Interruptions of the infrared light beams were measured and stored electronically. Experiments were performed in sound tight, diffusely illuminated boxes with water soaked food pellets in a corner. The actual activity was subsequently measured for 48 hours continuously to obtain two night and day activity cycles. Average activity counts were then calculated from the second 24-hour period, in order to minimize influence of stress-induced activity. The activity data of the mice were recorded per minute and expressed as the average total counts during the day and the night period.

2.8 Tissue weight and femur length

Adult mice were euthanized and the following tissues were collected and weighted: Brown adipose tissue (BAT; interscapular, subscapular and cervical), white adipose tissue (WAT; inguinal, epididymal and thorax), liver, brain and muscle (gastrocnemius). The length of the femur was chosen as an index of body size. Anaesthetized adult mice were immobilized on a plate with adjustable fixation bars for their teeth and paws. The animal was positioned with the right hind leg slightly outstretched such that the leg was at a 90° angle with their body. To measure the length, a ventral x-ray image of the femur was analyzed and assessed as the distance (mm) from the inferior border of the lateral epicondyle to the superior border of the femur head.

2.9 Blood collection and plasma analysis

On the day of blood collection, adult mice were removed from their housing room and were taken to an immediately adjacent separate area where blood was taken. To minimize stress response, the time from initial cage disturbance to being anaesthetized was less than 30 sec for each mouse. Blood samples were taken between 12:00 and 14:00 using wildtype and CK-*-/-* mice ad random. Blood was taken by means of an orbita puncture under ether anesthesia. Blood was col-

lected into an aprotinine (3000 units/ml) EDTA (1,5 mg/ml) tube, and was centrifuged at 6000 rpm at 4°C for 3 min. Plasma was collected and stored at -20°C until use. Measurements included leptin (mouse leptin ELISA kit, Crystal Chem Inc., Chicago, IL, USA), free fatty acids (NEFA C, WAKO Chemicals USA, Richmond, VA, USA), triglycerides (triglycerides kit, Sigma Diagnostics, St. Louis, MO, USA), and glucose (Infinity glucose reagent, Sigma Diagnostics).

2.10 BAT thermal response to NA infusion

The BAT thermal response to noradrenaline (NA) was performed as previously described (Ribeiro et al., 2000 and 2001). Adult mice were anaesthetized with urethan (560 mg/kg) and chloralose (38 mg/kg) injected intraperitoneally. Mice were kept on a warming pad through the course of the experiment. A polyethylene (PE-50) cannula was inserted in the left jugular vein and later was used for NA infusion. BAT temperatures (°C) were measured using a precalibrated thermistor probe secured under the interscapular BAT pad (model YSI 427; Yellow Springs Instrument Co., Yellow Springs, OH, USA). Body temperature was measured with a colonic probe (model YSI 423; Yellow Springs Instrument Co.). The probes were connected to a high-precision thermometer (YSI Precision 4000A Thermometer; Yellow Springs Instrument Co.). Body temperature and BAT temperature were monitored during a period of ~15 min to obtain a stable baseline, and then NA (2 mg/ml) infusion was started at a rate of 0.5 µl/min for 30 min. Data were plotted over time and expressed as the mean increase in BAT and body temperature (Δ BAT; Δ Body; °C).

2.11 Western blot analysis

Interscapular BAT, epididymal WAT, liver, brain and muscle (gastrocnemius) of adult mice were isolated and immediately frozen in liquid nitrogen. The tissues were homogenized in 150 mM NaCl, 1% triton X-100, 25 mM Tris pH 8.0, 2 mM EDTA and Protease Inhibitor Cocktail (Roche Diagnostics, Mannheim, Germany). Following a 20-min incubation at 4°C, the lysates were centrifuged at 15000 rpm for 20 min at 4°C. Protein concentration in the resulting supernatant was determined using the Bradford protein assay. The lysates were stored at -80°C until use. Protein samples were separated on a 10% SDS-page gel and

transferred to nitrocellulose membranes (ECL, Amersham Pharmacia Biotech BA, Piscataway AB, Uppsala, Sweden) by western blotting. The membranes were blocked with 5% non-fat dry milk in PBST (PBS, 0.1% Tween-20) for 60 min and incubated overnight with primary monoclonal anti-BCK 21E10 (1:1000; De Kok et al., 1995), polyclonal anti-UbCKmit #253 (1:1000; Friedman and Perryman, 1991), or polyclonal anti-UCP1 (1:5000, Chemicon International, Temecula, CA, USA) antibody at 4°C. The membranes were washed 3x5 min with PBST and incubated for 60 min with secondary peroxidase-conjugated Goat anti-Rabbit (Pierce Biotechnology Inc., Rockford, IL, USA) for use with UbCKmit and UCP1 antibodies, or ImmunoPure[®] Protein A/G (Pierce Biotechnology Inc) for use with BCK 21E10 antibodies. Following a 6x5 min wash with PBST, the immunoreactive bands were visualized using Lumi-Light Western Blotting Substrate (Roche Diagnostics) and exposed to autoradiography films (Kodak X-Omat, Eastman Kodak Company, Rochester, NY, USA). For the detection of brain specific creatine kinase isoforms in different tissues, an amount of 50 mg of total liver, muscle, brown and white adipose protein was loaded per lane. To prevent overexposure, the amount of total brain lysate was reduced to 10 mg. Also for the detection of UCP1 in BAT an amount of 10 mg of total protein was loaded. To accurately quantify UCP1 on the Western blot, direct infrared fluorescence detection on the Odyssey Imaging System was used.

2.12 Northern blot analysis

Interscapular BAT of naïve and 12-hour cold exposed wildtype and CK^{-/-} mice was isolated for Northern blot analyses and immediately frozen in liquid nitrogen. RNA of brown adipose tissue was isolated by the LiCl-Urea method. An amount of 3 mg of RNA was loaded on a 1% MOPS formaldehyde agarose gel. After overnight electrophoresis in MOPS buffer (20 mM MOPS pH 7.0, 0.5 mM sodium acetate, 1 mM EDTA), the RNA was transferred to a nylon membrane (Hybond-N, Amersham Pharmacia Biotech BA, Uppsala, Sweden) in 10xSSC (3 M NaCl, 0.3 M NaCitrate) overnight, and cross-linked by UV irradiation. The membranes were prehybridized for at least 1 hour in (pre)hybridization buffer (250 mM Na₂HPO₄ pH 7.2, 7% SDS, 1 mM EDTA) at 65°C. Purified cDNA probes (ESTs) were labeled with α -³²P-dCTP by random hexamer priming. After removing non-incorporated

radio-labeled nucleotides on Sephadex-G50 columns the probe was used for hybridization, performed overnight at 65°C. Then, blots were washed with 25 mM Na₂HPO₄ pH 7.2, 0.1% SDS, 1 mM EDTA and exposed to autoradiography films (Kodak BioMax XAR films, Eastman Kodak Company, Rochester, NY, USA). To accurately quantify UCP1 and GAPDH signals on the Northern blot, a PhosphorImager system was used. Detailed information on the ESTs and origin of the UCP1 or GAPDH cDNAs is available at www.ncmls.kun.nl/celbio (De Groof et al., 2001).

2.14 Immunohistochemistry for CK isoforms

Mice were anesthetized (hypnorm/dormicum/water; 0.21 ml/30 g BW) and perfused with 15 ml phosphate buffered saline (0.1 M PBS) and 30 ml 4% paraformaldehyde (PF) solution. Brain and interscapular BAT were isolated and immersed in a suitable amount of fixative for 12-15 hours at 4°C. Tissues were embedded in paraffin and 6 µm sections were placed on microscope slides (Superfrost/Plus glass slides, Menzel-Gläser, Braunschweig, Germany). Sections were incubated in 0.375% H₂O₂ and 0,1% Sodium Azide for 30 min at 37°C to inactivate endogenous peroxidase, rinsed in 0.01% PBST, and incubated in 1% BSA and 2% normal donkey serum for 30 min to reduce nonspecific background staining. Sections were incubated overnight at 4°C with polyclonal rabbit primary antibody for either BCK (1:1000; De Kok et al., 1995), or UbCKmit (1:1000; Friedman and Perryman, 1991), diluted in 0.01% PBS-T. After washing, sections were incubated for 60 min at room temperature with a secondary biotinylated donkey anti-rabbit antiserum (1:250 in PBS-T; Vector Laboratories, Burlingame, CA, USA). After a further washing step, the sections were incubated with Biotinylated enzyme Complex (Vectastain Elite ABC kit, Vector Laboratories). The peroxidase activity was detected with 0.04% DAB; 0.015% H₂O₂ and 0.025% Nickel ammoniumnitrate in 0.1 M Tris pH 7.6 for a maximum of 10 min. Subsequently, sections were rinsed with water and counterstained with haematoxylin for 3 min. Finally, sections were dehydrated with ethanol and xylene, embedded in Eukitt (Electron Microscopy Sciences, Fort Washington, PA, USA) and examined by light microscopy.

2.15 c-Fos immunoreactivity

To determine c-Fos protein expression following cold exposure (12 hours at 4°C), c-Fos immunostaining was performed on brain sections as previously described (Veening et al., 2004). Prior to perfusion, animals were anaesthetized by subcutaneous injection of a hypnorm/dormicum/water mixture (1:1:2; 0.21 ml/30 g BW). Perfusion was performed transcardially with 0.1 M phosphate buffered saline (15 ml PBS; pH 7.4), followed by 4% PF (in 0.1 M PBS, pH 7.4; 30 ml). Subsequently, brains were removed and post-fixed overnight in buffered 4% PF at 4°C. To cryoprotect before sectioning, brains were transferred to a 15% and 30% sucrose solution for 24 hours. Coronal sections of the brain (thickness: 40 µm) containing the median preoptic area (mPOA), paraventricular nucleus (PVN) and the dorsomedial hypothalamic nucleus (DMH) were cut on a freezing microtome and collected in 0.1 M PBS. The free-floating sections were washed twice in PBS and soaked for 1 hour in PBS containing 0.1% bovine serum albumin and 0.5% Triton X-100. Sections were incubated overnight (RT) with a polyclonal sheep anti-Fos antibody (1:10000; OA-11-824, Cambridge Research Biochemicals, Billingham, UK). After a washing step, sections were incubated for 60 min (RT) with donkey anti-sheep (1:400; Jackson ImmunoResearch Laboratories, West Grove, PA, USA) and for 120 min in ABC-elite (1:800 in PBS; Vectorstain elite ABC kit; Vector Laboratories, Burlingame, CA, USA). In between incubations, sections were washed with PBS. The c-Fos antibody peroxidase complex was visualized by DAB (3, 3'-diaminobenzidine tetrahydrochloride) staining. Sections were incubated for 10 min in a chromogen solution consisting of 0.02% DAB and 0.03% Ni-ammonium sulphate in 0.05 M Tris-buffer (pH 7.6) and subsequently for 10 min in chromogen solution containing hydrogen peroxide (10:1 of a 30% solution per 25 ml of reaction solution). All sections were rinsed several times with PBS.

The number of c-Fos positive cells in the hypothalamic mPOA, PVN and the DMH were counted using a light microscope (10x and 25x objective). For each region, we counted both sides of three continual sections and calculated the average of the six areas (Maruyama et al., 2003).

2.16 Histological analysis of brown adipose tissue

For the quantification of the brown adipocyte size, paraffin-embedded sections of interscapular BAT of adult wildtype and CK^{-/-} mice were examined histologically by means of hematoxylin-eosin staining. Three 500 mm distanced microscope slides each with four sections were used. Cells were photographed (40x objective) using a Nikon Coolpix 990 digital camera attached to the microscope. Fat cells from the digital images (150-200 cells per animal) were analysed with PC-image software to obtain the average brown adipocyte area (mm²), perimeter (mm) and diameter (mm).

For transmission electron microscopy, mice were transcardially perfused with 2% glutaraldehyde and 2% paraformaldehyde in 0.1 M sodium cacodylate buffer (pH 7.4). Interscapular BAT was removed and cut into ~1 mm³ thick pieces. The tissues were washed three times with 0.1 M sodium cacodylate buffer over a 48-hour period, and postfixed with 1% osmium tetroxide and 1% sodium ferrocyanide in 0.1 M cacodylate buffer (3 hours). After further washing (2x) with sodium cacodylate buffer for 3 hours, the sections were dehydrated through a series of graded ethanols to propylene oxide, and embedded in Agar 100 epoxy resin (Agar Scientific Ltd. Essex, UK). Thin (100-nm) sections were cut with a diamond knife (Element Six, Cuijk, The Netherlands) on a Leica UCT ultramicrotome (Leica Microsystems GmbH, Wetzlar, Germany) and placed on 75-mesh carbon coated copper grids (Stork Veco bv Eerbeek, The Netherlands). Sections were contrasted with uranyl acetate and lead citrate and micrographs were taken with a JEOL 1010 electron microscope (Jeol Ltd., Tokyo, Japan). For each animal, 4-7 randomly taken BAT micrographs were analyzed at a magnification of 5000x. Per genotype the average mitochondrial area (mm²) and density (number of mitochondria per 10 mm² of cytoplasm) over all micrographs was estimated using manual grid point counting.

2.16 Statistics

All data are presented as means \pm sem. The statistical significance of differences between two groups was assessed by two-tailed Student's t-test. For experiments with three groups (age- and weight-matched wildtype and CK^{-/-} mice), a one-way ANOVA followed by Bonferro-

ni's post-hoc test was performed. To analyze group differences over time the ANOVA repeated measures with post hoc analysis (Student's t-test) was used. All statistical procedures were performed using the SPSS 12.0 software package. Statistical significance was set at $P < 0.05$.

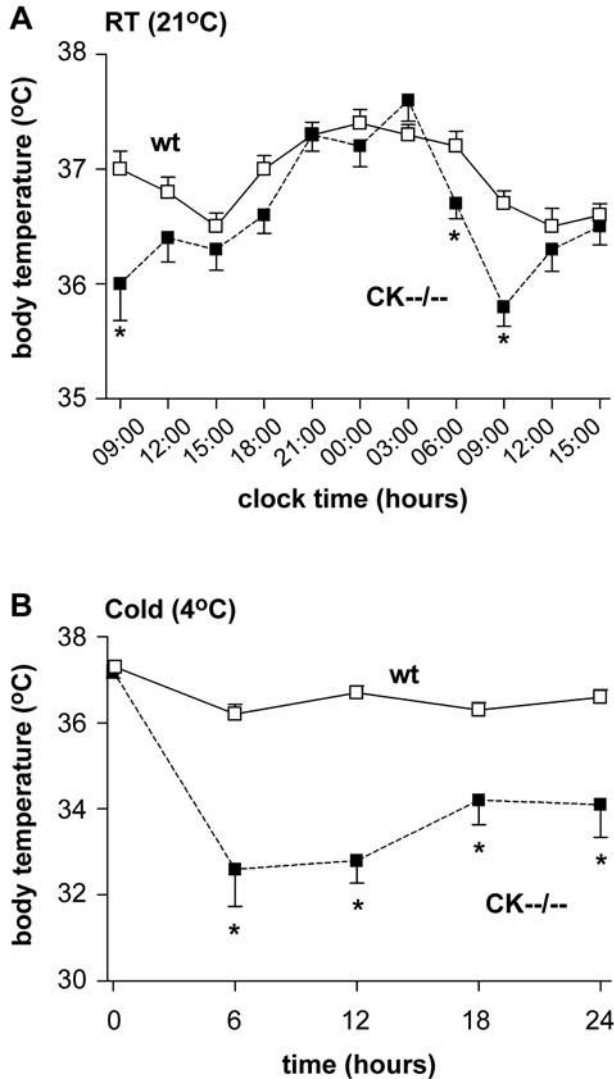


Figure 1: Body temperature profile of wildtype and CK-/- mice. (A) At room temperature (RT) CK-/- mice (black squares) demonstrated a significantly ($* P < 0.007$) lower morning body temperature compared to wildtype mice (white squares). (B) Upon cold challenge, CK-/- mice (black squares) were unable to sustain body temperature whereas wildtypes (white squares) could ($* P < 0.001$).

3. Results

3.1 CK^{-/-} mice have lower morning body temperature

The average body temperature profiles for both wildtype (n=20) and CK^{-/-} (n=18) mice showed a circadian rhythm (Fig. 1A). Wildtype mice, housed at room temperature, showed average body temperatures alternating between $36.7 \pm 0.1^\circ\text{C}$ and $37.3 \pm 0.1^\circ\text{C}$ during the day and night period, respectively. Throughout the three successive 30 hour periods of recording, the average body temperature of CK^{-/-} mice during the early night was similar to that of wildtypes but after 03:00 am the body temperature of CK^{-/-} mice started to decrease and remained lower for the next six hours. At 06:00, 1 hour before light-onset, CK^{-/-} body temperature was $\sim 0.5^\circ\text{C}$ lower than in wildtypes (wt: $37.2 \pm 0.1^\circ\text{C}$; CK^{-/-}: $36.7 \pm 0.1^\circ\text{C}$; $P < 0.007$), and dropped further to a $\sim 1^\circ\text{C}$ difference at 09:00 (wt: $36.9 \pm 0.1^\circ\text{C}$; CK^{-/-}: $35.9 \pm 0.2^\circ\text{C}$; $P < 0.001$). During the afternoon the average body temperature in CK^{-/-} mice slowly increased and was no longer significantly different from wildtypes thereafter. The consistence of the abnormally low morning body temperature was confirmed by additional temperature measurements (n=10 for both groups) between 09:00-11:00 during 12 days, showing an average body temperature of $36.7 \pm 0.1^\circ\text{C}$ for wildtypes and $35.6 \pm 0.2^\circ\text{C}$ for CK^{-/-} mice ($P < 0.001$).

3.2 CK^{-/-} mice are unable to sustain body temperature upon cold challenge

Next, to investigate the adaptive responses of CK^{-/-} mice (n=12) and wildtypes (n=10) to cold exposure, we transferred animals from room temperature to a 4°C environment and measured their body temperature after 6, 12, 18 and 24 hours (Fig 1B). At the start of the experiment (21:00), the body temperature of both genotype groups did not differ (wt: $37.4 \pm 0.2^\circ\text{C}$; CK^{-/-}: $37.6 \pm 0.2^\circ\text{C}$). During cold exposure, wildtype mice acclimatized well and kept their body temperature at $36.7 \pm 0.1^\circ\text{C}$, only 0.7°C below normal during the entire 24-hour cold period. Although wildtype mice were able to maintain normal thermoregulation, CK^{-/-} mice displayed significant reductions in body temperature during cold challenge. Within 18 hours of cold exposure, 33% of the CK^{-/-} mice (4 out of 12) showed severe hypothermia and died when their body tem-

perature dropped below 28°C. These animals were not included in the analysis. The remaining CK^{-/-} mice showed a physiologically strenuous 3-5°C body temperature drop ($F(1,16) = 38.658$, $P < 0.001$; Fig. 1B). Post hoc testing revealed that the body temperature declined significantly after the first 6 hours following cold exposure and remained consistently lower in CK^{-/-} mice compared to wildtypes (6 hours: $P < 0.001$; 12 hours: $P < 0.001$; 18 hours: $P < 0.007$; 24 hours: $P < 0.009$). It is of note that the CK^{-/-} mice are smaller (~23 g) compared to age-matched wildtype mice (~31 g; Streijger et al., 2005). Therefore, also wildtype animals with a similar low body weight (6 weeks old; ~22 g; $n=11$) as CK^{-/-} mice were subjected to cold exposure. Again, these weight-matched controls showed a reduction of approximately 0.5°C in body temperature, which remained constant during the entire 24-hour exposure period, indicating that genotype and not body size or weight is the dominant determining factor.

3.3 CK is expressed in various hypothalamic nuclei, and nerves and arteries innervating BAT

Using western blot analysis and immunohistochemistry, we examined the tissue specific expression of BCK and UbCKmit in specific hypothalamic brain areas, adipose tissue and muscle, which are important sites for cold-induced thermogenesis. As shown in Fig. 2A, BCK and UbCKmit were highly expressed in total brain lysates of wildtype mice, whereas no expression was observed in thermoregulatory active organs such as brown adipose tissue (BAT) and skeletal muscle. Only at very long exposure time, weak levels of UbCKmit could be detected in white adipose tissue (WAT) lysates. Additional immunohistochemistry of wildtype BAT (Fig. 2B) and WAT (data not shown) also revealed no BCK and UbCKmit staining in adipocytes itself. However, the nerves and arteries innervating the adipose tissue stained clearly positive for BCK (Fig. 2B). Interestingly, the BCK expression in blood vessels was restricted to the smooth muscle layer. Adipose tissue incubated with UbCKmit antibody showed no detectable staining in the innervating nerves, while a high degree of background staining was observed in the smooth muscle cells. Immunohistochemistry for BCK and UbCKmit on wildtype brain showed a strong expression throughout the brain, including regions known to be implicated in the central control of temperature, like the arcuate nucleus (Arc), medial preoptic area

(mPOA), and paraventricular nucleus (PVN) (Fig. 2C). This suggests a possible defect at the hypothalamic endpoint in the brain-fat axis for thermoregulation.

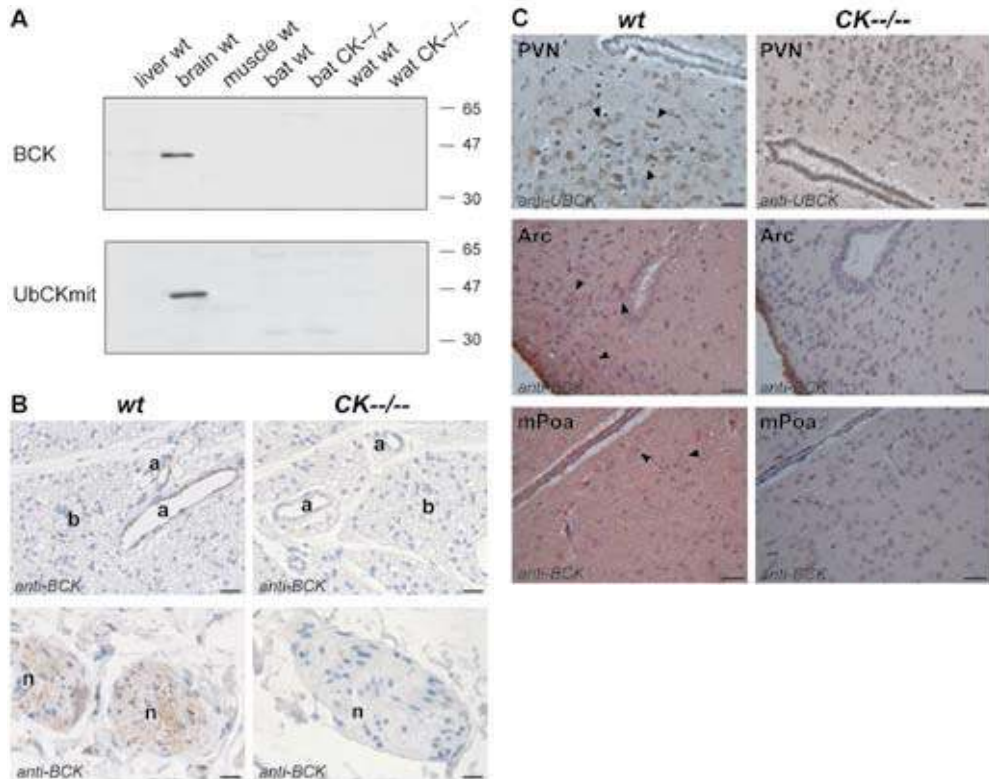


Figure 2: Brain creatine kinase (BCK) and ubiquitous creatine kinase (UbCKmit) expression in various tissues. (A) Western blot analyses revealed immunoreactivity towards BCK and UbCKmit in total brain lysates of wildtype (wt) animals. However, liver, muscle, brown adipose tissue (BAT) and white adipose tissue (WAT) of wildtype and CK^{-/-} mice remained negative. (B) This was consistent with the absence of immunostaining for creatine kinase in brown adipocytes (b). However, BCK was present in arteries (a) and nerves (n) innervating BAT. Horizontal black bar represents 100 μm. (C) BCK and UbCKmit were expressed in brain regions involved in thermoregulation like the paraventricular nucleus (PVN), arcuate nucleus (Arc) and medial preoptic area (mPOA). Horizontal black bar represents 25 μm.

3.4 Locomotor activity is normal in CK- $-/-$ mice

Increased skeletal muscle activity (exercise or shivering), tends to increase body temperature by accelerating fuel oxidation (Cannon and Nedergaard, 2004). So, to investigate alterations in heat-generating locomotor activity both groups were tested in an activity cage (Table 1). The activity profiles for wildtype and CK- $-/-$ mice were similar, with activity slowly decreasing after light onset and increasing just after the beginning of the dark phase. Wildtype mice (n=8) showed activity levels alternating between 1470 ± 129 counts and 2247 ± 425 counts during the day and night period, respectively (Table 1). While activity levels for CK- $-/-$ mice (n=8) appeared to be increased by ~30% during the light phase (1973 ± 262 counts) and night (3009 ± 570 counts), this was however not significantly different. (Table 1) Thus, our data does not support a model in which the lower morning body temperature is due to decreased locomotor activity.

Table 1. Comparative behavioral and physiological analysis of wildtype and CK- $-/-$ mice

| | wildtype | CK- $-/-$ | |
|--|-----------------|-----------------|-----|
| body weight (g) | 35.1 ± 0.7 | 25.4 ± 0.8 | *** |
| food intake per day | | | |
| absolute (g per animal) | 5.3 ± 0.1 | 4.4 ± 0.2 | *** |
| relative (mg per animal/g body weight) | 151.4 ± 4.9 | 175 ± 6.2 | ** |
| activity (counts) | | | |
| day | 1470 ± 129 | 1973 ± 262 | |
| night | 2247 ± 425 | 3009 ± 570 | |
| blood parameters | | | |
| glucose (mmol/l) | 10.2 ± 0.3 | 8.7 ± 0.4 | ** |
| leptin (ng/ml) | 1.3 ± 0.1 | 0.9 ± 0.1 | * |
| FFA (mmol/l) | 0.47 ± 0.04 | 0.36 ± 0.04 | |
| TG (mmol/l) | 0.60 ± 0.08 | 0.37 ± 0.04 | * |

Significantly different from wildtype (Student's t-test): *P < 0.05; **P < 0.01; ***P < 0.001.

3.5 CK^{-/-} mice consume less food

Thermoregulation is an adaptation of the basal metabolic rate in response to stimuli such as food intake (Cannon and Nedergaard, 2004). We therefore examined whether a change in food consumption could explain the abnormal body temperature regulation in our CK^{-/-} mice (Table 1). Analysis of food intake over a 3x24-hour time period revealed group differences for the absolute ($F(1,24) = 11.388$, $P < 0.001$) and relative food consumption ($F(1,24) = 13.447$, $P < 0.001$; Table 1). Wildtype animals consumed 5.3 ± 0.1 g of food per day ($n=9$), mainly eaten during the night. Food intake of CK^{-/-} mice was 17% lower than that of wildtypes, namely 4.4 ± 0.2 g per day ($n=9$, $P < 0.001$). However, because CK^{-/-} mice were leaner (Streijger et al., 2005), the food intake expressed per gram of body weight actually exceeded that of wildtypes by 16% (wt: 151 ± 4.9 mg per day/g BW; CK^{-/-}: 175 ± 6.2 mg per day/g BW; $P < 0.03$; Table 1). Moreover, young wildtype mice (~22 g) consumed similar amounts of food (4.5 ± 0.1 g per day; $n=7$) like CK^{-/-} mice, however exhibited normal body temperature. These data strongly suggest that the thermogenic problems in CK^{-/-} mice are not related to abnormal food consumption.

3.6 Reduced serum lipid and glucose content in CK^{-/-} mice

The carbohydrate and lipid fuels for BAT controlled thermogenesis are glucose, triglycerides and free fatty acids (Shimizu et al., 1991; Inokuma et al., 2005; Moira et al., 2005; Wu et al., 2006), substrates which may be used either directly or stored for later use. Leptin levels in serum usually adequately reflect (among other things) the status of the energy reserves of the animal. To reveal abnormal metabolic regulation we determined the serum levels of these fuel metabolites as well as leptin in wildtype ($n=11$) and CK^{-/-} mice ($n=10$; Table 1). In CK^{-/-} mice a significant reduction in serum triglycerides levels of ~39% was observed (wt: 0.60 ± 0.08 mmol/l; CK^{-/-}: 0.37 ± 0.04 mmol/l; $P < 0.03$; Table 1), whereas plasma glucose was down by 15% (wt: 10.2 ± 0.3 mmol/l; CK^{-/-}: 8.7 ± 0.4 mmol/l; $P < 0.005$). Although FFAs levels also appeared lower (wt: 0.47 ± 0.04 mmol/l; CK^{-/-}: 0.36 ± 0.04 mmol/l), this was not significant ($P < 0.08$; Table 1). The serum leptin concentration level were found to be decreased in CK^{-/-} mice (wt: 1.3 ± 0.1 ng/ml; CK^{-/-}: 0.9 ± 0.1 ng/ml; $P < 0.03$; Table 1). Combined, these

results indicate integral physiological changes in energy balance in the CK^{-/-} mice

3.7 CK^{-/-} mice show a similar fasting-induced body temperature response

CK enzymes play an essential role in cellular energy metabolism, and thermoregulation is closely tied to energy availability. During periods of inefficient energy supply, mammals lower their body temperature and metabolic rate to conserve fuel (Swan, 1974; Hudson, 1978; Hudson and Scott, 1979; Himms-Hagen, 1985; Nagashima et al., 2003; Overton and Williams, 2004). To investigate if CK deficiency has resulted in a negative energy balance at the whole body level, we analyzed whether CK^{-/-} mice were more sensitive to an overnight fast. Using temperature-sensitive transponders, the body temperature response was monitored prior to and following 12-hour fasting in CK^{-/-} mice and wildtypes (n=10 for both groups; Fig. 3A-B). In response to fasting, both genotype groups show an equal drop of 4-5°C in body temperature evident late in the dark phase. At 05:00, the average minimum temperature of wildtype mice dropped to $33.8 \pm 0.9^\circ\text{C}$ (Fig. 3A), whereas the body temperature of CK^{-/-} mice declined to an average of $32.2 \pm 1.0^\circ\text{C}$ (Fig. 3B). When food restriction was terminated by giving the animals free access to food, the fall in body temperature in wildtype and CK^{-/-} mice rapidly normalized back to initial values within 30 min (Fig. 3A-B).

3.8 CK^{-/-} mice have reduced adiposity

In Figure 4A-C we assessed the amount of WAT and BAT (wt, n=10-11; CK^{-/-}, n=9-10) and compared that to the weight of various other organs including muscle (n=5 both groups), brain (wt, n=11; CK^{-/-}, n=10) and liver (wt, n=11; CK^{-/-}, n=10). Additionally, the length of the femur was chosen as an index of body size (wt, n=12; CK^{-/-}, n=5). In wildtype mice, WAT was located predominantly intra abdominally around the epididymis (342.6 ± 40.4 mg), and in smaller amounts subcutaneously (inguinal: 237.9 ± 22.8 mg; thorax: 136.5 ± 15.4 mg) (Fig. 4A). CK^{-/-} mice contained a WAT mass which was reduced 40 to 50% in size, apparent in all three fat depots (epididymal: 173.3 ± 19.8 mg; $P < 0.001$; inguinal: 142.7 ± 14.4 mg; $P < 0.003$; thorax: 78.2 ± 11.0 mg;

$P < 0.006$). Additionally, $CK^{-/-}$ animals have distinctly smaller interscapular (wt: 81.6 ± 6.8 mg; $CK^{-/-}$: 51.4 ± 6.0 mg; $t(1,19) = 3.393$, $P < 0.003$), subscapular (wt: 50.3 ± 5.5 mg; $CK^{-/-}$: 25.8 ± 1.4 mg; $P < 0.001$), and cervical (wt: 16.0 ± 1.3 mg; $CK^{-/-}$: 11.6 ± 1.5 mg; $P < 0.04$) BAT depots as well (Fig. 4B). Liver ($P < 0.001$), brain ($P < 0.02$),

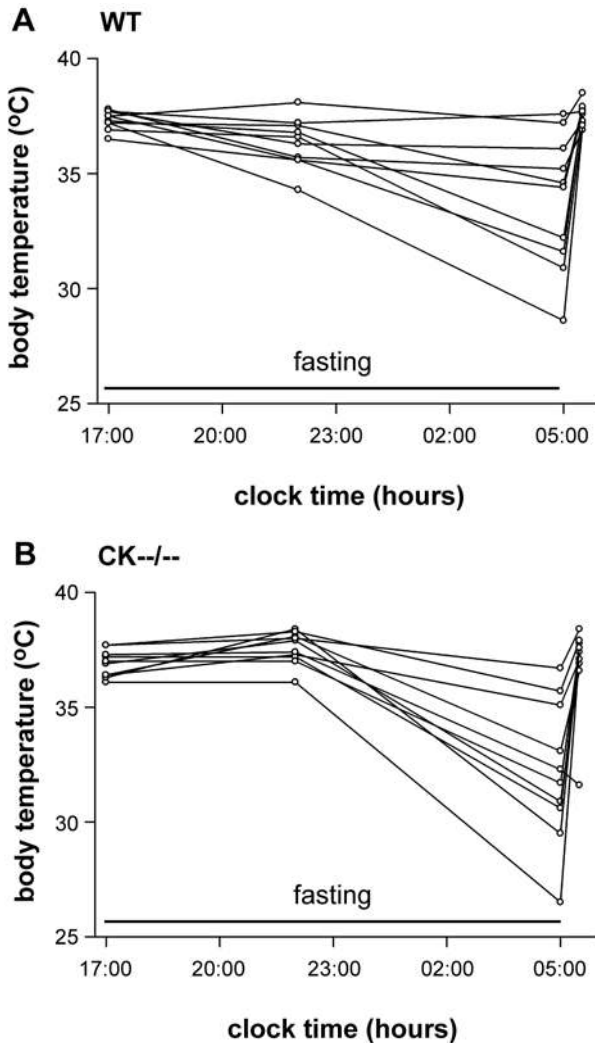
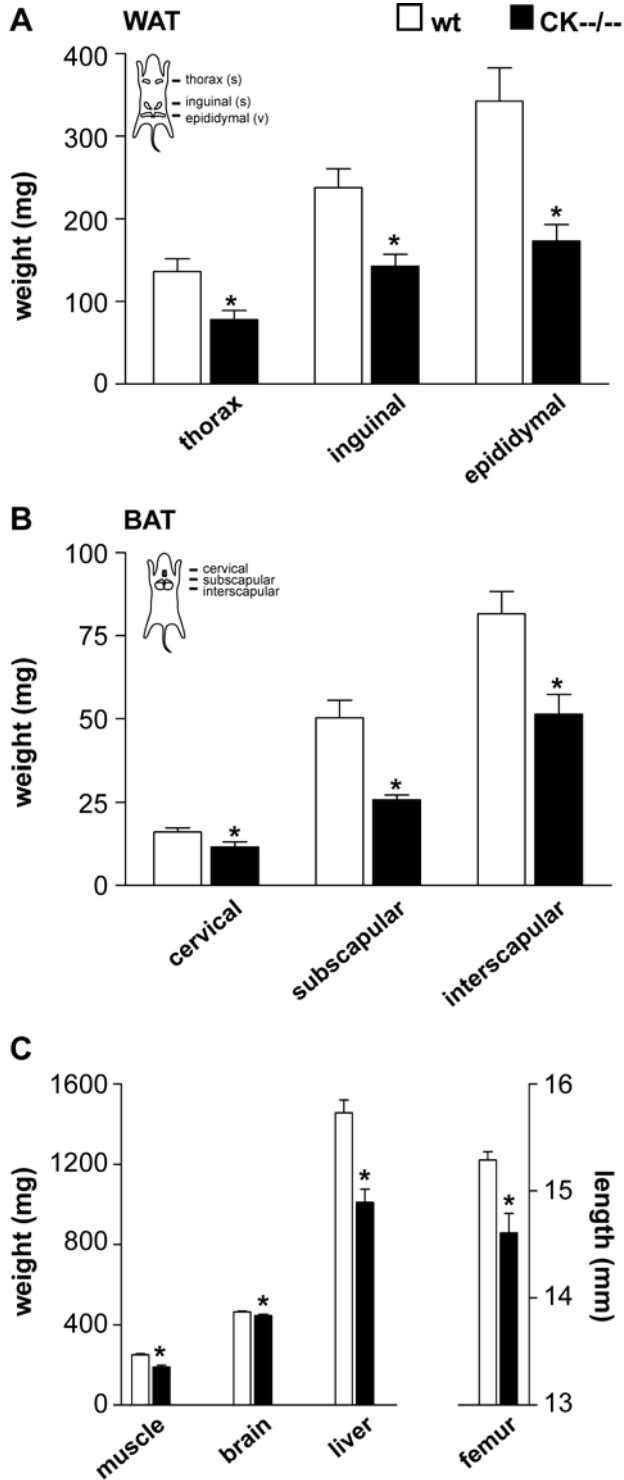


Figure 3: Fasting-induced body temperature response in wildtype and $CK^{-/-}$ mice. In response to 12-hour fasting, an equal drop of 4-5 °C in body temperature was evident late in the dark phase for (A) wildtype and (B) $CK^{-/-}$ mice. When food restriction was terminated the fall in body temperature in both groups rapidly normalized to initial values. Lines depicted are from individual animals.



muscle ($P < 0.001$) and femur ($P < 0.001$) were also smaller (Fig. 4C). When total adipose tissue was adjusted for body weight, a 19-29% reduction BAT (wt: 4.68 ± 0.5 mg/g BW; CK $^{-/-}$: 3.81 ± 0.5 mg/g BW; $P < 0.086$) and WAT (wt: 23.32 ± 3.6 mg/g BW; CK $^{-/-}$: 16.64 ± 2.35 mg/g BW; $P < 0.05$) was observed.

3.9 CK $^{-/-}$ mice have smaller brown adipocytes

Brown adipose tissue is responsible for a major portion of thermogenesis during cold exposure in rodents (Thomas and Palmiter, 1997; Bachman et al., 2002; Cannon and Nedergaard, 2004). To investigate if brain-type CK deficiency is associated with morphological changes in brown fat, we examined the histological appearance of BAT using light (Fig. 5A-B; $n=3$ for all groups) and transmission electron microscopy (Fig. 5C-D; wt: $n=2$, 9 pictures; CK $^{-/-}$: $n=3$, 18 pictures).

Brown adipocytes of adult (diameter: 25.0 ± 0.9 μm ; area: 331 ± 9 μm^2 ; Fig. 5C) and young (diameter: 25.7 ± 0.8 μm ; area: 335 ± 24 μm^2) wildtype mice displayed the typical morphological characteristics, ie. they were multilocular with the bulk of the cell being occupied by numerous round-shaped lipid droplets (Fig. 5A). Ultrastructurally, wildtype brown adipocytes are characterized by their high content of large mitochondria packed with cristae (Fig. 5E). In BAT of CK $^{-/-}$ mice the typical multilocular morphology appeared to be preserved (Fig. 5B). Evenso, no differences in mitochondrial appearance, area (wt: 0.55 ± 0.02 mm^2 ; CK $^{-/-}$: 0.61 ± 0.03 mm^2), or density (wt: 8 ± 0.6 mitochondria/10 mm^2 cytoplasm; CK $^{-/-}$: 9 ± 0.4 mitochondria/10 mm^2 cytoplasm) were observed (Fig. 5F). However, analyses revealed a significant group difference for brown adipocyte size as estimated by the cell diameter ($F(1,8) = 17.109$, $P < 0.003$) and area ($F(1,8) = 10.756$, $P < 0.01$). BAT adipocytes of CK $^{-/-}$ mice showed a marked ~13% reduction in diameter (21.8 ± 0.2 μm) compared to adult ($P < 0.01$) and young ($P < 0.005$) wildtype mice (Fig. 5C). A similar observation was seen for the average cell area of CK $^{-/-}$ brown adipocytes (Fig. 5D; 246 ± 4 μm^2 ; vs. adult wt: $P < 0.02$; vs. young wt: $P < 0.02$).

Figure 4: Organ weight distribution of wildtype and CK $^{-/-}$ mice. (A) CK $^{-/-}$ mice, compared to wildtypes, show an overall decline in white adipose tissue (WAT), and (B) brown adipose tissue (BAT) mass for all three indicated fat pads. (C) Since muscle, brain, liver, and femur were also smaller in CK $^{-/-}$ mice than in wildtypes. (For P values see results 3.7)

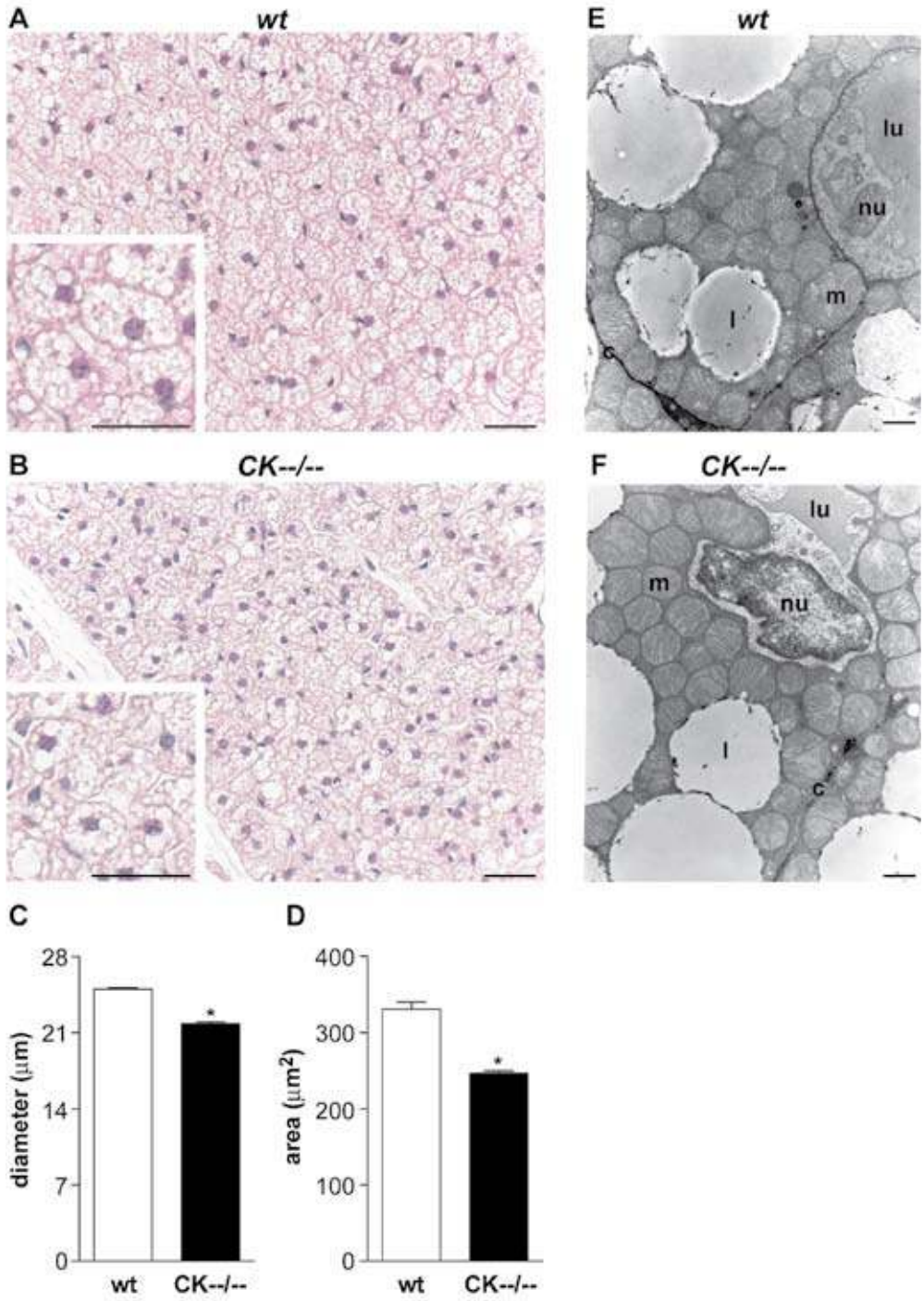
3.10 Noradrenaline infusion elicits normal BAT thermogenesis in CK^{-/-} mice

To determine if creatine kinase deficiency corresponds to abnormalities in BAT functioning, we investigated the ability of CK^{-/-} mice to mount a nonshivering thermogenic response. In an additional group of animals, we therefore measured noradrenaline-stimulated heat production in interscapular BAT (Fig. 6A; wt n=9; CK^{-/-} n=6). At the start of the experiment, the BAT temperature of both groups did not differ (wt: $35.6 \pm 0.3^\circ\text{C}$; CK^{-/-}: $36.2 \pm 0.2^\circ\text{C}$). Within 30 min, noradrenaline infusion elicited a rapid and progressive increase of about 2.5°C in BAT temperature (wt: $2.91 \pm 0.21^\circ\text{C}$; CK^{-/-}: $2.50 \pm 0.94^\circ\text{C}$). Notably, the temperature increment was higher in BAT (Fig. 6A) than in rectum (Fig. 6B), indicating that the BAT warming in either genotype group is not due to indirect warming of the body. These observations suggest that BAT in CK^{-/-} mice can respond normally to sympathetic noradrenaline activation.

3.11 CK^{-/-} mice show a similar BAT UCP1 mRNA response after cold exposure

The primary molecule involved in cold-induced thermogenesis is uncoupling protein-1 (UCP1), located in the inner membrane of mitochondria of brown adipocytes (Cannon and Nedergaard, 2004; Sell et al., 2004). Noradrenaline released from sympathetic nerve endings to BAT is the primary regulator of UCP1 activity and expression. β -Adrenergic-receptor stimulation increases UCP1 activity within seconds of stimulation, while chronic stimulation over hours and days results in

Figure 5: *Histological analysis of brown adipose tissue from wildtype and CK^{-/-} mice.* (A) Both wildtype and (B) CK^{-/-} mice showed a multilocular characteristic for brown adipocytes, with the cells being occupied by numerous round-shaped fat droplets of various sizes. The inset in B, compared to the inset in A, showed a reduced adipocyte size for CK^{-/-} mice. Quantification of brown adipocyte (C) diameter and (D) area is shown for both genotype groups. Horizontal black bar in A, B, inset A, and inset B represents 30 μm . * $P < 0.001$, significantly different from wildtype. EM-morphometric analysis of BAT indicated no differences in mitochondrial appearance or density between wildtype (E) and CK^{-/-} (F) mice. Horizontal black bar represents 1 μm . l, lipid droplet; m, mitochondria; nu, nucleus; c, cell membrane; lu, capillary lumen.



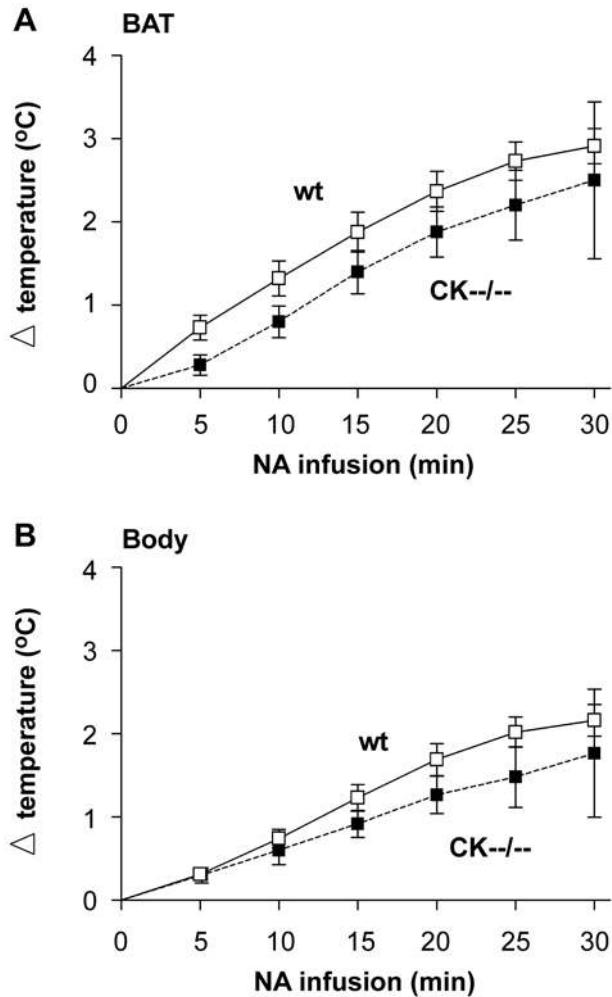


Figure 6: Physiological responses to noradrenaline in wildtype and $\text{CK}^{-/-}$ mice. (A) noradrenaline (NA) infusion increased brown adipose tissue temperature (BAT), and (B) body temperature to a similar extent in wildtype (white squares/circles) and in $\text{CK}^{-/-}$ (black squares/circles) mice.

increased amounts of UCP-1 protein (Lowell and Spiegelman, 2000). To examine whether $\text{CK}^{-/-}$ mice use the sympathetic outflow to BAT adequately, we used the induction of UCP1 as a reporter (Fig. 7). To determine UCP1 activation, we dissected interscapular BAT ($n=3$ for both groups) after 12-hour cold challenge, and measured UCP1 mRNA and protein levels.

Basal UCP1 mRNA levels were not significantly different in

wildtype and CK^{-/-} mice kept at room temperature (wt: 0.63 ± 0.05 a.u.; CK^{-/-}: 0.41 ± 0.25 a.u.; Fig. 7A). Cold exposure for 12 h at 4°C significantly increased UCP1 mRNA expression in brown adipose tissue of wildtype animals (1.83 ± 0.19 a.u.) and to a similar extent in that of CK^{-/-} mice (1.95 ± 0.10 a.u.; Fig. 7A). In both genotype groups, the levels of UCP1 protein had not changed and appeared similar before and after cold exposure (Fig. 7B-E). As no protein induction was seen, the period of cold exposure used may have been too brief to elicit an effect on UCP1 protein levels (Fig. 7D-E).

3.12 Cold treatment induced a higher increase of c-Fos in hypothalamic nuclei of CK^{-/-} mice

Expression of the inducible transcription factor c-Fos within the hypothalamus was used to investigate the neuronal responsiveness to cold exposure (Fig. 8A-D; Table 2). Specific subregions within the hypothalamus include the medial preoptic area (mPOA), paraventricular nucleus (PVN), and dorsomedial hypothalamus (DMH) which all increase c-Fos expression upon exposure to cold (Kiyohara et al., 1995; Baffi and Palkovits, 2000; Yoshida et al., 2005; Park et al., 2007). The positive staining for c-Fos was visible as a blue-black reaction product localized in the nucleus of neurons (Fig. 8A-D).

The amount of c-Fos positive cells within the mPOA, PVN, and DMH was not significantly different between wildtype and CK^{-/-} mice housed at room temperature (mPOA: 32 ± 3.3 vs. 45 ± 4.3 ; PVN: 17 ± 2.3 vs. 26 ± 4.1 ; DMH: 26 ± 5.3 vs. 35 ± 3.6 ; wt: n=4; CK^{-/-} n=7; Table 2). In both genotype groups, cold exposure for 12 h produced a significant increase in c-Fos expression in all three hypothalamic regions (Fig. 8A-D; Table 2). In wildtype mice (n=4), the number of c-Fos positive cells increased 2.0-, 2.4-, and 2.8-fold in respectively the mPOA, PVN and DMH areas (Fig. 8A, C; Table 2). While in CK^{-/-} brains the DMH region showed a similar 2.4-fold increase upon cold challenge, a significantly larger number of c-Fos positive cells was observed in the mPOA ($P < 0.01$) and PVN ($P < 0.001$) when compared to wildtypes (Fig 8A-D; Table 2). The more pronounced increase of ~3.3-fold in c-fos positive cell numbers for the mPOA and ~4.8-fold for the PVN area, can best be explained by an increased neuronal responsiveness in CK^{-/-} mice.

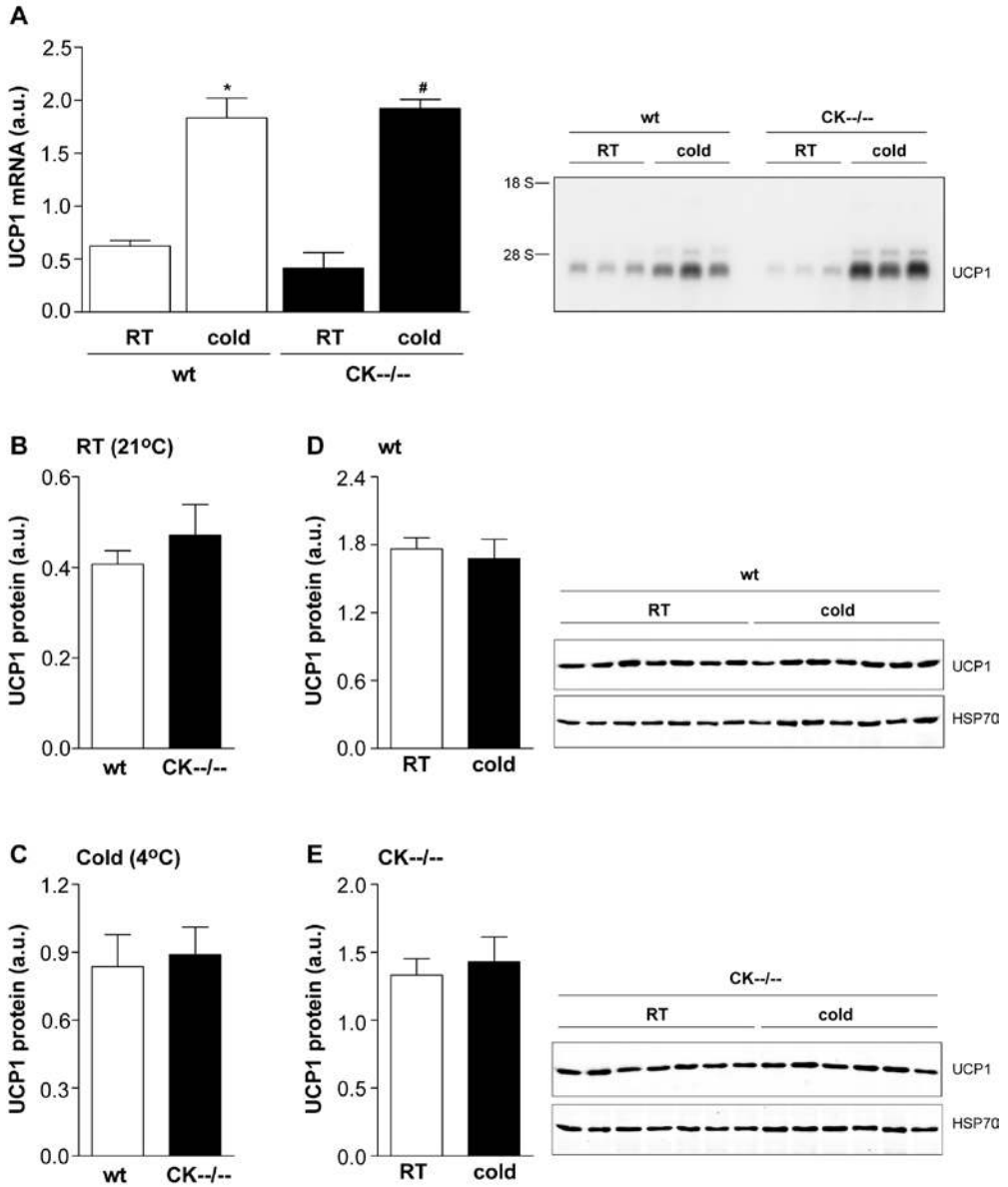


Figure 7: UCP1 response in brown adipose tissue of cold-exposed wildtype and CK^{-/-} mice. (A) UCP1 mRNA is adequately modulated upon a 12-hour cold challenge in both wildtype and in CK^{-/-} mice. (B) No differences were found for UCP1 protein levels under basal and (C) cold conditions. (D-E) In both genotype groups, 12-hour cold exposure on itself did not elicit a rise in protein level. Significantly different from cold exposed: * P < 0.031, # P < 0.011.

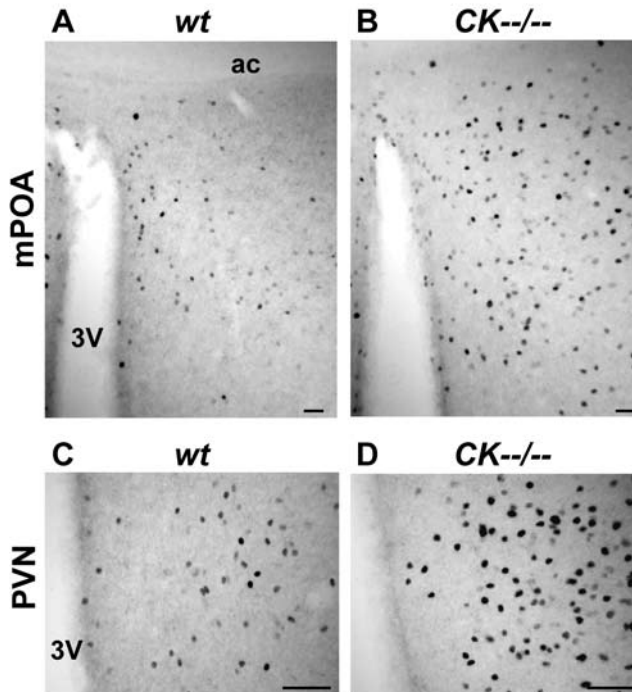


Figure 8: Distribution of *c-Fos* immunoreactivity in different brain regions after 12-hour cold exposure. (PVN). Panel A-B shows the median preoptic area (mPOA). Panel C-D shows the paraventricular nucleus (PVN). Upon cold exposure (4°C) the number of *c-Fos* expressing neurons within hypothalamic nuclei such as the mPOA and PVN was higher in CK^{-/-} (B and D) than in wildtype mice (A and C). Horizontal black bar represents 50 μm. 3V, third ventricle; ac, anterior commissure.

Table 2. Number of *c-fos* positive neurons in different hypothalamic nuclei

| | wildtype | CK ^{-/-} |
|---------------------------------|-------------|-------------------|
| room temperature (21°C) | | |
| mPOA | 31.6 ± 3.3 | 44.7 ± 4.3 |
| PVN | 16.6 ± 2.3 | 26.3 ± 4.1 |
| DHM | 26.0 ± 5.3 | 35.4 ± 3.6 |
| 12-h cold exposure (4°C) | | |
| mPOA | 64.1 ± 4.8 | 147.1 ± 21.0 * |
| PVN | 40.2 ± 5.2 | 125.5 ± 9.2 ** |
| DHM | 71.9 ± 12.5 | 84.7 ± 17.1 |

mPOA, median preoptic area; PVN, paraventricular nucleus; DMH, dorsomedial hypothalamus. Significantly different from wildtype (Student's t-test): *P < 0.01; **P < 0.0001.

4. Discussion

The present study shows that mice with complete brain-type creatine kinase deficiency have a lower body temperature and reduced capacity to maintain their temperature when exposed to cold. The cause of the abnormal body temperature maintenance is not simply a result of smaller body size. Small wild type mice, selected for comparable bodyweights and food intake as CK^{-/-} mice did not show the temperature drop below normal in the morning hours or when exposed to cold. The hypothermia at room temperature in CK^{-/-} mice was especially evident during the early inactive (light) phase of the day. For the rest of the day CK^{-/-} mice are capable of maintaining their body temperature at normal level, perhaps in part by using motor activity for heat production. Although not entirely significant, our locomotion analysis results showed that CK^{-/-} mice tend to be spontaneously hyperactive, suggesting that movement-generated heat is relatively more important to them than to wildtypes.

What and where could then be the origin of thermogenic changes in our CK^{-/-} mice? Basically there are two possible explanations for the thermoregulatory dysfunction in CK^{-/-} animals. Either CK deficiency affects the thermoregulatory neuronal circuitry or the effector organs. Based on the importance of CK for brain energetics, one might expect defective brain functioning as the most likely cause of impaired thermoregulation. Evidence suggests that efferent pathways governing the thermoeffectors involve the spinal cord, medulla oblongata, midbrain/pons, and hypothalamus (Nagashima et al., 2000; Romanovsky, 2007). Conti et al (2006) reported that overexpression of the UCP2 in hypocretin neurons results in elevated hypothalamic temperatures, forcing the hypothalamus to lower body temperature 0.3-0.5°C. In these transgenic mice the reduction of core body temperature during room temperature was more pronounced in the second part of the dark (active) phase of the day. Interestingly, this resembles closely what we observed in our cohorts of CK^{-/-} mice. This suggests that a purely neuronal alteration can be sufficient to cause a drop in baseline body temperature and that this could contribute to the hypothermia phenomenon seen in CK^{-/-} mice. Proper neuronal functioning is also critical for thermoregulatory coordination during acute cold exposure. A single, 3-hour exposure to cold (10°C) in rats elicits a strong c-Fos immunoreactivity in the medial preoptic area (mPOA) a crucial area in

the neuronal circuitry for thermoregulation (Baffi and Palkovits, 2000; Yoshida et al., 2005). Other areas in the hypothalamus, such as the paraventricular (PVN), dorsomedial, and ventromedial nuclei, and the posterior and lateral hypothalamic areas also participate in thermoregulation (Nagashima et al., 2000; Maruyama et al., 2003; Morrison, 2004; DiMicco and Zaretsky, 2007; Park et al., 2007; Romanovsky, 2007). CK protein expression is observed in various brain structures, including high levels in these thermoregulatory hypothalamic nuclei. CK deficiency may interrupt the functional system by damaging specific cellular areas or affecting the functional integrity of neurons. During cold exposure, a defect in central neuronal networks controlling different autonomic thermoregulatory effectors may arise, which in turn affects body temperature regulation. Surprisingly, we observed that CK^{-/-} mice had more cold-responsive c-Fos positive cells in hypothalamic nuclei such as the mPOA and PVN than wildtype mice. This may reflect a compensatory response, in an “attempt to correct” defective thermoregulatory signaling within the hypothalamus due to CK deficiency, or also reflect an adaptation with cellular rewiring that occurred during development and growth of the hypothalamus. Also other explanations remain possible, as not much is known about the precise relationship between c-Fos induction and cold signaling responses. We also show that the hyper-responsiveness to cold was not associated with a more strenuous increase in BAT UCP1 mRNA expression levels. When taken combined, these findings suggest impaired hypothalamic processing as the most likely cause of the impaired thermoregulation in CK^{-/-} mice.

Mammals normally maintain their body temperature within a narrow range, despite large fluctuations in environmental temperature and metabolic heat production. Body temperature homeostasis is facilitated by behavioral strategies and physiological responses, thereby balancing heat production and heat loss (Nagashima et al., 2000; Romanovsky, 2007). For instance, if an animal is acutely exposed to a cold environmental temperature it needs extra heat to compensate for the increased heat loss, to preserve its body temperature. Initially this will come from increased skeletal muscle activity (movement or shivering), to increase body temperature by accelerating fuel oxidation. On the other hand, control of arteriolar blood flow regulates how much heat is lost through specialized heat exchanges organs, such as the tail (Nagashima et al., 2003). Over time, shivering disappears

and other mechanisms become prominent like increased non-shivering thermogenesis in brown adipose tissue (BAT; Lowell and Spiegelman, 2000; Cannon and Nedergaard, 2004). Our results show that the thermogenic defect could not be explained at the level of intrinsic BAT functioning. Importantly, western blot analysis and immunohistochemistry of BAT indicated that the creatine kinases isoforms are not detectably expressed in brown adipocytes. In our histological analyses we used highly specific antibodies against both BCK and UbCKmit. We therefore attribute the finding of others (Berlet et al., 1976; Karmali et al., 1984), who reported creatine kinase activity in whole adipose tissue lysates, as a possible contamination by BCK originating from nerves and arteries innervating the BAT tissue. We do not exclude the possibility that creatine kinase deficiency could have resulted in alteration of mechanical properties of other compensatory mechanisms, like cutaneous vasomotion. CK protein is expressed in the smooth muscle layer of arteries. Blood flow between the body surface and the thermal core is a thermoregulatory mechanism for heat transfer between the environment and the body (Young and Dawson, 1982; Foster, 1986; Kikuchi-Utsumi et al., 2002; Nagashima et al., 2003; Nakayama et al., 2003; Wang et al., 2006). In hypothermic animals, vasoconstriction suppresses peripheral blood flow and slows heat transfer between the skin surface and the thermal core. Therefore, it is possible that differences in the ability to control cold loss through vasoconstriction could explain part of the thermoregulatory defect.

Some physiological conditions are also known to alter heat production, sometimes with pathological consequences but often with advantageous effects. For instance, under conditions of food restriction, hypothermia ($\leq 1^{\circ}\text{C}$ drop) is observed in several mammalian species to conserve energy by reducing metabolic heat production (Nagashima et al., 2003; Gelegen et al., 2006). With high energetic challenges mice even show a controlled drop in body temperature below 31°C , a condition known as torpor (Swan, 1974; Hudson, 1978; Hudson and Scott, 1979; Himms-Hagen, 1985; Overton and Williams, 2004). When an animal faces energy deficiency, body temperature gradually decreases selectively during the early onset of light (inactive) phase of the day, whereas body temperatures in the dark (active) phase is well maintained at the control level (for example see Nagashima et al., 2003). Although CK^{-/-} mice have rather normal brain ATP levels under basal conditions (In 't Zandt et al., 2004), it is interesting to note that

circulating serum levels of hormones and indicators of metabolic status like leptin, glucose and free fatty acids were reduced in our CK^{-/-} mice. A negative energy balance at the whole body level due to creatine kinase deficiency may thus also explain the inability to maintain their body temperature during a cold challenge. We found that CK^{-/-} mice showed severe hypothermia after only 6h cold exposure. Cold exposure increases O₂ uptake and basal metabolic state (Lowell and Spiegelman, 2000). Survival in the cold depends on increased energy expenditure and thus requires sustained substrate mobilization from the main energy stores such as liver glycogen and adipose tissue. A substantially reduced adiposity content (the amount of WAT, BAT and reduced brown adipocytes size) was observed in CK^{-/-} mice compared to wildtypes, limiting substrate availability for thermogenesis, or indirectly, for sympathetic nervous system functioning. However, if CK deficiency has resulted in a negative shift in energy homeostasis one would expect fasting-induced hypothermia to be more pronounced in CK^{-/-} mice. Paradoxically, we found that CK^{-/-} and wild type mice showed a similar temperature drop after 12h of fasting.

In conclusion, our evidence presented here has established a firm coupling between CK activity and basal thermogenesis regulation. Clearly, more experimental work is needed to delineate what are the integral physiological pathways involved in this coupling and to determine CK's exact position in the complex cascade of molecular events that control these pathways.

Acknowledgments

This research is supported by a research grant from the Radboud University Nijmegen Medical Centre. We want to thank Gaby Beckers for her help with the body temperature measurements, Huib Croes for paraffin histology and immunocytochemistry, Mietske Wijers for her help with the electron microscopy study, Arthur Kuipers for help with c-Fos immunostaining, and our colleagues in the Central Animal Facility for help and advice with the animal care.

References

Bachman ES, Dhillon H, Zhang CY, Cinti S, Bianco AC, Kobilka BK, Lowell BB (2002) β AR Signaling required for diet-Induced thermogenesis and obesity resistance. *Science* 297:843-845.

Baffi JS, Palkovits M (2000) Fine topography of brain areas activated by cold stress. A fos immunohistochemical study in rats. *Neuroendocrinology* 72:102-113.

Bamshad M, Kay Song C, Bartness TJ (1999) CNS origins of the sympathetic nervous system out flow to BAT. *Am J Physiol Regul Integr Comp Physiol* 276:1569-1578.

Berlet HH, Bonsmann I, Birringer H (1976) Occurrence of free creatine, phosphocreatine and creatine phosphokinase in adipose tissue. *Biochim Biophys Acta* 437:166-174.

Bessman SP, Carpenter CL (1985) The creatine-creatine phosphate energy shuttle. *Annu Rev Biochem* 54:831-862.

Cannon B, Nedergaard J (2004) BAT: function and physiological significance. *Physiol Rev* 84:277-359.

Conti B, Sanchez-Alavez M, Winsky-Sommerer R, Morale MC, Lucero J, Brownell S, Fabre V, Huitron-Resendiz S, Henriksen S, Zorrilla EP, de Lecea L, Bartfai T (2006) Transgenic mice with a reduced core body temperature have an increased life span. *Science* 314:825-828.

Cools A (1986) Mesolimbic dopamine and its control of locomotor activity in rats: differences in pharmacology and light/dark periodicity between the olfactory tubercle and the nucleus accumbens. *Psychopharmacology* 88:451-459.

De Groof AJ, Smeets B, Groot Koerkamp MJ, Mul AN, Janssen EE, Tabak HF, Wieringa B (2001) Changes in mRNA expression profile underlie phenotypic adaptations in creatine kinase-deficient muscles. *FEBS Lett* 506:73-78.

De Kok YJ, Geurds MP, Sistermans EA, Usmany M, Vlaskovits JM, Wieringa B (1995) Production of native creatine kinase B in insect cells using a baculovirus expression vector. *Mol Cell Biochem* 143:59-65.

DiMicco JA, Zaretsky DV (2007) The dorsomedial hypothalamus: a new player in thermoregulation. *Am J Physiol Regul Integr Comp Physiol* 292: R47-R63.

Foster DO (1986) *Brown Adipose Tissue*. Editors: Trayhurn P, Nicholls DG. London: Edward Arnold, pp31-51.

Friedman DL, Perryman MB (1991) Compartmentation of multiple forms of creatine kinase in the distal nephron of the rat kidney. *J Biol Chem* 266:22404-22410.

Gelegen C, Collier DA, Campbell IC, Oppelaar H, Kas MJ (2006) Behavioral, physiological, and molecular differences in response to dietary restriction in three inbred mouse strains. *Am J Physiol Endocrinol Metab* 291:E574-E581.

Himms-Hagen J (1985) Food restriction increases torpor and improves BAT thermogenesis in ob/ob mice. *Am J Physiol Endocrinol Metab* 248:531-539.

Hudson JW (1978) *Strategies in the cold: natural torpidity and thermogenesis*. Editors: Wang LCH, Hudson JW; Academic Press, New York, pp67-108.

Hudson JW, Scott IM (1979) Daily torpor in the laboratory mouse, *Mus musculus* var. albino. *Physiol Zool* 52:205-218.

Inokuma K, Ogura-Okamoto Y, Toda C, Kimura K, Yamashita H, Saito M (2005) Uncoupling protein 1 is necessary for norepinephrine-induced glucose utilization in brown adipose tissue. *Diabetes* 54:1385-1391.

In 't Zandt HJ, Renema WK, Streijger F, Jost C, Klomp DW, Oerlemans F, Van der Zee CEEM, Wieringa B, Heerschap A (2004) Cerebral creatine kinase deficiency influences metabolite levels and morphology in the mouse brain: a quantitative in vivo ¹H and ³¹P magnetic reso-

nance study. *J Neurochem* 90:1321-1330.

Kanosue K, Hosono, T, Zhang, YH, Chen, XM, (1998) Neuronal networks controlling thermoregulatory effectors. *Prog Brain Res* 115:49-62.

Karmali A, Montague DJ, Holloway BR, Peters TJ (1984) Comparative subcellular fractionation of control and cold-adapted rat brown and WAT with special reference to peroxisomal and mitochondrial distributions. *Cell Biochem Funct* 2:155-160.

Kikuchi-Utsumi K, Gao B, Ohinato H, Hashimoto M, Yamamoto N, Kuroshima A (2002) Enhanced gene expression of endothelial nitric oxide synthase in brown adipose tissue during cold exposure *Am J Physiol Regulatory Integrative Comp Physiol* 282:R623-R626.

Kiyohara T, Miyata S, Nakamura T, Shido O, Nakashima T, Shibata M (1995) Differences in Fos expression in the rat brains between cold and warm ambient exposures. *Brain Res Bull* 38:193-201.

Lowell BB, Spiegelman BM (2000) Towards a molecular understanding of adaptive thermogenesis. *Nature* 404: 652-660.

Maruyama M, Nishi M, Konishi M, Takashige Y, Nagashima K, Kiyohara T, Kanosue K (2003) Brain regions expressing Fos during thermoregulatory behavior in rats. *Am J Physiol Regul Integr Comp Physiol.* 285:R1116-R1123.

Morrison SF (2004) Central pathways controlling brown adipose tissue thermogenesis. *News Physiol Sci* 19:67-74.

Moura MA, Festuccia WT, Kawashita NH, Garófalo MA, Brito SR, Kettelhut IC, Migliorini RH (2005) Brown adipose tissue glyceroneogenesis is activated in rats exposed to cold. *Pflugers Arch* 449:463-469.

Nagashima K, Nakai S, Tanaka M, Kanosue K (2000) Neuronal circuitries involved in thermoregulation. *Auton Neurosci* 85:18-25.

Nagashima K, Nakai S, Matsue K, Konishi M, Tanaka M, Kanosue K (2003) Effects of fasting on thermoregulatory processes and the daily oscillations in rats. *Am J Physiol Regul Integr Comp Physiol* 284: R1486–R1493.

Nakayama A, Bianco AC, Zhang CY, Lowell BB, and Frangioni JV (2003) Quantitation of brown adipose tissue perfusion in transgenic mice using near-infrared fluorescence imaging. *Mol Imaging* 2:37-49.

O’Gorman E, Beutner G, Wallimann T, Brdiczka D (1996) Differential effects of creatine depletion on the regulation of enzyme activities and on creatine-stimulated mitochondrial respiration in skeletal muscle, heart, and brain. *Biochim Biophys Acta* 1276:161-170.

Oldfield BJ, Giles ME, Watson A, Anderson C, Colvill LM, McKinley MJ (2002) The neurochemical characterisation of hypothalamic pathways projecting polysynaptically to BAT in the rat. *Neuroscience* 110:515-526.

Overton JM, Williams TD (2004) Behavioral and physiologic responses to caloric restriction in mice. *Physiol Behav* 81:749-754.

Park JJ, Lee HK, Shin MW, Kim SJ, Noh SY, Shin J, Yu WS (2007) Short-Term Cold Exposure May Cause a Local Decrease of Neuropeptide Y in the Rat Hypothalamus. *Mol Cells* 23:88-93.

Ribeiro MO, Lebrun FL, Christoffolete MA, Branco M, Crescenzi A, Carvalho SD, Negrao N, Bianco AC (2000) Evidence of UCP1-independent regulation of norepinephrine-induced thermogenesis in brown fat. *Am J Physiol Endocrinol Metab* 279:314-322.

Ribeiro MO, Carvalho SD, Schultz JJ, Chiellini G, Scanlan TS, Bianco AC, Brent GA (2001) Thyroid hormone-sympathetic interaction and adaptive thermogenesis are thyroid hormone receptor isoform-specific. *J Clin Invest* 108:97-105.

Romanovsky AA (2007) Thermoregulation: some concepts have changed. Functional architecture of the thermoregulatory system. *Am J Physiol Regul Integr Comp Physiol* 292:37-46.

Sell H, Deshaies Y, Richard D (2004) The brown adipocyte: update on its metabolic role. *Int J Biochem Cell Biol* 36:2098-2104.

Shimizu Y, Nikami H, Saito M (1991) Sympathetic activation of glucose utilization in brown adipose tissue in rats. *J Biochem* 110:688-692.

Shin J, Streijger F, Beynon A, Peters T, Gadzalla L, McMillen D, Bystrom C, van der Zee CEEM, Wallimann T, Gillespie PG. (2007) Hair Bundles Are Specialized for ATP Delivery via Creatine Kinase. *Neuron* 53:371-386.

Streijger F, Oerlemans F, Ellenbroek BA, Jost CR, Wieringa B, van der Zee CEEM (2005) Structural and behavioral consequences of double deficiency for creatine kinases BCK and UbCKmit. *Behav Brain Res* 157:219-234.

Swan H (1974) *Thermoregulation and bioenergetics*. Elsevier, New York.

Thomas SA, Palmiter RD (1997) Thermoregulatory and metabolic phenotypes of mice lacking noradrenaline and adrenaline. *Nature* 387:94-97.

Veening JG, Bouwknecht JA, Joosten HJ, Dederen PJ, Zethof TJ, Groenink L, Van der Gugten J, Olivier B (2004) Stress-induced hyperthermia in the mouse: c-Fos expression, corticosterone and temperature changes. *Prog Neuropsychopharmacol Biol Psychiatry*. 28:699-707.

Wallimann T, Wyss M, Brdiczka D, Nicolay K, Eppenberger HM (1992) Intracellular compartmentation, structure and function of creatine kinase isoenzymes in tissues with high and fluctuating energy demands: the 'phospho-creatine circuit' for cellular energy homeostasis. *Biochem J* 281:21-40.

Wang Y, Kimura K, Inokuma K, Saito M, Kontani Y, Kobayashi Y, Mori N, Yamashita H (2006) Potential contribution of vasoconstriction to suppression of heat loss and homeothermic regulation in UCP1-deficient mice. *Pflugers Arch* 452:363-369.

Wu Q, Kazantzis M, Doege H, Ortegon AM, Tsang B, Falcon A, Stahl A (2006) Fatty acid transport protein 1 is required for nonshivering thermogenesis in brown adipose tissue. *Diabetes* 55:3229-3237.

Wyss M, Kaddurah-Daouk R (2000) Creatine and creatine metabolism. *Physiol Rev* 80:1107-1213.

Yoshida K, Konishi, M, Nagashima K, Saper CB, Kanosue (2005) Fos activation in hypothalamic neurons during cold or warm exposure: Projections to periaqueductal gray matter. *Neuroscience* 133:1039-1046.

Young AA, Dawson NJ (1982) Evidence for on-off control of heat dissipation from the tail of the rat. *Can J Physiol Pharmacol* 60:392-839.

Chapter 6

Complete brain-type creatine kinase deficiency in mice affects seizure activity and removal of intracellular calcium.


Streijger F¹, Scheenen WJJM², van Luijtelaar G³, Oerlemans F¹, Wieringa B¹, Van der Zee CEEM¹.

¹ Department of Cell Biology, NCMLS, Radboud University Nijmegen Medical Centre, Nijmegen, The Netherlands

² Department of Cellular Animal Physiology, EURON European graduate school of neuroscience, Radboud University Nijmegen, The Netherlands

³ Department of Biological Psychology, Nijmegen Institute for Cognition and Information, Radboud University Nijmegen, The Netherlands

in preparation



Abstract

In brain, cytosolic brain creatine kinase (BCK) and ubiquitous mitochondrial creatine kinase (UbCKmit) act as components of local phosphocreatine-ATP shuttles that help in the compartmentalization of cellular energy and serve to maintain pools of high-energy phosphate containing molecules in both neurons and glial cells. To know more about the role of these brain-type creatine kinases under extreme demanding conditions, we studied the physiological reactions of mice lacking both BCK and UbCKmit (CK^{-/-} mice) in response to chemical seizure induction using EEG recordings as well as behavioral monitoring.

In all CK^{-/-} mice, PTZ injection produced severe myoclonic jerking of limbs and body, however in only 4 out of the ten mice this evolved into a generalized seizure. EEG analysis showed that pre-seizure jerking was associated with increased high amplitude discharges that appear similar to wildtype mice. As the generalized seizure progresses, wildtype EEG recordings showed continuous runs of rhythmic 4-6 Hz activity. Interestingly, in CK^{-/-} mice that developed a seizure no rhythmic EEG activities were observed and only irregular discharges were recorded. Other CK^{-/-} mice (6 out of 10) displayed a sudden postictal depression without the development of a generalized seizure.

We hypothesized that altered intracellular Ca²⁺-regulation in synaptic transmission could play a role in these abnormalities. Strikingly, following repetitive KCl depolarization, CK^{-/-} hippocampal neurons exhibited a ~60% increase in removal rate of elevated intracellular Ca²⁺ levels. We argue that this altered Ca²⁺ clearance in CK^{-/-} neurons could play a crucial role in the abnormal EEG and seizure activity in these mice.

Introduction

Creatine Kinase isoenzymes belong to the large family of phosphagen kinases and are by far the most abundantly expressed members of this diverse family in vertebrates. By catalyzing the reaction $\text{MgATP}^{2-} + \text{Cr}$ (creatine) \leftrightarrow $\text{MgADP}^- + \text{PCr}^{2-}$ (phosphocreatine) + H^+ , creatine kinases (CK) are essential for storing and intracellular transport of high-energy phosphoryl metabolites (phosphagens), and thus ultimately

ATP buffering in tissues with fluctuating high energy demands such as muscle and brain (Bessman and Carpenter, 1985; Walliman et al., 1992; O’Gorman et al., 1996; Wyss and Kaddurah-Daouk, 2000; In ‘t Zandt et al., 2004). In brain, cytosolic brain creatine kinase (BCK) and ubiquitous mitochondrial creatine kinase (UbCKmit) serve to maintain the phosphotransfer shuttles that control ATP compartmentalization and feed into critical ATP-requiring processes. During development but also in adulthood, brain cells have to invest a high percentage of their ATP to fuel numerous energy-consuming processes including molecular transport, intracellular communication, actomyosin-based dynamic, dendritic spine or glial endfeet remodeling, electrogenic activity of Ca^{2+} - and Na^+/K^+ -ATPases, and for neurotransmitter cycling or neuroendocrine signaling (Barinaga, 1997; Bernstein and Bamburg, 2003; Hertz 2007).

To examine how defects in the creatine kinase system modulate brain energy metabolism and function, our group has generated knockout mice with deficiency for BCK, UbCKmit, or both CK isoforms. The CK mutants showed mutation-dependent abnormalities in brain morphology and behavior including impaired spatial learning, altered nestbuilding activity, and diminished acoustic startle reflex responses (Jost et al., 2002; Streijger et al., 2004; Streijger et al., 2005; chapter 2). Besides the behavior abnormalities, double deficient CK mice (CK $^{-/-}$ mice) displayed a typical smaller body size, and showed severe deficits in thermoregulation and hearing (Shin et al., 2007; chapter 5).

In this study, we tested brain performance of CK $^{-/-}$ mice under conditions of extremely high-energy demand. Therefore, animals were challenged with the seizure-inducing drug pentylenetetrazole (PTZ), a compound that elicits global depolarization waves involving the entire synaptic system (El Hamdi et al., 1992; Holtzman et al., 1997). Besides detailed behavioral analysis, simultaneous measurement of electroencephalography (EEG) was conducted to investigate brain functional connectivity in response to PTZ-induced seizure activity. Boero and colleagues (2003) showed that increased creatine kinase expression occurs because of enhanced neuronal activity, as in neurons with seizures. In addition, previous studies of BCK $^{-/-}$ mice revealed a prolonged pre-seizure period and a delayed development of pentylenetetrazole-induced seizures (Jost et al., 2002). Complete absence of PCr as energy buffer as occurring in CK $^{-/-}$ mice (In ‘t

Zandt et al., 2004) was therefore expected to have a truly dramatic effect on brain function.

Next, we examined a possible mechanism by which CK might function on neuronal transmission events. Interestingly, from muscle studies, we know that the CK-PCr system has an important role in Ca^{2+} homeostasis during repetitive muscle contractions (Rossi et al., 1990; Minajeva et al., 1996; Duke and Steele, 1999; De Groof et al., 2002). Furthermore, because of the importance of Ca^{2+} currents in seizure generation and in the establishment of epilepsy (Albowitz et al., 1997; Tashiro et al., 2002) we hypothesized that CK might be involved in neuronal Ca^{2+} kinetics thereby modulate intrinsic brain excitability. The effect of massive neuronal depolarization on Ca^{2+} transients was studied with the fura-2/AM probe in the dentate gyrus granule neurons, an area known to be involved in PTZ-induced seizures (Andre et al., 1998; Eells et al., 2004; Brevard et al., 2006).

Our findings demonstrated a tight coupling between creatine kinase activity and efficiency in the synaptic networks of the brain and provide us with useful entry points for further studies on the systems that fuel and control neuronal transmission events.

2. Material and methods

All procedures involving animals were approved by the Animal Care Committee of the Radboud University Nijmegen and were conform to the guidelines of the Dutch Council for Animal Care and the NIH. All efforts were made to reduce the number of animals used.

2.1 Animals

The generation of CK^{-/-} double knockout mice (further referred to as CK^{-/-} mice) and genotype analysis was described in detail elsewhere (Streijger et al., 2005). Studies were performed on 3- to 6-month-old male mice. All comparisons were made between age-matched animals of the same genetic background (25% 129/Ola and 75% C57BL/6). The animals were maintained on a standard 12h/12 h light-dark cycle (lights on at 07:00) and housed in standard cages (Macrolon type II) with ad libitum access to food and water. Room temperature was controlled at 21°C.

2.2 Electrode implantation

Mice were anesthetized with intraperitoneal injection of 0.21 ml/30 g hypnorm/dormicum/water (1:1:2). Their heads were shaved and the skin cleaned with 70% ethanol. After the depth of the anesthesia was periodically assessed via the limb withdrawal reflex, animals were placed into a mouse stereotax (Kopf Instruments, Tujunga, California, USA). The body temperature was maintained at 37°C using a heating pad. A topical analgesic (lidocaine) was applied to the scalp, and a small incision was made in the midline, which exposed the surface of the skull. Three holes were drilled into the skull onto the right frontal region (AP: +0.89, ML: -1.56), parietal frontal region (AP: -2.67, ML: -1.76) and the cerebellum (ground electrode, AP: -5.5, ML: +1.2) with the positioning relative to bregma. The stereotaxic coordinates were determined according to Paxinos and Watson (1997). The unilateral epidural electrodes were carefully bent into position and cut to an appropriate length to insert each of the wires through the nearest hole so that it lies on top of the dura mater. The electrode socket was fixed to the skull using two stainless steel jeweller screws and dental acrylic. The tissue was sutured and the mice were given a recovery period of 7 days.

2.3 PTZ administration

1 week after electrode implantation, the animals were randomly subjected to a high-energy demand stress situation created by pentylenetetrazole (PTZ)-induced seizures. Following an initial dose of 10 mg PTZ/kg body weight injected intraperitoneally, the individual mice were observed for 30 min. Subsequently, PTZ was administered in a dose of 10 mg/kg every 10 min until seizure onset. This PTZ-induced seizure method is very reliable and delivers a time- and dose-dependent occurrence of seizures (El Hamdi et al., 1992; Holtzman et al., 1997; Jost et al., 2002). For each animal, the PTZ-induced behavioral and EEG response was recorded.

2.4 Behavioral analyses

Besides video-recording each session for off-line analysis (~90 min), real-time observations were performed by two observers to determine

the different behavioral events: (1) Non-seizure activity; (2) Mice display typical jerking behavior (muscle spasms), mainly of the face and the skin on their backs. Principally, partial clonic events are short, lasting 1-2 sec, but they can occur repetitively over time (3) Myoclonic jerking of neck and forelimb; (4) Whole body clonus involving all four limbs and the tail; (5) Generalized clonic seizure episode characterized by loss of righting response, Straub tail (arching of the tail over the body), and maximal vigorous clonic movements in all limbs and the trunk.

2.5 EEG recordings

Concurrently the behavioral observation, electroencephalographic (EEG) activity was monitored. For EEG recordings, mice were connected to EEG leads and placed in transparent Plexiglas recording cages (15×30×35 cm). The EEG leads were connected to the EEG amplifier via a swivel to guarantee free movement of the animals. The EEG signals were amplified (200 mV), filtered (1-100 Hz; notch filter), digitized and stored on disk for subsequent off-line analysis. Baseline EEG was recorded for 5 min from each animal before PTZ administration. A single spike discharge was identified from the EEG as such if it included a sharp spike with an amplitude of at least 2x the initial baseline amplitude. A multi-spike complex was identified as a train of single sharp spikes (minimal of 3 successive single spikes). A generalized seizure was characterized as a train of spike discharges lasting ≤ 15 sec followed by a postictal depression. The postictal depression was determined as EEG activity with an amplitude of 0.5x the initial baseline. The latency to the first aberrant spike discharge, the inter-spike time, the amount of single and poly spikes and the latency and duration of the generalized seizure were determined for both wildtype and CK^{-/-} mice.

2.6 Measurements of intracellular Ca²⁺ levels

2.6.1 Slice preparation and fura-2 AM loading

All solutions during the experiment were continuously carbogenized (5% CO₂ -95% O₂ gas mixture). Brains of postnatal 14-16 day old mice were quickly removed and placed into ice-cold Krebs-Ringer's

buffer (135 mM NaCl, 25 mM NaHCO₃, 3 mM KCl, 1.25 mM NaH₂PO₄, 1 mM MgCl₂, 20 mM glucose, 2 mM CaCl₂, 2 mM Na-pyruvate, 0.5 mM myo-inositol, 0.1 mM ascorbic acid; pH 7.4). With a scalpel the olfactory bulb and cerebellum of the brain were removed. The remaining brain was glued onto a holding block of a slicing chamber, flooded with Krebs-Ringer's buffer. Coronal hippocampal brain slices (300 μm thick) were obtained using a vibratome (Leica VT1000S; Leica, Wetzlar, Germany) and were kept submerged on a grid in ice-cold Krebs-Ringer's buffer. The hippocampus slices were incubated at 37°C for 60 min and allowed to reach room temperature (60 min) before being used. The obtained brain slices were incubated for 20 min at room temperature in 10 mM fura-2/AM (Molecular Probes, Invitrogen, California, USA) in 1 ml Krebs-Ringer's buffer containing 0.02% pluronic acid and 3% bovine serum albumin. Upon loading the slices were washed for 60 min at room temperature in Krebs-Ringer's buffer to remove excess of extracellular non-hydrolyzed fura-2/AM and to allow complete intracellular de-esterification of the probe.

2.6.2 Ca²⁺ imaging

To measure intracellular Ca²⁺ levels, the hippocampus was isolated from the brain slice and fixed into a Leiden chamber (volume 1 ml; Ince et al., 1985) with a harp, made of stretched nylon wires glued onto a flattened u-shaped platinum wire. The chamber was continuously perfused with carbogenized Krebs-Ringer's buffer at 0.7 ml/min. The Leiden chamber was placed on the stage of an inverted microscope (Zeiss AxioVert 135 TV, Göttingen, Germany) and granule cells of the hippocampal dentate gyrus were studied (epifluorescent x40 magnification oil immersion objective; NA=1.4; Zeiss). Granule neurons of the hippocampal dentate gyrus from wildtype and CK^{-/-} brain slices were well loaded with fura-2 and could be readily distinguished by the shape and size of their cell soma. The light from a 100 W xenon lamp (Ushio UXL S150 MO; Ushio, Tokyo, Japan) was directed through a quartz neutral density filter (ND 2; Ealing ElectroOptics, Holliston, Massachusetts, USA) to reduce bleaching of the intracellularly trapped dye. The fluorescence emission was monitored at wavelengths above 460 nm. Ca²⁺ concentration was measured by the ratio F₃₄₀/F₃₈₀, where F₃₄₀ is the fluorescence intensity from Ca²⁺-bound fura-2 observed at the excitation wavelength 340 nm, and F₃₈₀ is the fluorescence

intensity of free fura-2 observed at the excitation wavelength 380 nm. Experiments were controlled and analyzed with Metafluor v.4.6 software (Universal Imaging Corporation, Downingtown, Pennsylvania, USA). Experiments were performed in a low-speed acquisition mode with a sample interval of 6 sec. Slices were challenged by a depolarizing 60 mM KCl concentration. The osmolarity of the Krebs-Ringer's buffer was kept constant by reducing the NaCl concentration. Basal ratio signals of the fura-2 fluorescence upon excitation to 340 and 380 nm were measured during 5 min after which a single 2-min KCl solution was applied (1x pulse protocol). After 15 minutes of recovery the brain slices were challenged with a repetitive (5x) 1-min KCl solution with an intrapulse time of 1 min (5x pulse protocol).

Basal intracellular ratio values, the potassium induced ratio peak increase and Ca^{2+} removal kinetics were calculated and compared between wildtype and CK--/-- double knockout brain slices during the 1x pulse and 5x pulse protocol. The basal ratio values of unstimulated cells were calculated as the mean ratio F340/F380 during the first 5 min of the experiment. The basal ratio values after a single KCl pulse were calculated during the 5 min before the 5x KCl protocol. The basal ratio values after repetitive KCl stimulation were calculated during the last minute of the experiment. The Ca^{2+} removal rate was calculated by determining the decay time constant using a non-linear regression curve fitting algorithm on a single exponential formula, in which R is the ratio value at any given time point t, a is the offset value and τ is the decay time constant:

$$R = a \cdot e^{-\tau \cdot t} \quad (\text{eg. 1})$$

All analyses were performed off-line using GraphPad Prism 4 (GraphPad Software, San Diego, California, USA).

2.7 Statistics

All data are calculated and displayed as the mean \pm SEM. Statistical differences ($P < 0.05$) between groups was assessed by two-tailed Student's t-test. All statistical analyses were performed with the SPSS 12.0 software package

2. Results

2.1 Number of animals displaying generalized seizure behavior was reduced in CK^{-/-} mice

To investigate whether CK deficiency changes brain function properties, wildtype (n=12) and CK^{-/-} mice (n=10) were subjected to a high-energy demand situation by inducing pentylenetetrazole (PTZ; GABAA receptor antagonist) evoked seizure episodes. Both genotype groups showed active exploration and locomotion in the 5-min period prior to the first PTZ injection. When wildtype mice had received up to four PTZ injections, the animals started to display subtle jerking or spasms mainly of the face and the skin on their backs. As the experiment proceeded and more PTZ was administered, myoclonic jerking of neck and limbs were observed of various severities. Finally, wildtype mice displayed severe vigorous whole-body jerking episodes with increasing frequency and duration (~2-5 sec), which finally evolved into a generalized seizure that often lasted for ~30 sec. Typically, 6-7 injections of PTZ evoked a seizure, which was followed by complete physical inactivity. For the CK^{-/-} mice, repetitive PTZ-injections also resulted in a progressive development of pre-seizure activity from neck twitches to severe myoclonic jerking. However, the occurrence of a generalized convulsion was reduced in CK deficient animals. In fact, only 4 out of 10 CK^{-/-} mice showed a generalized seizure behavior as observed in wildtypes. In all other mice (6 out of 10), PTZ injection did cause repeated whole-body jerking events of various severities and durations, however, the typical full-blown seizure remained absent. These results suggest a change in neuronal network excitability due to CK deficiency.

2.2 CK deficiency result in absence of rhythmic high amplitude spiking in brain

To determine the effect of CK knockout on brain activity, we performed electroencephalogram (EEG) monitoring of wildtype (n=12) and CK^{-/-}-mice (n=10) using surface electrodes (Fig. 1-3).

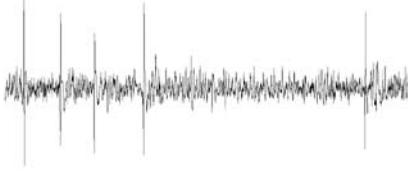
The baseline cortical activity showed a similar low-amplitude desynchronized EEG activity (wt: 148 ± 10 mV; CK^{-/-}: 123 ± 13 mV; Table 1; Fig. 1AB-I). About 60 min after the first PTZ injection abnormal

A. wildtype

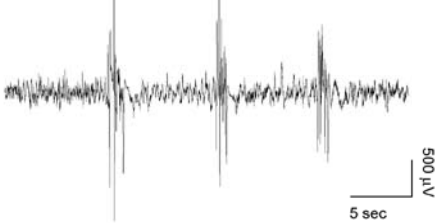
1



2



3

B. CK^{-/-}

1



2



3



Figure 1: Electroencephalograph (EEG) characteristics after administration of pentylenetetrazole in (A) wildtype and (B) CK^{-/-} mice. (I). Baseline brain activity before PTZ injections (II). Repetitive occurrence of single spikes that correlate with muscle jerking. (III) Poly-spikes episodes corresponding to bursts of myoclonic jerking. Vertical black bar represents 500 μ V, horizontal bar represents 5 sec.

brain activity was observed in both genotype groups (wt, 60 ± 2 min; CK^{-/-}, 64 ± 2 min). These abnormalities consisted of spontaneous single high voltage spikes (Fig. 1AB-II), each associated with a myoclonic jerk. The appearance of such a single EEG discharge, was not effected in CK^{-/-} mice as assessed by shape (Fig. 1AB-II) and firing duration (wt: 191 ± 4 ms; CK^{-/-}: 193 ± 4 ms; Table 1). As the experiment proceeded, more multi-spike complexes were observed, corresponding with more pronounced myoclonic jerking (Fig. 1AB-III). Interestingly, CK^{-/-} mice displayed a 2-fold increase in these multi-spike complexes (wt: $13.6 \pm 1.3\%$; CK^{-/-}: $26.0 \pm 1.1\%$; $t(1,20) = -7.298$,

Table 1. EEG analyses during repetitive PTZ injections.

| | wildtype (n=12) | CK ^{-/-} (n=10) |
|---------------------------------------|-----------------|-----------------------------|
| initial baseline amplitude (μ V) | 148 \pm 10 | 123 \pm 13 |
| latency first spike discharge (min) | 60 \pm 2 | 64 \pm 2 |
| duration single spike (ms) | 193 \pm 4 | 191 \pm 4 |
| spike interval, start (s) | 15 \pm 2 | 25 \pm 5 * |
| spike interval, end (s) | 5 \pm 1 | 5 \pm 1 |
| amount single spikes (%) | 86 \pm 1 | 74 \pm 1 * |
| amount polyspikes (%) | 14 \pm 1 | 26 \pm 1 * |
| latency ictal episode (min) | 88 \pm 6 | 101 \pm 9 |
| | | ^a [90 \pm 5] |
| duration ictal episode (s) | 26 \pm 1 | 26 \pm 4 |

^a Latency to postictal depression of CK^{-/-} mice (n=6 out of 10) not developing a clonic or clonic tonic seizure. Data reported are means SEM. *P < 0.05, significantly different from wildtype (Student's t-test)

P < 0.001). As a result, the amount of single spikes was significantly reduced in CK^{-/-} mice ($t(1,20) = 7.298$, P < 0.001). In both genotype groups, the time-interval between two successive discharge events became gradually shorter over time. First, the interspike interval obtained from CK^{-/-} mice (25 \pm 5 sec) was slightly increased compared to wildtype mice (15 \pm 2 sec; $t(1,20) = -2.359$, P < 0.03). However, as the seizure activity progresses, no significant differences in spike-interval was observed (wt, 5 \pm 1 sec; CK^{-/-}, 5 \pm 1 sec). 88 min after the first PTZ injection, all wildtype mice developed generalized convulsive seizures with the appearance of a continuous train of high-amplitude discharges (Fig. 2A; Table 1). Detailed analyses reveal that during the onset, EEG's of all wildtype mice started with a short period (~3-4 sec) of irregular high amplitude spikes (Fig. 3A). After the seizure initiation, but still relatively early in the episode, an organized rhythmic activity

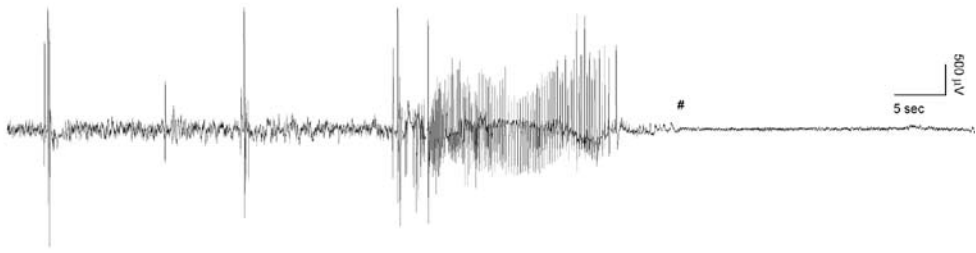
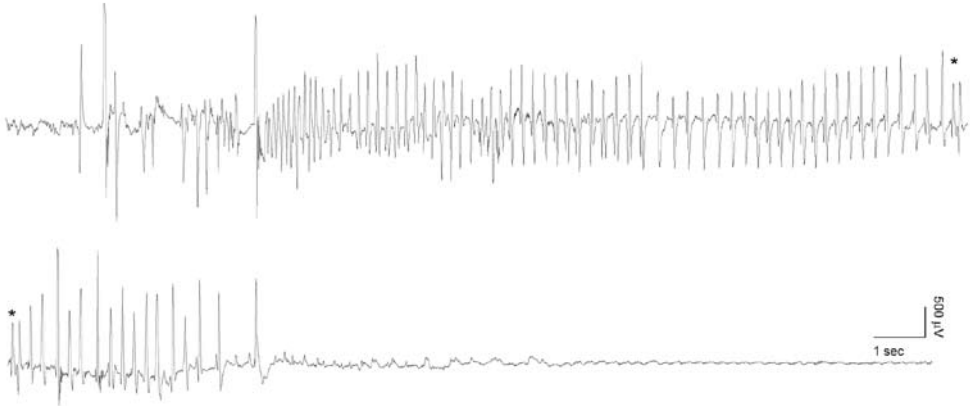
A. wildtype (n=12 out of 12)**B. CK-/-** (n=4 out of 10)**C. CK-/-** (n=6 out of 10)

Figure 2: *Electroencephalograph (EEG) recording during convulsion.* (A) All wildtype mice developed generalized convulsive seizures with the appearance of a continuous high amplitude discharges. The black arrow (↓) depicts the onset of the full seizure (B) In CK-/- mice Only 4 out of 10 CK-/- mice showed seizure-like EEG activity (C) Remarkably, 6 out of 10 CK-/- mice demonstrated a sudden transition to EEG inactivity (#). Vertical black bar represents 500 μ V, horizontal bar represents 5 sec.

was evident (Fig. 3A). At this time, the spike traces are characterized by continuous rhythmic high-amplitude discharges with frequencies ranging from 4 to 6 Hz. The seizure episode ended with the onset of an EEG suppression (postictal depression) period during which time the mice remained motionless. EEG traces of CK-/- mice (4 out of 10) also displayed intense seizure-like EEG discharges with similar latency and duration as wildtypes (Table 1). However, none of them

A. wildtype



B. CK^{-/-}

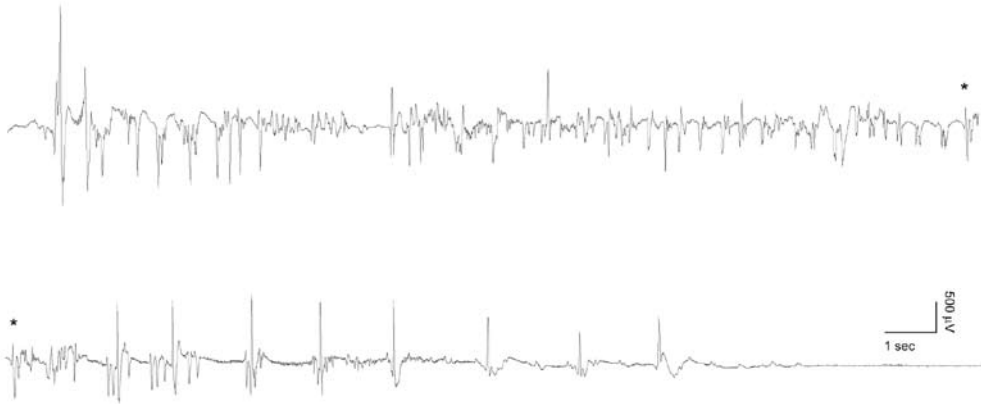


Figure 3: Enlarged view of an electroencephalograph (EEG) trace during convulsive seizure showing the synchronous 4-6 Hz spike discharge. (A) Wildtype brain EEG illustrates a train of rhythmic high amplitude spikes during the seizure episode (enlargement of Fig. 2A). (B) CK^{-/-} mice developing a seizure episode (4 out of 10) the train of spiking consisted of irregular non-synchronized spikes. (enlargement of Fig. 2B). Vertical black bar represents 500 μ V, horizontal bar represents 1 sec.

demonstrated the characteristic 4-6 Hz rhythmic high amplitude spikes in their EEG traces (Fig. 3B). In fact, the entire trace revealed irregular firing during the full seizure episode. Interestingly, those CK^{-/-} mice that did not display a behavioral seizure (6 out of 10), demonstrated after a total of \sim 7 PTZ-injections (\sim 90 min after the initial PTZ injection) a sudden EEG depression (Fig. 2C). Combined, these EEG patterns confirm alterations in brain network dynamics in CK^{-/-} mice.

2.4 Increased Ca^{2+} clearance in CK $^{-/-}$ neurons following repetitive depolarization

Evidence for the role of calcium in epileptogenesis has been shown in different animal experiments. During seizure, an increase in intracellular calcium is observed (Albowitz, 1997) by activating voltage-gated Ca^{2+} channels, as well as by release from intracellular stores (Berridge et al., 2003). Additionally, pharmacological tests with anti-seizure properties of Ca^{2+} antagonists and genetic mouse models have provided a direct link between Ca^{2+} channels and PTZ-induced seizures activity (Weiergräber et al., 2006; Shitak et al., 2007). Even so, Ca^{2+} extrusion is an important determinant of the time course of cytosolic Ca^{2+} signals, especially during the temporal integration resulting from repetitive activity (Sabatini et al., 2001; Berridge et al., 2003). Alterations in cellular processes within each of these categories might modify neuronal network behavior and ultimately animal behavior. To study if the lack of creatine kinase may have altered PTZ-susceptibility via effects on Ca^{2+} transients, we decided to analyze intracellular Ca^{2+} kinetics in acute brain slices. To this end, brain slices from wildtype (n=6) and CK $^{-/-}$ mice (n=6) were loaded with the fluorescent Ca^{2+} sensitive dye fura-2 and analyzed by dynamic video imaging. The ratio fluorescence emission during excitation at 340 nm and 380 nm (F340/F380) was evaluated for the estimation of change in intracellular calcium concentration (Fig. 4A-C).

In unstimulated hippocampal dentate gyrus granule neurons, the initial basal ratio values were similar between wildtypes and CK $^{-/-}$ mice, respectively 0.823 ± 0.03 and 0.735 ± 0.04 (Table 2). In both genotype groups, exposure of the brain slice to a 2 min pulse of KCl (60 mM) resulted in a rapid increase of the ratio fluorescence value within 30 sec (Fig. 5A-B). No significant difference was observed between wildtype and CK $^{-/-}$ cells regarding the maximal ratio value of intracellular Ca^{2+} levels after stimulation by a single KCl pulse (wt 1.210 ± 0.04 ; CK $^{-/-}$ 1.253 ± 0.02 ; Table 2). Following perfusion with Krebs-Ringer's buffer, fura-2 ratio values returned within 5 minutes to a resting ratio fluorescence level where it remained constant throughout the washout period (Table 2; Fig. 5A).

The recovered basal ratio values upon washout yielded non-significant differences between wildtype (0.828 ± 0.03) and CK $^{-/-}$ mice (0.739 ± 0.03 ; Table 2). To allow study of the effects of CK de-

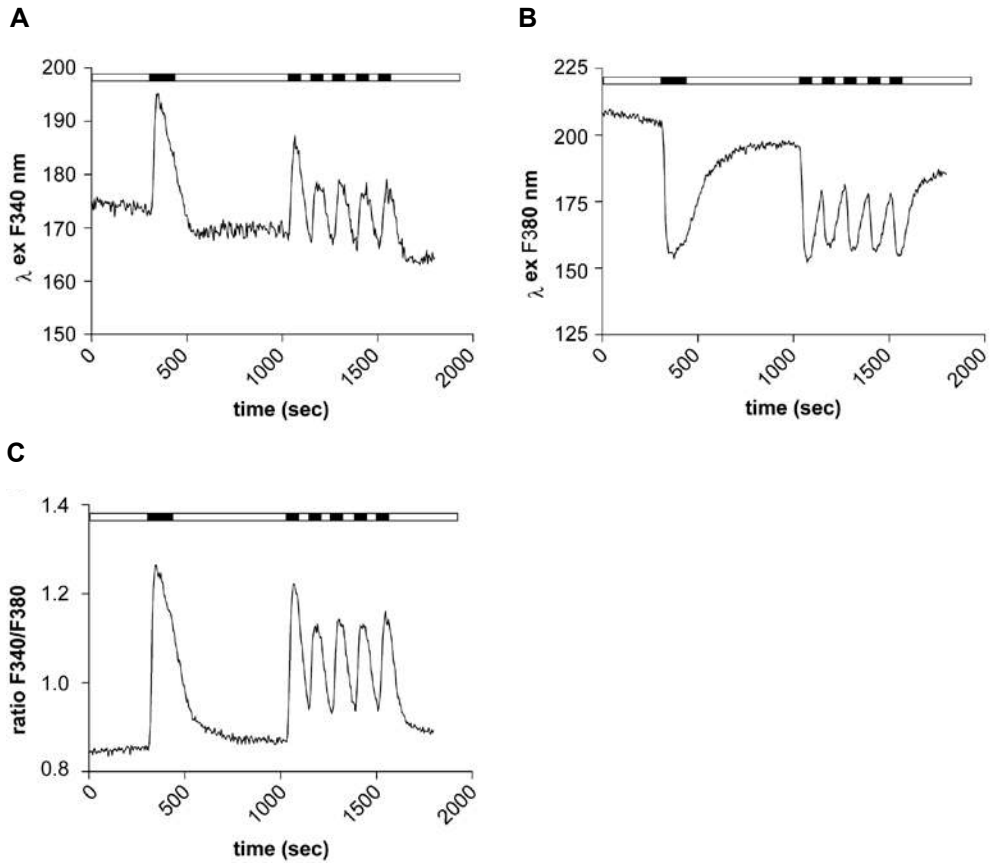


Figure 4: Typical recordings of the excitation spectra of fura-2 following KCl-induced depolarization of a mouse hippocampus brain slice. (A) The single excitation (ex) wavelength fura-2 fluorescence signals 340 nm and (B) 380 nm. (C) The 340 nm/380 nm ratio, which can be used as a linear indicator of intracellular Ca^{2+} levels.

iciency on Ca^{2+} signaling at increasing workloads, we developed a repetitive KCl depolarization (5x1 min) protocol. Interestingly, the use of repetitive stimulation showed differences in the temporal patterns of KCl-dependent calcium transients between wildtype and CK $^{-/-}$ cells. Although, similar maximum ratio values were observed, the minimal ratio value during the washout after each stimulus was significantly lower in CK $^{-/-}$ mice (Table 2; min-1: $t(1,10) = 2.397$, $P < 0.04$; min-2: $t(1,10) = 2.646$, $P < 0.02$; min-3: $t(1,10) = 2.710$, $P < 0.02$; min-4: $t(1,10) = 2.715$, $P < 0.02$). In order to compare Ca^{2+} removal in terms of single-exponential decay time constant, the ratio signals were normalized relative to the basal resting fura-2 ratio, a value to which all

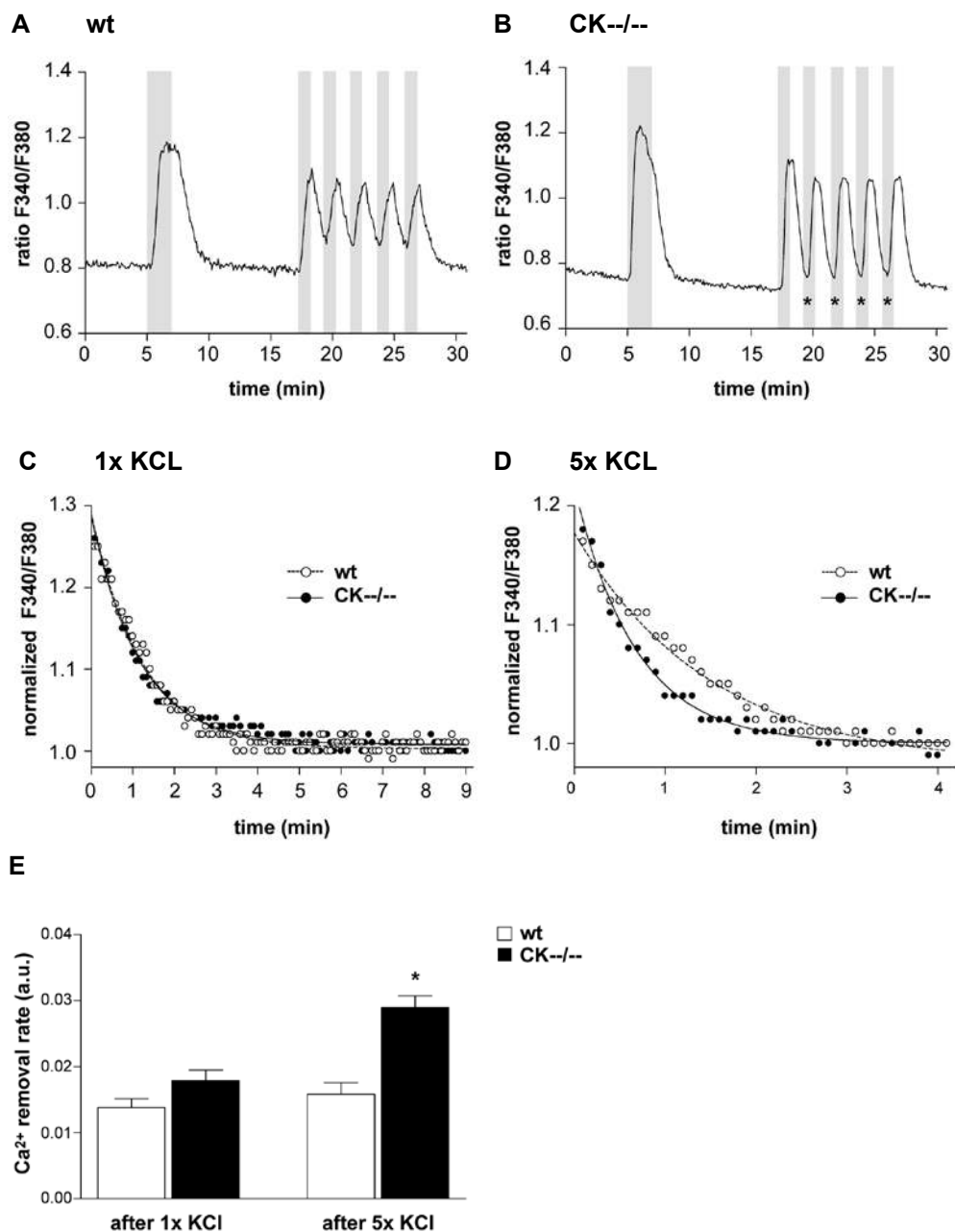


Figure 5: Intracellular calcium dynamics during KCl-induced depolarization of hippocampal brain slices. (A) Shows a representative KCl-induced intracellular Ca^{2+} flux of a wildtype and (B) CK $^{-/-}$ double knockout mouse. First gray bar equals a 2-min KCl pulse, the following five gray bars represents the 5x 1-min KCl pulses. (C) Normalized Intracellular Ca^{2+} decay kinetics after a 2-min KCl pulse and (D) after 5x 1-min KCl pulses of a wildtype (white circle, ; black line, curve fit) and a CK $^{-/-}$ double knockout (black circles, ; black dotted line, curve fit). (E) Mean intracellular Ca^{2+} extrusion values (K-values) of wildtype and CK $^{-/-}$ double knockout hippocampal brain slices (wt n=6, CK $^{-/-}$ n=6). Note that the CK $^{-/-}$ double knockout neurons exhibit a significantly higher K-value compared to wildtype neurons following the 5x 1-min KCl-pulse. (*, significantly different from wildtype (One-way ANOVA, $P < 0.05$), (#, significantly different from the single 2-min KCl-pulse (Paired T-Test, $P < 0.05$))



other values were related (Fig. 5C-D). By fitting a single exponential (eg. 1) to the average ratio signals, a fura-2 decay time constant was obtained for wildtype and CK $^{-/-}$ cells (Fig. 5E). This value represents the Ca^{2+} removal rate, the higher the value, the higher the removal rate. After a single KCl pulse, both in wildtype and CK $^{-/-}$ cells the intracellular Ca^{2+} -levels were back to pre-stimulatory levels within ~200 sec (Fig. 5C). Analyses revealed that the Ca^{2+} decay constant of wildtype and CK $^{-/-}$ cells were similar, respectively $0.01381 \pm 0.001 \text{ s}^{-1}$ and $0.01789 \pm 0.002 \text{ s}^{-1}$ (Fig. 5E). However, after a repetitive KCl pulse Ca^{2+} removal to basal levels was much quicker in CK $^{-/-}$ double knockout neurons (within 100 sec; Fig. 5D) compared to wildtype cells (within 125 sec; Fig. 5D). This difference in speed was also seen in the decay constant (figure 5E) demonstrating a ~60% higher t value in CK $^{-/-}$ cells ($0.02896 \pm 0.002 \text{ s}^{-1}$) compared to wildtype cells ($0.01582 \pm 0.002 \text{ s}^{-1}$), indicating a significantly faster Ca^{2+} removal rate ($t(1,10) = -5.233, P < 0.001$).

Discussion

After repetitive PTZ injections, mice will show generalized convulsive attacks exhibited by an evolving EEG pattern that (a) starts with irregular high voltage activity, (b) gradually change into a repetitive, 4-6 Hz rhythmic pattern, (c) evolve into a series of interrupted discharges, and (d) ends abruptly with a period of postictal depression. Understanding the dynamical mechanisms underlying the EEG activities and conditions that trigger transitions between these patterns is critical for understanding the brain. At the level of single neurons, both the pre-ictal

Table 2. Ratio values of fura-2 during KCL-induced depolarisation of hippocampal brain slices.

| | | wildtype (n=6 mice; 726 cells) | CK-/- (n=6 mice; 757 cells) |
|---|----------|--|---------------------------------------|
| initial baseline value | | 0.822 ± 0.03 | 0.735 ± 0.04 |
| maximal value single KCL ^a | | 1.210 ± 0.04 | 1.253 ± 0.02 |
| baseline after single KCL ^a | | 0.828 ± 0.03 | 0.739 ± 0.03 |
| maximal values repetitive KCL ^b | 1 | 1.145 ± 0.05 | 1.168 ± 0.03 |
| | 2 | 1.082 ± 0.04 | 1.040 ± 0.03 |
| | 3 | 1.069 ± 0.04 | 1.067 ± 0.02 |
| | 4 | 1.059 ± 0.04 | 1.051 ± 0.03 |
| | 5 | 1.058 ± 0.04 | 1.072 ± 0.02 |
| minimal values repetitive KCL ^b | 1 | 0.958 ± 0.04 | 0.837 ± 0.03 * |
| | 2 | 0.921 ± 0.04 | 0.798 ± 0.03 * |
| | 3 | 0.920 ± 0.03 | 0.804 ± 0.03 * |
| | 4 | 0.910 ± 0.03 | 0.800 ± 0.03 * |
| baseline after repetitive KCL ^b | | 0.824 ± 0.04 | 0.749 ± 0.03 |

^a single KCL: 1x2-minute potassiumchloride infusion

^b repetitive KCL: 5x1-minute potassiumchloride infusion, with a pulse interval of 1-minute

Data reported are means ± SEM. *P < 0.05, significantly different from wildtype (Student's t-test)

spikes, i.e. the single and multi-spike discharges, and the convulsive seizure episode consist of synchronized discharge of populations of neurons. The intracellular correlate of a pre-ictal spike on the EEG is an overt depolarization and results in the initiation of a high-frequency burst of action potentials (McCormick and Contreras, 2001). This burst mode firing of action potentials is a potent mechanism for increasing neural synchrony. The transition from brief bursts of synchronous population activity to more prolonged epochs has been associated with the gradual loss of the hyperpolarization between bursts and the progressive appearance of rhythmical action potentials during a sustained depolarization (Matsumoto and Ajmone-Marsan, 1964; Ayala et al., 1970; McCormick and Contreras, 2001). Kim et al (2001) showed that mice lacking burst mode firing of action potential are specifically resistant to the generation of the EEG spike-and-wave discharges characteristic

for absence seizures. Interestingly, intracellular recording with a current clamp also showed that these mice did have a normal repetitive mode firing and clonic-tonic seizures. These findings addressed the importance of different neuronal firing patterns underlying the various seizure activities (Kim et al., 2001).

The main conclusion of the present study is that double brain-type creatine kinase deficiency affects the generation of a prolonged state of intense rhythmic firing of 4-6 Hz frequencies, characteristic for convulsive seizures. Interestingly, the onset of the observed electrical silence in some of the CK^{-/-} mice is comparable with the latency to seizure onset in wildtype mice. Although we cannot rule out that higher doses eventually will lead to a behavioral seizure in these mice, we speculate that this is not the case since further treatment with PTZ initiated even a second period of isoelectric EEG depression (data not shown). Since no difference is observed between the start of seizure behavior upon PTZ injections this suggests an equal sensitivity to PTZ between wildtype and CK^{-/-} mice. It is thus likely that creatine kinase deficiency has not led to an altered numeric balance of GABAergic neurons. Thus, similar inhibitory control of excitatory neurotransmitter systems should exist in both mouse lineages.

Interestingly, the complete brain-type creatine kinase deficiency has affected the ictal activity, but not their pre-ictal activity. These findings suggest that at a neuronal level CK^{-/-} mice lack the continuous firing of action potentials, whereas they show the normal pattern of burst firing of action potentials. In addition, the ictal period of complete brain-type deficient mice was identified with irregular EEG activity, which was observed in wildtypes prior to the period of synchronized bursting. Possibly, the transition to continuous firing of action potentials is impaired in these mice resulting in prolonged neuronal burst firing recoded on the EEG as sustained irregular activity. In addition, the observed increased amount of polyspikes in the EEG could be a recurrent failure to initiate the actual ictal activity. In conclusion, we suggest that the creatine kinase deficiency selectively affects the repetitive mode firing of action potentials in CK^{-/-} neurons.

In hippocampal slices, it was shown that the large synchronized depolarization, associated with seizure events, leads to a large influx of Ca²⁺ into the neurons (Albowitz et al., 1997). In both repetitive and burst mode firing, substantial Ca²⁺ increases occur throughout the soma, nucleus, and proximal dendrite as measured in thalamic relay

cells (Zhou et al., 1997). In the tonic-firing mode, large Ca^{2+} signals were recorded during sustained depolarization, which produced sustained firing. Ca^{2+} signals that large were never produced in the burst mode. Using Ca^{2+} imaging, we showed that complete creatine kinase deficiency contributes to a faster Ca^{2+} extrusion following higher workloads in neurons. By shaping the time course of $[\text{Ca}^{2+}]$ transients in neurons, this can exert control on processes, which are dependent on the perfect timing and localization of Ca^{2+} gradients like transition to repetitive action potentials essential for the rhythmic seizure network. Ca^{2+} ion oscillations are involved in a large number of important cellular processes such as transmitter release, action potential conduction, synaptic plasticity, gene transcription, and neuronal development (Burgoyne and Morgan, 1995; Zucker, 1999; Hong et al., 2000; Peterson and Cancela, 2000; Zheng, 2000; Sabati et al., 2001; Konur and Ghosh, 2005; Berridge, 1998). The local amplitude and time course of Ca^{2+} signals are critical in determining the activation of Ca^{2+} -dependent pathways, depending on the spatial organization and kinetics of Ca^{2+} sources, buffers, and extrusion mechanisms (Sabatini et al., 2001; Berridge et al., 2003). For synaptic transmission, the effector systems respond to pulses within micro- to milliseconds. If the Ca^{2+} transients tend to last longer (seconds to minutes), the resulting signal usually spreads out as a propagating Ca^{2+} wave to reach targets that are distributed throughout the cell (Wolszon et al., 1994; Feller et al., 1996; Finch and Augustine, 1998; Nakamura, 2000). During prolonged stimulation, Ca^{2+} transients are repeated to set up regular Ca^{2+} oscillations that have been implicated in the control of many different processes, like those involved in epilepsy induction in neocortical slices (Tashiro et al., 2002). This supports the concept that changes in Ca^{2+} removal rate control dynamic or developmental changes in neurons. For example, during neuronal maturation, control of neuronal Ca^{2+} signaling becomes important for axon pathfinding (Hong et al., 2000; Peterson and Cancela, 2000; Zheng, 2000), neurotransmitter release (Burgoyne and Morgan, 1995), synapse formation, and synaptic signal integration (Zucker, 1999; Sabatini et al., 2001). Therefore, cytoplasmic Ca^{2+} is an important intracellular second messenger involved in regulating the neuronal circuitry in brain. The altered intracellular Ca^{2+} regulation in CK $^{-/-}$ mice might therefore disturb synapse formation leading to neuronal network disorganization, which could result in behavioral deficits as found in this study.

But how can complete brain-type specific deficiency lead to an increased Ca^{2+} removal rate in neurons following higher workloads while having no PCr available? A possible explanation for this may lie in a necessary compensatory adaptation contributing to the increased decay of $[\text{Ca}^{2+}]$ transients and the increase in capacity to handle and extrude the Ca^{2+} overload. The following events could be involved in this adaptation: (1) Ca^{2+} -dependent increase in Ca^{2+} buffer capacity; (2) decreased release of Ca^{2+} from Ca^{2+} sources activated during depolarization; and (3) increased surface expression of Ca^{2+} extrusion mechanisms like the mitochondrial uniporter, the intracellular Ca^{2+} buffers or the $\text{Na}^+/\text{Ca}^{2+}$ exchanger. Equally important are astrocytes, having a causal role in the maintenance and propagation of synchronous firing of large populations of neurons as during seizure activity (Kang et al., 2005; Tian et al., 2005). By releasing glutamate to activate neuronal receptors (Fellin et al., 2004), astrocytes can affect neuronal intracellular Ca^{2+} levels and thus shape the excitability and synaptic transmission, and coordinate activity across networks of neurons. Since BCK is also expressed in astrocytes (Jost et al., 2002; Tachikawa et al., 2004) we have to keep in mind that the defective simultaneously regulating neurotransmission could have had a neuronal-astrocytic basis.

In conclusion, in this study we provide evidence and propose a role for brain-type creatine kinases in repetitive neuronal firing. Altered Ca^{2+} kinetics could be a factor to explain the effect that ablation of both BCK and UbCKmit genes has on neuronal performance in our mutant CK mouse model. Further theoretical and experimental work is needed to determine precisely how and to what extent the creatine kinase energy system plays a role in neuronal excitability.

Acknowledgments

We want to thank Saskia Hermeling and Hans Krijnen for their expertise and advice with the electrode implantations, Dr. Tineke van Rijn for her indefinite help with the EEG analyses and our colleagues in the Central Animal Facility and the department of Biological Psychology for assistance and advice with the animal care.

References

- Albowitz B, König P, Kuhnt U (1997) Spatiotemporal distribution of intracellular calcium transients during epileptiform activity in guinea pig hippocampal slices. *J Neurophysiol* 77:491-501.
- André V, Pineau N, Motte JE, Marescaux C, Nehlig A (1998) Mapping of neuronal networks underlying generalized seizures induced by increasing doses of pentylenetetrazole in the immature and adult rat: a c-Fos immunohistochemical study. *Eur J Neurosci* 10:2094-2106.
- Ayala GF, Matsumoto H, Gumnit RJ (1970) Excitability changes and inhibitory mechanisms in neocortical neurons during seizures. *J Neurophysiol* 33:73-85
- Barinaga, M (1997) What makes brain neurons run? *Science* 276:196-198.
- Bernstein BW, Bamberg JR (2003) Actin-ATP hydrolysis is a major energy drain for neurons. *J Neurosci* 23:1-6.
- Berridge MJ (1998) Neuronal Ca²⁺ Signaling. *Neuron* 21:13-26.
- Berridge MJ, Bootman MD, Roderick HL (2003) calcium signaling: dynamics, homeostasis and remodeling. *Nat Rev Mol Cell Biol* 4:517-529.
- Bessman SP, Carpenter CL (1985) The creatine-creatine phosphate energy shuttle. *Annu Rev Biochem* 54:831-862.
- Boero J, Qin W, Cheng J, Woolsey TA, Strauss AW, Khuchua Z (2003) Restricted neuronal expression of ubiquitous mitochondrial creatine kinase: changing patterns in development and with increased activity. *Mol Cell Biochem* 244:69-76.
- Brevard ME, Kulkarni P, King JA, Ferris CF (2006). Imaging the neural substrates involved in the genesis of pentylenetetrazole-induced seizures. *Epilepsia* 47:745-754.

Burgoyne RD, Morgan A (1995) calcium and secretory-vesicle dynamics. *Trends Neurosci* 18:191-196.

Fellin T, Pascual O, Gobbo S, Pozzan T, Haydon PG, Carmignoto G (2004) Neuronal Synchrony Mediated by Astrocytic Glutamate through Activation of Extrasynaptic NMDA Receptors. *Neuron* 43:729-743.

De Groof AJ, Fransen JA, Errington RJ, Willems PH, Wieringa B, Koopman WJ (2002) The creatine kinase system is essential for optimal refill of the sarcoplasmic reticulum Ca^{2+} store in skeletal muscle. *J Biol Chem* 277:5275-5284.

Duke AM, Steele DS (1999) Effects of creatine phosphate on Ca^{2+} regulation by the sarcoplasmic reticulum in mechanically skinned rat skeletal muscle fibers. *J Physiol (Lond.)* 517:447-458.

Eells JB, Clough RW, Browning RA, Jobe PC (2004) Comparative fos immunoreactivity in the brain after forebrain, brainstem, or combined seizures induced by electroshock, pentylenetetrazole, focally induced and audiogenic seizures in rats. *Neuroscience* 123:279-292.

El Hamdi, G., de Vasconcelos, A.P., Vert, P. & Nehlig, A (1992) An experimental model of generalized seizures for the measurement of local glucose utilization in the immature rat. I. Behavioral characterization and determination of lumped constant. *Brain Res Dev Brain Res* 69:233-242.

Feller MB, Wellis DP, Stellwagen D, Werblin FS, Shatz CJ (1996) Requirement for cholinergic synaptic transmission in the propagation of spontaneous retinal waves. *Science* 272:1182-1187.

Finch EA, Augustine GJ (1998) Local calcium signaling by inositol-1-,4,5-trisphosphate in Purkinje cell dendrites. *Nature* 396:753-756.

Hertz L, Peng L, Dienel GA (2007) Energy metabolism in astrocytes: high rate of oxidative metabolism and spatiotemporal dependence on glycolysis/glycogenolysis. *J Cereb Blood Flow Metab* 27:219-249.

Holtzman D, Meyers R, Khait I, Jensen F (1997) Brain creatine kinase reaction rates and reactant concentrations during seizures in developing rats. *Epilepsy Res* 27:7-11.

Hong K, Nishiyama M, Henley J, Tessier-Lavigne M, Poo M (2000) Calcium signaling in the guidance of nerve growth by netrin-1. *Nature* 403: 93-98.

Ince C, Van Dissel JT, Diesselhoff MM (1985) A teflon culture dish for high-magnification microscopy and measurements in single cells. *Pflugers Arch* 403:240-244.

In 't Zandt HJ, Renema WK, Streijger F, Jost C, Klomp DW, Oerlemans F, Van der Zee CE, Wieringa B, Heerschap A (2004) Cerebral creatine kinase deficiency influences metabolite levels and morphology in the mouse brain: a quantitative in vivo ¹H and ³¹P magnetic resonance study. *J Neurochem* 90:1321-1330.

Jost CR, Van der Zee CEEM, In 't Zandt HJ, Oerlemans F, Verheij M, Streijger F, Franssen J, Heerschap A, Cools AR, Wieringa B (2002) Creatine kinase B-driven energy transfer in the brain is important for habituation and spatial learning behavior, mossy fiber field size and determination of seizure susceptibility. *Eur J Neurosci* 15:1692-1706.

Kang , Xu J, Xu Q, Nedergaard M, Kang J (2005) Astrocytic Glutamate Release-Induced Transient Depolarization and Epileptiform Discharges in Hippocampal CA1 Pyramidal Neurons. *J Neurophysiol* 94:4121-4130.

Kim D, Song I, Keum S, Lee T, Jeong M-J, Kim S-S, McEnery MW, Shin H-S, (2001) Lack of the Burst Firing of Thalamocortical Relay Neurons and Resistance to Absence Seizures in Mice Lacking a1G T-Type Ca²⁺ Channels. *Neuron* 31:35-45.

Konur S., Ghosh A (2005) Calcium signaling and the control of dendritic development. *Neuron* 46:401-405.

Matsumoto H, Ajmone-Marsan C (1964) Cortical cellular phenomena in experimental epilepsy: ictal manifestations. *Exp Neurol* 9:305-326.

McCormick DA, Contreras D (2001) On the cellular and network bases of epileptic seizures. *Annu Rev Physiol* 63:815-846.

Minajeva A, Ventura Clapier R, Veksler V (1996) Ca^{2+} uptake by cardiac sarcoplasmic reticulum ATPase in situ strongly depends on bound creatine kinase. *Pflugers Arch* 432:904-912.

Nakamura T, Nakamura K, Lasser-Ross N, Barbara JG, Sandler VM, Ross WN (2000) Inositol 1,4,5-trisphosphate (IP3)-mediated Ca^{2+} release evoked by metabotropic agonists and backpropagating action potentials in hippocampal CA1 pyramidal neurons. *J Neurosci* 20:8365-8376.

O'Gorman E, Beutner G, Wallimann T, Brdiczka D (1996) Differential effects of creatine depletion on the regulation of enzyme activities and on creatine-stimulated mitochondrial respiration in skeletal muscle, heart, and brain. *Biochim Biophys Acta* 276:161-170.

Paxinos G, Watson C (1997) *The rat brain in stereotaxic coordinates*, Academic Press, San Diego.

Peterson OH, Cancela JM (2000) Nerve guidance: attraction or repulsion by local Ca^{2+} signals. *Curr Biol* 10:R311-R314.

Rossi AM, Eppenberger HM, Volpe P, Cotrufo R, Wallimann T (1990) Muscle-type MM creatine kinase is specifically bound to sarcoplasmic reticulum and can support Ca^{2+} uptake and regulate local ATP/ADP ratios. *J Biol Chem* 265:5258-5266.

Sabatini BL, Maravall M, Svoboda K (2001) Ca^{2+} signaling in dendritic spines. *Curr Opin Neurobiol* 11:349-356.

Shin J, Streijger F, Beynon A, Peters T, Gadzalla L, McMillen D, Bystrom C, van der Zee CEEM, Wallimann T, Gillespie PG. (2007) Hair Bundles Are Specialized for ATP Delivery via Creatine Kinase. *Neuron* 53:371-386.

Shitak R, Sahai AK, Hota D, Chakrabarti A (2007) Evaluation of the modulatory role of nimodipine in seizures induced by kainic acid and

pentylentetrazole in mice. *Methods Find Exp Clin Pharmacol* 29:11-17.

Streijger F, Jost CR, Oerlemans F, Ellenbroek BA, Cools AR, Wieringa B, Van der Zee CEEM (2004) Mice lacking the UbCKmit isoform of creatine kinase reveal slower spatial learning acquisition, diminished exploration and habituation, and reduced acoustic startle reflex responses. *Mol Cell Biochem* 256-257:305-318.

Streijger F, Oerlemans F, Ellenbroek BA, Jost CR, Wieringa B, Van der Zee CEEM (2005) Structural and behavioral consequences of double deficiency for creatine kinases BCK and UbCKmit. *Behav Brain Res* 157: 219-234.

Tachikawa, M., Fukaya, M., Terasaki, T., Ohtsuki, S., and Watanabe, M. (2004). Distinct cellular expressions of creatine synthetic enzyme GAMT and creatine kinases uCK-Mi and CK-B suggest a novel neuron-glia relationship for brain energy homeostasis. *Eur J Neurosci* 20:144-160.

Tashiro A, Goldberg J, Yuste R (2002) Calcium oscillations in neocortical astrocytes under epileptiform conditions. *J Neurobiol* 50:45-55.

Tian GF, Azmi H, Takano T, Xu Q, Peng W, Lin J, Oberheim N, Lou N, Wang X, Zielke HR, Kang J, Nedergaard M (2005) An astrocytic basis of epilepsy. *Nat Med* 11:973-981.

Wallimann T, Wyss M, Brdiczka D, Nicolay K, Eppenberger HM (1992) Intracellular compartmentation, structure and function of creatine kinase isoenzymes in tissues with high and fluctuating energy demands: the phosphocreatine circuit for cellular energy homeostasis. *Biochem J* 281:21-40.

Weiergräber M, Henry M, Krieger A, Kamp M, Radhakrishnan K, Hescheler J, Schneider T (2006) Altered Seizure Susceptibility in Mice Lacking the Cav2.3 E-type Ca^{2+} Channel. *Epilepsia* 47:839-850.

Wolszon LR, Rehder V, Kater SB, Macagno ER (1994) Calcium wave fronts that cross gap junctions may signal neuronal death during development. *J Neurosci* 14:3437-3448.

Wyss M, Kaddurah-Daouk R (2000) Creatine and creatinine metabolism. *Physiol Rev* 80:1107-1213.

Zheng JQ (2000) Turning of nerve growth cones induced by localized increases in intracellular calcium ions. *Nature* 403:89-93.

Zhou Q, Godwin DW, O'Malley DM, Adams PR (1997) Visualization of calcium influx through channels that shape the burst and tonic firing modes of thalamic relay cells. *J Neurophysiol* 77:2816-2825.

Zucker RS (1999) calcium- and activity-dependent synaptic plasticity. *Curr Opin Neurobiol* 9:305-313.

Chapter 7

Summarizing discussion



1. Function of the brain creatine kinases

For any living cell it is essential to keep energy demand and production well balanced, and have energy homeostasis – i.e. ATP level - under tight regulation. Cells maintain their ATP level and viability by either respiration or glycolysis, whereby the energy provided is needed for the synthesis and modification of small and macromolecular constituents of the cell, for cellular movement, maintenance of osmolar and electrical gradients, molecular transport, maintenance of protein integrity, and in warm-blooded animals, for the generation of body heat (Barinaga, 1997; Lowell and Spiegelman, 2000; Bernstein and Bamberg, 2003; Hertz 2007; Ikemoto et al., 2003). The cellular network for allocation of ATP and distribution of high-energy phosphate groups among phosphometabolites in mammalian cells consists of several redundant pathways, in which glycolytic enzymes, members of the creatine kinase and adenylate kinase families of enzymes and nucleoside diphosphate kinases play a determining role. Creatine kinase (CK), also known as phosphocreatine kinase or creatine phosphokinase, is expressed in various tissues. The function of the enzyme is the catalysis of the reversible conversion of phosphocreatine to creatine, consuming ADP and generating ATP. In tissues that consume ATP rapidly, like skeletal muscle, heart and brain, creatine phosphate serves as a reservoir for the rapid generation of ATP in periods during which energy consumption threatens to exceed energy production. Remarkably, although this system has been extensively studied in-vitro and in-vivo, it is still largely unknown how its proposed functions translate into biological significance in the intact animal. In the study described in this thesis much effort was spent to investigate the role of the brain specific creatine kinase-phosphocreatine (CK-PCr) circuit. Using gene-knockout approaches we have generated mice strains that carry null mutations for either cytosolic BCK (BCK^{-/-} mice) or mitochondrial UbCKmit (UbCKmit^{-/-} mice), or for both enzymes in double knock-outs (CK^{-/-} mice; Van Deursen and Wieringa, 1994; Steeghs et al., 1995; In 't Zandt et al., 2004). For phenotyping of these mice, a battery of many different behavioral paradigms was developed and used to study the relationship between phosphocreatine-creatine energetics and task performance.

2. CK and behavior

What is the exact role of the brain specific creatine kinases in the control of animal behavior? As described in chapter 2-6 the absence of CK function has striking behavioral effects. Single creatine kinase deficient mice have mild behavioral and anatomical abnormalities like decreased spatial cognition, less habituation and activity, and reduced startle responses to multiple high intensity sound (Jost et al., 2002; Streijger et al., 2004; chapter 2). In principle, the plasticity of the creatine kinase reaction in cells could allow for reciprocal compensation when either BCK or UbCKmit is absent, at least in cell types where they are co-expressed. Thus we speculated that - although both CK isoenzymes occur in different cellular locales - this functional redundancy will warrant reversible ATP/PCr exchange in single knockout mice, explaining their relatively mild phenotype (Jost et al., 2002; Streijger et al., 2004; chapter 2). In chapter 3 (Streijger et al., 2005) we therefore extended our study and examined whether ablation of both BCK and UbCKmit indeed has more detrimental effects than single knockout in our mouse models. As anticipated, we observed that double mutants were significantly more affected than the single mutants. The phenotype included growth deficiency, body temperature deficits, hearing loss, altered seizure characteristics, brain abnormalities, and particular deficits in hippocampal-dependent spatial learning dysfunction (Jost et al., 2002; Streijger et al., 2004; Streijger et al., 2005; chapter 3-6). Although BCK^{-/-}, UbCKmit^{-/-} and CK^{-/-} mice all showed reduced spatial cognition, spatial learning deficits were most severe when CK was fully absent. The Morris water maze and 12-circular hole board tasks highlight these differences clearly, showing that the difference between CK^{-/-} mice and the control group remain over time, while both single knockout groups eventually learn the task. However, normal learning was shown in the non-hippocampus-dependent learning task such as the visible platform water maze. Besides the specificity of the learning impairments, a few other neurological phenotypes have been reported. Some behavioral features (e.g., increased activity in an open field, and decreased nestbuilding activity) are correlated with morphological alterations in the hippocampus (Schwegler & Crusio, 1995; Spooren et al., 1999; Ramirez-Amaya, 2001). Additionally, although creatine kinase is not essential for life since CK^{-/-} mice are viable, the enzyme does appear necessary for normal brain development. To illustrate this

point, we found that both single and double creatine kinase deficient mice displayed abnormal brain morphology (Jost et al., 2002; Streijger et al 2005; chapter 3). This deviant morphology was most apparent in CK^{-/-} mice, demonstrating a smaller brain size, and changes in the hippocampus and intra-infra projection field (Streijger et al., 2005; chapter 3). Subsequent studies revealed that mice lacking both CK's have a profound hearing impairment as well (Streijger et al., 2005, Shin et al., 2007; chapter 3-4). Although the sensory structures within the CK mutant animals' ears appeared to develop normally, hearing studies showed that a 20-30 dB greater intensity signal was required to elicit auditory threshold in CK^{-/-} mice, indicating hearing loss (Shin et al., 2007; chapter 4). Notably, the behavioral phenotype of mice with deficiency for CK resembles some of the hallmarks of the human creatine deficiency syndrome and knockout mouse model of GAMT deficiency such as reduced PCr signal in brain, cognitive dysfunction and a marked reduction in body weight (Schmidt et al., 2004).

3. CK at the system level

The specific behavioral phenotype of CK^{-/-} mice lead in turn to the following question: How might these aspects of behavior be explained by the function and activity of the creatine kinase in the entire organism? In this thesis we correlated most of the abnormal behavior of CK mutant mice with alterations in brain systems (Chapter 2-3; chapter 5-6). However, we have shown in collaboration with the lab of Peter Gillespie that BCK is present in hair bundles within the cochlea of the inner ear at high enough levels to be primarily responsible for ATP delivery in these cells (Shin et al., 2007; chapter 4). Hair cells stimulation generally occurs through the deformation of the cell's stereocilia, which lead to the direct opening of transduction channels thereby changing the membrane potential resulting, eventually, in a nervous impulse (Grant and Fuchs, 2007). Although, metabolic energy is not required for mechanodeflection of the stereocilia itself, ATP is essential for mechanisms involved in adaptation to the auditory transduction accomplished by the influx of Ca²⁺-ions (Mammano et al., 2007) leading to myosin movement along actin filaments reducing tension and allowing channels to close (Schneider et al., 2002; Gillespie and Cyr, 2004; Hirono et al., 2004; Lin et al., 2005). Our results are consistent with this specific energy-supply role since CK inhibition in hair cells re-

sulted in reduced adaptation and CK mutant mice demonstrated loss of hearing (Shin et al., 2007; chapter 4). This reduced hearing sensitivity could also explain the conspicuous reduction in startle responses upon high-intensity auditory stimulation (Jost et al., 2002; Streijger et al., 2005; chapter 3).

To further investigate the physiological function of creatine kinase in brain, CK^{-/-} mice were subjected to PTZ-induced seizures in order to create a robust challenge for overall brain energy metabolism (Chapter 6). EEG monitoring studies revealed that excessive electrical neuronal discharges as during seizures, is severely impaired in CK^{-/-} mice despite normal baseline synaptic transmission (Jost et al., 2002; chapter 6). To what extent the altered overall brain activity contributes to the behavioral phenotype of the CK mutants, remains to be elucidated. Although many brain disorders have an energetic base, the role of the metabolic impairment in the disease process is highly variable (Beal, 2000; Escartin et al., 2006; Lin and Beal, 2006; Palop et al., 2006; Rubinsztein, 2006). Some pathological conditions can be very direct and straightforward as after a stroke when the acute disruption in energy supply will lead to a massive cell death in the infarct core (Lo et al., 2003; Escartin et al., 2006). On the other hand, neuronal dysfunction in some genetic disorders, such as GLUT1 deficiency syndrome, is caused by a mutation of a key metabolic enzyme or transporter (Wang et al., 2005). Thus, the brain is highly vulnerable to energetic dysfunction. In the present study, we have described first steps on a long road towards the delineation of the biological role the creatine kinases in brain energetic. From the overview of data given here it is apparent that CK isoenzymes may have an accessory role if we consider global brain physiology at the systems-level. Many factors might influence behavioral outcome and considering the ubiquitous expression pattern of BCK and UbCKmit in brain, one might suggest that the lack of creatine kinase in the CNS might affect neural activities at multiple levels, including the disruption of molecular pathways, synapses, neuronal subpopulations and local circuits in specific brain regions, as well as high-order neuronal networks.

By comparing (remaining) creatine kinase enzyme activity between brains from wildtype and knockout mice we were able to estimate the relative expression levels of BCK and UbCKmit in brains of mice at different time points after birth (chapter 3; streijger et al., 2005). Our data demonstrate a postnatal increase of the total CK en-

zyme activity, with a peak between 3-6 weeks of age and an estimated contribution of BCK and UbCKmit, of around 67% and 33%, respectively to total CK activity. Of note, the peak of highest CK activity coincides with the time period in which brains of mice undergo a period of very rapid development and organization. This period is characterized by a dramatic increase in cell number of both neurons and astrocytes, with highly dynamic pathfinding, shaping and pruning activity (Bhide et al., 1996; Clancy et al., 2001). Neuroanatomical studies and analyses with functional MRI (In 't Zandt, 2004; Streijger et al., 2005; chapter 3; chapter 5) provided further evidence that the neural organization in creatine kinase deficient mice is abnormal, and that the roots of the cognitive aspects of the phenotype may lie in the disruption of normal neurodevelopment. Furthermore, also the altered seizure susceptibility (chapter 6), involving a global depolarization of large brain areas, may point into the direction of a general loss-of-function or altered cellular wiring and developmental adaptation. CK-related late-prenatal and post-natal developmental impairment of brain growth is evident if we consider the overall smaller brain size (Streijger et al., 2005; chapter 3). Evidence for further structural alterations was obtained from analysis of the mossy fiber area of the hippocampus (Jost et al., 2002; Streijger et al., 2005; chapter 2-3). Most easily, these findings can be explained by absence of pruning or abnormal neuron-astrocyte cooperation during subregional brain development, possibly in the postnatal period. It is unlikely that the extended SP-MF/IIP-MF structures are caused by improved dendrite development in the absence of CK.

The role of BCK in brain may even be much more complex, however, as its expression is not confined to neurons but also prominent in cells of the astrocytes-glia cell lineage (Jost et al., 2002; Tachikawa et al., 2004). Neuronal networks contain a variety of glial cells with which neurons have complex reciprocal interactions (Magistretti and Pellerin 1999; Ames, 2000; Escartin et al., 2006; Halasa et al., 2006; Pellerin et al., 2007). Glial cells maintain local ion concentrations and pH homeostasis in the extracellular space, supply neurons with nutrients and remove byproducts of metabolism and neurotransmitters released into the synaptic cleft (Martin, 1992; Nedergaard et al., 2003). Astrocytes also regulate synapse neurogenesis (Barres, 1999), and synaptogenesis (Barres, 1999; Ullian et al., 2001; Ullian et al., 2004). Not surprisingly, disturbances in astrocyte function have been implicated in mechanisms of increased neuronal excitability leading to sei-

zures (Steinhauser and Seifert, 2002; D'Ambrosio, 2004; Tian et al., 2005). Furthermore, a currently held concept suggests that astrocytes may coordinate synapses into synchronously neuronal firing that define epileptic seizures (Kang et al., 2005; Tian et al., 2005).

The capacity for reorganization and change is a critical feature of brain development. Ongoing synaptic spine remodeling and cell-contact (endfeet) reshaping lead to continuous alteration in synaptic connectivity and strength between neuronal partners, affecting the efficacy of synaptic communication during development, growth into adulthood and even during ageing. Changing and remodeling of the brain is not only important early in life, but also provides the basis for learning in the adult brain. Changes in synaptic number, spine density and spine morphology within the hippocampus (Harms and Dunayevsky, 2006; Kopec and Malinow, 2006) have been reported with memory acquisition. The finding that lack of creatine kinase function in the brain associated with cognitive deficits (chapter 2-3; Jost et al., 2002; Streijger et al., 2005) thus suggests a possible relationship between (sub)cellular energy metabolism and the maintenance of structural and functional plasticity during adulthood. A role for creatine kinase during cellular shape changes and cell motility is indirectly supported by work of Wang et al (1998), who showed that arginine kinase, another member of the guanidine phosphotransferase family of enzymes and the insect homologue of BCK, is concentrated along moving edges of lamellipodia of migrating glia and growth cones in migrating neurons. Also, creatine kinase inhibitors reduce tumor cell motility (Mulvaney et al., 1998) and preliminary evidence suggests that BCK may participate in axonal branching (H. Pluk, personal communication). Several studies indicate that glial cells in epileptic tissue undergo not only physiological but also morphological alterations (Eduardo and Benarroch, 2005). It is therefore interesting to note here, that Mahajan et al (2000) showed that knockdown of BCK expression prevents thrombin-mediated morphological changes in astrocytes, indicating that CK is indeed important in astrocyte shape modulation. Combined these literature data suggests that creatine kinase deficiency can also impair neurons indirectly through impairment of astroglial function. Therefore, both glia and neurons could be equally well involved in the CK^{-/-} abnormalities.

4. CK at the molecular level

The results described in this thesis have led to assumption that brain CK's are essential for the efficient functioning of plasma membrane Ca^{2+} -ATPases in brain cells (chapter 6) and hair cells within the cochlea of the inner ear (Shin et al., 2007; chapter 4). A similar correlation has also been demonstrated in muscle (Rossi et al., 1990; Minajeva et al., 1996; Duke and Steele, 1999; Steeghs et al., 1997; De Groof et al., 2002). Direct supporting evidence was provided by studies on calcium extrusion mechanisms of hippocampal brain slices of CK mutant mice. Experimental-induced depolarization resulted in a substantially altered intracellular clearance of large Ca^{2+} loads in neuronal cell. From these studies, we propose a model of impaired intracellular Ca^{2+} regulation contributing to the behavioral phenotype of our CK $^{-/-}$. Numerous studies have indicated that modulation of intracellular Ca^{2+} levels is particularly important for cellular cell changes and motility during development and adulthood. During axon growth, regulation of growth cone Ca^{2+} levels influences the rate and direction of axon elongation (Kater and Mills 1991; Zheng, 2000). In addition, intracellular Ca^{2+} signals controls influence many cellular processes such as neurotransmitter release, synaptic vesicle recycling (Reuter and Porzig, 1995; Bouron and Reuter, 1996) and plasticity (Zucker, 1996). Recently, work of Jeon et al (2003) showed that hippocampal neurons of mice with a functional deletion of the plasma membrane $\text{Na}^{+}/\text{Ca}^{2+}$ exchanger 2, exhibited a significantly clearance of elevated Ca^{2+} concentrations following depolarization. Behaviorally, these mutant mice showed an enhanced performance in several hippocampus-dependent learning and memory tasks together with enhanced long-term potentiation. This study indicated that activity-dependent increase in postsynaptic intracellular Ca^{2+} levels and subsequent activation of Ca^{2+} -dependent pathways play a critical role in synaptic plasticity that may serve as a cellular cognate of memory acquisition and consolidation. It will be interesting to examine if the impaired spatial memory of CK $^{-/-}$ mice underlies lack of long-term plasticity due to altered Ca^{2+} extrusion.

Although our observations in CK $^{-/-}$ mice support the concept that brain CK's are essential for normal Ca^{2+} regulation (Shin et al., 2004; chapter 4; chapter 6), we do not exclude the existence of other plausible mechanisms or a combination of processes. Dynamic modulation of the actin cytoskeleton is a major ATP consuming process in

brain (Bernstein and Bamburg, 2003) and is essential for pathfinding of neurons, ensheating of neurons by astrocytes projections, spine dynamics (Da Silva and Dotti, 2002; Fischer et al., 1998; Dunaevsky et al., 1999; Park et al., 2006). Recently, evidence from our lab suggests that mobilization of BCK may also participate in processes based on actin motility in glial and neuronal cells (Kuiper et al., in preparation). Accordingly, in osteoclast cells the PCr is utilized to maintain cellular ATP content during the cyclical processes of migration, attachment and resorption (Chang et al., submitted). The efficiency of these processes depends critically on actin cytoskeleton modulation. We thus propose that the creatine kinase in brain cells could in part also be necessary for the delivery of ATP for the energetically demanding task involving actine cytoskeleton reorganization.

It might be questioned whether all behavioral characteristics of the CK^{-/-} mice can be explained by the defect of a single mechanism. One future approach that will help us in the further deconvolution of the physiological role of CK at the molecular level will be to compare behavioral phenotypes between our CK mice and mice with knockout mutations in partner proteins for CK's. To our knowledge, currently only one such a model is available: The hypomorphic KCC2-deficient mouse (Tornberg et al., 2005), which has lost one allele of the potassium-chloride co-transporter KCC2. KCC2 is a membrane protein, which interacts with BCK, and has a role in hyperpolarizing fast inhibitory neurotransmission (Inoue et al., 2006). Interestingly, KCC2 hypomorphs are smaller, exhibit altered habituation behavior and show impaired learning ability. However, PTZ sensitivity was increased and not impaired as in our CK-mutants. Perhaps parallel testing should be done to reveal more similarities and differences, but ultimately this may help to interpret the relative importance of components in the CK circuit itself, and the structurally or functionally coupled systems.

5. Concluding remarks

The main objective of the studies described in this thesis was to obtain more insight in the biological importance of the brain specific creatine kinases, BCK and UbCKmit, for an organism. Our current behavioral phenotyping abilities are not powerful enough to discriminate between the many potential mechanisms that could underlie the phenotype of our CK deficient mice. However, the results of this study confirm the

suggestion that brain-type creatine kinases play a role in Ca^{2+} regulation, actomyosin sliding and perhaps other energy-dependent processes in brain cells and hair bundles. Continuation of the work described in this thesis is thus necessary. At the one hand we must characterize whether the patterns of CK expression or - perhaps better, CK activity - correlate with regional effects on brain development and the role of neurons and glial cells therein. Comparison of viability parameters, ion-homeostasis and/or actomyosin dynamics in primary neurons or astrocytes obtained from these regions may eventually help us to make further progress in our understanding of the CK system at the cellular level. At the other hand, we need high-resolution brain-imaging techniques like fMRI to delineate the most vulnerable nodal regions in the cellular brain network, regions that lose functional integrity in the absence of CK. Here a general decline in the homeostatic ATP reserve or more specific metabolic loss-of-function effects may be involved, with similarity to effects of ageing or neurodegenerative disease like Alzheimer's, Parkinson and Huntington's, diabetes type II or mitochondrial disorders. Research on CK function in brain may thus ultimately contribute not only to the topic of CK-Cr significance itself, but also help in a better understanding of how [ATP] functions within the normal physiological range or is associated with cell death or pathophysiological dysfunction in disease.

References

Ames A III (2000) CNS energy metabolism as related to function. *Brain Res Rev* 34:42-68.

Bailey SR, Eid AH, Mitra S, Flavahan S, Flavahan NA (2004) Rho kinase mediates cold-induced constriction of cutaneous arteries: role of α_2c -adrenoceptor translocation. *Circ Res* 94:1367-1374.

Barinaga M (1997) What makes brain neurons run? *Science* 276:196-198.

Barres BA (1999) A new role for glia: generation of neurons! *Cell* 97:667-670.

Bernstein BW, Bamburg JR (2003) Actin-ATP hydrolysis is a major energy drain for neurons *J Neurosci* 23:1-6

Beal MF (2000) Energetics in the pathogenesis of neurodegenerative diseases. *Trends Neurosci* 23:298-304.

Bhide PG, Day M, Sapp E, Schwarz C, Sheth A, Kim J, Young AB, Penney J, Golden J, Aronin N, DiFiglia M (1996) Expression of normal and mutant huntingtin in the developing brain. *J Neurosci* 16:5523-5535.

Clancy B, Darlington RB, Finlay BL (2001) Translating developmental time across mammalian species. *Neurosci* 105:7-17.

D'Ambrosio R (2004) The role of glial membrane ion channels in seizures and epileptogenesis. *Pharmacol Ther.* 103:95-108.

Da Silva JS, Dotti CG (2002) Breaking the neuronal sphere: regulation of the actin cytoskeleton in neuritogenesis. *Nat Rev Neurosci* 3:694-704.

De Groof AJ, Fransen JA, Errington RJ, Willems PH, Wieringa B, Koopman WJ (2002) The creatine kinase system is essential for optimal refill of the sarcoplasmic reticulum Ca^{2+} store in skeletal muscle.

J Biol Chem 277:5275-5284.

Duke AM, Steele DS (1999) Effects of creatine phosphate on Ca^{2+} regulation by the sarcoplasmic reticulum in mechanically skinned rat skeletal muscle fibres. J Physiol 517:447-458.

Dunaevsky A, Tashiro A, Majewska A, Mason C, Yuste R (1999) Developmental regulation of spine motility in the mammalian central nervous system Proc Natl Acad Sci USA 96:13438-13443.

Eduardo E, Benarroch MD (2005) Neuron-Astrocyte Interactions: Partnership for Normal Function and Disease in the Central Nervous System. Mayo Clin Proc 80:1326-1338.

Escartin C, Valette J, Lebon V, Bonvento G (2006) Neuron-astrocyte interactions in the regulation of brain energy metabolism: a focus on NMR spectroscopy J Neurochem 99:393-401.

Fischer M, Kaech S, Knutti D, Matus A (1998) Rapid actin-based plasticity in dendritic spines. Neuron 20:847-854.

Foster DO (1986) Brown Adipose Tissue. Editors: Trayhurn P, Nicholls DG. London: Edward Arnold, pp31-51.

Gillespie PG, Cyr JL (2004) Myosin-1c, the hair cell's adaptation motor. Annu Rev Physiol 66:521-545.

Grant L, Fuchs PA (2007) Auditory transduction in the mouse. Pflugers Arch 454:793-804.

Harms KJ, Dunaevsky A (2006) Dendritic spine plasticity: Looking beyond development. Brain Res [Epub ahead of print].

Halassa MM, Fellin T, Haydon PG (2007) The tripartite synapse: roles for gliotransmission in health and disease. Trends Mol Med 13:54-63.

Hertz L, Peng L, Dienel GA (2007) Energy metabolism in astrocytes: high rate of oxidative metabolism and spatiotemporal dependence on glycolysis /glycogenolysis. J Cereb Blood Flow Metab 27:219-249.

Hirono M, Denis CS, Richardson GP, Gillespie PG (2004) Hair cells require phosphatidylinositol 4,5-bisphosphate for mechanical transduction and adaptation. *Neuron* 44:309-320.

Ikemoto A, Bole DG, Ueda T (2003) Glycolysis and glutamate accumulation into synaptic vesicles. Role of glyceraldehyde phosphate dehydrogenase and 3-phosphoglycerate kinase. *J Biol Chem* 278:5929-5940.

Inoue K, Yamada J, Ueno S, Fukuda A (2006) Brain-type creatine kinase activates neuron-specific K^+ - Cl^- co-transporter KCC2. *J Neurochem* 96:598-608.

In 't Zandt HJ, Renema WK, Streijger F, Jost C, Klomp DW, Oerlemans F, Van der Zee CEEM, Wieringa B, Heerschap A (2004) Cerebral creatine kinase deficiency influences metabolite levels and morphology in the mouse brain: a quantitative in vivo 1H and ^{31}P magnetic resonance study. *J Neurochem* 90:1321-1330.

Jeon D, Yang YM, Jeong MJ, Philipson KD, Rhim H, Shin HS (2003) Enhanced Learning and Memory in Mice Lacking Na^+/Ca^{2+} Exchanger 2. *Neuron* 38: 965-976.

Jost CR, van der Zee CEEM, In 't Zandt HJ, Oerlemans F, Verheij M, Streijger F, Fransen J, Heerschap A, Cools AR, Wieringa B (2002) Creatine kinase B-driven energy transfer in the brain is important for habituation and spatial learning behavior, mossy fibre field size and determination of seizure susceptibility. *Eur J Neurosci* 15:1692-1706.

Kang , Xu J, Xu Q, Nedergaard M, Kang J (2005) Astrocytic Glutamate Release-Induced Transient Depolarization and Epileptiform Discharges in Hippocampal CA1 Pyramidal Neurons. *J Neurophysiol* 94:4121-4130.

Kater SB, Mills LR (1991) Regulation of growth cone behavior by calcium. *J Neurosci* 11: 891-899.

Kikuchi-Utsumi K, Gao B, Ohinato H, Hashimoto M, Yamamoto N, Kuroshima A (2002) Enhanced gene expression of endothelial nitric

oxide synthase in brown adipose tissue during cold exposure *Am J Physiol Regulatory Integrative Comp Physiol* 282:R623–R626.

Kopec C, Malinow R (2006) Neuroscience. Matters of size. *Science* 314:1554-1555.

Lin HW, Schneider ME, Kachar B (2005) When size matters: the dynamic regulation of stereocilia lengths. *Curr Opin Cell Biol* 17:55–61.

Lin MT, Beal MF (2006) Mitochondrial dysfunction and oxidative stress in neurodegenerative diseases. *Nature* 443:787-795.

Lo EH, Dalkara T, Moskowitz MA (2003) Mechanisms, challenges and opportunities in stroke. *Nat Rev Neurosci* 4:399-415.

Lowell BB, Spiegelman BM (2000) Towards a molecular understanding of adaptive thermogenesis. *Nature* 404:652-660.

Magistretti PJ, Pellerin L (1999) Astrocytes Couple Synaptic Activity to Glucose Utilization in the Brain. *News Physiol Sci* 14:177-182.

Mahajan VB, Pai KS, Lau A, Cunningham DD (2000) Creatine kinase, an ATP-generating enzyme, is required for thrombin receptor signaling to the cytoskeleton. *PNAS* 97:12062-12067.

Mammano F, Bortolozzi M, Ortolano S, Anselmi F (2007) Ca²⁺ Signaling in the Inner Ear. *Physiology* 22:131-144.

Martin DL (1992) Synthesis and release of neuroactive substances by glia. *Glia* 5:81-94.

Minajeva A, Ventura Clapier R, Veksler V (1996) Ca²⁺ uptake by cardiac sarcoplasmic reticulum ATPase in situ strongly depends on bound creatine kinase. *Pflugers Arch* 432:904-912.

Mulvaney PT, Stracke ML, Nam SW, Woodhouse E, O'Keefe M, Clair T, Liotta LA, Khaddurah-Daouk R, Schiffmann EZ (1998) Cyclocreatine inhibits stimulated motility in tumor cells possessing creatine kinase. *Int J Cancer* 78:46-52.

Nagashima K, Nakai S, Matsue K, Konishi M, Tanaka M, Kanosue K (2003) Effects of fasting on thermoregulatory processes and the daily oscillations in rats. *Am J Physiol Regul Integr Comp Physiol* 284:R1486-R493.

Nakayama A, Bianco AC, Zhang CY, Lowell BB, and Frangioni JV (2003) Quantitation of brown adipose tissue perfusion in transgenic mice using near-infrared fluorescence imaging. *Mol Imaging* 2:37-49.

Nedergaard M, Ransom B, Goldman SA (2003) New roles for astrocytes: redefining the functional architecture of the brain. *Trends Neurosci* 26:523–530.

Palop JJ, Chin J, Mucke L (2006) A network dysfunction perspective on neurodegenerative diseases. *Nature* 443:768-773.

Park M, Salgado JM, Ostroff L, Helton TD, Robinson CG, Harris KM, Ehlers MD (2006) Plasticity-induced growth of dendritic spines by exocytic trafficking from recycling endosomes *Neuron* 52:817-830.

Pellerin L, Bouzier-Sore AK, Aubert A, Serres S, Merle M, Costalat R, Magistretti PJ (2007) Activity-dependent regulation of energy metabolism by astrocytes: An update. *Glia* 55:1251-1262.

Ramirez-Amaya V, Balderas I, Sandoval J, Escobar ML, Bermudez-Rattoni F (2001) Spatial long-term memory is related to mossy fiber synaptogenesis. *J Neurosci* 21:7340-7348.

Rossi AM, Eppenberger HM, Volpe P, Cotrufo R, Wallimann T (1990) Muscle-type MM creatine kinase is specifically bound to sarcoplasmic reticulum and can support Ca^{2+} uptake and regulate local ATP/ADP ratios. *J Biol Chem* 265:5258-5266.

Rubinsztein DC (2006) The roles of intracellular protein-degradation pathways in neurodegeneration. *Nature* 443:780-786.

Schneider ME, Belyantseva IA, Azevedo RB, Kachar B (2002) Rapid renewal of auditory hair bundles. *Nature* 418:837-838.

Schwegler, H. & Crusio, W.E. (1995) Correlations between radial-maze learning and structural variations of septum and hippocampus in rodents. *Behav Brain Res* 67:29-41.

Shin J, Streijger F, Beynon A, Peters T, Gadzalla L, McMillen D, Bystrom C, van der Zee CEEM, Wallimann T, Gillespie PG. (2007) Hair Bundles Are Specialized for ATP Delivery via Creatine Kinase. *Neuron* 53:371-386.

Spooren WPJM, Lubbers L, Jenks BG, Cools AR (1999) Variation in hippocampal dynorphin b-immunoreactive mossy fiber terminal fields of apomorphine-(un) susceptible rats. *J Chem Neuroanat*, 17:59-64.

Steeghs K, Benders A, Oerlemans F, De Haan A, Heerschap A, Ruitenbeek W, Jost C, Van Deursen J, Perryman B, Pette D, Bruckwilder M, Koudijs J, Jap P, Veerkamp J, Wieringa B (1997) Altered Ca^{2+} responses in muscles with combined mitochondrial and cytosolic creatine kinase deficiencies. *Cell* 89:93-103.

Steinhauser C, Seifert G (2002) Glial membrane channels and receptors in epilepsy: impact for generation and spread of seizure activity. *Eur J Pharmacol* 447:227-237.

Streijger F, Oerlemans F, Ellenbroek BA, Jost CR, Wieringa B, Van der Zee CEEM (2005) Structural and behavioral consequences of double deficiency for creatine kinases BCK and UbCKmit. *Behav Brain Res* 157:219-234.

Streijger F, Jost CR, Oerlemans F, Ellenbroek BA, Cools AR, Wieringa B, Van der Zee CEEM (2004) Mice lacking the UbCKmit isoform of creatine kinase reveal slower spatial learning acquisition, diminished exploration and habituation, and reduced acoustic startle reflex responses. *Mol Cell Biochem* 256-257:305-318.

Tachikawa M, Fukaya M, Terasaki T, Ohtsuki S, Watanabe M (2004) Distinct cellular expressions of creatine synthetic enzyme GAMT and creatine kinases uCK-Mi and CK-B suggest a novel neuron–glial relationship for brain energy homeostasis *Eur J Neurosci* 20:144-160.

Tian GF, Azmi H, Takano T, Xu Q, Peng W, Lin J, Oberheim N, Lou N, Wang X, Zielke RH, Kang J, Nedergaard M (2005) An astrocytic basis of epilepsy. *Nat Med* 11:973-981.

Tornberg J, Volkmar V, Savilahti H, Rauvala H, Airaksinen MS (2005) Behavioral phenotypes of hypomorphic KCC2-deficient mice. *Eur. J. Neurosci.* 21, 1327-1337.

Ullian EM, Christopherson KS, Barres BA (2004) Role for glia in synaptogenesis *Glia* 47:209-216.

Ullian EM, Sapperstein SK, Christopherson KS, Barres BA (2001) Control of synapse number by glia. *Science* 291:657-661.

Wang YE, Esbensen P, Bentley D (1998) Arginine kinase expression and localization in growth cone migration. *J Neurosci* 18:987-998.

Wang D, Pascual JM, Yang H, Engelstad K, Jhung S, Sun RP, De Vivo DC (2005) Glut1 deficiency syndrome: clinical, genetic, and therapeutic aspects. *Ann Neurol* 57:111-118.

Wang Y, Kimura K, Inokuma K, Saito M, Kontani Y, Kobayashi Y, Mori N, Yamashita H (2006) Potential contribution of vasoconstriction to suppression of heat loss and homeothermic regulation in UCP1-deficient mice. *Pflugers Arch* 452:363-369.

Young AA, Dawson NJ (1982) Evidence for on-off control of heat dissipation from the tail of the rat *Can J Physiol Pharmacol* 60:392-839.

Zheng JQ (2000). Turning of nerve growth cones induced by localized increases in intracellular calcium ions. *Nature* 403:89-93.

Zucker RS (1996) Exocytosis: a molecular and physiological perspective. *Neuron* 17:1049-1055.

Samenvatting - Dutch summary



Samenvatting

De meeste cellen in ons lichaam gebruiken ATP als voornaamste direct beschikbare energiebron. ATP wordt gegenereerd via metabole routes zoals glycolyse en oxidatieve fosforylering. Onder normale omstandigheden is in een levende cel de vraag naar energie in balans met de productie daarvan. Wanneer deze balans verstoord wordt doordat plotseling heel veel energie geconsumeerd wordt, kan gebruik worden gemaakt van het creatine kinase-fosfocreatine (CK-PCr) systeem. In weefsels zoals spierweefsel en hersenen, dient fosfocreatine (PCr) als tijdelijke energiebuffer. Het enzym creatine kinase (CK) zorgt voor de synthese van PCr door de reversibele overdracht van de energierijke fosfaat groep van ATP naar creatine (Cr). De functie van het CK-PCr systeem in spierweefsel is veelvuldig en diepgaand bestudeerd, maar het biologische belang van de brein specifieke CK's in zoogdieren is nog grotendeels onbekend. Om deze rol nader te onderzoeken, zijn in onze groep muizenmodellen ontwikkeld waarbij de individuele CK isoenzymen ieder afzonderlijk zijn uitgeschakeld met behulp van genetische modificatie. In dit proefschrift wordt beschreven hoe deze transgene muis modellen zijn gebruikt in onderzoek naar de rol van het cytosolisch BCK en het mitochondrieel UbCKmit in diverse hersengestuurde processen. In de **hoofdstukken 2-6** is beschreven hoe en in welke mate CK gestuurde reacties zijn gekoppeld aan gedrag, leervermogen, en regulatie van lichaamsfysiologie.

In **hoofdstuk 2** wordt de consequentie van UbCkmit deficiëntie ten aanzien van het gedrag in muizen beschreven. Observationale en gedragsexperimentele technieken werden gebruikt om gedragskenmerken zoals motivatie, emotie, motor functie en cognitie te analyseren. Bij UbCKmit^{-/-} muizen in hun natuurlijke omgeving werden in eerste instantie geen grote afwijkingen geconstateerd met betrekking tot gezondheid, ontwikkeling, maximale levensduur, of kooiactiviteit. Onderzoek naar meer complexere gedragingen liet echter zien dat deze dieren minder exploratie en habituatie gedrag vertonen in een nieuwe omgeving. Tevens hebben ze een verminderd vermogen om ruimtelijke taken te leren. Afwijkingen in motorische of visuele functies zijn niet aangetoond. Verder laten wij zien dat UbCkmit^{-/-} muizen een verlaagd vermogen hebben om acuut te reageren op onvoorspelbare akoestische prikkels. De resultaten van dit onderzoek leveren een beter begrip omtrent de gedrags relevante processen die verstoord kunnen zijn bij een defect creatine kinase energie systeem in de her-

senen.

Wij veronderstellen in **hoofdstuk 2** dat de nog aanwezige activiteit van het BCK isoenzym in UbCK^{-/-} muizen en eventueel andere fosfo-energie transfer-systemen compensatie kunnen bieden voor de verstoorde energie homeostasis. In **hoofdstuk 3** wordt deze hypothese verder belicht en wordt onderzocht welke functies worden aangetast als genoemde compensatie niet meer kan optreden. Hiervoor is gebruik gemaakt van transgene muizen met een complete CK deficiëntie, d.w.z. volledige inaktivering van zowel BCK als UbCKmit in CK^{-/-} muizen. Ons onderzoek liet zien dat een enkele mutatie van BCK of UbCKmit een relatief mild fenotype geeft in vergelijking met de (gedrags)veranderingen die worden aangetoond bij complete CK deficiëntie. Naast ernstige cognitieve defecten, vertonen CK^{-/-} muizen ook een postnatale groeivertraging en blijven deze dieren achter in zowel lichaamsgrootte als ook breinontwikkeling. De ernstige gedragsafwijkingen gaan gepaard met kenmerkende morfologische afwijkingen in de hippocampus, waaronder de 'dentate gyrus regio-inferior' en het 'intra-infra-pyramidaal mossy fiber' projectie gebied. Deze structurele veranderingen duiden o.i. op een belangrijke rol voor creatine kinase in de ontwikkeling en maturatie van neuronen en astrocyten, hetgeen kan leiden tot grootschalige functionele neurologische ontregelingen. In **hoofdstuk 4** werd met behulp van immunohistochemie BCK expressie aangetoond in haarcellen in de cochlea. Dit gehoororgaan is verantwoordelijk voor signaaltransductie in het binnenoor. De mechanische verplaatsing van de stereocilia van de haarcellen ten opzichte van het tectoriaal membraan, leidt tot opening van mechanotransductiekanaalen. Dit veroorzaakt cel depolarisatie welke gepaard gaat met opening van voltage-afhankelijke calcium kanalen in de basolaterale membraan, neurotransmitter afgifte en activatie van axonen. De effectiviteit van de elektrische prikkel vermindert uiteindelijk doordat actine filamenten en myosine eiwitten in de stereocilia actief langs elkaar schuiven waardoor de spanning vermindert en de kanalen sluiten. In hoofdstuk 4 tonen we aan dat dit adaptatieproces in haarcellen wordt beïnvloed door creatine kinase. Onze resultaten laten namelijk zien dat CK deficiëntie leidt tot een verminderd adaptatie proces met als gevolg een verslechterd gehoor in CK transgene muizen. Mogelijk ligt hierin ook de verklaring waarom onze mutante muizen een verlaagd vermogen hebben om acuut te reageren op onvoorspelbare akoestische prikkels (**hoofdstuk 2-3**).

In **hoofdstuk 5** wordt aangetoond dat één aspect van de li-

chaamsfysiologie, namelijk de regulatie van lichaamstemperatuur, heel kenmerkend afwijkend is in CK^{-/-} muizen. Uit ons onderzoek is gebleken dat de temperatuur van CK^{-/-} muizen elke dag $\sim 1^{\circ}\text{C}$ lager is in de vroege ochtend uren in vergelijking met controle dieren. Ook hebben de dieren een sterk verminderd vermogen om hun lichaamstemperatuur te handhaven in een koude omgeving. Controle dieren daarentegen kunnen hun lichaamstemperatuur wel constant houden onafhankelijk van de temperatuur van hun omgeving. Zodra hypothermie optreedt, zullen er (neuro)fysiologische processen op gang gebracht worden samen met veranderingen in gedrag. In **hoofdstuk 5** is gekeken naar de betrokkenheid van verscheidene thermo-effectoren in de afwijkende thermoregulatie van CK^{-/-} muizen. Onderzoek wees uit dat de hypothermie in deze muizen niet lijkt te worden bepaald door het kleiner zijn van de dieren, doordat ze minder lichaamsvet hebben, of minder voedsel innemen. Opvallend aan CK^{-/-} muizen is tevens dat het serumniveau van glucose, leptine en vrije vetzuren (FFA) lager is dan in controle dieren. Het is niet bekend hoe bij creatine kinase deficiëntie een verlaging van deze metabolieten en hormonen wordt veroorzaakt, maar een koppeling met inadequate energie-homeostase in het brein is wel waarschijnlijk. Verder zijn er geen veranderingen gevonden in het functioneren van het bruin vetweefsel, een cruciaal orgaan voor warmteproductie in perioden van koude. Echter, geheel tegen onze verwachting in, werden in CK^{-/-} muizen, na een koude behandeling, juist meer c-Fos positive neuronen aangetoond in specifieke hypothalamus gebieden. Gebaseerd op deze waarnemingen zou de defecte thermoregulatie in CK^{-/-} dieren wellicht samen kunnen hangen met een inefficiënt neuronaal functioneren.

In **hoofdstuk 6** wordt beschreven hoe hersenen met een complete CK deficiëntie functioneren in situaties waarbij de energie consumptie globaal en dramatisch verhoogd is en er er dus aanzienlijk meer ATP wordt verbruikt dan gevormd. Daartoe werden in controle en CK^{-/-} muizen kunstmatig convulsies opgewekt door middel van herhaaldelijke injecties met de convulsant pentylenetetrazole (PTZ). Als uitlezing werd bij dit deelonderzoek de elektrische activiteit van de hersenen gemeten door een elektroencefalogram (EEG) te maken met epiduraal geplaatste elektroden. Uit de EEG patronen was af te lezen dat in alle controle dieren een epileptische aanval gepaard gaat met een aaneengesloten serie van regelmatige 4-6Hz pieken. Het EEG patroon van CK^{-/-} dieren werd juist gekenmerkt door een zeer onregelmatige reeks van asymmetrisch pieken. Onze bevindingen duiden

op een verstoorde of ontregelde neurodynamiek. Calciumionen spelen hierin een cruciale rol, met name bij de exciteerbaarheid en neurotransmitter afgifte in neuronen. In het tweede deel van **hoofdstuk 6** laten we zien dat in CK^{-/-} muizen veranderingen zijn opgetreden in het vermogen om calcium uit hippocampale cellen te verwijderen. Een verhoogde extrusie van calciumionen kan mogelijk een effect hebben gehad op het vuurpatroon van neuronen en daarmee het “seizure gedrag” beïnvloeden.

Tot slot, in dit proefschrift hebben we nader bestudeerd hoe creatine kinase activiteit in de hersenen is gekoppeld aan sturing van gedrag, ontwikkeling en lichaamsfuncties. Waarschijnlijk beschermt het CK-PCr systeem tegen (tijdelijke) energie-overvraag. Drastische verstoring van dit systeem heeft dus grote pathofysiologische gevolgen, direct voor neuronale cellen en het functioneren van de hersenen zelf, maar indirect daarmee ook voor het functioneren van het hele organisme. Vervolgonderzoek naar de rol van creatine kinases in de energie-homeostase van verschillende celtypen in de hersenen, bijvoorbeeld t.a.v. de neurodynamische werking van neuronen of de rol van astrocyten tijdens de groei en voortdurende remodellering van hersenstructuren, is ook na mijn promotieonderzoek beslist nog nodig. Op termijn zal dit ons nieuwe mogelijkheden bieden om de betekenis van creatine kinases nog verder te verduidelijken en de enorm complexe interactie tussen molecuul, hersenaanleg en (leer)gedrag verder bloot te leggen.

Dankwoord

1916: First successful divorce case based on failure of author to thank his wife, in the foreword of his book, for typing the manuscript. D.D. Jackson, in *Science with a Smile*, 1992

Je weet hoe het gaat. Je krijgt een boekje, je kijkt naar de cover, maakt een beslissing: mooi/niet mooi en dan ga je gelijk door naar het dankwoord. Wetende dat iedereen het dankwoord zal lezen, maakt het schrijven ervan bepaald geen makkelijke opgave. Zeker omdat je niemand wilt vergeten of teleurstellen wat kan leiden tot desastreuze gevolgen.

Allereerst mijn promotor Bé Wieringa. Tijdens de afgelopen jaren, eerst als student, toen als analist en later als AIO, heb ik vooral je aanspreekbaarheid erg gewaardeerd. Heel erg bedankt voor je begeleiding, het 'denken in hoofdstukken' en de tijd die je nam om ondanks de overvolle agenda toch nog mijn hoofdstukken te corrigeren (of volledig te herschrijven). Verder wil ik Ineke, mijn co-promotor en begeleidster, nog in het bijzonder bedanken. Wat ik het meeste aan je bewonder is wel je enorme betrokkenheid. Of ik nu langs je zat op de flex kamer of zoals de laatste tijd aan de andere kant van de wereld, je hebt altijd het beste met me voor gehad en deed er alles aan om me verder te helpen. Jouw immense energie, enthousiasme en doorzettingsvermogen waren bewonderenswaardig en aanstekelijk. De grote mate van zelfstandigheid die je me gaf, heeft erg stimulerend gewerkt. Dank je wel voor het vertrouwen in mij. Verder natuurlijk Helma. Als ik terug kijk op mijn tijd bij celbiologie krijg ik bijna medelijden met je. De vele vragen die ik op je afgevuurd heb over blotjes, gelletjes, PCR's en ga maar door. Wist ik iets niet, dan hadden we altijd onze eigen 'Helma-wikipedia'. Ook jij hebt er voor gezorgd dat ik dit dankwoord zit te schrijven. Super bedankt. Frank, mijn eerste onderzoeksproject als student onder jouw begeleiding is de start geweest voor mijn verdere 'carrière' bij de afdeling Celbiologie. Als ik iemand uit moet leggen wie Frank is, dan zal ik zeggen dat hij van een CD hoesje een professioneel fixatie systeem voor muizen kan maken. Het komt maar zelden

voor dat het woord 'helaas' uit zijn mond komt. Je enthousiasme en natuurlijk je gezelligheid was een enorme stimulans voor mij. Huipie, vaak wist je al dat zodra ik je iets vroeg dat het je aardig wat ellende en 'bench-hours' zou bezorgen. Ontzettend bedankt voor al je hulp, ook alvast voor de toekomst, want je bent nog niet van me af. De komende jaren zal ik nog menig keer komen met vragen, verzoeken of gewoon zomaar ook al zit ik in Canada. Mietske, allereerst enorm bedankt voor jouw EM bijdrage in dit boekje. Zoals je ziet waren de foto's te mooi om niet te gebruiken. En dan mijn labmaatjes: Gönül, Lieke, Marloes, Suus en Yvet. Niet alleen collega's maar ook nog eens super goede vriendinnen. Jullie zijn stuk voor stuk top meiden en zou jullie vriendschap niet willen missen! Lieke, jou wil ik nog een keer speciaal bedanken voor alles wat je voor me gedaan hebt de afgelopen jaren. Vaak had het excuus 'sorry maar de trein had vertraging' wel iets met jou te maken. Even een biertje op Vrijdag (of Maandag), of lekker een hapje eten, het ging altijd gepaard met een telefoontje naar huis. Zie ik je volgend jaar met de sleurhut in Vancouver? Edwin, Marco, Ad, Jan K, en Bas. In de vier jaar hebben we zowel onnoemelijk veel onzinnige maar ook zinnige gesprekken gehad. Ik twijfel nog over de balans tussen die twee, maar ik had ze beiden niet willen missen. In dit rijtje horen natuurlijk ook de overige nog niet genoemde (ex)leden van celbiologie: Rick, Walter, Renee, en Ralph, Rinske, Jack, Wiljan, Jan S, Mary, Marianne, Hans (24 december 1944 - 12 november 2001), Marieke en Mariska. Ik heb het altijd zeer gewaardeerd dat je bij iedereen kon aankloppen voor van alles en nog wat. De gezellige atmosfeer, de ontspannende lunch pauzes en de collegialiteit waren een extra stimulans bij het onderzoek. Zonder jullie was het maar een saaie bedoeling geweest. Ook de NS moet even genoemd worden. Ruim een kwart miljoen kilometer in totaal heeft de trein me tussen Nijmegen en Eindhoven heen en weer gereden. Vaak met vertragingen en soms zelfs met geen enkel treinverkeer. Gelukkig was ik nooit alleen, want altijd was daar mijn NS maatje: El Magnifico: Muuuuuuuuhahahahaha. Magda. Ik wil jou natuurlijk ook bedanken voor jouw steun bij al het papierwerk dat een promotie met zich meebrengt. Het versturen van een belangrijke envelop is vaak van onzichtbaar maar groot belang. Dank

je wel voor je geduld met FedEx. Wilma (14 mei 1968 - 22 november 2006) ook jou wil ik op deze manier nog enorm bedanken. Door jouw bereidheid om net even iets extra's te doen voor een ander, is het mij gelukt om dit project tot een goed einde te brengen. Natuurlijk mogen de collega's van moleculair dierfysiologie niet ook vergeten worden: Nick, Jeroen, Jos, Dorien, Karen, Eric, Gerard, Gerrit, François, Rob, Jessica, Marcel, en Karel (19 december 1952 - 17 oktober 2004). En natuurlijk 'de Boertjes': Godfried, Alwin, en Peter. Bedankt voor de gezelligheid op de afdeling, en niet te vergeten de zeer gedenkwaardige 'dagjes uit' en kerstdiners met de afdeling. Iedereen heel erg bedankt! Ook ben ik veel verschuldigd aan de medewerkers van het centraal dierenlaboratorium en in het bijzonder Helma, Nancy, Aglaja, en Laura. Bedankt voor de gezelligheid en voor jullie inzet, ondersteuning en hulp bij het verzorgen van de muizen. Veder wil ik Wim Scheenen enorm bedanken voor zijn inzet. Ontelbare keren hebben jij, Ineke en ik onder het genot van een kop thee prettig gediscussieerd over de soms frustrerende calcium resultaten. Gilles Luijtelaar, voor alle tijd die jij in mij geïnvesteerd met betrekking tot de seizure experimenten. Bedankt voor je inspirerende ideeën. Ook mogen de buitenlandse samenwerkingen niet ongenoemd blijven. I thank Peter G. Gillespie and his lab in Portland, OG, USA for their work on the hair cell experiments. I really appreciate the fruitful collaboration. Furthermore, I would like to thank my current supervisor, Wolfram Tetzlaff. My work with him is not directly related to the CK project, and even though it was not in my job description, he never complained about the time I spent working on my thesis.

Naast de directe werkomgeving is de steun van familie en vrienden natuurlijk ook heel erg belangrijk voor een succesvolle promotieperiode. Lisette, Yvonne, Manon, Judit, Janneke, Tamara, en Yvonne Zoetermeer, ik neem aan dat jullie nog steeds niet goed begrijpen waar ik eigenlijk de afgelopen vier jaar mee bezig ben geweest. Maar toch hebben jullie altijd geïnteresseerd geluisterd als ik mijn ei weer eens kwijt moest. Ik wil jullie graag danken omdat jullie er steeds voor me zijn geweest en omdat ik altijd op jullie kon rekenen! Paps, mams en Michiel ontzettend bedankt voor alle ondersteuning over de afgelopen

jaren. Jullie hebben mij onvoorwaardelijk gesteund ook toen ik besloot om naar Vancouver te vertrekken wat vast niet makkelijk is geweest. Nodeloos om te zeggen dat ik het niet had kunnen doen zonder jullie. Natuurlijk wil ik ook Charlotte, Jan, Lotje en Wouter bedanken voor alle gezellige tijden. Ik heb me altijd welkom gevoeld in jullie knusse geheel. Merán. Jij hebt mij altijd gestimuleerd en vrij gelaten om mijn eigen keuzes te volgen, ook al bracht die weg ons naar de andere kant van de planeet. Hoe cool kan je vriend zijn?

Tenslotte; ik weet dat velen deze tekst als eerste (en laatste) lezen, en zich dan stiekem afvragen: "word ik genoemd"? Als ik je nu toch ongehoopt ben vergeten dan is deze voor jou: bedankt!

Zonder jullie allemaal
was het nooit gelukt

-X- Franke
16 oktober 2007

Curriculum Vitae

Femke Streijger was born on 30 November 1976 in Nijmegen, the Netherlands. In 1994 she finished high school at the Rommert Casimir (Eindhoven, the Netherlands). After one year of Gymnasium she started the study Animal management at the Van Hall Institute, Leeuwarden, The Netherlands. As part of her practical training, she started her internship at the National Institute of Public Health and the Environment, (Bilthoven, The Netherlands) under supervision of prof. dr. CFM Hendriksen. There she worked as a trainee on the project "The evaluation of humane endpoints in pertussis vaccine potency testing". In her final year, she became a trainee at the department of Cell Biology, Radboud University Nijmegen Medical Center, The Netherlands. In 1999 she graduated on the project "Non-invasive temperature measurements in mice", supervised by dr. I. van der Zee and F. Oerlemans and obtained her bachelor degree for Animal Management, specialization Animal Laboratory. Femke Streijger worked a few months as a technician at the animal facility of the Erasmus University Rotterdam, The Netherlands. In 2000 she rejoined the department of Cell Biology of prof. dr. B. Wieringa to work as a technician developing and adapting behavioral tests for mice phenotyping under supervision of dr. Catharina E.E.M. van der Zee. In 2002 she became a PhD student unraveling the biological role of phosphocreatine-creatine kinase cellular energy circuit in mice, which resulted in the present thesis. At the moment she is employed as a Postdoctoral Research Fellow at ICORD, Dept Zoology, University of British Columbia, Vancouver, Canada performing research on spinal cord injury.

Publications

Chapters

1. Streijger F, In 't Zandt HJA, Renema WKJ, Oerlemans F, Heerschap A, Kuiper J, Pluk H, Jost CR, Van der Zee CEEM, Wieringa B (2007) Developmental and Functional Consequences of Disturbed Energetic Communication in Brain of Creatine Kinase Deficient Mice: Understanding CK's role in fuelling of behavior and learning. Editor: Valdur Saks, Wiley Book Series, in press.

Refereed Journal Articles:

2. Shin JB, Streijger F, Beynon A, Peters T, Gadzala L, McMillen D, Bystrom C, Van der Zee CEEM, Wallimann T, Gillespie PG (2007) Hair bundles are specialized for ATP delivery via creatine kinase. *Neuron* 53:371-386.

3. Streijger F, Oerlemans F, Ellenbroek BA, Jost CR, Wieringa B, Van der Zee CEEM (2005) Structural and behavioral consequences of double deficiency for creatine kinases BCK and UbCKmit. *Behav Brain Res.* 157:219-234.

4. In 't Zandt HJ, Renema WK, Streijger F, Jost CR, Klomp DW, Oerlemans F, Van der Zee CEEM, Wieringa B, Heerschap A (2004) Cerebral creatine kinase deficiency influences metabolite levels and morphology in the mouse brain: a quantitative in vivo ¹H and ³¹P magnetic resonance study. *J Neurochem* 90:1321-1330.

5. Kolkman MJM, Streijger F, Linkels M, Bloemen M, Heeren D, Henderiks WJAJ, Van der Zee CEEM (2004) Mice lacking Leukocyte common Antigen-Related (LAR) protein tyrosine phosphatase domains demonstrate spatial learning impairment in the two-trial water maze and hyperactivity in multiple behavioral tests. *Behav Brain Res* 154:171-182.

6. Streijger F, Jost CR, Oerlemans F, Ellenbroek BA, Cools AR, Wieringa B, Van der Zee CEEM (2004) Mice lacking the UbCKmit isoform of creatine kinase reveal slower spatial learning acquisition, diminished exploration and habituation, and reduced acoustic startle reflex responses. *Mol Cell Biochem* 256-257:305-318.

7. Jost CR, Van der Zee CEEM, In 't Zandt HJ, Oerlemans F, Verheij M, Streijger F, Fransen J, Heerschap A, Cools AR, Wieringa B (2002) Creatine kinase B-driven energy transfer in the brain is important for spatial learning behavior, mossy fiber field size and determination of susceptibility. *Eur J Neuroscience* 15:1692-1706.

Articles in preparation

8. Streijger F, Oerlemans F, Bianco AC, Ribeiro MO, Pluk H, Wieringa B, Van der Zee CEEM. Deficiency for brain-type creatine kinases in mice causes defective thermoregulation. In preparation.

9. Streijger F, Scheenen WJJM, van Luijtelaar G, Oerlemans F, Wieringa B, Van der Zee CEEM. Complete brain-type creatine kinase deficiency in mice affects seizure activity and removal of intracellular calcium. In preparation.

10. Plunet WT, Streijger F, Lam CK, Lee JHT, Tetzlaff W. Dietary restriction implemented after spinal cord injury improves functional recovery. Submitted to *Brain* 2007.

